Climatic Effects on Pavement and Geotechnical Infrastructure

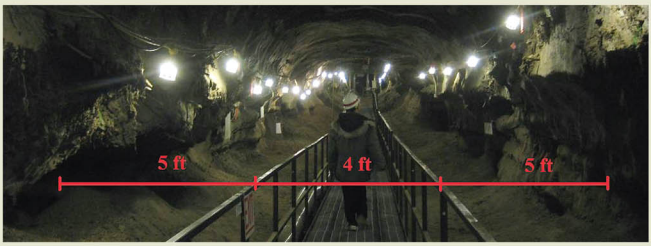

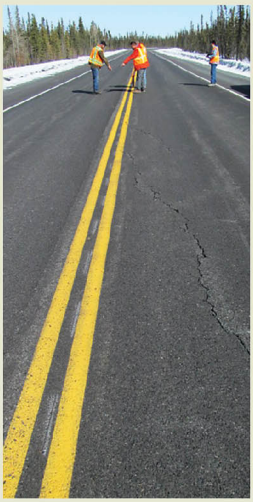

Proceedings of the
International Symposium of Climatic Effects on Pavement and Geotechnical Infrastructure 2013

Edited by

Jenny Liu, Ph.D., P.E.; Peng Li, Ph.D.;
Xiong Zhang, Ph.D., P.E.; and
Baoshan Huang, Ph.D., P.E.

ASCE

CONSTRUCTION INSTITUTE

CLIMATIC EFFECTS ON PAVEMENT AND GEOTECHNICAL INFRASTRUCTURE

PROCEEDINGS OF THE INTERNATIONAL SYMPOSIUM OF CLIMATIC EFFECTS ON PAVEMENT AND GEOTECHNICAL INFRASTRUCTURE 2013

August 4–7, 2013
Fairbanks, Alaska

SPONSORED BY
The Construction Institute of the American Society of Civil Engineers

EDITED BY
Jenny Liu, Ph.D., P.E.
Peng Li, Ph.D.
Xiong Zhang, Ph.D., P.E.
Baoshan Huang, Ph.D., P.E.

Published by the American Society of Civil Engineers

Cataloging-in-Publication Data on file with the Library of Congress.

Published by American Society of Civil Engineers
1801 Alexander Bell Drive
Reston, Virginia, 20191-4382
www.asce.org/bookstore | ascelibrary.org

Errata: Errata, if any, can be found at http://dx.doi.org/10.1061/9780784413326

ISBN 978-0-7844-1332-6 (paper)
ISBN 978-0-7844-7831-8 (PDF)
Manufactured in the United States of America.

Cover photo credits: Jenny Liu, Ph.D., P.E.; Xiong Zhang, Ph.D., P.E.; and Billy Connor, P.E.

Preface

Climatic Effects on Pavement and Geotechnical Infrastructure selects 22 papers that represent the latest developments and advances of the impact of various climatic factors, such as freeze and thaw, wet and dry cycle, rainfall, flooding, etc., on designing, building, preserving and maintaining transportation infrastructure.

Many of the selected papers were presented at the International Symposium of Climatic Effects on Pavement and Geotechnical Infrastructure 2013 held in Fairbanks, Alaska, USA from August 4 to 7, 2013. The conference was hosted by the University of Alaska Fairbanks in collaboration with the University of Alaska Anchorage in USA, Tongji University in China, Harbin Institute of Technology in China, Chang'An University in China, International Association of Chinese Infrastructure Professionals (IACIP), the American Society of Civil Engineers (ASCE), and the University of Tennessee, Knoxville in USA.

The papers presented within the *Climatic Effects on Pavement and Geotechnical Infrastructure* Special Technical Publication (STP) are divided into four groups. The first group contains four papers which provide an international perspective on climate change and infrastructure and climate network. The second group of papers contains five papers focused on preservation, maintenance, and operations of pavement and geotechnical infrastructure in correspondence to various climatic conditions. Eight papers are collected in the third group on advancing innovative sustainable materials and design for transportation infrastructure use. Furthermore, five papers on various analysis and evaluation approaches to assess the climatic effects on performance and life of infrastructure are provided.

Two or more reviewers along with the editors evaluated each paper published in this ASCE STP. All published papers are eligible for discussion in the *Journal of Materials in Civil Engineering*, and are eligible for ASCE awards.

We would like to acknowledge the great support from Laura Ciampa and Marvin Oey from the ASCE Construction Institute (CI) that makes it possible for this high quality peer reviewed STP. Most importantly, we would like to thank the peer reviewers who spent their time and efforts in ensuring the exceptional quality of the papers presented within this STP. Without their contributions this publication would not be possible.

This page intentionally left blank

Contents

Author List

Impact of Climate Change on Pavement Performance: Preliminary Lessons Learned through the Infrastructure and Climate Network (ICNet)

Jo Sias Daniel[1], M. ASCE, Jennifer M. Jacobs[2], M. ASCE, Ellen Douglas[3], M. ASCE, Rajib B. Mallick[4], M. ASCE, Katharine Hayhoe[5]

[1]Professor, Department of Civil Engineering, University of New Hampshire, Durham, NH 03824, jo.daniel@unh.edu
[2]Professor, Department of Civil Engineering, University of New Hampshire, Durham, NH 03824, jennifer.jacobs@unh.edu
[3]Associate Professor, School for the Environment, University of Massachusetts at Boston, Ellen.Douglas@umb.edu
[4]Professor, Civil and Environmental Engineering Department, Worcester Polytechnic Institute (WPI), Worcester, MA 01609, rajib@wpi.edu
[5]Director, Climate Science Center, and Associate Professor, Department of Political Science, Texas Tech University, Lubbock TX 79409, hayhoe@atmosresearch.com

ABSTRACT: The Infrastructure and Climate Network (ICNet) was established to develop collaborative networks and platforms needed to integrate the multidisciplinary areas of climate change, pavement design and performance, and economics. Preliminary network activities, described in this paper, have rapidly expanded our knowledge of pavement performance under future climates and provide insights for future research. Specifically, increases in the frequency and/or severity of many types of extreme weather events have already been observed; projected future changes in air temperature, rainfall, sea level rise and hurricanes on pavement performance are significant; and future costs are expected to increase very significantly and non-linearly. Combining these findings, we offer a set of recommendations for future research to address our key research question: *How does climate non-stationarity differentially impact transportation infrastructure design, performance and life span?*

INTRODUCTION

The nation's infrastructure is becoming increasingly vulnerable to damage from changing weather patterns resulting from global climate change. Observations, models, and even paleohydrologic studies identify the potential for changes in climate characteristics that directly impact infrastructure design. Observed and projected future changes in infrastructure-relevant climate characteristics include the average, variability, and extreme values of temperature, solar radiation, snow and rainfall, freeze-thaw cycles, groundwater levels, and streamflow. Increases in sea level and

changes in the intensity of tropical storms and hurricanes carry additional implications for coastal infrastructure.

Pavements constitute the most widely used part of the nation's infrastructure for the transportation of people and goods. Changing climate can impact the properties of the pavement layers, making them susceptible to accelerated damage under traffic loading, reducing their serviceable life span, and increasing maintenance costs, all of which would have a major negative impact on the nation's economy. An increase in pavement temperature as a result of rising air temperature, reduction in subgrade and hot mix asphalt (HMA) modulus due to high rainfall (saturation), and flooding due to rise in sea water level (in coastal areas) and stronger hurricanes are all factors that should be considered to design and construct pavements that will perform under non-stationary future climate conditions.

We argue that the key to constructing resilient pavements is accounting for the fact that climate can no longer be assumed to be a stationary process – in other words, that the past is no longer a reliable guide to the future. Instead of relying solely on historic datasets and single-valued design parameters, engineering methods must be able to accommodate changing parameters and a range of projected climate futures to ensure that pavements are designed to withstand the conditions that are likely to occur over their lifetime.

There are many challenges to incorporating information from climate projections into the existing pavement design methodologies and also more generally into the knowledge community supporting long-range infrastructure decisions. The Infrastructure and Climate Network (ICNet), a network of engineers and scientists, was formed to integrate climate science and engineering research for sustainable transportation infrastructure in New England and is funded by a U.S. National Science Foundation (NSF) research grant from the RCN-SEES program (CBET-1231326). ICNet uses joint knowledge-building approaches which are appropriate for complex problems and have slowly permeated into the planning and policy communities as well as a few large-scale institutions like the U.S. Army Corps of Engineers (http://www.sharedvisionplanning.us/).

ICNet's goal is to integrate climate change and adaptation research into infrastructure engineering by addressing the problem as a network of researchers and practitioners, rather than as individual investigators. ICNet members are identifying, prioritizing and developing climate impact information and resources needed to make decisions about building bridges and roads today that will last longer and cost less to maintain under the uncertain conditions of tomorrow. A distinctive part of our strategy is to build community and develop resources to support knowledge-sharing and prioritization among ICNet researchers and to link that knowledge to the community of user institutions. This is being done through interactive workshops with researchers and stakeholders, webinars, and a knowledge commons that is readily accessible (theicnet.org). ICNet is an open community that encourages participation in network activities and the development of new collaborations among researchers and practitioners in New England. This paper presents outcomes from ICNet's early exploration process in which the research and practitioner communities jointly collaborated to identify relevant climate information, to use that information to

identify research needs and to explore the impact of future climate on pavement performance at multiple scales.

CLIMATE CHANGE AND SEA LEVEL RISE

Climate defines the range of conditions (both "normal" and extreme)—in terms of temperature, precipitation, humidity, etc.—experienced over multiple decades. The notion of climate stationarity assumes that average conditions do not change over time and that climate variability remains within a quantifiable range. This assumption has allowed engineers to design infrastructure that are reliable to an acceptable level of failure risk. However, both the validity and utility of this assumption has been called into question (Milly et al., 2008; Lins and Cohn, 2011). Climate is already changing, here in North America and around the world (USGCRP, 2009) and decades of research has demonstrated that extreme events are more sensitive to climate change than average events; in fact, "a changing climate … can result in unprecedented extreme weather and climate events" (IPCC, 2012). Despite large increases in heavy precipitation events, it has been difficult to tease out the influence of climate change on flooding, given the complex nature of watershed processes, natural climate variability and anthropogenic factors such as land use change, urbanization and flow regulation (i.e., Shaw and Riha, 2011; Smith et al., 2011). However, the observed and projected impacts of climate change on temperature extremes are direct and clear: the number of cold days and cold extremes is decreasing, while the frequency, magnitude and duration of heat waves and heat extremes are increasing.

New England has already experienced increases in annual and seasonal temperatures and changes to hydrologic processes (for information and publications, see www.climatechoices.org/northeast). These changes are expected to accelerate into the future as human emissions of carbon dioxide and other heat-trapping gases continue to rise. For example, an average summer in New England could feel like a summer below the Mason-Dixon line by mid- to late century. For coastal areas, rising sea level is one of the most certain and potentially devastating impacts of climate change. Globally, the ocean is expanding and rising as an estimated 93% of the excess heat trapped within the Earth's climate system by human emissions is being absorbed by the ocean (Levitus et al., 2012). Atmospheric warming is accelerating glacial ice melt and the increased ocean heat content is destabilizing ice sheet margins in Antarctica and Greenland (Joughin et al., 2012). Kemp et al. (2011) suggested that the increase in sea level since the 19th century along the eastern Seaboard represents the steepest century-scale increase in sea level over the past two millennia. Sallenger et al. (2012) identified the Northeast U.S. coastline as a SLR "hot spot", with SLR rates 3-4 times faster than the global rate. Add to that a potential two- to seven-fold increase in extreme "Katrina-magnitude" storm surge events along the U.S eastern and Gulf coast (Grinstead et al., 2013) and the likelihood of future damage to infrastructure increases dramatically.

RESILIENT PAVEMENT DESIGN IN A CHANGING CLIMATE

It is evident that pavements are at increasing and critical risk from climate-driven stressors; anticipated changes could alter the frequency, duration, and severity of road failures as well as the time and cost of reconstructing the pavement systems. ICNet members conducted a detailed review of pavement systems in New England to better understand potential impacts of climate change on pavement design and maintenance in the future and to identify limitations in the sector's knowledge. ICNet's findings indicate that pavements face failure from a combination of temperature and water impacts. Higher temperatures will decrease the stiffness of the asphalt concrete pavement, increasing susceptibility to rutting, while more freeze thaw cycles would increase the damage from frost heaves and potentially increase thermal fatigue cracking. Increased precipitation, flooding events, and/or SLR will increase the moisture content of the granular (soil) sub layers under the pavement surface. The increase could be permanent (in case of higher groundwater tables) or temporary (longer drainage times). Coastal roadways, especially local and secondary roads, will be flooded more frequently as the limit of high tide moves landward and storm surge and wave effects reach farther inland than in the past. Higher moisture contents weaken the pavement base and subgrade; this can lead to increased cracking or rutting of the pavement surface due to loss of underlying support, hastening failure of the entire pavement structure. Flooding can also lead to sudden catastrophic failure (washout) if the event is sufficiently large. Impacts from temperature and water ultimately will require new pavement designs, roadway elevation or re-routing in order to accommodate expected changes.

Better understanding of these potential modes and consequences of failure is critical to the evaluation of options with regard to infrastructure (Transportation Research Board, 2009). ICNet members have conducted some initial research activities to quantify changes in pavement failure modes under future climates in New England. The sections below briefly describe research and results from two pilot studies that evaluated local-scale pavement design and pavement system dynamics. Challenges and opportunities for future research are presented in each section.

Pilot Study 1: Local Scale Evaluation of Climate Change Impacts on Pavements

The impact of a changing climate on pavement performance has been investigated by a few researchers in the past (Mills et al. 2009) and most recently, ICNet members presented a methodology to assess the impact of future climate change on pavement deterioration (Meagher et al. 2012). Instead of relying on historic observations, they conducted a mechanistic-empirical analysis of pavement structures (designed for four sites across New England) with projected future temperatures, and evaluated their effects on the rutting and cracking performance of the pavements. The effect on the rutting potential of the asphalt concrete layer was found to be significant. The authors demonstrated and proposed the use of high-resolution future climate projections to create modified hourly climatic inputs for the mechanistic empirical pavement design guide/software (MEPDG/S). For example, Meagher et al. used the North American Regional Climate Change Assessment Program's (NARCCAP) products to provide

modeled output for two periods, 1971-2000 and 2041-2070, at a spatial resolution of 50 km, based on the SRES (Special Report on Emissions Scenarios) A2 mid-high emissions scenario. Because there often is a bias between model output and the required MEPDG site information, a cumulative distribution function transformation method was used to adjust the NARCCAP temperature data to site-specific data for use in the MEPDG. The importance of this probabilistic transformation was underscored by the shift in historical and future temperature forecasts once the observed statistical characteristics were matched. This method is fundamentally different from a recent study completed by Truax et al. (2011) for the state of Mississippi which also evaluated the impact of climate on pavement performance using the MEPDG. Truax et al. used decadal output from a single regional climate model (RegCM2) for the 1990s and 2040s to calculate the change in precipitation and temperature due to climate change. This 'delta' was then applied to the historic MEPDG climate files to create future climate files. While both approaches are reasonable, their differences make comparisons across studies difficult.

Even if the climate projections are consistent across studies, challenges will still arise from how to best use that information. For example, the MEPDG/S requires climate projections at an hourly time resolution that are not readily available from either global or regional climate models, so Meagher et al. applied average values to each of the corresponding three-hour intervals. However, the use of averages reduces the extreme temperatures that are critical to predicting rutting and thermal cracking. Also, one must consider that different climate variables have different degrees of uncertainty associated with them: lower uncertainty for projected temperature changes, higher for precipitation, sunshine, relative humidity, and a great deal higher for wind speed and direction. MEPDG/S requires forecasted modifications to all variables to completely assess net impacts of climate change and the decoupling of the interactions among the variables could change predictions of future pavement performance.

Pilot Study 2: A Systems Dynamics Approach for Evaluating Climate Change Impacts on Pavements

The effect of climate change on the entire life cycle of pavements (and pavement systems) including maintenance costs may be best evaluated through a systems dynamics approach. Systems dynamics modeling has the ability to link elements across disciplines (such as climate science and civil engineering), to model the interdependencies, and to utilize feedback loops (causal loops) to identify non-linear trends in responses, if any, which may appear only at a later period. A system dynamics model linking climatic changes to pavement maintenance and costs was developed by members of the ICNet group (Mallick et al., 2014). The effects of climate change which are considered include increases in average annual rainfall, maximum air temperature, hurricane frequency and SLR. These parameters will affect the pavement systems by increasing the pavement temperature and number of months during which the subgrade is saturated. Pavement state variables were linked to stiffness (represented through modulus) of the HMA and subgrade. The life of the

pavement is represented by rutting evaluated using the MEPDG to illustrate the framework.

The model was run for a time span of 100 years for two cases, with and without climate change. The average pavement life decreased from 16 (without climate change) to 4 years (with climate change) as a result of reduced effective subgrade and HMA modulus due to climate change. The maintenance costs increased after 20 years for both cases; a linear increase was observed when climate change was not considered whereas consideration of climate change resulted in a non-linear increase.

At the end of 100 years, the cost of maintenance considering climate change increased 160%, as compared to the less than 60% increase without the impact of climate change. The study recommends that, for making long-term predictions and optimizing pavement performance for expected changes, engineers must integrate available climate, pavement and economic (as well as environmental) data in a systems dynamics approach. There is a critical need for accurate and reliable data regarding climate changes, particularly those that will have significant effects on pavement performance.

The data requirements and challenges for the systems approach differed greatly from that of the site-specific MEPDG study. In order to capture the overall system performance and ultimately maintenance cost increases, empirical relationships are more appropriate to link climate data to pavement state and performance than a complex physical model (e.g., MEPDG's mechanistic approach). However, the empirical relationships are derived from a database of results that are generated from mechanistic-empirical analyses. The reduction in model complexity allows the systems model to broadly evaluate the relative contribution from many climate forces that potentially cause deterioration and to deploy sensitivity analyses.

Even when targeting simplified methods, developing estimates of subgrade saturation and inundation frequency is a nontrivial process. There is no direct method to translate precipitation to subgrade saturation. Mallick et al. used a simple one-dimensional water balance model to predict the change in the number of times the soil could be expected to be at or close to saturation. While this approach can account for the arrival of rain events, it requires additional subgrade soil properties to be specified. Inundation frequency presented the greatest challenge because it is a function of both SLR and hurricanes. While reasonable estimates of SLR are available, the impact of SLR is sensitive to the road location. Inundation frequency due to hurricanes is difficult to quantify because there is no consistent dataset that links hurricane arrivals and intensity to roadway inundation and only recently have climate modelers been able to provide some estimate of future hurricane frequencies.

Pavement temperatures are more readily determined and provide an opportunity to examine the uncertainty among model output of future temperatures. The maximum pavement temperature was determined empirically from the maximum air temperatures model (LTTP model). The LTTP approach could readily be used to develop ranges of future maximum pavement temperatures if an ensemble of climate models were used to determine future maximum air temperatures. Temperature changes are readily determined using the delta method (differencing current and future climate variables) available. The primary difficulty is determining which models and scenarios are appropriate for the study region. Mallick et al. used only

one climate model output for their estimates of temperatures in their initial systems analysis. Extending beyond a single model adds to the complexity and points to the need for a suite of climate models with output that is readily composited into pavement relevant variables.

CONCLUSIONS

The future can never be predicted with certainty. What is certain, however, is that climate is changing. Most existing pavement design and management practices use historic climate records and do not include our current understanding of future variability in sea and river water levels, storm frequency and intensity, and temperature means and extremes when predicting the response and remaining service life of roads. Pavement and other infrastructure design based on specifications from historical climate average conditions and extremes is no longer valid today, and will certainly not be valid in the future as temperatures increase, precipitation patterns change, and sea level rises. Transportation agencies should adjust or adapt to the challenges posed by changing climate and use scenarios of possible future climates to find adaptation strategies that function reasonably well over all climate conditions (so-called robust solutions), employ adaptive management adjusting to impacts as they occur, or most likely, a combination of these.

Incorporating climate projections and other information on a changing climate into pavement design standards, however, is complicated. The information produced by one field of research (i.e, climate science) is not necessarily the information most directly useful to another field of research (i.e., engineering design). Approaches that build regional knowledge and improved collaboration between climate scientists and transportation engineers such as ICNet are critical so that engineers understand the uncertainties and limitations of future climate projections and climate scientists can generate the best possible model output for end users. There is a need to use system dynamics approach to integrate the multidisciplinary topics of climate change, pavement design and performance, and economics to determine the key factors and responses, and the nature of responses. The goal should be the assessment and prioritization of risks of climate change and their economic consequences and determination through simulation, of innovative, sustainable, cost-effective and practical approaches to meet the demands of the changing climates. This approach is necessary to make sure that appropriate materials and methods are developed and that the optimal combination (for road construction) is utilized in the future, for long term positive outcomes. The work should be carried out under two main subject areas – risk assessment (which determines the risk to pavement performance and the transportation network), economic assessment (to determine the cost of damage) and risk management (which involves the evaluation of innovative materials and techniques for cost-benefit data). ICNet participants, who include transportation planners, designers and researchers, will be instrumental in highlighting the long-term implications of such impacts as well as helping to promote research that will lead to more permanent solutions.

REFERENCES

Grinsted, A., Moore, J. C., and Jevreieva, S.(2013). "Projected Atlantic hurricane surge threat from rising temperatures." *Proceedings of the National Academy of Science*, www.pnas.org/cgi/doi/10.1073/pnas.1209980110.

IPCC[Field, C.B., Barros, V., Stocker, T.F., Qin, D., Dokken, D. J., Ebi, K.L., Mastrandrea, M.D., Mach, K. J., Plattner, G. K., Allen, S. K., Tignor, M., and Midgley, P.M. (eds.)] (2012). "Managing the Risks of Extreme Events and Disasters to Advance Climate Change Adaptation." *A Special Report of Working Groups I and II of the Intergovernmental Panel on Climate Change*. Cambridge University Press, Cambridge, UK, and New York, NY, USA, pp. 1-19.

Joughin, I., Alley, R. B., and Holland, D. M. (2012). "Ice-Sheet Response to Oceanic Forcing." *Science*, 338:1172-1176.

Kemp, A. C., Horton, B. P., Donnelly, J. P., Mann, M. E., Vermeer, M., and Rahmstorf, S. (2011). "Climate related sea-level variations over the past two millennia." *Proceedings of the National Academy of Sciences*, 108 (27): 11017–11022.

Levitus, S., Antonov, J. I., Boyer, T. P., Baranova, O. K., Garcia, H. E., Locarnini, R. A., Mishonov, A. V., Reagan, J. R., Seidov, D., Yarosh, E. S., and Zweng, M. M. (2012). "World ocean heat content and thermosteric sea level change (0–2000 m), 1955–2010." *Geophysical Research Letters*, 39, L10603.

Lins, H. F. and Cohn, T. A. (2011). "Stationarity: Wanted Dead or Alive?" *Journal of the American Water Resources Association*, 47(3):475-480.

Mallick, R. B., Radzicki, M. J., Daniel, J. S., and Jacobs, J. M. (2014). "Use of System Dynamics to Understand the Long Term Impact of Climate Change on Pavement Performance and Maintenance Cost." Paper submitted for consideration for presentation at the *2014 Annual Meeting of the Transportation Research Board (TRB) and Publication in the TRB Research Record: Journal of Transportation Research Board.*

Meagher, W., Daniel, J. S., Jacobs, J., and Linder, E. (2012). "A Methodology to Evaluate the Implications of Climate Change on the Design and Performance of Flexible Pavements" *Transportation Research Record*, Vol. 2305/ 111-120.

Mills, B., Tighe, S., Andrey, J., Smith, J., and Huen, K. (2009). "Climate Change Implications for Flexible Pavement Design and Performance in Southern Canada." *Journal of Transportation Engineering*-ASCE 135(10): 773-782.

Milly, P. C. D., Betancourt, J., Falkenmark, M., Hirsch, R. M., Kundzewicz, Z. W., Lettenmaier, D. P., and Stouffer, R. J. (2008). "Stationarity is dead: whither water management?" *Science,* 319: 573-574.

Sallenger, A. H., Doran, K. S., and Howd, P. A, (2012). "Hotspot of accelerated sea-level rise on the Atlantic coast of North America." *Nature Climate Change*, 2: 884–888.

Shaw, S.B. and Riha, S. J. (2011). "Assessing possible changes in flood frequency due to climate change in mid-sized watersheds in New York State, USA." *Hydrological Processes* 25(16): 2542-2550.

Smith, J. A., Villarini, G., and Baeck, M. L. (2011). "Mixture Distributions and the Hydroclimatology of Extreme Rainfall and Flooding in the Eastern United States." *J. Hydrometeorology*, 12: 294-309.

Transportation Research Board. (2009). "A Transportation Research Program for Mitigating and Adapting to Climate Change and Conserving Energy." *Special Report 299*. Washington, D.C.

Truax, D., Heitzman, M., Takle, G., Herzmann, D., and Timm, D. (2011). "Developing MEPDG Climate Data Input Files for Mississippi." *Final Report FHWA/ME-DOT-RD-11-232*.

USCGRP [Karl, T. R., Melillo, J. M., and Peterson, T.C. (eds.)] (2009). *Global Climate Change Impacts in the United States*. Cambridge University Press, available online at www.globalchange.gov/usimpacts.

Test and Analysis of Vibration Characteristic for Asphalt Pavement Energy Harvesting

Hongduo Zhao[1], Luyao Qin[2], Yinghui Liang[3]

[1]Professor, Key Laboratory of Road and Traffic Engineering of Ministry of Education, Tongji University, Shanghai 201804 China; hdzhao@tongji.edu.cn

[2]Master, Key Laboratory of Road and Traffic Engineering of Ministry of Education, Tongji University, Shanghai 201804 China; luyao1215@vip.qq.com

[3]Master, Key Laboratory of Road and Traffic Engineering of Ministry of Education, Tongji University, Shanghai 201804 China; liangliangasi@163.com

ABSTRACT: The purpose of this paper is to explore the vibration characteristic of asphalt pavement with various structures for harvesting mechanical energy via finite element analysis (FEA) and analytic model. Part of energies in asphalt pavement caused by mechanical vibration can be harvested by piezoelectric transducers. In order to get more energy from pavement, the sensitivity of structure parameters such as thickness, modulus, mass and stiffness are analyzed by using semi-rigid asphalt pavement as an example. Finite element model and analytic model are established in the analysis, which are calibrated by field measurement and laboratory test. The results show that the vibration frequency of typical semi-rigid asphalt pavement is between 10Hz and 20Hz, which is far lower than frequency of typical piezoelectric transducers. The fundamental frequency of asphalt pavement decreases with increasing thickness and mass of surface, base and subbase. However, the fundamental frequency is increase with the modulus and stiffness of subgrade, the increment is about 23Hz/10MPa and $0.7Hz/10^6(N/m)$.

INTRODUCTION

Piezoelectric technology is the most potential technology for harvesting mechanical energies from asphalt pavement because its ability to convert stress into electricity. The use of piezoelectric materials to capitalize on ambient vibrations surrounding a system is one method for energy harvesting. Bimorph, Unimorph, PVDF (Polyvinylidene fluoride) and MFC (Macro Fiber Composite) based cantilevers are typical piezoelectric transducers that used to harvest the vibration energy (Roundy 2003 and Galhardi 2008). The cantilevers are designed to work at resonance state driven by the ambient vibration. In order to harvest more energy from asphalt pavement, the vibration characteristic should be

analyzed at pavement environment.

Current vibration characteristic of asphalt pavement research shows that the value of vibration frequency cause by vehicle load is about 4-80Hz and the rang of acceleration speed is about $0.005m/s^2$-$2m/s^2$ (Rainer et al. 1994). Some factors such as vehicle type, vehicle speed and road surface condition were analyzed through field test and simulation model. Toshikazu proposed that dynamic vehicle loading has a great effect on vibration and the stiffness of pavement structure is the main factor (Hanazato 1991). However, there is little research work at the influence of different pavement structures on vibration characteristic for energy harvesting.

This paper is aiming at discussing the vibration characteristic of asphalt pavement with various structures for harvesting mechanical energy via finite element analysis (FEA) and analytic model. Field measurement and laboratory test are used to prove the consistency of the finite element (FE) model and analytic model. At the same time, the fundamental frequency related to the thickness, modulus, mass and stiffness is presented.

VIBRATION TEST

Field Measurement

The measurement site is Caoan Highway near Anhong Road in Shanghai, which is 8-lanes double-way with asphalt pavement. The structure parameters of Caoan Highway are showed in Table 1.

Table 1. Structure Parameters of Caoan Highway

Structure layers	Thickness (cm)	Density (Kg/m^3)	Modulus (MPa)	Poisson's ratio
Wearing course	4	2400	1600	0.25
Binder course	6	2400	1200	0.25
	8	2400	1000	0.25
Base	35	2000	1500	0.25
Subbase	20	1800	550	0.30
Subgrade	--	1800	20	0.35

Accelerometer was used in this vibration test, which was made by Beijing Shenzhou Xiangyu Company. Its measuring range is between 0.35Hz~4000Hz and resolution is 0.00004g. In the experiment, Accelerometer was stuck on pavement to gather the vibration information. When the moving vehicles passed by, the voltage signal would be converted into vibration acceleration signal by modem, then those vibration acceleration signal was stored in software DASYLab9.0 to analyze frequency. All the test data showed that the vibration frequency of Caoan Highway structure is about 15Hz. Typical vibration frequency is showed as FIG. 1, when a truck passed on the curb lane.

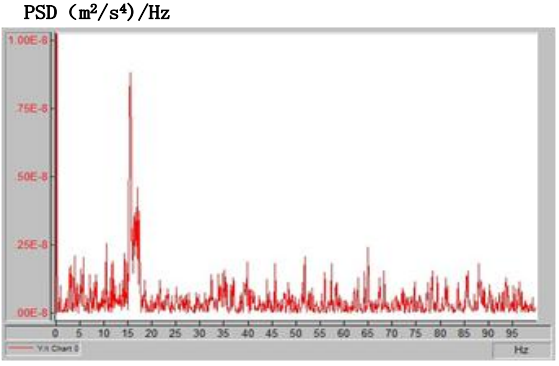

Frequency (Hz)

FIG. 1. Vibration frequency of Caoan Highway pavement structure

Laboratory Test

Handheld Falling Weight Deflectometer is used as excitation in laboratory test. This equipment uses a weight about 10kg that is lifted by hand to a given height and then is dropped, which impacts a transient load on the pavement surface. The parameter of pavement structure in laboratory is showed as Table 2.

Table 2. Parameters of Pavement Structure in Laboratory

Structure layers	Thickness (cm)	Density (Kg/m^3)	Modulus (MPa)	Poisson's ratio
Wearing course	4	2400	1800	0.25
Binder course	5	2400	1600	0.25
	8	2400	1500	0.25
Base	40	2000	1500	0.25
Subbase	30	1800	300	0.30
Subgrade	200	1900	30	0.35

In laboratory test, the method of data collection and analysis is the same as field measurement. All the test data showed that the vibration frequency of road structure in laboratory is between 15Hz and 20Hz. FIG. 2 shows the vibration frequency of asphalt pavement in laboratory under the impact load. Compared with FIG. 1 and FIG. 2 shows more vibration peaks because the Handheld Falling Weight Deflectometer repetitive impacts to pavement in the process of bounce.

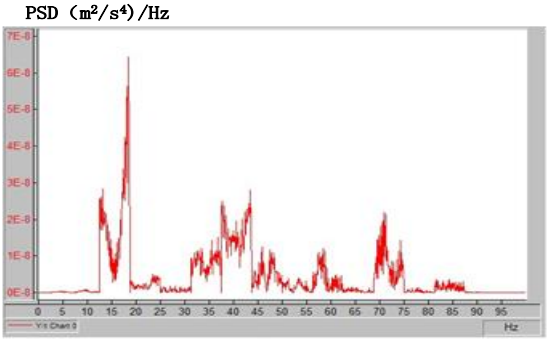

Frequency (Hz)

FIG. 2. Vibration frequency of Road structure in laboratory

FINITE ELEMENT ANALYSIS

FE Model and Parameters

Dae-Wook Park (2004) advised the longitudinal and lateral value should not be less than 3m in X-Y plane. In order to meet the size and meshing requirements, the model with 3m×3m of plane size and 2m of subgrade thickness was analyzed in this paper.

In FE model, elastic material properties are used for asphalt pavement. Considering the material properties and the deformation of each layer, the constraint between two layers are set as "tie" and the layer interface is continuity condition. As for the boundary condition of the model, top surface is no constraints; displacement in X-Y direction and torque around the Z axis are limited on the lateral (U_x=U_y=0, UR_z=0); subface is fully constraints (U_x=U_y=U_z=0, UR_x=UR_y=UR_z=0). By using C3D8 element type, the FE model is meshing to15cm of size in X-Y direction. Base course and subbase divided into three layers, subgrade would be divided into fifteen layers and the surface divided layers depend on the particular case.

Validation of FE Model

In order to observe the change trend of frequency, the degree of linear frequency step is set as 10. FEA shows that the Caoan Highway with fundamental frequency of 13Hz and 2~10 degree natural frequency of 13.9Hz error is 7.3%; The road in laboratory with fundamental frequency of 17.1Hz and 2~10 degree natural frequency of 8.5Hz error is 7.5%.

It can be summarized that the difference between the model and measured data is within 7.5%. In normal conditions, the frequency caused resonance is not only a specify value, but a range of frequency when the damping coefficient is small (Wu 1987). This range is about 0.8f~1.1f. By comparing, it can be found that the difference between the model and measured data is reasonable.

Parameter Sensitivity

By using semi-rigid asphalt pavement as an example, the sensitivity of subgrade and pavement structure parameters are analyzed in this paper. The semi-rigid asphalt pavement structure parameters are showed as Table 3. FEA shows that the fundamental frequency of this pavement structure is 12.6Hz and the 2~10 degree frequency is 12.9Hz.

Table 3. Parameters of Semi-rigid Asphalt Pavement Structure

Structure layers	Thickness (cm)	Density (Kg/m^3)	Modulus (MPa)	Poisson's ratio
Surface	15	2400	1200	0.25
Base	30	2000	1500	0.25
Subbase	15	1800	200	0.30
Subgrade	200	1800	20	0.35

FIG. 3 and FIG. 4 show that the fundamental frequency with various thickness and modulus of surface and base. It can be concluded that the fundamental frequency decrease with increasing thickness of surface and base. But it does not change with the increasing modulus of surface and base. In addition, the surface and base with various thicknesses and modulus have no influence on the 2~10 degree frequency.

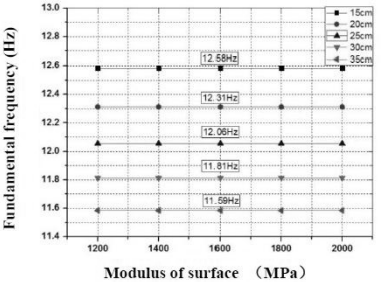

FIG. 3. Sensitivity of surface thickness and modulus

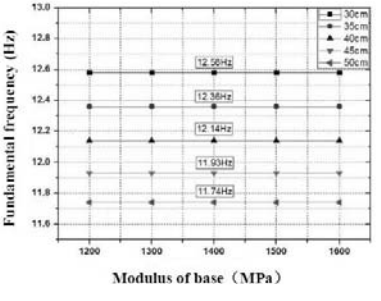

FIG. 4. Sensitivity of base thickness and modulus

In this method, it can be founded that the fundamental frequency decreases with increasing thickness of subbase and increase slightly with increasing modulus of subbase. However, the subbase with various thicknesses and modulus has no influence on the 2~10 degree frequency. In addition, the fundamental and the 2~10 degree frequency are increase with subgrade modulus and the increment is about 23Hz/10MPa. However, the increment of the fundamental frequency and the 2~10 degree frequency is reduced as the modulus increasing.

FREQUENCY ANALYTIC MODEL

Model and Parameters

In road engineering, the modulus of surface, base and subbase is different from the subgrade. Thus, they are divided and simplified to two distinct parts, which composed the two-mass equivalent model. According to vibration characteristic, this model is assumed to be a two degree of freedom system (see FIG. 5).

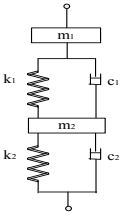

FIG. 5. Two degree of freedom system

Where, c_1 is damping of surface, base and subbase; c_2 is the damping of subgrade; k_1 is the stiffness of surface, base and subbase; k_2 is the stiffness of subgrade; m_1 is the mass of surface, base and subbase; m_2 is the mass of subgrade.

The damping coefficient can be ignored in modeling, because the materials compose the surface, base, subbase and subgrade is low damping. Thus, the differential equation of motion for two-mass equivalent model can be described as Eq.(1).

$$[M]\{\ddot{x}\}+[K]\{x\}=\{0\} \tag{1}$$

Where, K is the stiffness; M is the mass; x is the displacement; $\ddot{x}$ is the accelerated velocity.

The size of model should be determined firstly because it can influence the mass and stiffness. Research shows, the vertical displacement is smaller and later flattens when the vertical depth is greater than 3m; the vertical dynamic stress is relatively small when the distance away from the surface is greater than 1.75m (Wu 2010). Combined with finite element analysis on the model size, the thickness of the model at 3m is decided as the reasonable thickness. For the level scope, the model plane size of 3.8m×2m can be calculated through a load influence area calculation equation proposed by Schwartz (2002).

In the calculation process, the spring and damping are weightless and used to present the properties of the pavement structure. Thus, the model mass is the mass of pavement structure under the selected size. Due to this paper only focuses on the vibration characteristic of surface under the vertical load, it can be assumed that the subgrade reaction is uniform distribution. Consequently, the vertical displacement and stiffness of bottom center can be described as Eqs.(2) and (3).

$$K_{\upsilon} = \frac{\pi aE}{2(1-\upsilon)(1+\upsilon)} \tag{2}$$

$$\delta_z = \frac{2P(1-\upsilon)(1+\upsilon)}{\pi aE} \tag{3}$$

Where, a is the radius of load area; E is the resilient modulus; K_v is the stiffness of bottom center; P is the external load; v is the Poisson's ratio; δ_z is the vertical displacement of bottom center.

In order to reduce the error, the weighted average of each material Poisson's ratio would be used in the equations. And the equivalent resilient modulus of each part would be obtained by the modulus equations (JTG D50-2006). By using the equivalent resilient modulus, the equivalent stiffness also can be obtained in Eq.(2).

Validation of Analytic Model

Base on the mass and equivalent stiffness, the system equation of motion is calculated by Eq.(1).

$$\{x\} = \begin{Bmatrix} X_1 \\ X_2 \end{Bmatrix} = C_1 \begin{Bmatrix} 1 \\ r_1 \end{Bmatrix} \sin(w_1 t + \varphi_1) + C_2 \begin{Bmatrix} 1 \\ r_2 \end{Bmatrix} \sin(w_2 t + \varphi_2) \tag{4}$$

$$r_1 = \frac{X_2^{(1)}}{X_1^{(1)}} = -\frac{(k_1 + k_2) - m_1 w_1^2}{-k_1} \tag{5}$$

$$r_2 = \frac{X_2^{(2)}}{X_1^{(2)}} = -\frac{(k_1 + k_2) - m_1 w_2^2}{-k_1} \tag{6}$$

$$w_i^2 = \frac{k_i}{m_i} \tag{7}$$

$$f = \frac{1}{2\pi}\sqrt{\frac{k}{m}} \tag{8}$$

Where, f is the frequency; k_1 is the equivalent stiffness of surface, base and subbase; k_2 is the stiffness of subgrade; m_1 is the mass of surface, base and subbase; m_2 is the mass of subgrade; r_1 is the amplitude ratio base on w_1; r_2 is the amplitude ratio base on w_2.

According to the parameters of pavement structure, the frequency and displacement can be calculated by Eqs.(4)-(8). Comparing with FEA and Bisar, the results are listed in Table 4. It can be found that the error of frequency and displacement from analytic model is within 10%. Thus, this frequency analytic model is reliable.

Table 4. Results of Frequency and Displacement

	Frequency(Hz)			Displacement(m)		
Pavement types	**FEA**	**Analytic model**	**Error**	**BISAR**	**Analytic model**	**Error**
Typical structure	12.6	13.5	6.7%	4.77×10^{-4}	4.32×10^{-4}	9.4%
Caoan Highway	13.0	14.2	8.5%	3.76×10^{-4}	3.72×10^{-4}	8.5%
Pavement in laboratory	17.1	18.6	8.1%	2.70×10^{-4}	2.67×10^{-4}	9.9%

Parameter Sensitivity

The semi-rigid asphalt pavement structure with various mass and stiffness are calculated by the model, and the trends of fundamental frequency are showed as FIG. 6 ~ FIG. 9. As show in FIG. 6 and FIG.7, the fundamental frequency decrease with increasing m_1 and m_2 and the influence effect of m_1 and m_2 is nearly the same. The curves in FIG. 8 and FIG. 9 show that the fundamental frequency increase with k_1 and k_2. The increment of k_2 is about 0.7Hz/10^6(N/m) and the increment of k_1 is about 0.1Hz/10^7(N/m). The increment of k_2 greater than k_1, which is consistent with the FEA.

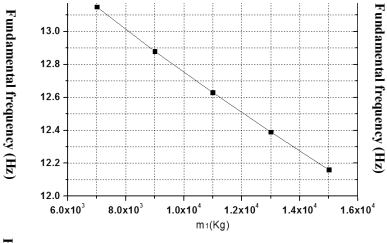

FIG. 6. Sensitivity of m_1

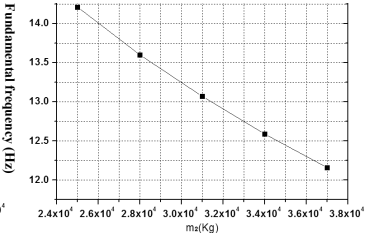

FIG. 7. Sensitivity of m_2

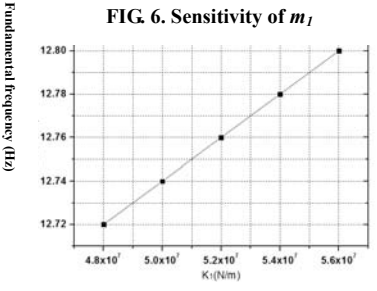

FIG.8. Sensitivity of k_1

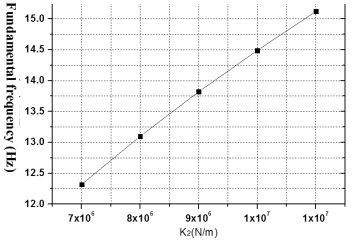

FIG. 9. Sensitivity of k_2

DISCUSSION

Bimorph, Unimorph, THUNDER or MFC based cantilever are widely accepted to harvest the energy from the ambient vibration (Roundy 2005). By using the effect of piezoelectricity, the transducer can transform the mechanical vibration into electric charge. In theory, the maximum energy would be generated when the ambient vibration frequency is close to the frequency of transducer. The natural frequency of those piezoelectric transducers is more than 100Hz. However, the frequency of asphalt pavement from the moving vehicle load is 10-20Hz. It means that the energy transmission ability is great limited when those piezoelectric transducers are embedded in asphalt pavement.

Even the piezoelectric transducers are unsuited to asphalt pavement, the above analysis can provide the basal theory to find a combination of pavement structure to satisfy those piezoelectric transducers or design a new piezoelectric transducer for pavement environment.

CONCLUSIONS

This paper analyzed the vibration characteristic of asphalt pavement with various structures for harvesting mechanical energy. FE model and analytic model are used in the analysis, which are proved by field measurement and laboratory test. At the same time, the sensitivity of the thickness, modulus, mass and stiffness is presented. Base on the test and analysis presented in this paper, the following conclusions are made:

(1) The vibration frequency of Caoan Highway structure is about 15Hz. The vibration frequency of road structure in laboratory is between 15Hz and 20Hz. Combine with FEA and analytic model analysis, it can be concluded that the vibration frequency of typical semi-rigid asphalt pavement is between 10Hz and 20Hz.

(2) The difference between the FEA results and test is within 7.5%, which is reliable in the permitted range of frequency (0.8f~1.1f).

(3) The FEA results of parameter sensitivity shows that the fundamental frequency decreases with increasing thickness of surface, base and subbase, however it does not change with the modulus of surface, base and subbase. In addition, the surface, base and subbase with various thicknesses and modulus have no influence on the 2~10 degree frequency. In the case of subgrade, the fundamental frequency and 2~10 degree frequency are increase with the modulus and the increment is about 23Hz/10MPa.

(4) Comparing to the results from FEA and BISAR, the error of frequency and displacement from the analytic model is within 10%. It can be found that the two-mass equivalent model can meet the requirement of precision.

(5) By using the analytic model, the sensitivity of mass and stiffness are analyzed. The results show that the fundamental frequency decreases with increasing m_1 and m_2 but increase with k_1 and k_2. The increment of k_2 is about $0.7\text{Hz}/10^6(\text{N/m})$, which is greater than k_1.

ACKNOWLEDGEMENTS

This paper is support by the National High Technology Research and

Development (863 program) of China under Grant 2012AA112505, Science and Technology Commission of Shanghai Municipality Project under Grant 11231201800 and National Natural Science Foundation of China Project No.50908177.

REFERENCES

Galhardi, M. A., Guilherme, T. H., and Junior, V. L. (2008). "Dynamics, Control and Application. " *FCT-Unesp at Presidente Prudente*, *Proc. 7th conf*. SP, Brazil.

Hanazato, T., Ugai, K., Mori, M., and Sakaguchi, R. I. (1991). "Three-dimensional Analysis of Traffic induced Ground Vibrations." *Journal of geotechnical engineering*, vol. 117(8): 1133-1151.

Industry standard of PRC.(2006). *Specifications for Design of Highway Asphalt Pavement* (JTG D50-2006). Ministry of Communications of PRC.

Park, D. W. (2004). "Characterization of Permanent Deformation in Asphalt Concrete Using a Laboratory Prediction Method and an Elastic-Viscoplastic Model." *PhD Thesis*, Texas: A&M University.

Rainer, O, Hunaidi, J. H., and Pernica, G. (1994). "Measurement and analysis of traffic-induced vibrations." *Second International Symposium - Transport Noise and Vibration*, St. Petersburg, Russia, October 4-6: 103-108.

Roundy, S. J. (2003). "Energy scavenging for wireless sensor nodes with a focus on vibration to electricity conversion." *A dissertation* submitted in partial satisfaction of the requirements for the degree of Doctor of Philosophy in Engineering-Mechanical Engineering in graduate division of the University of California, Berkeley, California.

Roundy, S. J. (2005). "On the effectiveness of vibration-based energy harvesting." *J. Intel. Mat. Syst. Str*., 16(10): 809-823.

Schwartz, C. W.(2002). "Effect of Stress-Dependent Base Layer on the Superposition of Flexible Pavement Solutions." *The International Journal of Geomechanics*. Vol. 2, No. 3, ASCE, Reston/VA: 311-352.

Wu, F. G. Cai, C. W.(1987). *Vibration Theory*. Beijing Higher Education Press. Beijing: 26-28.

Wu, Z. H.(2010). "The Study about Road Friendliness Characteristic Basing on Vehicle-Road Coupled System." *Master Degree Thesis*, Chongqing Jiaotong University.

Damage Types and Countermeasures of Highway Lifeline of Yunnan Earthquake in China

Benmin Liu[1], Donglana Su[2], Zhongyin Guo[3]

[1]Associate professor , The Key Laboratory of Road and Traffic Engineering of the Ministry of Education, School of Transportation Engineering, Tongji University, NO. 4800 Cao'an Road, Shanghai, 201804, P. R. China, liubenming@tongji.edu.cn
[2]Ph.D student, The Key Laboratory of Road and Traffic Engineering of the Ministry of Education, School of Transportation Engineering, Tongji University, Building 2, Box 208, NO. 4800 Cao'an Road, Shanghai, 201804, P. R. China, 2011sudonglan@tongji.edu.cn
[3]Professor, The Key Laboratory of Road and Traffic Engineering of the Ministry of Education, School of Transportation Engineering, Tongji University, NO. 4800 Cao'an Road, Shanghai, 201804, P. R. China, zhongyin@tongji.edu.cn

ABSTRACT: This paper investigated highway damage caused by the earthquake recently occurred in Yunnan province of China. The damage types of highway lifelines in the earthquake were analyzed. The influence factors to highway damage in the earthquake were summarized, which mainly included geological hydrological and meteorological conditions and road conditions. Based on the analysis results, the highway lifeline damage classifications standard in earthquakes was proposed. Several emergency countermeasures of highway damage caused by earthquakes were also recommended, including the emergency traffic management, comprehensive traffic connection and emergency management plan. The research results of this paper provided reference for the damage analysis and emergency management of highway damage in earthquakes, improved the emergency response and rescue speed, and reduced casualties and property losses.

INTRODUCTION

Earthquakes have significant impact on traffic and transportation which have great influence on the rescue after the earthquake. It is of great importance to investigate the highway damage caused by earthquakes and to develop effective countermeasures for the emergency rescue. Yunnan province of China locates on the east side of Indian Ocean plate and the Eurasian plate collision (subduction) zone. Due to the geological structure complex, nontectonic movement and the modern tectonic activity are strong, and earthquakes happen frequently. 4.1% of the land area of the country releases 20% of the total earthquake energy. The biggest earthquake recorded had a magnitude of 8. In recent 100 years destructive earthquakes above magnitude 5 total 383 times in recent 100 years, more than magnitude 7 earthquake is 10 group 13

times. For the frequency of earthquakes, magnitude 5 to 5.9 earthquakes happened 3 times per year on average, magnitude 6 to 6.9 earthquakes occurred once every 2 years on average, and magnitude 7 to 7.9 earthquake occurred once every 8 years.

Wang et al. (1988) analyzed more than 100 destructive earthquakes occurred in Yunnan, and summarized the characteristics of those as follows:

- The casualties were high and the distributions were relatively concentrated.
- The seismic performances of buildings were poor.
- The seismic landslide, collapse and debris flow were very common.
- The floods caused by earthquake were all over the province.
- The fire caused by earthquake could not be ignored.
- Earthquakes usually caused interruption of the traffic.

According to the seismic network in Yunnan province, Yunnan province and the surrounding area (20ºto 30ºN , 96ºto107ºE) have had 5007 earthquakes, which can be classified as ML1.0 magnitude in 2012 as shown in FIG. 1.

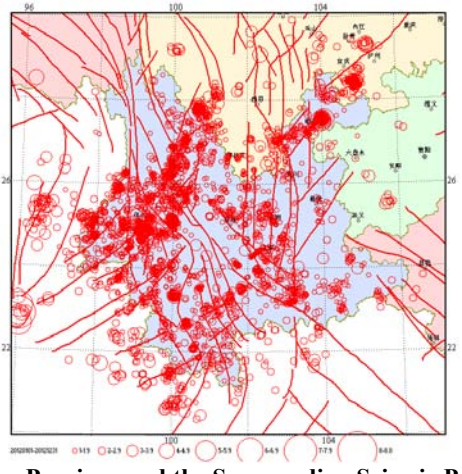

FIG. 1. Yunnan Province and the Surrounding Seismic Profiles in 2012

Some scholars investigated the earthquakes in Yunnan and had attained some valuable findings. Ren and Cao (2011) collected earthquake data from 1831 BC to 1980 AD, and discussed the time and location characteristics of earthquakes and their influences based on the Geographic Information System (GIS) technology. In Yunnan province, the earthquakes with low intensity also have great influences on the transportation systems, due to the reasons that Yunnan province is in the Pleistoseismic zone, and it has complex geographical environments with more mountains.

FAILURE MODELS OF HIGHWAY DAMAGE IN EARTHQUAKE

Based on the literature review, the failure models of highways due to earthquakes can be summarized as follows:

Subgrade and Pavement

The subgrade and pavement suffer various damages, including embankment sliding, subgrade sliding, subsidence, subgrade uplift, extrusion, collapses and landslides, waterlogging of lake inundated roads, roadbed failure caused by falling rocks, retaining structures failure.

Bridge

The bridge damage models include beam falling, block damage, horizontal and vertical displacement of the upper structure, bearing and telescopic device damage, bridge pier shift, concrete piers crushing, collar beam crack, retaining wall damage, pier uplift or subsidence, bridge abutment conical slope system damage (displacement of retaining wall damaged or collapsed, after packing), the whole bridge collapse or direct damage, buried by landslides, rock breaking, lake flooding and other secondary disasters.

Tunnel

Huang et al. (2010) summarized the tunnel damage models:

- Lining shear displacement. This damage often happen when the tunnel is built on fault fracture belt.
- Tunnel structure damage caused by slope failure.
- Lining damage. Because the linings are rigid supporting and the bending shear capacity is low, it is prone to crack in the earthquake damage, which may lead to the lining of landslides in high intensity area.
- Sidewall damage.
- Tunnel collapse caused by the tunnel landslide.

INFLUENCE FACTORS OF HIGHWAY DAMAGE IN EARTHQUAKE

The seismic damages to highway system mainly include road, bridge and tunnel structure damage. To prevent the various types of damage and develop countermeasures, it is necessary to analyze the influence factors of highway damage in earthquake. Generally, the influence factors of highway traffic lifeline damage include focal depth, distance to epicenter, road grade, and geological geomorphology condition.

Earthquake Magnitude

Earthquake magnitude is determined according to the seismograph records of wave amplitude, usually measured by the Richter scale. The Magnitude (M) is determined according to the log of maximum wave amplitude, recorded by the standard seismograph about 100 km from the epicenter. Earthquake magnitude is the main index to reflect earthquake intensity. There is a direct relation between earthquake

magnitude and road damage. Thus, the earthquake magnitude is the first factor affecting highway lifeline damage.

Focal Depth

The origin of seismic place is called its focus. The vertical projection of the focus on the ground is called the epicenter. It is the earliest parts to accept vibration. The depth of focus to epicenter called focal depth. Focal depth is one of the factors affecting the earthquake size, and is the second influence factors of highway lifeline damage. According to the focal depth, the earthquake can be divided into shallow-focus earthquake, intermediate-focus earthquake and Palintectic earthquake:

- Shallow-focus earthquake has a focal depth of 0~60 km. Shallow-focus earthquake threatened structures mostly. At the same earthquake magnitude, the smaller focal depth, the greater the destructive power.
- Intermediate-focus earthquake has a focal depth of 60~300 km.
- Palintectic earthquake has a focal depth greater than 300km. Currently, the deepest observable earthquake is 720 kilometers.

For earthquakes of same magnitude, because of the different focal depth, the degree of ground damage is different. The smaller focal depth, the greater damage, but the smaller affected scope.

Distance to Epicenter

Distance to epicenter is the linear distance between any ground point and the epicenter. For the same magnitude earthquake, the smaller distance to epicenter, the heavier damage. The distance to epicenter determines the impact strength of the earthquake. With the increase of the distance to epicenter, the damage caused by earthquake reduces gradually. According to the distance to epicenter; the earthquake can be divided into three kinds:

- Local shock: the distance to epicenter is less than 100 km.
- Near earthquake: the distance to epicenter is between 100~1000 km.
- Distant earthquake: the distance to epicenter is greater than 1000km.

Highway Grade

Highway grade is divided based on road usage, function and traffic flow. In China, highways can be divided into the expressway, first class roads, second class roads, third class roads and fourth class roads. The grade and quality of highway construction is directly related to the post-diaster damage. Under the same earthquake situation, the susceptible highway would be easy to be damaged seriously. Although the shock-resistance and robustness of highway is difficult to evaluate by any standard, a certain highway grade represents a certain level of road construction. Higher road grade means higher shock-resistance and robustness. Therefore, road grade is a comprehensive index reflecting earthquake resistance of highway.

Hydrogeology Condition

Hydrogeology refers to the natural phenomenon of various kinds of change and movement of groundwater. Geological and hydrological condition is an important factor which closely relates to a regional groundwater, and geothermal, earthquakes, geological environment, and etc. It may influence the potential flood and thus also have significant influence on the earthquake caused highway damage.

CLASSIFICATION OF HIGHWAY DAMAGE IN EARTHQUAKE

The emergency traffic guide, comprehensive connection, rescue work post-earthquake are determined by the degree of highway damage in earthquake and. Therefore, in order to facilitate disaster emergency management, it is necessary to investigate the highway damage in earthquake.

Classification Basis

Roads, Bridges and tunnels in earthquake will appear many kinds and different degrees of damage which affect the connectivity of highway lifeline network. When the earthquake strikes, different earthquake magnitude, focal depth and distance to epicenter may cause different damage to the highway lifeline. In addition, different grades of highway may experience different levels of damage in the same disaster zone. However, at present, there is little research on the relationship between highway lifeline damage and earthquake magnitude, focal depth, distance from the epicenter, road grade, etc. Based on the influence of different factors, the highway damage level can be established

Classification Standard

By analyzing the relationship between highway damage and earthquake magnitude, focal depth, distance to epicenter, highway grade and hydrogeology condition, the highway lifeline damage in earthquake can be divided into three levels as shown in Table 1. This can provide basis for connecting reliability evaluation of highway lifeline, rescue path selection, comprehensive transportation connection and emergency preplan activation.

Table 1. Classification of Highway Damage in Earthquake

Highway damage level	Earthquake magnitude (M)	Focal depth (km)	Distance to epicenter (km)	Highway grade	Hydrogeology condition	Highway damage qualitative description
One-level	6.0~6.9	＜70	＜100	Low Grade Road	Brittle rocks, loose mountain, high underground water level	Severe damage, vehicle cannot pass, lifeline interrupt.
	≥7	≥300	≥1000	High Grade Road	Hard rocks, solid mountain, low underground water level	
	≥7	＜300	＜1000	Highway under class II	Relatively brittle rocks, relatively loose mountain, underground water upper average	
Two-level	6.0~6.9	≥70	≥100	Highway of class II and above class II	Relatively hard rock, relatively solid mountain, underground water level below average	Partly damage, only large rescue vehicles can pass.
		＜70	＜100	Highway of and above class II	Brittle rocks, loose mountain, high underground water level	
Three-level	5.0~5.9	≥70	≥100	Highway of and above class III	Relatively hard rock, relatively solid mountain, underground water level below average	almost no damage.
		＜70	＜100	Highway of and above class II	Brittle rocks, loose mountain, high underground water level	
		≥70	＜100	Low Grade Road	Brittle rocks, loose mountain, high underground water level	

Note: High grade road refers to the senior pavement, large traffic flow of road.
Low grade road refers to the poorer pavement, small traffic flow of road.

MANAGEMENT MEASURES

Emergency Traffic Management

Rescue should be conducted in earthquake areas immediately after the earthquake. Vehicles within the earthquake area need to be evacuated and the external aid needs transported to the earthquake area as quickly as possible. Emergency transportation after the earthquake needs effective guidance and management. Therefore, this paper recommended the traffic management countermeasures according to different degree and affect range of earthquakes, which aims to rationally utilize limited traffic facilities, and ensure that relief supplies reach earthquake areas fast.

Confirmation of the Influence Extent

Confirmation of the range of earthquake damage is the precondition for the implementation of emergency traffic management. In order to evacuate congestion traffic flow after the earthquake, avoid further deterioration of congestion, and determine rescue and aid strategy, it is significant to determine the damage area of the earthquake. Considering the damage of roads and other infrastructure in earthquake, influence extent is divided into four levels as shown in Table 2.

Table 2. Classification of seismic influence extents

Influence extent	Extent I	Extent II	Extent III	Extent IV
Characteristics of classification	Network destruction thoroughly, traffic paralysis.	Network destruction partly, it can repair in a short time.	Highway facilities damage partly, road network is complete.	Surrounding road network was not damage.

Determination of Evacuation Area

According to the classification of seismic influence extents, evacuation area can be determined by analyzing the influence of earthquake and land use. The evacuation area can be divided into mandatory evacuation area, voluntary evacuation area and safety area.

Emergency Traffic Organization

In order to reduce the effects of earthquake on the road network traffic flow, and ensure the safety of network operation, a variety of traffic control and management methods should be utilized to organize and manage emergency traffic. According to the level of action, the earthquake emergency traffic management strategies can be divided into: macroscopic emergency traffic management strategy and microcosmic emergency traffic management strategies.

Macro emergency traffic management strategy refers to the overall emergency traffic control strategy, which can be divided into the control strategy and regional evacuation closed control strategy. The main purpose of the former is to evacuate people from the affected areas to perimeter security area, and the latter is to control the vehicle into the affected areas. Micro emergency traffic management strategy includes seven major categories: lane management, vehicle traffic restrictions, traffic limit, shunt induced, the survival safeguard measures, engineering measures and other traffic management measures of emergency.

Comprehensive Traffic Connection

Earthquake is a devastating natural disaster, damaging roads and other infrastructure severely and paralyzing highway network. However, compared to the highway, waterway and air transport are less affected, which can be utilized in rescue. To improve the effectiveness of rescue, it is necessary to integrate highway, railway, water and air transport.

Connection between Aviation and Highway

The ground lifeline is not connected at the beginning of earthquake. In that state, air transport is the only mode of transportation. Yunnan province has 12 civil airports. As long as the linkage between the airports and highway network are established, a proper airport emergency strategy can be developed.

Railway and Highway

As the national economy aorta and lifeline, railway system plays an important role in the rescue of the Wenchuan earthquake. But the railway line in Yunnan province is weak. It does not form network and are located unreasonable due to the mountainous geography. Most of the railway lines are still under construction. In the railway network design, various modes of transportation have to be considered as an integral

body, including the railway and highway, aviation, water transportation and other transportation infrastructures.

Waterways and Highways connection

Since water transportation is of large transport capacity but low speed, it is mainly used in the later stage of the disaster relief work. In order to make full use of the comprehensive transportation system, the combination of highway and water, or railway and highway transportation can reduce the pressure on road transport. It is recommended to make full use of the water transportation system in Yunnan province to reach the earthquake area through the port connected with highways.

Utilization of Helicopters

Helicopter has the characteristics of flexible handle, no need for specific airport and runway, and it can land at many places such as land, water, ship, the roof. Therefore, it plays an important role in the disaster emergency rescue. But the number of helicopters in China is only 1/52 of the world's average level, and there is no heavy transport helicopter. In addition, the equipment of the helicopter airborne equipment is relatively backward and lack of airborne radar, forward looking infrared, anti-collision system, accurate navigation system, GPS, etc. Therefore, in the major natural disasters, the helicopter can't react quickly.

Emergency Management Plan

Many cities in China specialized GIS-based earthquake disaster reduction system (Li et al. 2007). Nanning City Emergency Response System is the first set of City Emergency Response System (Xie and Tao 2000). Shanghai set up municipal emergency command geographic information system (Lan 2008). Earthquake emergency management plan is important to make a timely and correct response after the earthquake. Based on the analysis of relevant research results, several recommendations on emergency management plan were proposed.

Prevention and Preparation Phase

- Monitoring and submit information: earthquake monitoring stations and networks at all levels conduct (including the volcano monitoring information) detection, transmission, analysis, processing, storage and submit seismic monitoring, group monitoring nets observed macro exception of earthquake and timely reported. Chinese earthquake networks center tracks earthquake situation.
- On the basis of short-term earthquake prediction, Chinese Seismological Bureau organizes tracking earthquake situation and develop the views of the impending earthquake prediction, report to the Government in predicted areas. The Government decides to release imminent earthquake prediction, announced the area into the impending earthquake emergency period.
- According to the earthquake situation and road structures along the seismic

capacity, release suspension notice, where necessary.
- Prepare for emergency relief supplies and distribute it to management and construction units along the highway.
- Arrangements for the practical implement, prepare for the preparatory work.
- The monitoring center should be strengthened with the meteorological department to establish long-term early warning mechanism.
- Highways departments strengthen field patrols.
- Highways department get linkage and coordination with highway traffic police department, establish an effective linkage mechanism with Highways traffic police.
- Improve the monitoring and forecasting of secondary disasters.

Emergency response phase

Emergency response refers to a system of activities when certain types of emergencies occur after the pre-set conditions. The pre-set corresponding measures must be taken once a specific level is reached. According to the affected severity and the affected area, the response of the emergency response phase is divided into three levels, including commanding an order, repair work of the damaged section, opening up rescue channel, releasing disasters and traffic guidance information, maintaining traffic order, traffic guidance, diversion, information reporting and etc.

Recovery Phase

The recovery phase generally includes four parts:
- Alert clear, clean up the scene and restore normal traffic order.
- Infrastructure rehabilitation.
- Emergency Summary.
- Event statistical analysis.

CONCLUSIONS

By investigating the highway damage caused by the earthquake, the highway damage types, influencing factors and countermeasures were analyzed and developed. The failure models of highway damage, including subgrade, pavement, bridge and tunnel, in the Yunnan earthquake were summarized through comprehensive survey. The influence factors of highway damage in earthquake included focal depth, distance to epicenter, road grade, and geological geomorphology condition. A damage classification standard was then proposed in this paper according to the earthquake states parameters, hydrogeology condition and highway condition. Recommendations were provided to help guide earthquake rescue of the earthquake.

ACKNOWLEDGEMENT

This research was supported by the Science-Technology Programs of Transportation Commission of Yunnan Province (Project No.:2011(B) 06-b) and

Social Development Science Programs of the Department of Science and Technology of Yunnan Province (Project No.:2012CA004), Yunnan Province, China.

REFERENCES

Chen, J. (2000). "Damage of bridge caused by earthquake in Yunnan." *Journal of Seismological Research*. 4, 436-443.

Huang, M., Liu, M., and Wang, A. (2010). "The research of tunnel earthquake damage forms and the reasons." *Technoligy & Economy in Areas of Communications*. 1, 60-62.

Lan, Y. (2008). "Plan Reasoning Research and Fuzzy Evaluation for City Traffic Emergency Management System." *Master's thesis*. Beijing Jiaotong University.

Li, P., Tao, X., and Yan, S. (2007). "3S-based quick evaluation of earthquake damage." *Journal of Natural Disasters*. 6, 109-113.

Ren, H., and Cao, X. (2011). "Spatial and temporal distributions and types of impacts of earthquake disasters on transportation from 1831 BC to 1980 AD in China." *Progress in Geography*. 7, 875-882.

Wang, D., Guo, X., and Sun, Z. (2009). "Damage to highway bridges during Wenchuan Earthquake." *Journal of Earthquake Engineering and Engineering Vibration*. 3, 84-94.

Wang, J. (1988). "Characteristics of earthquake hazard in Yunnan Area." *Journal of Seismological Research*. 9, 492-499.

Xie, L. and Tao, X. (2000). "A GIS based earthquake losses assessment and emergency response system for Daqing oilfield." *12th World Conference on earthquake engineering. Auckland*.

Analysis of Road Surface Heat Flux Based on Energy Balance Theory

Xiaoling Zou[1], Danny X. Xiao[2], A.M. ASCE and Boming Tang[3]

[1]Assistant professor, Chongqing Jiaotong University, No. 66 Xuefudadao, Nanan District, Chongqing, 400074, China; zouxiaoling2775@126.com
[2]Research associate, Louisiana Transportation Research Center, 4101 Gourrier Avenue, Baton Rouge, LA 70808, United States; xxiao@lsu.edu
[3]Professor and president, Chongqing Jiaotong University, No. 66 Xuefudadao, Nanan District, Chongqing, 400074, China; tbm@netease.com

ABSTRACT: Understanding the interaction between pavements and the ambient temperature is critical for mitigating urban heat islands. The objective of this paper is to investigate the variation of heat flux from different pavement materials based on a field experiment in Ningbo, China. One-year observation, including total surface solar radiation, reflective radiation and net total radiation, are analyzed. Quantitative variations of the heat flux are then determined using energy balance theory. Results show that the average daily heat flux (Q_d) of asphalt pavements is higher than that of concrete pavements. Seasonally, summer has a larger Q_d than spring has, and winter has the smallest Q_d. On average, the daily heat flux varies from 4 to 12 W/m^2. Weather condition influences heat flux. Ranking from the maximum to the minimum is clear days (11.8 W/m^2), cloudy days (7.9 W/m^2), and rainy days (4.2 W/m^2).

INTRODUCTION

The exchange of heat between road surface and the atmosphere is a key parameter of pavement temperature field (Tan et al. 2010). It also provides the surface boundary condition, a required input for numerical modeling (Huntingford et al. 1995; Vogel et al. 1995; Mihailovic and Ruml 1996). In recent years, severe summer-time heat islands have occurred in major urban-industrial regions and metropolitans all over the world. Besides the increase in energy consumption and heat generated by industry, business and transportation, numerous researches attribute urban warming to the decrease of bare soil and wooded areas and the increase of paved surface with asphalt or cement concrete (Asaeda et al. 1996). Doll (1983) showed that the urban climate was significantly influenced by the direct heating from heated pavement surface. While several studies (Tran et al. 2009; Boriboonsomsin and Reza 2007) were conducted to reduce urban heat island by using innovative pavement materials, very few researches have been undertaken to quantitatively analyze the variation of heat flux from different pavement surfaces. Knowledge of the heat flux is critical for

understanding how pavements influence the surrounding thermal environment.

The objective of this paper is to evaluate the variation of heat flux from different road surface materials with contrasting thermal properties. Since the temperature of urban or regional-scale areas is directly dependent upon land use and material properties, this study would provide useful information for simulating urban and regional mixed-layer dynamics in boundary-layer models.

EXPERIMENT DESIGN AND INSTRUMENTATION

The relationship between ppavement temperature field and surface energy was a part of a recent study conducted at Ningbo, China (Yao 2012). The site was located at east longitude 121º33', north latitude 29º47' and altitude 5 m. Four types of materials commonly found in urban and rural environment were included in the study: asphalt concrete (AC), Portland cement concrete (PCC), bare soil and grassy soil. Fig. 1 illustrates the instrumentation layout and pavement structures.

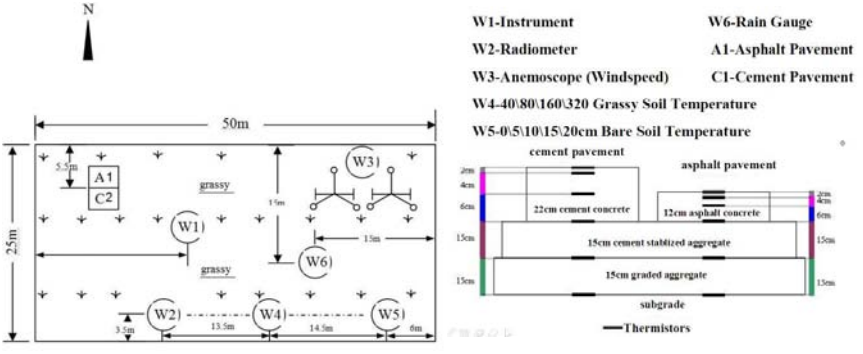

(a) **(b)**

FIG. 1. (a) Instrumentation layout, (b) pavement structure.

Radiation data were collected to measure albedo effects. Total radiation was measured with pyranometers (model DFY4 and model TBQ 2). Reflective radiation was measured using TRT-2 reflective pyranometers. Swissteco (model S-1) net pyranometers were used to measure the net radiation. All pyranometers were placed 1.2 m above the ground surface. Fig. 2 shows some of these instruments.

Ambient air temperatures were collected at 1.5 m above the surface. Surface temperature sensors were placed directly on the asphalt or concrete surface and covered with a thin layer of asphalt or cement mortar to achieve a good contact. Subsurface temperature measurements were obtained from a network of platinum thermocouple probes embedded in the pavement structure at various depths. To assure good contact between temperature probes and pavement materials, probes were first placed at the required level, and then repacked with road materials. Subsurface temperature measurements were obtained to a depth of 0.52 m beneath the concrete

pavement and 0.42 m beneath the asphalt pavement.

Other weather data such as wind speed and precipitation were also collected throughout the study period. All data were recorded at 10 minutes interval.

FIG. 2. Pyranometers: (a) field installation, (b) a pyranometer to measure total radiation, (c) a net pyranometer.

METHODOLOGY AND ASSUMPTIONS

The heat flux on concrete, asphalt and grass overlay materials is determined from the vertical component of the Fourier heat conduction equation:

$$\frac{dQ}{dt} = -\rho C \frac{dT}{dz} \tag{1}$$

where Q = road surface heat flux, W/m^2,
ρ = density, kg/m^3,
C = specific heat capacity, J /(kg·°C),
T = temperature, °C, and
z = depth (surface is at $z = 0$), m.

By integrating Eq. 1 from zero to a certain depth, with average values of ρ, C, and T at each interval, the heat flux Q can be determined. However, this method has to assume the composition and material parameters due to the difficulty in estimating the boundary condition and heat stored in a pavement. These assumptions may reduce the accuracy of this method.

In this study, the heat flux is determined using energy balance theory at the road surface, given by

$$Q = (1-\alpha) R_S + R_L + R_C + H + L_E \tag{2}$$

where R_s = total solar radiation (short-wave), W/m^2
a = albedo of road surface，
R_L = net radiation on road surface (long-wave), W/m^2
R_C = heat flux due to convection ,W/m^2
H = sensible heat flux, W/m^2, and
L_E = latent heat flux due to evaporation ,W/m^2.

Heat flux due to convection R_C is assumed to be proportional to wind speed as well as the difference between surface temperature and air temperature. It can be calculated from the following equation (Zhang et al. 2006):

$$R_C = Bc \times \Delta T \tag{3}$$

where ΔT = the difference between surface temperature and air temperature,
B_C = convectional coefficient, W/(m$^2\cdot$°C), given by

$$B_C = (9.55 + 3.5v + 0.035\Delta T) \tag{4}$$

where v = wind speed, m/s.

In order to isolate the consequence of heated ground from other effects, this study assumes a homogeneous flat pavement with full exposure to solar radiation. Sensible heat flux and latent heat flux due to evaporation are not considered.

In total, one-year observation from June 2009 to May 2010 with continuous records at 10 minutes interval is analyzed.

RESULTS ANLAYSIS

Monthly Variation

The one-year data is first averaged by month. The result is named monthly average road surface heat flux, Q_M, as listed in Table 1. Positive heat flux means that heat energy in the pavement increases (i.e., the pavement gains heat). On the contrary, negative heat flux means that heat energy in the pavement decreases (i.e., the pavement loses heat). It is found from Table 1 that asphalt pavements and concrete pavements have a similar process in term of Q_M: gaining heat in the summer and losing heat in the winter. Q_M changes from positive to negative in autumn (as road surface temperature decreases), and changes back in spring (as road surface temperature decreases). The positive maximum occurs in June and the negative

maximum happens in November.

Table 1. Monthly Average Road Surface Heat Flux, Q_M (W/m^2)

	Jun 2009	Jul 2009	Aug 2009	Sep 2009	Oct 2009	Nov 2009	Dec 2009	Jan 2010	Feb 2010	Mar 2010	Apr 2010	May 2010
AC	33	30	25	3	-4	-38	-28	-13	-6	7	16	30
PCC	17	8	4	-6	-10	-32	-20	-9	-7	-10	1	7

Slight difference is also observed. Asphalt pavements have a shorter "negative season" (five months, gray colored in Table 1) than concrete pavements do (seven months). This may be attributed to the difference of thermal conductivity and heat capacity between the two types of materials, as shown in Table 2. Comparing to AC, PCC has a larger thermal conductivity, a smaller heat capacity and a smaller absorptivity. This means that, in comparison to AC, PCC conducts heat faster while stores less heat energy and absorbs less energy from the sun.

Table 2. Thermal Properties of AC and PCC (ARA 2004)

	Thermal conductivity W/(m·°C)	Heat capacity J/(kg·°C)	Short wave absorptivity
AC	0.76~1.38	921.10~1674.72	Weathered AC (gray): 0.80-0.90 Fresh AC (black): 0.90-0.98
PCC	1.73~2.60	837.36~1172.30	0.70-0.90

Seasonal Variation

The average daily heat flux Q_d is determined using the one-year observed data. Since weather is an important factor affecting heat flux, only daily averages under the same weather condition are comparable. Fig. 3 presents the daily average on clear days.

A clear trend is found for Q_d: decreasing from summer to winter and increasing from winter to summer. In addition, asphalt pavements and concrete pavements present a similar seasonal trend.

But the magnitude of Q_d is different for the two types of pavement. The daily heat flux for asphalt pavements ranges from -49 to 95 W/m^2 with an average of 26 W/m^2, while the range for concrete pavements is between -47 and 69 W/m^2 with average at 14 W/m^2. Generally speaking, asphalt surface has a greater heat flux than concrete surface does. The main reason may due to the albedo. With a lower albedo, asphalt pavements could have a larger heat gain than concrete pavements have according to Eq. 2. The heat energy in asphalt pavements is later released to the air, creating a heat island.

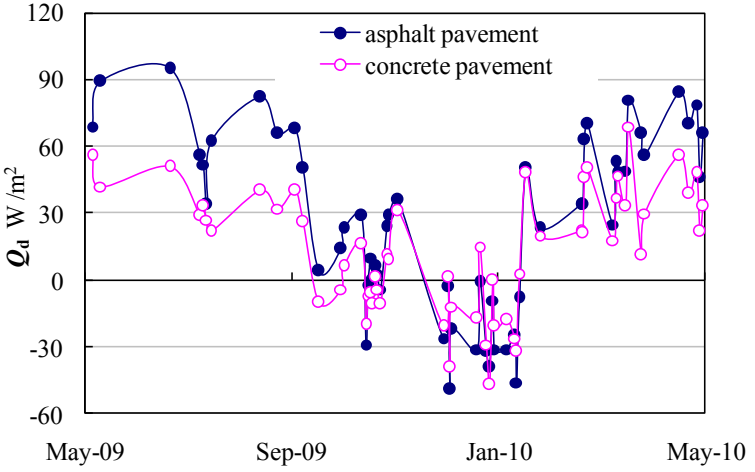

FIG. 3. Average daily heat flux Q_d on clear days.

Interestingly, one may also note in Fig. 3 that the heat flux between asphalt pavements and concrete pavements is very close to each other in autumn and spring. In other words, Q_d between the two becomes similar when the solar elevation and angle change.

Relationship between Heat Flux and Daily Temperature

It can be inferred from Eq. 1 that heat flux Q_d is proportional to the temperature gradient. But this relationship may not be linear and may depend on other parameters such as weather condition and material properties.

Starting from a linear model (Eq. 5), observed data in this study were analyzed.

$$Q_d = m + n \cdot T_g \tag{5}$$

where T_g = temperature gradient, °C/cm, and

m, n = regression coefficients.

It was found that coefficients m and n change with weather condition and daily temperature fluctuation ratio ξ. Fig. 4 shows the variation of regression coefficient m, n and correlation coefficient R for Eq. 5. It is clear that (1) as the fluctuation ratio ξ increases, the intercept m increases but the slope n decreases; (2) The ranking of dependence on weather condition is clear days > cloudy days > rainy days.

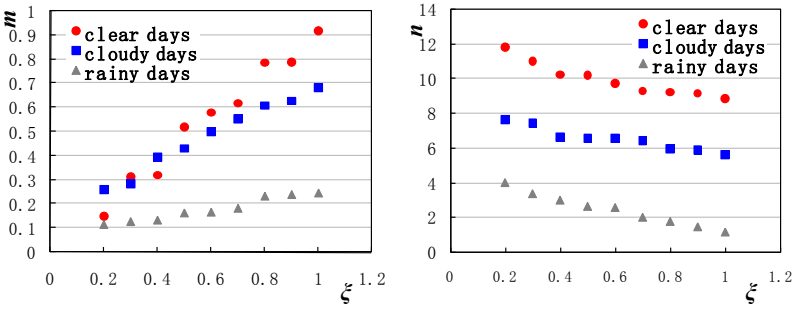

FIG. 4. Variation of regression coefficient *m* and *n* for Eq. 5.

Based on previous analyses, the quantitative relationship between heat flux Q_d and temperature gradient T_g can be given by

$$Q_d = (m_0 + m_1\xi) + (n_0 + n_1\xi)T_g \tag{6}$$

where $\xi = (T_{max}\text{-}T_{min})_{z=0}/(T_{max}\text{-}T_{min})_z$

m_0, m_1, n_0 and n_1 are regression coefficients.

Table 3 lists the regression coefficients for different weather conditions. If the temperature fluctuation ratio ξ is 0.1 and the temperature gradient T_g is a constant of 1°C/cm, the average heat flux Q_d is between 4 and 12 W/m^2. Clear days would have the maximum heat flux (11.8 W/m^2) while rainy days have the minimum (4.2 W/m^2), and cloudy days are in between (7.9 W/m^2). The effect of ξ on the Q_d is considerable.

Table 3. Regression Coefficients for Eq. 6

Weather condition	*m*			*n*		
	m_0	m_1	Relative error (%)	n_0	n_1	Relative error (%)
clear days	0.001	0.924	0.534	12.000	-3.412	0.745
cloudy days	0.150	0.553	0.276	7.974	-2.418	4.231
rainy days	0.071	0.177	0.503	4.435	-3.353	0.829

One application of the relationship between heat flux and daily temperature is to estimate the temperature gradient T_g. Eq. 6 can be written as

$$T_g = \frac{Q_d - (m_0 + m_1\xi)}{n_0 + n_1\xi} \tag{7}$$

where denotations are the same as aforementioned. For example, if the heat flux Q_d

and the temperature fluctuation ratio ξ for a clear day were determined to be 11.8 W/m^2 and 0.5, respectively, the temperature gradient T_g at the depth of 20cm in a pavement could be estimated as 1.10 ℃/cm.

$$T_g = \frac{11.8 - (0.001 + 0.924 \times 0.5)}{12.0 + (-3.412) \times 0.5} = 1.10 \tag{8}$$

CONCLUSIONS

Using energy balance theory, the variation of heat flux for different road surface types is analyzed based on one-year observation at Ningbo, China. Results show that the average daily heat flux Q_d of asphalt pavements is higher than that of concrete pavements. The largest heat flux occurs in summer and the weakest happens in winter. The average Q_d changes from 4 to 12 W/m^2 through a year. Clear days have a higher heat flux than cloudy days have and rainy days have the lowest.

ACKNOWLEDGEMENTS

This study was funded by the Chinese Postdoctoral Science Foundation, Zhejiang Province Department of Communications and the Chinese Government & Local United Engineering Laboratory of Transportation and Civil Engineering Materials at Chongqing Jiaotong University.

REFERENCES

ARA Inc., ERES Consultants Division, (2004). “Guide for mechanistic-empirical pavement design of new and rehabilitated pavement structures.” *Final Report*, *Part 2, Chapter 2*, Champaign, Illinois: 33-58.

Asaeda, T., Ca, V. T., and Wake, A. (1996). “Heat storage of pavement and its effect on the lower atmosphere.” *Atmospheric Environment*. 30 (3): 413-427.

Boriboonsomsin, K. and Reza, F. (2007). “Mix design and benefit evaluation of high solar reflectance concrete for pavements.” *Transportation Research Record: Journal of the Transportation Research Board*, No. 2011, Washington, D.C.:11–20.

Doll, D. (1983). “Diurnal variability of the surface energy budget fluxes for three contrasting land use surface materials.” *Master Thesis*, North Carolina State University. Raleigh, North Carolina, 132 p.

Huntingford, C., Allen, S.J., and Harding, R.J. (1995). “An intercomparison of single and dual-source vegetation-atmosphere transfer models applied to transpiration from Sahelian Savannah.” *Boundary-Layer Meteorology*. 74 (4): 397-418.

Mihailovid, D. T. and Ruml, M. (1996). "Design of land-air parameterization scheme (LAPS) for modeling boundary layer surface processes." *Meteorology and Atmospheric Physics*. 58: 65-81.

Tan, Z. M., Zou, X. L., and Liu, B. Y. (2010). "Numerical solution to pavement temperature fields and discussion on several key issues." *Journal of Tongji University: Natural Science*, 38 (03): 374~379.

Tran, N., Powell, B., Marks, H., West, R., and Kvasnak, A. (2009). "Strategies for design and construction of high-reflectance asphalt pavements." *Transportation Research Record: Journal of the Transportation Research Board*, No. 2098, Washington, D.C.: 124–130.

Vogel, C. A., Baldocchi, D. D., Luhar, A. K., and Rao, K. S. (1995). "A comparison of a hierarchy of models for determining energy balance components over vegetation canopies." *Journal of Applied Meteorology*. 34: 2182-2196.

Yao, Z. K. (2012). "Methods research on asphalt pavement structure design based on multi-index." *Final Report, Part 1*, Shanghai, China.

Zhang, J. R. and Liu, Z. Q. (2006). "A study on the convective heat transfer coefficient of concrete in wind tunnel experiment." *China Civil Engineering Journal*. 39 (09): 39-42.

Field Evaluation of Crack Sealing of AC Pavements in Alaska

Anthony Mullin[1], P.E, M. ASCE, Juanyu Liu[2], Ph.D, P.E., M. ASCE,
Robert McHattie[3], MCE, P.E., M. ASCE

[1]Graduate Research Assistant, Department of Civil and Environmental Engineering, University of Alaska Fairbanks, Fairbanks, AK 99775-5900; apmullin@alaska.edu
[2]Associate Professor, Department of Civil and Environmental Engineering, University of Alaska Fairbanks, Fairbanks, AK 99775-5900; jliu6@alaska.edu
[3]Consulting Engineer, GZR Engineering, Fairbanks, AK; rlmchattie@gci.net

ABSTRACT: Sealing cracks in asphalt concrete (AC) pavements is a widely used preventive maintenance strategy, and has long been regarded as a necessary annual procedure in most of the United States and other countries. However, many years of careful observations in Alaska have conjectured that certain thermal crack types may sometimes be ignored, i.e., left completely unsealed, for the life of the pavement with no negative effects. This paper presents a recently completed field study on evaluating crack sealing of thermal cracks in older AC pavements in northern and central Alaska. Two distinct types of thermal cracks, differentiated as 1) lessor thermal cracks and 2) major transverse thermal cracks, were formally recognized and assessed using a special thermal crack evaluation (STCE) method. Based on field data collection, analysis, and interpretation, it was concluded that significant maintenance funds can be saved or redirected by not sealing or by reduced sealing of certain types of thermal cracks in AC pavements. The study recommends that lessor thermal cracking receive no maintenance except on delaminating pavements. Maintenance treatment of major transverse thermal cracks can be greatly reduced based on inexpensive, long-term assessments following new pavement construction.

INTRODUCTION

Sealing cracks in asphalt concrete (AC) pavements is a widely used preventive maintenance strategy, and has long been regarded as a necessary annual procedure in most of the United States and other countries (Chen et al. 2003; Rajagopal and Minkarah 2003; Masson 2005; Shatnawi et al. 2006; Yildirim et al. 2010; Yang et al. 2010). The Alaska Department of Transportation and Public Facilities (AKDOT&PF) has promoted routine sealing of cracks in AC pavements for many years. Approximately $450,000 is spent on crack sealing each year in the Northern Region. The total figure is more than $1,000,000 per year if Central and Southeast Regions' efforts are added. Until new technology is developed that can eliminate thermal cracking, a lot of funds will continue to be spent on crack sealing and minor patching.

Since the FHWA sponsored an implementation project (LTPP Pavement Maintenance Materials: SHRP AC Crack Treatment Experiment) to assist states with evaluation of preventive maintenance treatments in 1999, a number of resources have become available to address the benefits of cracking sealing, how to select the appropriate sealing treatment for the pavement conditions, preparation methods, procedures and equipment selection, material placement, treatment materials evaluations, and traffic safety issues (Dickens 2000; Stevenson and Chehovits 2001; FHWA 2001; Heydorn 2002; Zinke et al. 2005). In addition, researchers and highway agencies are spending efforts on verifying the effectiveness of crack sealing programs on pavement condition and life (Rajagopal and Minkarah 2003; Chen et al. 2003; Zinke et al. 2005; Shuler 2006; Al-Qadi et al. 2009; Yang et al. 2010). It has been suggested that this process extends the life of a pavement surface and can therefore reduce an agency's pavement replacement and rehabilitation costs.

Although relevant literature and research in progress almost invariably indicate that sealing of all cracks is absolutely necessary for good pavement performance, many years of careful observations in Alaska (McHattie et al. 1980; Raad et al. 1997) have indicated that certain cracks (including map/grid cracks) may sometimes be ignored, i.e., left completely unsealed, for the life of the pavement with no negative effects. Many example areas of highly cracked, but never-sealed, older pavements in interior Alaska are evident. Such observations seem to hold particularly true in the Northern Region where the climate is classified as semi-arid. It is economically wise, if possible, to delineate areas of the State where such sealing is (or is not) necessary.

Hence, a recently completed field study was conducted to evaluate current crack sealing practices of thermal cracks on older AC pavements in northern and central Alaska. The main objective of that study was to provide sealing recommendations, specific to thermal crack type, aimed at economically optimizing the way Alaska's maintenance and operations (M&O) funds are spent on crack sealing. This paper presents a summary of the field examination performed on these 20 plus year old sections, in which a qualitative evaluation method named the "special thermal crack evaluation" (STCE) method was developed to identify two recognized forms of thermal cracking. Both a LTPP crack evaluation, quantitative, and a PASER evaluation, qualitative, were performed and can be read in the original paper. This paper focuses on the above mentioned STCE method findings followed by conclusions and recommendations.

FIELD WORK AND DATA COLLECTION

Selecting Field Sites

AKDOT&PF records indicated the existence of 52 sections of AC pavement that were 20 or more years old, and spread reasonably throughout the contiguous non-urban road system of AKDOT&PF's Northern and Central Regions. Researchers decided on a sampling size of 120 locations to be apportioned throughout the 52 old pavement sections. The total number of evaluated locations became 91 after several weeks of field work due to unexpected or problematic pavement types such as newer

than expected, recent maintenance overlay, very poor foundation conditions, surface treatment pavement type, and safety concerns, etc. This final sampling size (91 individual field locations) was considered large enough to reasonably represent the performance of older AC pavements throughout the areas of Alaska's highway system being studied.

All sample locations were 0.1 mile in length and centered approximately at the milepost, and located on highways including Elliott Highway, Steese Highway, Richardson Highway, Parks Highway, Alaska Highway, Tok Cutoff, Glenn Highway, and Sterling Highway. Urban pavement sections were not included because of the danger of conducting fieldwork, and because the non-urban sampling was considered sufficiently large to provide a basis for valid conclusions.

STCE Method

In this study, only certain crack types are the subject of speculation regarding required sealing. These include the two most common types of thermal cracks found on nearly every paved road in colder areas of Alaska, as shown in Figure 1. The major transverse thermal crack, commonly known as a "thumper," usually extends across the entire width of the pavement surface, or nearly so, and tends to be oriented perpendicular to the roadway centerline. The driver can usually feel a definite bump when driving over a major transverse crack. Lessor thermal cracks may be almost as wide as major transverse cracks, and are interconnected in a map-like or blocky grid. By definition, both types of cracks are thermally induced.

(a) (b)

FIG. 1. Examples of (a) lessor thermal cracking, and (b) major thermal cracking

The special thermal crack evaluation (STCE) method was developed for the specific purpose of evaluating these two types of thermal cracking on older asphalt pavement sections of Alaska's northern and central roads. The STCE method collects data to help answer three basic questions that are important to Alaska's pavement maintenance strategy: To what degree does vehicle traffic affect thermal cracking? Is the interaction between thermal cracking and traffic a significant contributing factor in producing additional forms of damage in AC pavements? Does the maintenance practice of sealing thermal cracks significantly improve general pavement

performance? In the STCE method, these questions were addressed by 1) comparing the condition of thermal cracks in wheel path versus non-wheel path areas on old pavements, 2) examining the pavement near thermal cracking on old pavements for signs of fatigue cracking, potholing, excess rutting, or other signs of structural softening, and 3) comparing the condition of sealed cracks versus non-sealed cracks on old pavements. Each field location was photographed and visually examined in order to obtain a general impression of the long term value of crack sealant practices (sealed versus non-sealed) at that location.

FIELD DATA ANALYSIS

Pavement Age and Temperature Data

The objective of the research was to evaluate the sealing of thermal cracks on 20 plus year old pavement sections in Alaska, so the importance of pavement age and local temperature was emphasized in selecting field locations. A synergy of asphalt cement weathering and low temperatures produced thermal cracking in every old AC pavement in colder areas of Alaska. Figure 2 shows the minimum age, maximum age, average age, and number of sections for each of the indicated highways. Each individual column contains all of the mentioned information as indicated by the number on each section of the column as described in Figure 2's legend. The overall height is not necessarily important.

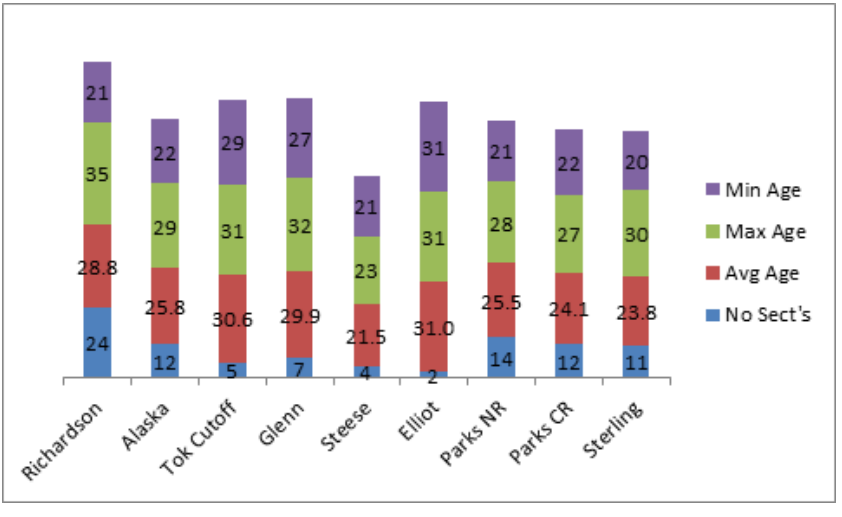

FIG. 2. Ages of road sections evaluated

Table 1 summarizes the extreme air and pavement surface temperatures as per AKDOT&PF'S Road Weather Information System (RWIS) website data recorded for the past five to six years. It can be seen that pavement surface is subjected to a range

of temperature cycling much larger than that indicated by air temperatures alone. Summertime pavement surface temperature may run as high as 30° to 40° F above the ambient air temperature. Maximum temperature differences between air and pavement surface would be expected on cloudless, dry, summer days with no wind. Minimum air/surface temperature differences would be expected: 1) on rainy and/or windy summer days, or 2) during spring/fall nights with cloud cover, or 3) during the darker winter months.

Table 1. Min and Max Air and Pavement Temperatures (°F) (AKDOT&PF RWIS)

	Rich	AK	Tok Cutoff	Glenn	Steese	Elliot	Parks NR*	Parks CR*	Sterling
Min Air	-40	-40	-40	-40	-30	n/a	-40	-35	-29
Max Air	89	87	87	85	84	n/a	87	90	87
Air Range	129	127	127	125	118	n/a	127	125	116
Min Pave	-32	-39	-37	-35	-24	n/a	-37	-28	-23
Max Pave	129	120	120	123	122	n/a	114	128	123
Pave Range	161	159	157	158	146	n/a	151	156	146

* NR = AKDOT&PF Northern Region, CR = AKDOT&PF Central Region

STCE Data Interpretation

Figure 3 looks at whether portions of major and lessor thermal cracks within wheel paths performed worse than portions outside the wheel paths. Consistent, large differences in performance between the two locations would indicate that traffic loadings played an important part in degrading pavement near the cracks themselves. Differences were observed 35 percent of the time, and large differences only 11 percent of the time for major thermal cracks. This suggests that there is usually no marked softening of the pavement structure in the wheel path. For lessor thermal cracks, there was almost no difference between wheel path and non-wheel path areas. Only at one site out of 84 was a difference observed representing approximately one percent. Therefore, based on the project data, lessor thermal cracking seems unrelated to subsequent softening of the pavement structure.

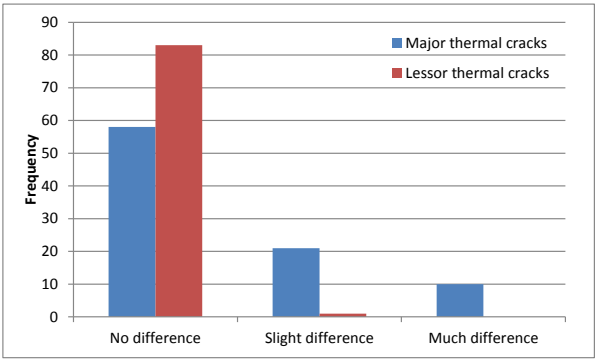

FIG. 3. Conditions of thermal cracks (wheel path vs. non-wheel path areas)

The maximum observed crack widths of major transverse crack zones are summarized in Figure 4. It supports Figure 3 in that, not only is there usually little damage difference between wheel path and non-wheel path locations, but there is usually no damage (let alone significant softening) very far beyond the transverse crack's centerline.

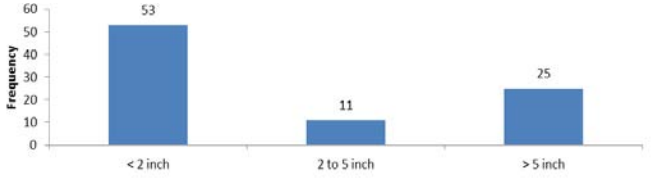

FIG. 4. Maximum observed width of major transverse crack zone

Figure 5 indicates that most lessor thermal cracks are no wider than 1/8 inch (94 percent). Perhaps most important in this finding is that vehicle action, water, and time (20 years or more in this study) did not combine to widen lessor thermal cracks or noticeably degrade/damage pavement materials adjacent to those cracks.

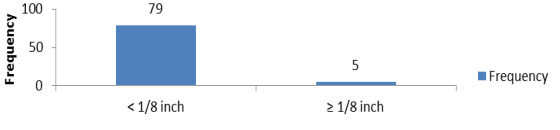

FIG. 5. Maximum observed width of lessor thermal crack zone

Figure 6 addresses the question of whether or not there were obvious signs that rutting, alligator cracking, raveling, or potholes were associated more with the near-vicinity of major transverse thermal cracks than areas of the road located farther away from the major cracks. As shown in Figure 6, only 7 (about 8 percent) of the examined pavements ("slightly noticeable" and "very noticeable" categories) showed

any signs that major transverse cracks affected pavement performance beyond the immediate vicinity of the crack zone itself. It is important to note that the 8 percent indicated here were all in areas where multiple layers of pavement were present and in the process of delaminating.

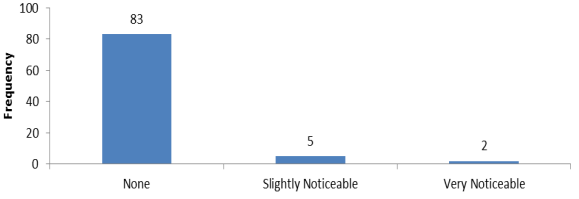

FIG. 6. General pavement deterioration due to major transverse cracking

Figure 7 indicates that no sites could be found where lessor thermal cracks appeared to be influencing other aspects of pavement performance. Very few exceptions were found where minor potholing occurred at intersections of lessor crack segments. This observation held true for most of the delaminating pavements examined during the study. It should be noted that while lessor thermal cracks may be interconnected with major thermal cracks they are primarily a result of thermal stresses on the remaining contiguous block asphalt between major thermal cracks and other lessor thermal cracks. Lesser thermal cracks were not confused with alligator cracking which, for the road sections evaluated, were easily recognized as an obviously different crack form. Again, all road sections evaluated were 20 plus years old; the cracking patterns were therefore very mature and crack types easily differentiated.

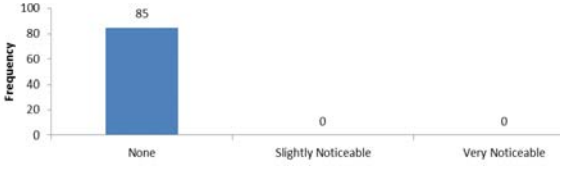

FIG. 7. General pavement deterioration due to lessor thermal cracking

Figure 8 indicates that more than half the sites contained major transverse cracks that had been sealed at some time (at 48 sites). There had been an attempt to seal all thermal cracks at only 28 sites. At 14 additional sites the sealant was so old and worn as to be barely visible (and had sealed nothing for many years) — or perhaps sealant had never been applied at all. It is very possible that some locations where sealant could not be seen in 2012 may have in fact been sealed at one time. Pavement maintenance records in Alaska do not identify specific locations where crack sealants were applied in past decades.

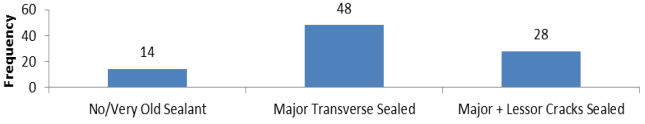

FIG. 8. Presence of crack sealant

Figure 9 shows that of the 83 sites where sealants were recognized (some old sealants were very difficult to see), only about 13 percent of those sites still exhibited effective sealants. Even sites that generally contained effectively sealed thermal cracks offered plenty of the unsealed variety for study.

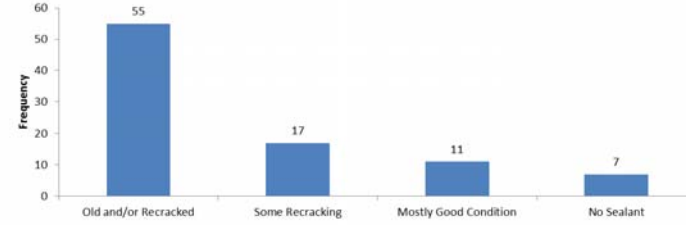

FIG. 9. Present condition of sealant

Interpretation of Photos and Miscellaneous Comments

This subsection summarizes and interprets thermal crack characteristics and aspects of crack sealing performance based on photos and miscellaneous comments accumulated during project fieldwork.

Natural major transverse thermal cracks usually do not extend across the road in a simple, straight line nearly perpendicular to the centerline. Based on all observations, only about 50% of the major thermal cracks were both fairly straight and perpendicular to the centerline. About 50% were not perpendicular to the centerline and/or not straight. The majority, 95% of these cracks, had widths between ¼ inch and ½ inch. The remaining 5% exhibited widths of not more than about 1 inch. Only 5% displayed deep depressions along the crack edges and 15% exhibited spalling along the crack zone. In terms of depth, these cracks always extended through both the AC and base course layers, and apparently well into underlying layers of the

pavement structure. Miscellaneous observations and photos suggest that relatively little of the major transverse thermal cracking seen on old pavements would significantly benefit from sealing at present.

Unlike major transverse cracks, lessor thermal cracks have a much less consistent general appearance. Lessor thermal cracks usually first appear as individual hairline crack segments perpendicular to the centerline. As lessor thermal cracking matures, crack segments tend to intersect and interconnect to form irregular net-like or orthogonal grid-like patterns. These cracks did not display zones of depression or spalling along their edges. Nearly all observations and photos suggest that none of the lessor thermal cracking seen on old pavements requires sealant. Once formed, it appears that this crack type does not deteriorate to the point that general pavement performance is affected.

Wheel Path Versus Non-Wheel Path Conditions

For major transverse thermal cracks, visual observations backed by photographic evidence identified only a relatively small percentage of locations where wheel path damage was noticeably worse than non-wheel path damage.

For lessor thermal cracking, observations identified very few instances where the condition of lesser thermal cracking was worse in wheel path areas than non-wheel path areas. The few examples where lesser thermal cracking showed more damage in the wheel paths were in areas where pavement delamination was occurring. Figure 10 shows the typical appearance of nearly all lessor thermal cracks seen during field work for this research. Note that there is essentially no difference in performance between wheel path and non-wheel path locations. Pavement condition does not vary as a function of distance perpendicular to the edge of any individual crack.

FIG. 10. Lessor thermal cracks showing same performance in wheel path and non-wheel path locations (common appearance)

Overall, during the entire course of 2012 field work, almost no consistent evidence was found to support the generally accepted theory that open pavement cracks always allow enough surface water infiltration to facilitate load-related pavement damage. In theory, the severely damaging consequences of water-vehicle interaction should have been obviously and abundantly evident within the more heavily trafficked wheel path areas of the pavement — in fact there was usually no such evidence at all.

Influence of Cracking on Adjacent Pavement Areas

Theoretically, pavement condition should vary as a function of distance from a crack. The worst condition would be expected near the crack because of the interaction of water and traffic loadings. At most sites there was no obvious correlation between pavement condition and distance from the edge of a crack except for the usual influence zone (usually less than 2 inches wide) adjacent to major transverse thermal cracks. Figure 11 shows examples of the typical case where pavement damage does not extend far beyond the crack edge. Most observations failed to support the assumption that thermal cracks allow enough water past the AC pavement layer to generally soften the pavement structure in any obvious way.

FIG. 11. Severe major transverse cracks with little influence on pavement performance beyond crack edges

Effect of Maintenance "Banding"

A wide form (several feet wide) of patch/seal was examined in a number of areas in AKDOT&PF's Northern Region. This type of maintenance treatment is applied to major transverse thermal cracks with the apparent intention of simultaneously accomplishing sealing, patching and re-leveling. However, except for the newest of these treatments, nearly every band had re-cracked to reveal the old thermal crack. Failure of the sealing function appeared to cause no problem however. Regardless of not providing a permanent seal, these bands did appear to be performing a valuable function. Most of the banded transverse cracks (even those with old bands) still provided a permanent re-leveling of the area adjacent to the crack, and less of a bump for the driving public than without the band. Figure 12 shows two examples of maintenance banding in AKDOT&PF's Northern Region. Observations concerning the effectiveness of the bands provide more evidence that thermal cracks can be allowed to remain open without necessarily causing further pavement damage.

FIG. 12. Examples of patch/seal band maintenance of major transverse thermal cracks

Effect of Pavement Delamination

The problem of pavement delamination was observed at several of the research field sites. This problem was easy to identify where 1) much potholing and raveling were present, and 2) where another pavement layer could be found at the bottoms of the potholes and heavily raveled areas. Only in areas of delaminating pavement was pothole formation apparently associated with thermal cracking. Delamination tended to increase the severity of spalling along major transverse cracks. Fortunately, relatively few miles of Alaska's paved roads exhibit delamination.

CONCLUSIONS

The following conclusions are derived from observations of 20 plus years old pavements in Northern and Central Alaska, specifically mentioned in this study. These pavements have had sufficient time to accumulate very mature patterns of thermal crack damage as well as the other common damage types associated advanced pavement age in Alaska.

The characteristics of lessor thermal cracks appear to be the same within and outside of wheel paths at any given location (only 1 case was slightly different). Lessor thermal cracks do not appear to deteriorate after formation. Zones of pavement adjacent to lessor thermal cracks show no more deterioration than the pavement surface in general. The condition of lessor thermal cracks and areas of pavement adjacent to those cracks appear to be similar regardless of whether or not the lessor thermal cracks were sealed (general observation during the study without apparent exceptions). From this study it is recommended not to seal lessor thermal cracks in asphalt pavements in the northern and central regions of Alaska.

The condition of a major transverse crack within the wheel path versus outside the wheel path is the same or only slightly different (about 89% of the sections where major transverse cracking was present). Major transverse cracks almost always exhibit a narrow zone of influence (a depressed and/or spalled zone) that extends parallel to and along both sides of each crack. Only about 28% of those cracks have influence zones more than 5 inches in total width. Major transverse cracks were not associated with noticeable pavement problems in 92% of the sections where that crack type was present. Most major transverse cracks are characterized by a

depressed zone that produces the familiar vehicle tire thump whether sealed or not. However, wide bands of sealing/patching applied to major transverse cracks appear to have lessened tire thump in many instances. Except for very recent applications, all seal/patches of this type (wide bands) were found to be re-cracked providing no seal. Observations made throughout the course of this study strongly suggest that much less sealing of major transverse thermal cracks may be a practical economic possibility that is compatible with acceptable long-term pavement performance. For the time being however, it is recommended to continue the routine pavement preservation exercise of sealing major thermal cracks as a general precautionary strategy pending additional field testing.

A few pavement sections evaluated during this research were found to be generally damaged by the process of pavement delamination. Delamination tended to be accentuated wherever cracks in the pavement surface allowed water to access the interface between delaminating pavement layers. Based on these observations, paving methods that might lead to delamination should be avoided if at all possible, and any observed breaks in a delaminating pavement surface should be sealed if possible.

Assessment of the need to seal thermal cracks should be continued. A field testing process may be established to document the long-term performance of sealed versus non-sealed cracks. Such experiments will finally provide the hard evidence to support or reject the routine practice of sealing major transverse thermal cracks. Research is needed as well to develop an understanding of why, contrary to accepted engineering belief, heavily trafficked pavements can indeed survive quite well for decades with many thermal cracks and little or no sealing.

Further research applying statistical methodologies related to other climatic events such as precipitation and snowfall, as well as base and subgrade parameters, drainage and bearing capacity is recommended. The research reported herein has shed interesting light on what has actually happened to a number of old pavement sections in Alaska. The recommended research is intended to provide answers to important questions about why the pavement has performed the way it has — contrary to usual dire expectations regarding the interaction of pavement cracks, water, and vehicle traffic.

REFERENCES

AKDOT&PF Road Weather Information System http://www.dot.state.ak.us/iways/roadweather/forms/About.html, accessed 9/30/2012.

Al-Qadi, I. L., Yang, S., Fini, E. H., Masson, J-F., and McGhee, K. K. (2009). "Performance-Based Specification Guidelines for the Selection of Bituminous-Based Hot-Poured Crack Sealants." *Journal of the Association of Asphalt Paving Technologists*, 78, 491-534.

Chen, D-H, Lin, D-F, and Luo, H-L. (2003). "Effectiveness of Preventative Maintenance Treatments Using Fourteen Sps-3 Sites in Texas." *ASCE Journal of Performance of Constructed Facilities*, 17(3), 136-143.

Dickens, R. (2000). "Sealing the Crack... and the Sale." *Pavement: Advancing the World of Pavements*, 15 (2), 46-52.

Federal Highway Administration. (2001). "Crack Seal Application." *Research Report,* FHWA-IF-02-005, Federal Highway Administration, Washington, DC.

Heydorn, A. (2002). "Crack Repair Study." *Pavement: Advancing the World of Pavements*, 17 (3), 48 and 50.

Masson, J.F. (2005). *Bituminous Crack Sealants in Canada: Research and Performance Specifications*. National Research Council of Canada, Ottawa, Canada.

McHattie, R., Connor, B., and Esch, D. (1980). "Pavement Structure Evaluation of Alaskan Highways." *Research Report*, *Alaska Department of Transportation and Public Facilities*, FHWA-AK-RD-80-1, Juneau, AK.

Raad, L, Sabounjian, S., Sebaaly, P., Epps, J., Camilli, B., and Bush, D. (1997). "Low Temperature Cracking of Modified AC Mixes in Alaska, Volume I." *INE/TRC 97.05*, University of Alaska Fairbanks, AK.

Rajagopal, A. S., and Minkarah, I. A. (2003). "Effectiveness of Crack Sealing on Pavement Serviceability and Life." *FHWA/OH-2003/009 Report*, University of Cincinnati, Cincinnati, OH.

Shatnawi, S., Marsh, R., Hicks, G. R., and Zhou, H. (2006). "Pavement Preservation Strategy Selection in California." *11th AASHTO-TRB Maintenance Management Conference*, Charleston, South Carolina.

Shuler, S. (2006). "Evaluation of the Performance, Cost-Effectiveness, and Timing of Various Preventive Maintenances: Interim Report." *CDOT-DTD-R-2006-6*, Colorado State University, Fort Collins, CO.

Stevenson, J, and Chehovits, J. (2001). "Crack Sealing and Filling Treatments for Asphalt Concrete Pavements." *FHWA-IF-03-019, Federal Highway Administration*, Washington, DC.

Yang, S., Al-Qadi, I. L., McGraw, J., Masson, J-F., and McGhee, K. (2010). "Threshold Identification and Field Validation of Performance-Based Guidelines to Select Hot-Poured Crack Sealants." *Transportation Research Record* 2150, 87-95.

Yildirim, Y., Yurttas, Y., and Boz, I. (2010). "Service Life of Crack Sealants." *First International Conference on Pavement Preservation*, Newport Beach, CA.

Zinke, S., Hogge, B., O'Brien, C., and Mahoney, J. (2005). "Evaluation of Pavement Crack Treatments - Literature Review." *CT-2241-F-05-6*, University of Connecticut, Storrs, CT.

Highway Winter Maintenance Operations at Extremely Cold Temperatures

Xianming Shi[1], M. ASCE, P.E., Jiang Huang[2], Dan Williams[3], Michelle Akin[4], P.E., and David Veneziano[5]

[1] Research Professor/Program Manager, Civil Engineering Department and Western Transportation Institute, Montana State University, P.O. Box 174250, Bozeman, MT 59717-4250; xianming_s@coe.montana.edu
[2] Research Associate, Western Transportation Institute, P.O. Box 174250, Bozeman, MT 59717-4250; jiang.huang@coe.montana.edu
[3] Senior Research Associate, Western Transportation Institute, P.O. Box 174250, Bozeman, MT 59717-4250; kdzagn@hughes.net
[4] Research Engineer, Western Transportation Institute, P.O. Box 174250, Bozeman, MT 59717-4250; michelle.akin@coe.montana.edu
[5] Research Scienstist, Western Transportation Institute, P.O. Box 174250, Bozeman, MT 59717-4250; david.veneziano@coe.montana.edu

ABSTRACT: Winter maintenance operations are crucial for achieving a reasonable level of motorist safety and public mobility on highways in cold regions. Such activities become essential when a storm with extremely cold temperatures hits the area, either as a result of normal fluctuations or as a result of climate change. Once the pavement temperature drops below 10°F, the traditional tools (e.g., granular salt) become ineffective. To achieve a drivable pavement friction condition, excessive amount of plowing, chemicals, and/or abrasives is often used, which leads to substantial cost increases and environmental concerns. The most severe 20 percent of the storms can cost 80 percent of an agency's annual budget for winter maintenance. In this context, it is necessary to examine the best practices of highway winter maintenance operations with a renewed perspective, so as to target these extreme storms. This work presents a synthesis of relevant information in the published domain, with a focus on the traditional and innovative strategies potentially useful for highway agencies to fight extremely cold storms. This information can be valuable in the context of climate change, as certain areas may experience unusually cold snow or ice storms and face devastating consequences if unprepared for such scenarios.

INTRODUCTION

Winter maintenance operations are crucial for achieving a reasonable level of motorist safety and public mobility on highways in cold regions (Strong et al. 2010). Such activities become essential when a storm with extremely cold temperatures hits the area, either as a result of normal fluctuations or as a result of climate change.

Once the pavement temperature drops below 10°F, the traditional tools (e.g., granular salt) become ineffective. To achieve a drivable pavement friction condition, excessive amount of plowing, chemicals, and/or abrasives is often used, which leads to substantial cost increases and environmental concerns (Fay and Shi 2011, 2012, Shi et al. 2009, 2010a, 2010b, 2013, Staples et al. 2004). In this context, it is necessary to examine the best practices of highway winter maintenance operations with a renewed perspective. FIG. 1 illustrates the interrelated components and processes in winter maintenance operations that define the scope of this work.

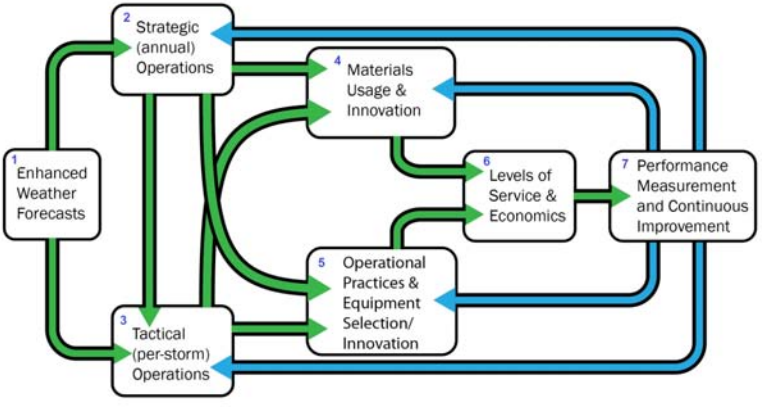

FIG. 1. Key components and processes in winter transportation operations

In addition to geographical location, intensity of precipitation, and cost, *pavement temperature* is a key parameter to consider when selecting the operational strategies and/or the application rate of materials for removing snow and ice from roads during winter storms. Traditionally, large amounts of salt (sodium chloride, NaCl) are used for snow and ice control on roads, which works well down to approximately 10 ºF (-12.2°C). As the pavement temperature gets colder, higher volumes of salt are required to achieve a reasonable level of service (LOS). As such, the use of salt is no longer cost-effective and highway agencies thus utilize other chemicals either alone or as prewetting agents to enhance the performance of salt (Ohio DOT 2011) or apply abrasives to provide a traction layer on pavement. Abrasives are usually used at pavement temperatures below 12°F (-11ºC), and on roads with low traffic and low LOS (Blackburn et al. 2004). Furthermore, plowing is the most commonly used tool for snow removal, especially when the temperatures are extremely low.

Based on the field experience by Montana Department of Transportation (DOT) professionals, there are a number of considerations that affect winter maintenance operations when ambient and surface temperatures get very cold (e.g., below 0°F). These considerations are listed as follows, mostly related to various components in FIG. 1: forecasts and recovery (Component 1); roadside design and maintenance impacts on drifting (Component 2); turbulence from vehicles (Component 4); performance and storage of winter chemicals (Component 4); proactive vs. reactive strategies (Component 5); rural vs. urban environments (Component 5); and target LOS (Component 6). Road design and snow fences are important considerations

especially in open and windy areas. Tools have been developed to account for blowing and drifting snow in the highway design process, such as SnowMan® from the New York DOT (Chen and Lamanna 2006). However, roadside vegetation is often overlooked regarding its role in drift control.

In the U.S., northern tier and mountain states tend to feature much colder temperatures and greater snow amounts than the southern tier. However, even the southern tier may experience extremely cold temperatures occasionally. In the context of climate change, certain areas may experience unusually cold snow or ice storms and face devastating consequences if unprepared for such scenarios. Extremely cold conditions bring different considerations for taking care of roads in the winter season. For instance, the moisture content of snowfall in very cold conditions is very low and this dry snow does not pack well and is readily disturbed by wind or vehicle turbulence. Winter maintenance managers and staff must assess their specific areas of interest to determine their needs and viable strategies.

BEST PRACTICES FOR FIGHTING EXTREMELY COLD STORMS

The effectiveness and efficiency of a highway winter maintenance program hinge on a number of factors, including the selection and proper execution of operational strategies and tactics that are effective under the prevailing conditions. Based on existing knowledge and research, several effective strategies for highway winter maintenance operations during extremely cold storms have been identified from the published domain and detailed in this section. These include weather forecasting, snow storage, chemical usage, plowing, abrasive usage, and pavement innovations. These strategies may be used individually or synergistically to achieve a reasonable LOS on highway pavement, at a reasonable cost.

The NCHRP Report 526 provided guidelines for snow and ice control methods and operations (Blackburn et al. 2004). Mechanical removal (e.g., plowing) was indicated to be effective at low temperature pavement conditions (below 12º F) where deicers may become ineffective. Abrasives were indicated to be effective at all temperatures, while combinations of strategies (e.g., abrasives and chemicals) can also be effective in many cases. The Maine DOT conducted field evaluation of various approaches to treating an Interstate highway during a low-temperature January 2011 snowstorm that lasted about 7 to 8 hours (CTC & Associates 2011). The agency found that applying prewetted sand with a 70/30 blend of salt brine and Ice B'Gone (a proprietary $MgCl_2$ blend) was more cost-effective relative to two other approaches (three applications of salt, or early salting followed by sanding).

Weather Forecasting

Weather forecasting is particularly important for fighting extremely cold storms for which resource allocation needs to be optimized as much as possible. In order to meet highway winter maintenance challenges, it is crucial to obtain and utilize accurate weather information (Ohio DOT 2011). Otherwise, the consequences could be: excessive use of chemicals and materials, failure to respond in a timely matter to a storm event (resulting in greater crash risk and user delay), unplanned use of overtime

staffing, etc. (Strong and Fay 2007). Improvements in weather information can help in all stages of winter storm response, including pre-, during and post-storm.

Near-real-time weather and road condition information and customized weather service are valuable to the success of proactive maintenance strategies (Shi et al. 2007, Ye et al. 2009a, 2009b). Anti-icing is more sensitive to weather conditions than other winter maintenance practices, since anti-icing is a proactive practice that is sensitive to pavement temperature, dilution, and other factors (Blackburn et al. 2004). When considering the choice between spatially or temporally improved forecasts, Fu et al. (2009) found that improved spatial resolution of forecast data will provide greater expected benefit to service levels. Strong and Shi (2008) estimated the value and additional saving potential of the UDOT customized weather service to be 11–25 percent and 4–10 percent of the UDOT labor and materials costs for winter maintenance, respectively. The UDOT Weather Information Program was estimated to feature a benefit–cost ratio of 11:1. Mesonets that integrate observational data from a variety of sources can provide a more comprehensive and accurate picture of current weather conditions (Strong et al. 2010). These data management systems are expected to maximize availability and utility of road weather observations and facilitate more accurate, route-specific forecasting of road weather conditions.

Three case studies by Ye et al. (2009b) and Shi et al. (2007) collectively showed that winter maintenance costs decreased as the use of weather information increased or its accuracy improved. Ye et al. (2009b) recommended that the use of weather information be more focused towards the road environment, in order to develop better winter maintenance strategies. In addition, agencies should continue to invest in road weather information with high accuracy and to ensure high usage of the existing road weather information services.

Snow Storage

Highway agencies have indicated that snow storage is an effective strategy as it removes snow from the roadway environment that may be susceptible to drifting (Yang and Ying 2010, CTC & Associates 2011). The simplest solution is to store the snow adjacent to the roadside, but this may not be feasible everywhere, especially in urban areas. Other options include: removing the snow to dedicated snow storage areas, which may be equipped with facilities to treat the melt water (impurities can include deicers, oil, grease, heavy metals, litter, and dirt, as detailed in Tatarniuk et al. 2009); or using mobile snow melters (Transportation Association of Canada 2003). Considerations should be made for snow storage in the planning process of road design or reconstruction (CTC & Associates 2011).

Chemical Usage

Best practices of winter chemical usage are implemented to *apply the right type and amount of materials in the right place at the right time* for snow and ice control. Laboratory data demonstrate that, relative to NaCl, the use of calcium chloride ($CaCl_2$) for comparable deicing performance between 0 and 10°F within 1 hour, would introduce five times fewer chloride anions and ten times fewer cations (Brandt 1973). Another laboratory study demonstrated that at 15°F and 5°F $CaCl_2$ produced more

undercutting of ice on pavement materials than NaCl (Blackburn et al. 1991). A corn steepwater demonstrated higher melting performance than the salt/sand mixture with respect to both duration and strength. The steepwater deicer also showed active ice melting at temperatures as low as 7.5°F, whereas the salt/sand mixture ice melting stopped around 20°F (Janke and Johnson 1997). Alkoka and Kandil (2002) examined a blend of agricultural byproducts and liquid magnesium chloride ($MgCl_2$) and found its working temperature for deicing to be down to -20ºF.

Some chemicals (especially $CaCl_2$) used at low temperatures were indicated to have the potential to create an ice film. Packed snow and thin layers of ice can be difficult to remove at low temperatures, although scarifying or ice chipping blades have been effective in such cases (CTC & Associates 2011). Boselly et al. (2005) recommended that for air temperatures below 12 ºF, the suitable maintenance strategy would be mechanical removal without chemicals if snow and/or ice were unbonded to the pavement, or the application of chemicals and (as needed) abrasives if snow and/or ice were bonded.

The NCHRP Report 577 also provided guidance on application rates and temperatures for different maintenance operations. Anti-icing was cited as being applicable down to an air temperature of 10ºF, deicing applicable down to 0ºF (prewet salt applicable down to -1ºF.), prewet and dry abrasives were applicable at all temperatures, and abrasive/salt mixes were applicable down to -1ºF (Levelton Consultants 2007). A synthesis by CTC & Associates (2009) suggested that anti-icing with solid or prewetted chemicals is not a good strategy when the pavement temperature drops below 15ºF. However, the laboratory investigation by Cuelho et al. (2010) revealed that liquid anti-icing materials improved the ability of a plow to remove snow from the pavement surface, even at temperatures lower than 14ºF. Among the common chemicals investigated, $CaCl_2$ performed best on asphalt surfaces at all temperatures, while potassium acetate (KAc) performed best on concrete at all temperatures (0 ºF, 10 ºF, 15 ºF and 30 ºF). Luker et al. (2004) compared the performance of dry rock salt and six prewet salt mixtures in the laboratory. The rate of prewetting was explored at 4, 8, and 12 gallons of liquid chemical per ton of rock salt respectively, and the melting of compacted snow improved with the rate of prewetting. Prewetting salt slightly decreased its performance at relatively warm temperatures (–1°C and –5°C) in some cases but "all of the prewet mixtures were effective at –10°C, unlike the dry rock salt".

In summary, chemicals can be used primarily for deicing or prewetting during extremely cold winter storms. If used in combination with mechanical removal, the chemical usage can be a cost-effective option. There are still ongoing efforts towards the development of more cost-effective and environmentally responsible chemicals as well as the appropriate timing and application rate of chemical deicers under given road weather scenarios.

Plowing

Plowing is the most ubiquitous method of removing snow and ice from roadways. Snow with low moisture content and at temperatures far from the melting point can be more easily plowed from a road surface. Frequent plowing can help prevent snow

and ice from sticking to the road surface. Lannert (2008) discussed the use of wider (14-ft wide) front plows to clear a 12-ft lane in one pass in Missouri. The cost of this conversion was less than $400 per foot of plow. The benefits obtained from this practice included: a reduction in the number of passes needed, saved fuel, and reduced labor. The use of trailer plow (*TowPlow*) was also discussed, which produced the benefits of one snowplow truck and operator clearing over 24 feet of lane at high speeds while reducing fuel usage. The author noted that *TowPlows* also can reduce an agency's capital investment needs by 20% to 30% and still achieve the same amount of work. The Wisconsin DOT implemented *TowPlow* during the 2009-2010 winter season, and estimated a 32%-43% operational cost savings relative to a regular plow truck (Santiago-Chaparro et al. 2012). Macfarlane (2001) discussed the use of a reversible plow and switchable wing mounting, which could be used for all multi-lane and conventional operations by swinging the plow and mounting the appropriate wing. The trials by the New Brunswick DOT in 1995 identified several benefits, including: improved plowing efficiency and equipment versatility, reduced run-up collisions, and improved visibility for the plow operator.

Abrasive Usage

During heavy snowfall, sand and grit are often used to provide traction. Abrasives are typically used at pavement temperatures below 12°F and on roads with low traffic and low level of service (Blackburn et al. 2004). Prewetting has shown to increase the performance of solid chemicals or abrasives and their longevity on the roadway surface, thereby reducing the amount of materials required (O'Keefe and Shi 2005).

Heated sand or prewetting abrasives with liquid deicers or hot water can greatly reduce bounce and scatter and contribute to improved friction even with vehicular traffic (Perchanok 2008, Perchanok et al. 2010). Dahlen and Vaa (2001) found that "by using heated materials or adding warm water to the sand it is possible to maintain a friction level above the standard, even after the passage of 2,000 vehicles". Hot water in particular results in a sandpaper-like appearance on compacted snow and ice and is commonly used at airports in Norway during periods of prolonged cold temperatures (Klein-Paste and Sinha 2007). Field tests during the 2003-2004 winter season compared salt prewet with hot water versus prewet with brine. The two showed similar performance on thick ice, and prewetting with hot water provided better friction improvements on thin ice (Lysbakken and Stotterud 2006). Vaa and Sivertsen (2008) examined Norway's highway winter maintenance operations and found that mixing hot water and sand was an effective alternative to salting when temperatures were low. While a specific temperature associated with this operation was not specified, subsequent text indicated salting was performed down to 12ºF (-8ºC).

Pavement Innovations

An interesting approach to snow and ice control at extremely cold temperatures leverages recent advances made in pavement technologies. Of particular interest are heated pavement technologies, which prevent the ice formation or facilitate the

removal of snow and ice from the pavement surface. As such, these technologies reduce or eliminate the need for using chemicals, abrasives, or mechanical removal. Depending on the relative location of heating source to the pavement, they can be classified as internal heating [e.g., geothermal heat pumps (Seo et al. 2011) and electrical resistive heating (Yehia et al. 1999, 2000, Chang et al. 2009, Yang et al. 2011)] and external heating (e.g., microwave and infrared heating). Table 1 presents cost estimates by the Iowa DOT for various heating systems (Zhang et al. 2009).

Table 1. Cost Estimates for Various Heating Systems for Snow and Ice Control

Heating	Approximate Capital Cost	Power Consumption	Operating Cost
Infrared Heat Lamp	\$96/m^2 (\$8.9/ft^2)	75 W/m^2 (7 W/ft^2)	Not available
Electric Heating Cable	\$54/m^2 (\$5/ft^2)	323–430 W/m^2 (30–40 W/ft^2)	\$4.8/m^2 (\$0.45/ft^2)
Hot Water	\$161/m^2 (\$15/ft^2)	473 W/m^2 (44 W/ft^2)	\$250/Storm, 3-inch snow
Heated Gas	\$378/m^2 (\$35/ft^2)	Not available	\$2.1/m^2 (\$0.2/ft^2)
Conductive Concrete Overlay	\$48/m^2 (\$4.5/ft^2)	516 W/m^2 (48 W/ft^2)	\$5.4/m^2 (\$0.5 ft^2)

In Japan, Marita (2000) introduced and evaluated the Gaia Snow-melting System that utilizes the geothermal heat from the shallow ground and its auxiliary solar heat in the summer. The first system installed in Ninohe, Iwate Prefecture in 1996 has shown that even under very low temperatures for the month of January (averaging -8.3°C), the system was effective in snow and ice melting and environmentally benign. However, modifications would be needed to guarantee its proper operations in very cold days and recommendations on future improvements were proposed to achieve higher performance. In 2006, Yasukawa (2007) summarized the advantages of geothermal heat pump application of "Gaia System". These include: reduced consumption of fossil fuels, reduced consumption of electricity with higher coefficient of performance, and reduced urban heat-island effect with heat exhaust into underground. Hiroshi et al. (1998) reported the use of a snow-melting technology utilizing tunnel spring water and hot spring water on a highway through the Abo Pass, where average minimum temperature was around -18°C during the past five years with average annual accumulated snow fall depth of 500 cm. They concluded that the system using tunnel spring water and hot spring water are practical ways to melt snow where such thermal energy and large site are available.

The conductive pavement technology has also found its application to airport runways. One such example is the Snowfree® system installed and operated at O'Hare International Airport (Derwin et al., 2003). Snowfree® electrically conductive asphalt pavement uses a unique blend of graphite and asphalt and was used to electrically heat the runway surface and break the ice bond to pavement. It was installed and operated for four years since November 1994. The installation costs were at \$15 per square foot. The conductive asphalt showed similar durability as regular asphalt concrete and "consistently melted snow in all but the most severe conditions". It was able to increase the pavement temperature 3 to 5°F per hour as designed. A benefit/cost analysis was conducted, which showed that the system on

high-speed exits could have a payback time of three years. In severe snow storms, Snowfree would expedite the runway reopening after the shutdown, leading to safety benefits and cost savings for airlines and airports. The system was effective even when temperatures went down to -10°F in one of the winter seasons. Its ability to increase the pavement temperature 22°F confirmed its effectiveness in the extremely cold weather.

For microwave and infrared heating, very limited technical information was found during the literature research. The knowledge is still lacking on their performances and cost-effectiveness (Long et al. 1995, Hopstock and Zanko 2005). The infrared heaters can be mounted on a truck or on the bridge-side structures to provide heat from the lamps to melt the snow and ice on the bridge deck. In 2001, Switzenbaum et al. (2001) described its application on aircraft. Microwave heating shares the similarities in the installation of infrared heaters and can be mounted on a truck or on the bridge-side structures (Johnson 2006).

In summary, heated pavement technologies hold great promise for snow and ice control at specific locations where the site conditions and economics warrant their deployment. They have demonstrated outstanding abilities in fighting cold storms. Yet, some technical or economic barriers remain before they can be widely implemented.

CONCLUDING REMARKS

Successfully implementing a highway winter maintenance program requires appropriate selection of chemicals or pavement treatments for snow and ice control, obtaining the right equipment, having well-trained staff, making informed decisions, and proper execution of strategies and tactics. There is a substantial amount of knowledge regarding best practices of highway or airport winter maintenance. However, most of these best practices are versatile and there are limited research dedicated to best practices of snow and ice control at extremely low temperatures, which highlights the need for more research in this field.

Table 2 summarizes the best practices identified in the published domain for fighting extremely cold storms. There is still room in improving operating strategies, weather forecasting, and equipment, so as to optimize the timing of winter maintenance operations and to maximize the outcome (LOS) and resilience of winter maintenance with the limited resources at hand. Chemical usage still holds great promise in improving the effectiveness and efficiency of snow and ice control under such conditions, as new cost-effective chemical deicers emerge on the market. Conventional practices for fighting winter storms at extremely low temperatures focus on the use of abrasives and plowing. Pavement treatments generally bear higher cost per lane mile than the use of chemicals for snow and ice control, and thus should be targeted for problem locations where the best return on investment can be expected. Pavement treatments offer the benefit of reducing chemical usage and associated environmental footprint, enhancing agency preparedness, and quicker recovery to bare pavement. Despite the limited reports, certain technologies (geothermal heating and conductive pavement) seem to indicate positive performance

at cold temperatures. For innovative technologies, some technical or economic barriers remain before they can be widely implemented.

This work provides a synthesis of information that can be valuable in the context of climate change, as certain areas may experience unusually cold snow or ice storms and face devastating consequences if unprepared for such scenarios. Continued research and development can be expected in the aforementioned enabling technologies, while efforts are made to advance the knowledge base underlying the key interactions and processes occurring in the "dynamic layer", i.e., those between the pavement, snow/ice, and chemicals. It is highly recommended to monitor the developments in this field and periodically revisit the research to determine when innovations become practical for widespread use. Furthermore, for the identified best practices, field and/or laboratory validation may be necessary before their adoption by highway agencies for their specific road weather environments.

ACKNOWLEDGEMENTS

The authors extend our sincere appreciation to the Clear Roads pooled fund and its sponsor states. They would like to specifically thank the Clear Roads Technical Advisory Subcommittee and Colleen Bos of CTC & Associates for the feedback throughout the course of the research project.

Table 2. Best Practices for Fighting Extremely Cold Storms

Component in FIG. 1	Winter Maintenance Tool	Best Practices	Benefits	Comments
#1	Weather forecasting	Improved spatial resolution and usage; Integrated observational data; Customized weather service	Optimal resource allocation; Timely response and planned staffing	Pre-, during and post-storm; Especially crucial for proactive practices
#2	Snow storage	Store the snow adjacent to the roadside or remove it to dedicated snow storage areas; use mobile snow melters	Reduce snow drifting	Consider snow storage in the planning process of road design or reconstruction
#4	Chemical usage (for deicing above 0ºF and anti-icing with liquids above 10ºF or with prewet solids above 15ºF)	Combine chemical usage with plowing; Use prewet salt; Use some agro-by products and their blends	Cost-effective solution	Apply the right type and amount of materials in the right place at the right time

#5	Plowing	Wider front plows; trailer plow (*TowPlow*); Reversible plow and switchable wing mounting	Minimal environmental damage	Improved plowing efficiency and equipment versatility, reduced run-up collisions, and improved visibility for the plow operator
#5	Abrasive usage	Prewetting with hot water (vs. liquid deicer); Heated sand	Reduce bounce and scatter; Improve friction even with vehicular traffic	Typically used at pavement temperatures below 12°F and on roads with low traffic and low LOS
#5	Pavement innovations	Heated pavement technologies (geothermal heating and conductive pavement)	Reduce or eliminate the need for using chemicals, abrasives, or mechanical removal; Improve agency preparedness	Suitable for some key site locations; Some technical or economic barriers remain

REFERENCES

Akin, M., Huang, J., Shi, X., Veneziano, D., and Williams, D. (2013). "Snow removal at extreme temperatures." *Research report*, Minnesota Department of Transportation and the Clear Roads Program. St. Paul, MN.

Alkoka, M., and Kandil, K. (2002). "Effectiveness of using organic by-products in decreasing the freezing point of chemical solutions." *New challenges for winter road service: XIth International Winter Road Congress*. Sapporo, Japan.

Blackburn, R. R., Bauer, K., McElroy, A. D., and Pelkey, J. E. (1991). "Chemical undercutting of ice on highway pavement materials." *Transportation Research Record*, Vol. 1304: 230-242.

Blackburn, R. R., Bauer, K. M., Amsler, D. E., Boselly, S. E., and McElroy, A. D. (2004). "Snow and ice control: Guidelines for materials and methods." *Research Report*, National Cooperative Highway Research Program, National Research Council. Washington, D.C.

Boselly, S. E., Robert, R. B., and Amsler, D. E. (2005). "Procedures for winter storm maintenance operations." *Research report*, Arizona Department of Transportation. Phoenix, AZ.

Brandt, G. H. (1973). "Environmental degradation by de-icing chemicals and effective countermeasures: Potential impact of sodium chloride and calcium chloride de-icing mixtures on roadside soils and plants." *Highway Research Record*, Vol. 425: 52-65.

Chang, C., Ho, M., Song, G., Mo, Y. L., and Li, H. (2009). "A feasibility study of self-heating concrete utilizing carbon nanofiber heating elements." *Smart Materials and Structures*, Vol. 18(12): 127001.

Chen, S. and Lamanna, M. (2006). *Control of blowing snow using SnowMan (Snow Management): User manual*. New York State Department of Transportation. Albany, NY.

Cuelho, E., Harwood, J., Akin, M., and Adams, E. (2010). "Establishing best practices of removing snow and ice from California roadways." *Research report*, California Department of Transportation. Sacramento, CA.

CTC & Associates (2009). "Anti-icing in winter maintenance operations: Examination of research and survey of state practice." *Research report*, Minnesota Department of Transportation. St. Paul, MN.

CTC & Associates (2010). "Multiple-blade snowplow project." *Final report*, Wisconsin Department of Transportation. Madison, WI.

CTC & Associates (2011). "Snow and ice control at extreme temperatures." *Research report*, Wisconsin Department of Transportation. Madison, WI.

Dahlen, J., and Vaa, T. (2001). "Winter friction project in Norway." *Transportation Research Record*, Vol. 1741: 34-41

Derwin, D., Booth, P., Zaleski, P., Marsey, W., and Flood Jr., W. (2000). "Snowfree®, heated pavement system to eliminate icy runways." *SAE Technical Paper Series. Report No.* 2003-01-2145. Warrendale, PA.

Fay, L., and Shi, X. (2011). "Laboratory investigation of performance and impacts of snow and ice control chemicals for winter road service." *ASCE Journal of Cold Regions Engineering*, Vol. 25(3): 89-114.

Fay, L., and Shi, X. (2012). "Environmental impacts of chemicals for snow and ice control: State of the knowledge." *Water, Air & Soil Pollution*, Vol. 223: 2751–2770.

Fu, L., Trudel, M., and Kim, V. (2009). "Optimizing winter road maintenance operations under real-time information." *European Journal of Operational* Research, Vol. 196(1): 332–341.

Hiroshi, T., Nobuhiro, T., and Nobuo, K. (1998). "Development of highway snow melting technology using natural energy." *Proceedings of the 10th PIARC International Winter Road Congress*. Lulea, Sweden.

Hopstock, D., and Zanko, L. (2005). "Minnesota taconite as a microwave-absorbing road material for deicing and pothole patching applications." *Research report*, Center for Transportation Studies, University of Minnesota. Minneapolis, MN.

Janke, G.A. and Johnson Jr., W.D. (1997). "Deicing composition and method." *US Patent No. 5*,635,101.

Johnson, G. (2006). "Smart roads can de-ice itself: Pavement overlay releases chemical in bad weather." *The Calgary Herald*. Calgary, Canada.

Klein-Paste, A. and Sinha, N.K. (2007). "Study of warm, pre-wetted sanding method at airports in Norway." *Transport Canada*. Ontario, Canada.

Lannert, R.G. (2008). "Plowing wider and faster on 21st-century highways by using 14-ft front plows and trailer plows effectively." *Seventh International Symposium on Snow Removal and Ice Control Technology*. Indianapolis, IN.

Levelton Consultants (2007). "Guidelines for the selection of snow and ice control materials to mitigate environmental impacts." *Research report*, National Cooperative Highway Research Program, National Research Council. Washington, D.C.

Long, H.W. et al. (1995). "Asphaltic Compositions and Uses Therefor." *US Patent* No.5, 441,360.

Luker, C., Rokosh, B., and Leggett, T. (2004). "Laboratory melting performance comparison: Rock salt with and without pre-wetting." *Transportation Research Circular Number E-C063*. *Proceedings of the Sixth International Symposium on Snow Removal and Ice Control Technology*. Spokane, Washington.

Lysbakken, K. R., and Stotterud, R. (2006). "Prewetting salt with hot water." *PIARC XII International Winter Roads Congress*. Torino, Italy.

Macfarlane, D. (2001). "Plow truck with reversible plow and wing." American Public Works Association. *APWA Reporter*, Vol. 68(10): ---.

Morita, K. (2000). "Operational characteristics of the Gaia snow-melting system in Ninohe, Iwate, Japan." *Research report*, National Institute for Resources and Environment. Tokyo, Japan.

Ohio DOT (2011). "Snow & ice practices." *Research report*, Ohio Department of Transportation. Columbus, OH.

O'Keefe, K., and Shi, X. (2005). "Synthesis of information on anti-icing and pre-wetting for winter highway maintenance practices in North America." *Research report*, Pacific Northwest Snowfighters Association in Collaboration with the Washington State Department of Transportation. Olympia, WA.

Perchanok, M. (2008). "Making sand last: MTO tests hot water sander." *Road Talk*, 14(2): ---.

Perchanok, M., Fu, L., Feng, F., Usman, T., McClintock, H., Young, J., and Fleming, K. (2010). "Snow and ice control: Guidelines for materials and methods." *2010 Annual Conference of the Transportation Association of Canada*. Halifax, Nova Scotia.

Santiago-Chaparro, K.R., Chitturi, M., Szymkowski, T., and Noyce, D.A. (2012). "Evaluation of the performance of AVL and TowPlow for winter maintenance operations in Wisconsin." *Transportation Research Record*, Vol. 2272: 136–143.

Seo, Y., Seo, U., Eum, J., and Lee, S.-J. (2011). "Development of a geothermal snow melting system for highway overlays and its performance validations." *Journal of Testing and Evaluation*, Vol. 39(4): 1-11.

Shi X, O'Keefe K, Wang S, and Strong C. (2007). "Evaluation of Utah department of transportation's weather operations/RWIS program: Phase I." *Research report*, Utah Department of Transportation. Salt Lake, UT.

Shi, X., Fay, L., Yang, Z., Nguyen, T.A., and Liu, Y. (2009). "Corrosion of deicers to metals in transportation infrastructure: Introduction and recent developments." *Corrosion Reviews*, Vol. 27(1-2): 23-52.

Shi, X., Fay, L., Peterson, M.M., and Yang, Z. (2010a). "Freeze-thaw damage and chemical change of a portland cement concrete in the presence of diluted deicers." *Materials and Structures*, Vol. 43(7): 933-946.

Shi, X., Liu, Y., Mooney, M., Berry, M., Hubbard, B., and Nguyen, T.A. (2010b). "Laboratory investigation and neural networks modeling of deicer ingress into Portland cement concrete and its corrosion implications." *Corrosion Reviews*, 28(3-4): 105-153.

Shi, X., Fortune, K., Smithlin, R., Akin, M., and Fay, L. (2013). "Exploring the performance and corrosivity of chloride deicer solutions: Laboratory

investigation and quantitative modeling." *Cold Regions Science and Technology*, Vol. 86: 36-44.

Strong, C.K., Z. Ye, and Shi, X. (2010). "Safety effects of winter weather: The state of knowledge and remaining challenges." *Transport Reviews*, Vol. 30(6): 677-699.

Staples, J.M., Gamradt, L., Stein, O., and Shi, X. (2004). "Recommendations for winter traction materials management on roadways adjacent to bodies of water." *Research report*, Montana Department of Transportation. Helena, MT.

Strong, C., and Fay, L. (2007). "RWIS usage report." *Research report*, Alaska Department of Transportation and Public Facilities. Juneau, AK.

Strong, C., and Shi, X. (2008). "Benefit-cost analysis of weather information for winter maintenance: A case study." *Transportation Research Record*, Vol. 2055: 119-127.

Switzenbaum, M. S., Veltman, S., Mericas, D., Wagoner, B., and Schoenberg, T. (2001). "Best management practices for airport deicing stormwater." *Chemosphere*, Vol. 43(8): 1051-1062.

Tatarniuk, C., Donahue, R., and Sego, D. (2009). "Freeze separation of salt contaminated melt water and sand wash water at snow storage and sand recycling facilities." *Cold Regions Science and Technology*, Vol. 57(2): 61-66.

Transportation Association of Canada (2003). *Synthesis of best Practices: Road salt management*. Chapter 8. Snow storage and disposal. Transportation Association of Canada. Ontario, Canada.

Vaa, T., and Sivertsen, A. (2008). "Winter operations in view of Vision Zero." Transportation Research Circular Number E-C126. *Surface Transportation Weather and Snow Removal and Ice Control Technology: Fourth National Conference on Surface Transportation Weather and Seventh International Symposium on Snow Removal and Ice Control Technology*. Indianapolis, IN.

Yang, H., and Ying, Z. (2010). "Discover the causes of road hazards in blowing and drifting snow climate and design highway embankment cross section." In *Proceedings of the Second International Conference on Computational Intelligence and Natural Computing Proceedings (CINC),* Vol. 1: 361-364.

Yang, T., Yang, Z. J., Singla, M., Song, G., and Li, Q. (2011). "Experimental study on carbon fiber tape–based deicing technology." *Journal of Cold Regions Engineering*, Vol. 26(2): 55-70.

Yasukawa, I. (2007). "Direct use of geothermal energy in Japan." *The 12th Annual Eastern Snow Expo*. Columbus, OH.

Ye, Z., Shi, X., Strong, C.K., and Greenfield, T.H. (2009a). "Evaluation of the effects of weather information on winter maintenance costs." *Transportation Research Record*, Vol. 2107: 104-110.

Ye Z, Strong C, Fay L, and Shi X. (2009b). *Cost benefits of weather information for winter road maintenance*. Iowa Department of Transportation. Des Moines, IA.

Yehia, S., and Tuan, C.Y. (1999). "Conductive concrete overlay for bridge deck deicing." *ACI Materials Journal*, Vol. 96(3): 382-391.

Yehia, S., Tuan, C.Y., Ferdon, D., and Chen, B. (2000). "Conductive concrete overlay for bridge deck deicing: Mixture proportioning, optimization, and properties." *ACI Materials Journal,* Vol. 97(2): 172-181.

Zhang, J., Das, D.K., and Peterson R. (2009). "Selection of effective and efficient snow removal and ice control technologies for cold-region bridges." *Journal of Civil, Environmental, and Architectural Engineering*, Vol. 3(1): 1-14.

Potential Deicer Effects on Concrete Bridge Decks: Developing Exposure Maps

Jing Gong[1], Jiang Huang[2], Shaowei Wang[3], P.E., Steve Soltesz[4], and Xianming Shi[5], M. ASCE, P.E.

[1] Associate Professor, School of Civil Engineering and Architecture, Wuhan Polytechnic University, Wuhan 430023, China; gongjingshao@163.com
[2] Research Associate, Western Transportation Institute, P.O. Box 174250, Bozeman, MT 59717-4250; jiang.huang@coe.montana.edu
[3] Principal, ITSNode LLC, 4520 Glenwood Dr., Bozeman, MT 59718; swang@itsnode.com
[4] Research Engineer, Oregon Department of Transportation, Research Unit, 200 Hawthorne SE, Suite B-240, Salem, Oregon 97301-5192; Steven.M.Soltesz@odot.state.or.us
[5] Research Professor/Program Manager, Civil Engineering Department and Western Transportation Institute, Montana State University, P.O. Box 174250, Bozeman, MT 59717-4250; xianming_s@coe.montana.edu

ABSTRACT: The use of ice control chemicals has become a crucial tool in providing a reasonable level of service on wintery roadways. Yet, there is little research on how the durability of concrete decks in cold climate might be affected by their exposure to deicers. This work presents a streamlined method of developing exposure maps that can be used to better understand the potential effects that deicer usage and other relevant variables may have on an agency's concrete infrastructure. Using the Oregon Department of Transportation (ODOT) as a case study, this work started with a survey of two relevant stakeholder groups, followed by the collection of relevant data for developing exposure maps for 12 selected representative ODOT concrete bridge decks. Some issues with data availability and quality were identified. It is recommended that deicer type and application rates, traffic volume, climatic conditions, and concrete mix design and rehabilitation data should be documented into an integrated deck preservation program, or be added to the existing bridge management systems. The inventory of such data would ultimately enable the agency to examine the role of various factors in the premature deterioration of its concrete bridge decks.

INTRODUCTION

There are multiple dimensions to the use of chemicals for snow and ice control on roadways. These chemicals, referred to as deicers, are important tools used by roadway agencies to maintain a reasonably high level of service during wintery weather, as there are substantial implications in highway safety, reliability, and mobility (Qiu and Nixon 2008, Usman et al., 2010, Shahdah and Fu, 2010, Strong et

al. 2010, Ye et al. 2013). Yet, there have been growing concerns over the potential negative effects of such chemicals on the natural environment, transportation infrastructure and motor vehicles (Ramakrishna and Viraraghavan 2005, Spragg et al. 2011, Fay and Shi 2011, 2012, Pan et al. 2008, Shi et al. 2009a, 2010a, 2012, 2013, Özgan et al. 2013). The U.S. spends approximately $2.3 billion annually to keep highways free of snow and ice, and the associated corrosion and environmental impacts add at least $5 billion to that cost (FHWA 2005). The corrosive effect of chlorides-based deicers on embedded steel reinforcement is well-known (Jang et al 1995, Shi et al. 2010b). Existing laboratory research also suggested that chloride deicers may have detrimental effects on concrete through their reactions with cement paste and/or aggregates and thus reduce concrete integrity and strength (Neville 1995, Shi et al. 2009b).

Accumulative studies have been conducted in the laboratory setting, often in an accelerated manner, which reported the physicochemical deterioration of concrete as a function of deicer type and test protocol (Sutter et al. 2008, Shi et al. 2010a, 2011, Fay and Shi 2011). These results illustrate the complexity of this concrete durability issue and suggest that there are more than one mechanisms at work. Thus far, there is little research on how the durability of concrete decks in cold climate might be affected by their exposure to the deicers. The exposure to deicers at a specific site may depend not only on application frequency but also on deicer type, environmental and traffic conditions. Hong and Hooton (1999) revealed that "a good relationship exists between the depth of (sodium) chloride penetration and the square root of the number of (wet/dry) cycles". It remains unclear whether the chemical or physical attack of ice control chemicals would lead to significant degradation of concrete infrastructure in the field environment, where the deicer/concrete interactions are complicated by many other factors at play. In order to isolate the effect of a single factor (e.g., deicer exposure) on the durability of concrete, groundwork is needed to establish a framework under which the relevant data can be identified, collected, integrated, and made ready for subsequent analyses.

In this context, this work presents a streamlined method of developing exposure maps that can be used to better understand the potential effects that deicer usage and other relevant variables may have on an agency's concrete infrastructure. The Oregon Department of Transportation (ODOT) was used as a case study to illustrate the processes, elements, and challenges in developing exposure maps.

METHODOLOGY

This work started with a survey of two relevant stakeholder groups, the ODOT winter maintenance managers and the ODOT bridge managers. The survey helped to achieve a high-level understanding of the current and past practices of ODOT practitioners in managing their winter roads and concrete bridge decks. Subsequently, a process was established to selected decks that would represent the population of ODOT concrete bridge decks with various levels of age, winter severity (deicer usage), and traffic volume. Finally, relevant data were collected to develop the exposure maps for 12 selected representative ODOT concrete bridge decks. These include: the recent annual Average Daily Traffic (ADT) data and the percent of truck

traffic; the number of freeze/thaw cycles estimated using the historical air temperature data from a nearby weather station; the bridge category, concrete mix design, and deck rehabilitation information from the ODOT bridge management system; the accumulative or annual deicer usage data from past winter season(s), and the annual precipitation total. Ultimately, a graphic information system (GIS)-based map showing the estimated amount of deicers used on the selected ODOT concrete bridge decks (along with the other key parameters) was developed.

Bridge Deck Selection Process

To describe how specific bridge decks were selected for exposure maps, a guideline along with a flowchart (FIG. 1) is provided in this section. In this case study, the deck selection avoided the coastal districts where chlorides from the marine environment may reach the deck and compromise the role of deicer-borne chlorides in the investigation. Decks without nearby weather station and decks that have been rehabilitated with a polymer sealer or microsilica overlay were also avoided, as the investigation focused on the effects of deicers on the PCC decks themselves.

By using the ArcGIS (or any other GIS software), a bridge geo-database was created to include the shape files of: ODOT maintenance districts, highway functional classification, concrete bridges, and road weather information system (RWIS)/MesoWest weather stations, each with the required attributes available. Then, the bridge deck selection process was initiated, following the steps detailed below.

Firstly, the ODOT maintenance districts were selected based on their geolocation and winter severity. Specifically, the districts along the coastal line were eliminated from the selection, so as to avoid the possible effect of marine-borne chlorides. Then, the remaining districts were grouped into low or high winter severity, based on their estimated deicer usage from past winter seasons. In this case study, this information was obtained from the survey of winter maintenance managers.

Secondly, the bridge decks were further sub-grouped by the bridge age. Specifically, for the list of low-winter-severity concrete bridges, they were categorized according to their built year: 1996-2011, 1981-1995, and before 1980. This generated three table lists and their associated files. The same approach was applied to the list of high-winter-severity concrete bridges. Therefore, a total of six table lists and shape files were generated.

Thirdly, the bridge decks were further sub-grouped by the annual ADT. Specifically, the bridges within the aforementioned six lists were categorized based on its most recent annual ADT value. The cutoff level was set to 10,000. In the end, a total of 12 table lists and shape files were generated to group the ODOT concrete bridge deck population into 12 categories.

Fourthly, in each of the 12 categories mentioned above, only the bridges within 10-mile radius of a RWIS or MesoWest weather station were selected. Only one bridge was randomly selected from each of the 12 groups of remaining bridges. If the deck was overlaid with microsilica or rehabilitated with a polymer sealer, then it was eliminated and another random selection from the group was conducted. In the end, a total of 12 concrete bridge decks were selected, each representing one category of the ODOT concrete bridge deck population.

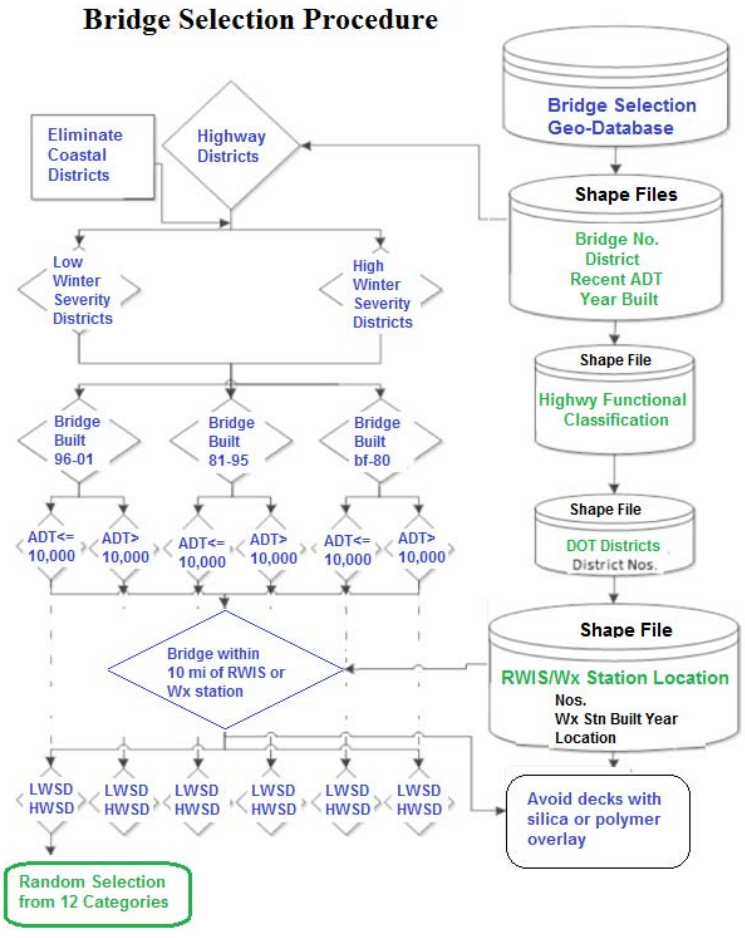

FIG. 1. The Bridge Selection Procedure in a Flowchart

Data Collection for the Exposure Map Development

For developing the exposure maps to fully illustrate the factors that might have played a significant role in the properties and durability of ODOT concrete bridge decks, a wide array of data elements was collected for each specific bridge site, as detailed in this section. The bridge mix design, ADT, and other relevant bridge data were obtained from the ODOT bridge management system. For some agencies, the deicer usage data may be available from their maintenance management system. For this case study, the deicer usage data were not available in any digital form; instead, paper records were sorted before it was possible to estimate the amount of deicers used on the selected decks over the past winter seasons.

The number of annual freeze/thaw cycles for the selected bridge decks was estimated by dividing the number of times the ambient air temperature crossed the 0ºC (32ºF, freezing point of moisture) threshold by two. It is based on the fact that the surface temperature of bridge decks usually tracks the ambient air temperature more closely than do the adjacent roadway pavements (Roosevelt 2004). In this case study, hourly and sub-hourly historical air temperature data from a nearby weather station were utilized for estimating the number of annual freeze/thaw cycles. This approach is different from how hourly air temperature data from weather stations were utilized to determine the number of freeze/thaw cycles in the new mechanistic empirical pavement design guide (MEPDG) developed by the American Association of State Highway and Transportation Officials (AASHTO). In the latter case, a heat balance equation is used to simulate the freeze/thaw conditions in the pavement as a function of time (Zapata et al., 2007).

RESULTS AND DISCUSSION

Stakeholder Perspectives: Winter Maintenance Managers

The 2011 winter maintenance survey was designed and distributed to understand the ODOT current and past winter maintenance practices in managing their winter highways. The ODOT is presently divided into five geographic regions with 16 maintenance districts. Each maintenance district has developed its own strategies to address the needed level of service for their winter highways. Eight out of the sixteen districts responded to this survey, which resulted in a 50% response rate.

All the participating districts were using chemicals for anti-icing and deicing. With the exception of one district (D2B), seven out of the eight districts had used anti-icing as well as deicing for over ten years. Only one district (D10) used pre-wetting for less than ten years, while the other seven districts did not use pre-wetting at all. The primary chemical type used in all these eight districts was $MgCl_2$. Six of the eight districts reported a change in the type of chemical used in the past years. Some ODOT districts had used calcium magnesium acetate (CMA), until they successfully switched to the use of $MgCl_2$ over the past five to ten years. One district (D10) used CMA both in liquid and solid forms during 1998 to 2001, which did not work well with the colder climate; as such a transition to $MgCl_2$ was made in 2002. All eight ODOT districts had observed an increased usage of chemicals and attributed this change to the following facts: better understanding of advantages of the chemicals over sanding, higher level of service expectations, higher traffic volumes, and colder weather.

Most winter maintenance managers (seven out of the eight districts) did not consider chloride deicers to pose a significant risk or negative impact on the durability of concrete bridge decks. Only one district (D2B) reported moderately negative effect observed for concrete pavement and bridge decks. Most districts had observed little negative effect of ice control chemicals on the asphalt concrete or PCC pavements or concrete bridge decks.

Stakeholder Perspectives: Bridge Managers

The 2011 bridge management survey was designed and distributed to understand the ODOT current and past winter maintenance practices in managing their concrete bridge infrastructure. The ODOT bridge managers oversee the design, construction, operation, and maintenance of the bridges located in the State of Oregon highway system using a centralized bridge management system. They regularly conduct inspections, assessment of condition and strength, repairs, and rehabilitation. As such, the bridge managers of the ODOT headquarters, Region 3, Region 4, and Region 5 were approached to achieve a high-level understanding of ODOT bridge management practices, with a focus on the potential effects of deicer exposure and freeze-thaw cycling on bridges decks. Among the five ODOT construction regions, Regions 1 and 2 did not respond to the survey as they featured mostly mild climate and rarely used deicers except on mountain passes.

The bridge managers were asked about which external factors influenced the premature deterioration of concrete bridge decks in Oregon, including cracking, spalling, delamination or other forms of deterioration related to the concrete itself and/or rebar corrosion. A majority of ODOT bridge managers responded that freeze-thaw damage and chloride deicers contribute to the premature deterioration of ODOT bridge decks, while a consensus could not be reached on the level of influence posed by the chloride deicers. In addition, cracking caused by traffic loading, natural calamities (earth quake, fire, storm surge, flood, and excessive rain), spalling, and tire studs were also considered as external factors that contributed to the premature deterioration of ODOT bridge decks.

The ODOT bridge managers had started to consider chloride contamination as a factor in influencing the decision making for the maintenance, repair, and rehabilitation of bridge decks. In addition, the ODOT had changed the guidelines for concrete design and construction practices for concrete decks in the effort to prevent their premature deterioration.

A Method of Developing Exposure Maps: ODOT Case Study

The results from the aforementioned ODOT surveys revealed a discrepancy in the perceived risk of chloride deicers to concrete bridge decks, between the winter maintenance managers and the bridge managers. This highlighted the need for a systematic study to investigate this issue, as it has lasting economic and environmental implications. Using the ODOT as a case study, this section presents a streamlined method of developing exposure maps that can be used to better understand the potential effects that deicer usage and other relevant variables may have on an agency's concrete infrastructure.

Bridge Selection: A total of 12 categories were identified through the bridge selection process described earlier (FIG. 1). Then one representative concrete bridge deck from each identified category was selected to showcase the methodology of developing exposure maps.

Mix Design Data: The mix design of concrete plays a crucial role in their performance and durability in the service environment. As such, this is an important data set for investigating the premature deterioration of concrete bridge decks. A

typical mix design provides information on concrete proportioning (type and amount of cement and mineral admixtures; gradation, absorption and amount of fine and coarse aggregates; water-to-cement ratio) and properties of fresh concrete (slump and air content) and hardened concrete (density and compressive strength).

ADT Data: The most recent annual ADT data were obtained from the ODOT bridge management system. In addition, the data on the percent of (heavy) truck traffic in the ADT were collected, which do not include vans, pickup trucks, or other light delivery trucks.

Availability of Deicer Usage Data: Complete records of ice control chemical applications were necessary to assess the relative level of deicer exposure for a given concrete deck. In this case study, manually recorded daily deicer rate data along with the relevant air temperature data were collected, and then quality-controlled to calculate the annual deicer application rate total for each bridge site. The ODOT deicer usage data were only available in daily records and in paper form, ranging from fiscal year (FY) 2005 to FY2011. The deicer most commonly used by the ODOT was shown to be magnesium chloride and it is still used exclusively statewide from FY2006. The log had application date/time, application rate (gallons/lane mile), pavement condition, and air temperature by the time of application recorded.

Quality of Deicer Usage Data: Proper chemical application rates for snow and ice control vary as a function of the pavement temperature characteristics and the type and volume of precipitation as well as the target level of service and the traffic volume. Application rates are determined by the current road conditions as well as the anticipated weather and road conditions, as stated by Martinez and Poecker (2006). According to the ODOT survey results, typical application rates for anti-icing and deicing ranged from 15 to 50 gallons per lane mile. As such, a preliminary range check was made to identify the extreme values for further examination. Less than 1% of the data were found problematic. Suspect values were then identified manually, and several approaches were employed to verify the values. For instance, the high application rates (e.g., 60 gallons/lane mile) might occur before a large snow event or freezing rain. When the air temperature was slightly below 32^{o}F, there could often be wet snow, sleet, freezing rain, or a mix of all; in such worst icing conditions, the value for daily application rate might go up as needed. When the air temperature was very cold (e.g., below 19^{o}F), the ice/snow was less slick and the traction could be better, hence requiring lower application rates of chemicals. Once validated, the daily application rate data were summarized to obtain the total deicer usage for each winter season.

Infilling the Missing Deicer Usage Data: In this case study, a large number of missing deicer usage data occurred for four of the 12 selected bridge sites. These four bridges had six out of eight years' deicer usage data missing. Under the assumption that all bridges were treated with $MgCl_2$ liquids since FY2006, incompleteness of the data would be a major barrier before a complete picture of deicer use on these bridge decks could be obtained. To address this challenge, the district level deicer usage data were obtained from the ODOT maintenance management system, from FY2000 to FY2011. The districts of concern were Districts 2B, 8, 12, and 13. These data were employed to determine the temporal trends of $MgCl_2$ use by these ODOT Maintenance Districts.

Assuming that the temporal evolution of application rates on specific bridge decks followed the district-level trend, the deicer usage data for the missing years were infilled from the data from the existing years. Note that the chemical application rates are site-specific and depend on a variety of factors including type of deicer used, air and pavement temperatures, amount of snow on the ground, and steepness of the roadway (Fischel 2001). As such, the district deicer usage data should be considered as correlated information and not a statistical representation for the bridge site's actual deicer usage.

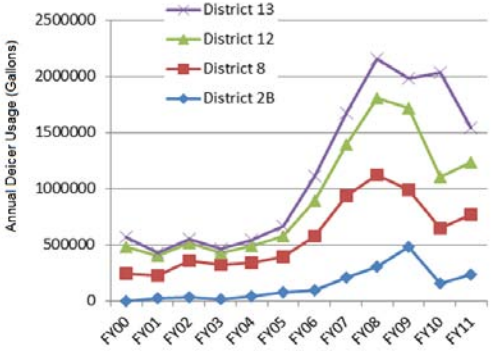

FIG. 2. Annual Deicer Usage Data for the ODOT District 13, 12, 8 and 2B

Freeze/Thaw Cycles Data: Yet another influential factor is the number of freeze/thaw cycles that bridge decks were exposed to. The freeze/thaw cycling can pose a significant risk to the durability of concrete bridge decks, as such cycling can lead to the physical deterioration of the concrete microstructure (Shi et al. 2009b).

The severity of freeze/thaw exposure varies with different areas of Oregon. In this case study, a total of nine MesoWest weather stations were close enough to the 12 selected bridge sites. Over a period of eleven years, more than 2.5 million records of historical air temperature data were collected from these weather stations. The reporting frequencies for these air temperature sensors were every 10, 15 or 20 minutes. The amount of missing data for all these selected weather stations was less than 5%.

Table 1 presents the summary of freeze/thaw cycles data of all the 12 bridges from FY2005 to FY2011. To align with the other ODOT data, the freeze/thaw cycles data were estimated for each fiscal year. Based on the results, the freeze-thaw cycles tend to increase dramatically for areas with higher elevation (>1000 feet). For a missing winter season, the data could be infilled by the values calculated from a similar winter. More data and research would be warranted to potentially establish the annual number of freeze/thaw cycles as a function of geolocation (latitude, longitude, elevation). If such a function was established, it would greatly facilitate the infilling of missing data for a given bridge site with known geolocation.

Note that this method of using ambient air temperature to estimate the number of freeze/thaw cycles has its own caveats. It tends to substantially overestimate the actual number of freeze/thaw cycles that occurred inside the concrete, especially

when the presence of deicer solution significantly reduced the freezing point temperature of the pore solution.

Table 1. Estimated Freeze/thaw Cycles for Fiscal Years 2005 – 2011

Bridge No.	Elev. (ft)	2005	2006	2007	2008	2009	2010	2011
576	1290	NA	NA	57	61	28	32	48
08958F	270	18	18	13	17	14	9	13
8682	1491	39	37	49	79	76	54	55
09268S	270	4	18	13	17	14	9	13
16844	915	NA	NA	52	60	41	22	49
16358	270	4	18	13	17	14	9	13
16440	190	82	85	85	101	85	81	71
16534	270	4	18	13	17	14	9	13
18525	1360	38	60	49	66	70	47	23
18940	100	15	33	29	22	20	13	19
19268	1700	65	69	74	96	89	47	71
19681	2900	143	123	121	155	125	100	117

Bridge Deck Exposure Maps: The exposure map for FY2011 was developed to provide a snapshot of the statewide exposure conditions for the 12 selected ODOT decks (see FIG. 3). The underlying data structure was composed of bridge geolocation (latitude, longitude, and elevation), built year, category, ADT along with percent truck traffic, annual deicer usage in gallons per lane mile, and estimated annual number of freeze/thaw cycles, as well as annual precipitation total.

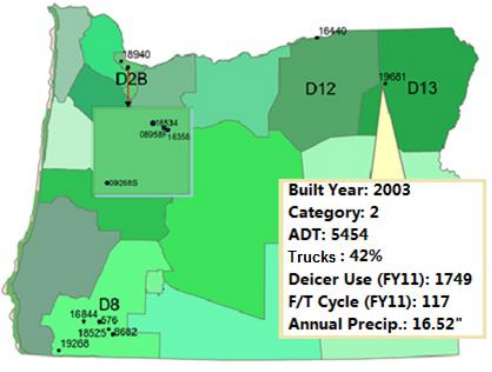

FIG. 3. FY2011 Exposure Map for the 12 selected ODOT Bridge Decks

CONCLUDING REMARKS

Anti-icing strategy with $MgCl_2$ liquids has been widely used by ODOT districts and is believed to be very successful by participating winter maintenance survey respondents. Usage of ice control chemicals has generally been increasing during the past ten years due to colder weather, higher traffic volumes and higher level of service. This trend seems to be continuing and has raised some concerns regarding its negative effects on existing highway infrastructure. Nonetheless, the vast majority of the participating ODOT winter maintenance managers did not think that there has been any significant deteriorating effect of $MgCl_2$ on the ODOT concrete bridge decks. In contrast, a majority of bridge managers believed that freeze-thaw damage and chloride deicers both contribute to the premature deterioration of bridge decks, even though they disagreed on the level of influence.

This study, while focusing on examining the relevant data from Oregon, has demonstrated the general approach that other agencies could implement or adopt in developing exposure maps for their infrastructure. In order to investigate the root cause of premature deterioration of concrete bridge decks in cold climate, it is important to develop their exposure maps over time. Nonetheless, this study has revealed that currently agencies may not have complete and well-defined records of the relevant data. It is highly recommended that deicer type and application rate, traffic volume and truck traffic volume, road weather conditions (deck temperature, air temperature, precipitation, etc.), concrete mix design, and deck maintenance records be archived into an integrated bridge preservation program. Alternatively, such data should be added to the existing bridge management system. The inventory of such data would then enable agencies to investigate the role of such variables in the durability of their concrete bridge decks and potentially alter their approach to winter maintenance operations and/or other practices accordingly.

This work unravels great challenges in data collection. Significant amount of historical air or deck temperature data are required to calculate the number of freeze/thaw cycles. Ideally, more detailed records on precipitation and traffic volumes would also facilitate the understanding of how weather, deicer, traffic, etc. might contribute to the premature deterioration of concrete bridge decks. While beyond the scope of this paper, future study should examine how such exposure maps would facilitate decision-making, once sufficient data become available for data mining and statistical analyses.

ACKNOWLEDGEMENTS

This study was financially supported by the Oregon DOT and the USDOT RITA (via Alaska UTC and Western Transportation Institute). The authors thank the professionals who responded to the surveys and the ODOT engineers (Rick Poecker, Bert Hartman, Erick Cain, Adam Bradford, Susan Mead, Gretchen Harvey, Chad Crockett), as well as other members of the technical panel.

REFERENCES

Fay, L., and Shi, X. (2011). "Laboratory investigation of performance and impacts of snow and ice control chemicals for winter road service." *ASCE Journal of Cold Regions Engineering*, Vol. 25 (3): 89-114.

Fay, L., and Shi, X. (2012). "Environmental impacts of chemicals for snow and ice control: State of the knowledge." *Water, Air & Soil Pollution*, Vol. 223: 2751–2770.

FHWA. (2005). "How do weather events impact roads?" Federal Highway Administration, Washington, D.C.

Fischel, M. (2001). "Evaluation of selected deicers based on a review of the literature." *Research report*, Colorado Department of Transportation. Denver, CO.

Hong, K., and Hooton, R. D. (1999). "Effects of cyclic chloride exposure on penetration of concrete cover." *Cement and Concrete Research*, Vol. 29(9): 1379-1386.

Jang, J. W., Iwasaki, I., Gillis, H. J., and Weiblen, P. W. (1995). "Effect of corrosion-inhibitor-added deicing salts and salt substitutes on reinforcing steels: I. Influence of concentration." *Advanced Cement Based Materials*, Vol. 2(4): 145-151.

Martinez, F., and Poecker, R. (2006). "Evaluation of deicer applications on open graded pavements." *Research report*, Oregon Department of Transportation. Salem, OR.

Neville, A. (1995). "Chloride attack of reinforced concrete: an overview." *Materials and Structures*, Vol. 28(2): 63-70.

Özgan, E., Serin, S., Gerengi, H., and Arslan, İ. (2013). "Multi-faceted investigation of the effect of de-icer chemicals on the engineering properties of asphalt concrete." *Cold Regions Science and Technology*, Vol. 87: 59–67.

Pan, T., He, X., and Shi, X. (2008). "Laboratory investigation of acetate-based deicing/anti-icing agents deteriorating airfield asphalt concrete." *Journal of the Association of Asphalt Paving Technologists (AAPT)*, Vol. 77: 773-793.

Qiu, L., and Nixon, W. A. (2008). "Effects of adverse weather on traffic crashes: systematic review and meta-analysis." *Transportation Research Record: Journal of the Transportation Research Board*, Vol. 2055: 139-146.

Ramakrishna, D. M., and Viraraghavan, T. (2005). "Environmental impact of chemical deicers–a review." *Water, Air, and Soil Pollution*, Vol. 166(1-4), 49-63.

Roosevelt, D. (2004). "Bridge deck anti-icing system in Virginia: Lessons learned from a pilot study." *Research report*, Virginia Transportation Research Council. Richmond, VA. http://www.virginiadot.org/vtrc/main/online_reports/pdf/04-r26.pdf.

Shahdah, U., and Fu, L. (2010). "Quantifying the mobility benefits of winter road maintenance – A simulation based analysis." *TRB 89th Annual Meeting Compendium of Papers DVD. Transportation Research Board. Washington, D.C.*

Shi, X., Fay, L., Yang, Z., Nguyen, T.A., and Liu, Y. (2009). "Corrosion of deicers to metals in transportation infrastructure: Introduction and recent developments." *Corrosion Reviews*, Vol. 27(1-2): 23-52.

Shi, X., Akin, M., Pan. T., Fay, L., Liu, Y. and Yang, Z. (2009b). "Deicer impacts on pavement materials: Introduction and recent developments." *The Open Civil Engineering Journal*, Vol. 3: 16-27.

Shi, X., Fay, L., Peterson, M.M., and Yang, Z. (2010a). "Freeze-thaw damage and chemical change of a Portland cement concrete in the presence of diluted deicers." *Materials and Structures*, Vol. 43(7): 933-946.

Shi, X., Liu, Y., Mooney, M., Berry, M., Hubbard, B., and Nguyen, T.A. (2010b). "Laboratory investigation and neural networks modeling of deicer ingress into Portland cement concrete and its corrosion implications." *Corrosion Reviews*, Vol. 28(3-4): 105-153.

Shi, X., Fay, L., Peterson, M.M., Berry, M., and Mooney, M. (2011). "A FESEM/EDX investigation into how continuous deicer exposure affects the chemistry of Portland cement concrete." *Construction and Building Materials*, Vol. 25(2): 957-966.

Shi, X., Goh, S.W., Akin, M., Stevens, S., and You, Z. (2012). "Exploring the interactions of chloride deicer solutions with nano/micro-modified asphalt mixtures using artificial neural networks." *ASCE Journal of Materials in Civil Engineering*, Vol. 24(7): 805–815.

Shi, X., Fortune, K., Smithlin, R., Akin, M., and Fay, L. (2013). "Exploring the performance and corrosivity of chloride deicer solutions: Laboratory investigation and quantitative modeling." *Cold Regions Science and Technology*, Vol. 86: 36-44.

Spragg, R. P., Castro, J., Li, W., Pour-Ghaz, M., Huang, P. T., and Weiss, J. (2011). "Wetting and drying of concrete using aqueous solutions containing deicing salts." *Cement and Concrete Composites*, Vol. 33(5): 535-542.

Strong, C.K., Z. Ye, and Shi, X. (2010). "Safety effects of winter weather: The state of knowledge and remaining challenges." *Transport Reviews*, Vol. 30(6): 677-699.

Sutter, L., Peterson, K., Julio-Betancourt, G., Hooton, D., Vam Dam, T., and Smith, K. (2008). "The deleterious chemical effects of concentrated deicing solutions on Portland cement concrete." *Research report*, South Dakota Department of Transportation. Pierre, SD.

Usman, T., Fu, L., and Miranda-Moreno, L. F. (2010). "Quantifying safety benefit of winter road maintenance: Accident frequency modeling." *Accident Analysis & Prevention*, Vol. 42(6): 1878-1887.

Ye, Z., Veneziano, D., and Shi, X. (2013). "Estimating statewide benefits of winter maintenance operations." *Transportation Research Record*, Vol. 2329: 17-23.

Zapata, C. E., Andrei, D., Witczak, M. W., and Houston, W. N. (2007). "Incorporation of environmental effects in pavement design." *Road Materials and Pavement Design*, Vol. 8(4): 667-693.

Measuring Fatigue Damages from an Instrumented Pavement Section due to Day-Night and Yearly Temperature Rise and Fall in Desert Land of the West

Rafiqul A. Tarefder[1], M. ASCE, P.E. and Md Rashadul Islam[2], S.M. ASCE

[1]Associate Professor, Dept. of Civil Engineering, University of New Mexico, MSC01 1070, 1 University of New Mexico, Albuquerque, NM 87131, USA; tarefder@unm.edu
[2]Ph.D. Student, Dept. of Civil Engineering, University of New Mexico, MSC01 1070, 1 University of New Mexico, Albuquerque, NM 87131, USA; mdislam@unm.edu

ABSTRACT: This study measures the fatigue damage due to temperature fluctuations and hence, the fatigue life of asphalt concrete using data from an instrumentation pavement section in the desert land of New Mexico for real time climate conditions. As a first step, fatigue life prediction models have been developed for both vehicle and temperature fluctuations based on stiffness and strain of Hot Mix Asphalt (HMA) collected from the instrumentation section located on Interstate 40 (I-40) in New Mexico. In the second step, traffic and thermal strains at the bottom of asphalt concrete are measured by Horizontal Asphalt Strain Gauges (HASGs). In the third step, using these strain values, fatigue damage at the bottom of asphalt concrete is determined. Results show that thermal damage is responsible for 98.2% of total fatigue damage in asphalt concrete. In addition, yearly temperature fluctuation produces greater damage (95.8 % of total damage) than the damage caused by daily temperature variations (2.4% of total damage).

BACKGROUND

Bottom up fatigue cracking (i.e., alligator cracking) in Mechanistic-Empirical Pavement Design Guide (MEPDG) is predicted based on accumulated damage caused by repeated cycles of traffic loading. Since the number of thermal expansion and contraction is small compared to the number of traffic loads, MEPDG does not consider damage due to the thermal load in fatigue cracking calculation of an asphalt pavement. However, thermal damage may be significant and possibly causes premature failure of asphalt pavement especially in zones where diurnal and annual temperature variations are relatively large.

Temperature affects the flexible pavement in two ways. Firstly, the structural responses due to temperature variations changes which is considered by seasonal effects. Secondly, the thermal expansion and contraction due to the day-night and the summer-winter temperature variations which cause low-temperature cracking and thermal fatigue cracking (Jackson and Vinson 1996, Shen and Kirkner 1999).

Thermal cracking has been widely explored since early 1960s and is currently recognized as one of the major failure mechanisms in flexible pavements in MEPDG (Rajbongshi and Das 2009). However, the thermal strain at the bottom of Hot Mix Asphalt (HMA) in a flexible pavement has been neglected till this date. In addition, recently developed Mechanistic-Empirical Pavement Design Guide (MEPDG) predicts fatigue performance of asphalt concrete based on tensile strain at the bottom of asphalt concrete due to repeated traffic loads neglecting thermal strain due to thermal expansion and contraction. The expansion and contraction of HMA is not negligible in areas where day-night temperature variations are relatively large like New Mexico (NM). Bayat and Knight (2010) measured daily strain fluctuations as high as 650 microstrain (μm/m) and yearly strain fluctuations as high as 2544 μm/m per year at the bottom of HMA. These values are vastly greater than vehicle induced strain although these values are dependent on ambient temperature fluctuations, geometry of pavement and mixture design. Therefore, thermal strain though small in number may have significant effect in causing damage to flexible pavement.

The present study for the first time evaluates the effect of thermal damage at the bottom of HMA through laboratory testing and field measured strain value on the instrumentation section on Interstate 40 (I-40) in New Mexico. Stiffnesses of HMA at different period of year were determined by conducting Falling Weight Deflectometer (FWD) test and thermal and vehicle induced transverse horizontal tensile strains (as the transverse horizontal strain is measured 20% greater than the longitudinal one (Islam and Tarefder 2013)) at the bottom of HMA were measured by installed Horizontal Asphalt Gauges (HASGs) from May 2012 to April 2013.

OBJECTIVES AND METHODOLOGY

The main objective of the present study is to evaluate the effect of thermal damage in fatigue life of asphalt concrete in flexible pavement. Specific objectives are mentioned below:

- Predicting fatigue life (and damage) of I-40 pavement due to traffic loads based on laboratory developed fatigue model using the field measured stiffness and counted traffic.
- Determining damage for temperature induced strain at the bottom of HMA using the developed fatigue model for thermal load. Horizontal strains at the bottom of HMA due to both diurnal and annual temperature fluctuations are considered.
- Compare the above determined vehicle and thermal induced damages and evaluate the contribution of thermal strain in fatigue life of asphalt concrete.

To accomplish this, fatigue life of I-40 pavement is predicted for vehicle load only which is the procedure of MEPDG. Then, damages for diurnal and yearly thermal strains are included with vehicle induced damage. The contributions of vehicle, daily and yearly transverse longitudinal horizontal strains in the fatigue damage of HMA were then evaluated.

INSTRUMENTATION SECTION

Layers and Materials

The instrumentation section was used to measure the tensile strain at the bottom of HMA for different axle loads in different periods of the year for both traffic and thermal loads. These values were used in the fatigue life model to predict the allowable number of load repetitions. The section is located on I-40 east bound lane at mile post 141 near the city of Albuquerque in the state of New Mexico, USA. Sensors installation works were conducted in collaboration with National Center for Asphalt Technology (NCAT) at Auburn University and New Mexico Department of Transportation (NMDOT).

The section has four layers. The surface layer is a 300 mm (12 in) thick HMA layer composed of SuperPave (SP), type SP-III mixture with 35% Reclaimed Asphalt Pavement (RAP) materials. Performance Grade (PG) polymer modified binder PG 70-22 was used 4% by weight. The maximum aggregate size was 25 mm (1 in). The base layer is 144 mm (5.75 in) thick and composed of granular crushed stone aggregates and 50% RAP materials. The 200 mm (8 in) thick subbase layer (locally known as Process Place and Compact) was prepared by mixing previous 100 mm thick HMA layer and 100 mm thick base layer.

Sensors Installation

Twelve Horizontal Asphalt Strain Gauges (HASGs) were installed at the bottom of HMA to measure the vehicle and thermal induced horizontal strains. The gauges were installed in the driving lane at the outer wheel path. Six gauges were installed in longitudinal direction and the other six were embedded in transverse direction. Both longitudinal and transverse gauges are identical. Three axle sensing strips were installed to measure the wheel wander and speed of traffic passing through the instrumentation section. The ASSs sensors were installed ahead of the HASGs array. Measuring wheel wander of traffic is essential as small deviation of traffic wheel from the sensors' centerline produces much different in stress-strain responses.

DEVELOPING FATIGUE LIFE MODELS

Sample Preparation

Fatigue Life prediction model has been developed in the laboratory through Beam Fatigue Test following AASHTO T321-07 (2010) test protocol. Plant produced, dense graded SP-III mixture which was used in the reconstruction of the instrumented pavement section was used to prepare beam samples to determine the flexural stiffness and fatigue life. The mix was compacted with kneading compactor at 150 °C (300 °F). Prior to compaction, the mix was oven heated for half an hour at 155 °C (312 °F). Beam slabs of 450 mm (18 in) x 150 mm (6 in) x 75 mm (3 in) were prepared first. Then, each slab was cut into two beams of 380 mm (15 in) x 63 mm

(2.5 in) x 50 mm (2 in) using a laboratory saw. The air voids of the samples ranges 5.1% to 5.6% with an average value of 5.3%.

Beam Fatigue Test

Beam Fatigue tests were conducted only at 20 °C using a negative sinusoidal waveform of 10 Hz with no rest period at different strain levels which are the requirements of AASHTO T 321-07 (2007) test protocol. In future study, the test will be conducted at different temperatures. Negative waveform means the sample is to be forced to its original position at the end of each load pulse. Tests were conducted on fourteen beam samples at seven different strain levels to cover a wide range of horizontal strain that may occur in real pavement. Two beams were tested at each strain level and the average values were used in the analysis. According to the AASHTO T 321-07 test standard, the stiffness at the 50^{th} cycle of loading was considered the initial stiffness and the number of cycles at 50% reduction of initial stiffness was considered the number of load cycles to cause failure of the beam.

Fatigue Model for Vehicle Load

Regression equation was developed based on the tests results. The detailed test results and the model development can be found in the study of Islam and Tarefder (2014). The regression model is presented in Eq. 1 whose coefficient of regression (R^2) is 0.992.

$$N_{fv} = 0.1 \left(\frac{1}{\varepsilon_{tv}}\right)^{5.79} \left(\frac{1}{E}\right)^{2.03} \quad (1)$$

where N_{fv}, ε_{tv} and E are predicted allowable number of load repetitions for vehicle, transverse tensile strain at the bottom of surface layer (m/m) and initial stiffness of the mixture in psi respectively. This model has been used to predict the fatigue life for vehicle loads. Considering the wheel wander and long rest period of vehicle, the field fatigue life is 5 to 700 times (18.4 times by Asphalt Institute) longer than the laboratory predicted fatigue life (Huang 2004). In the present study, no laboratory to field shift factor was assumed to remain more conservative.

Fatigue Model for Thermal Load

Fatigue life model for vehicle load was developed with Beam Fatigue Testing at 10 Hz. However, frequency of thermal load is very low. Usually, it takes 24 hours to complete a daily thermal cycle. No temperature load was applied to develop temperature induced fatigue model. In future studies, actual temperature load will be applied on restrained samples. Thermal expansion and contraction produce thermal stress or strain in the material. This equivalent stress or strain was attained by applying mechanical load in a strain controlled beam fatigue test apparatus. Beam fatigue tests were conducted at three different frequencies (0.15, 5 and 10 Hz) at 1000 με and 20 °C following AASHTO T321-07 test standard with one replicate sample of

each. Allowable numbers of load repetitions at different frequencies of loadings are plotted in Fig. 1. Using this data, the failure cycles for lower frequency (such as, 1.16×10^{-5} Hz for day-night temperature cycle and 3.17×10^{-8} Hz for yearly temperature cycle). It can be observed that at lower frequency the effect of frequency is negligible and number of cycles at failure is close to 3391 (11.3% of that of 10 Hz). Therefore, the developed fatigue model for vehicle is multiplied by a factor of 0.113 to determine the fatigue model for thermal load. This finding agrees with the laboratory finding of Sugawara and Moriyoshi (1984).

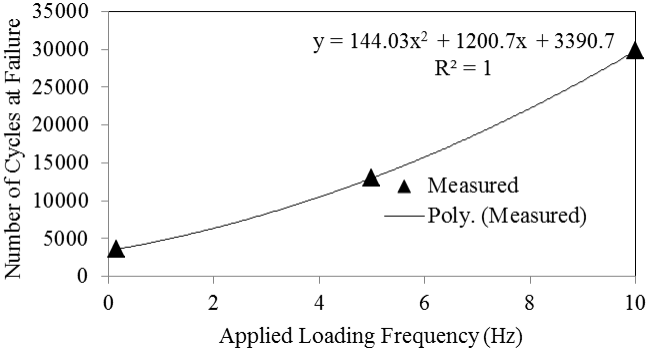

FIG. 1. Variations of allowable load repetitions with frequency of loading for strain level of 1000 με.

The fatigue model for thermal loading is presented in Eq. 2.

$$N_{ft} = 0.113\,[0.1\left(\frac{1}{\varepsilon_{tt}}\right)^{5.79}\left(\frac{1}{E}\right)^{2.03}] \quad (2)$$

where N_{ft}, ε_{tt} and E are predicted allowable number of load repetitions for thermal load, tensile strain at the bottom of surface layer (m/m) and initial stiffness of the mixture in psi respectively.

PREDICTING FATIGUE LIFE

Traffic Load

Fatigue life of I-40 pavement has been assessed through the laboratory developed fatigue model presented in Eq. 1. Note that the HMA mixture used on I-40 pavement reconstruction has also been used in laboratory to prepare samples for developing the fatigue model. Daily traffic loads have been counted for ten days at different times of a day and calculated for the whole year considering no seasonal and wheel wander effect.

Table 1 lists the traffic distribution, measured transverse horizontal strain at the bottom of HMA through the instrumentation section, calculation of damage ratio and fatigue life prediction.

Table 1. Predicting Fatigue Life for Traffic Load

Month	Stiffness (MPa)	Vehicle Loads per Year		
		Single Axle	Tandem Axle	Tridem Axle
		1127694	1517318	23732
		Measured Tensile Strain		
January	9315 (1350 ksi)	35	44	47
February	7935 (1150 ksi)	53.5	67	71
March	6210 (900 ksi)	70.5	91	97
April	4485 (650 ksi)	89	123	123
May	2933 (425 ksi)	113.5	161	156
June	1380 (200 ksi)	142	185	199
July	1518 (220 ksi)	119	156	151
August	2070 (300 ksi)	96.5	141	123
September	3105 (450 ksi)	77	105	99
October	4485 (650 ksi)	57	84	79
November	6210 (900 ksi)	43.5	62	64
December	7935 (1150 ksi)	35	44	47
Measured Fatigue Life (million), $N_{fv} = 0.1\left(\frac{1}{\varepsilon_{tv}}\right)^{5.79}\left(\frac{1}{E}\right)^{2.03}$				
January		2266045	602325	411126
February		268915	73081	52239
March		89510	20419	14108
April		44959	6906	6906
May		26058	3442	4132
June		32897	7111	4661
July		75416	15728	18993
August		135216	15047	33181
September		219380	36416	51197
October		593294	62836	89644
November		1465666	188338	156713
December		3137830	834050	569294
Damage Ratio (D_R)		0.00011793		
Design Life (years)		8479		

The whole year is divided into twelve months (i.e., January to December). Stiffnesses of HMA material at these twelve periods are determined based on routine FWD test. Tensile strain at the bottom of HMA is measured using the strain gauges. MEPDG calculates the tensile strain at the bottom of HMA using linear elastic analysis based on provided traffic load and stiffness. In addition, seasonal variations

in stiffness are predicted based on the input climate data which very often differs from actual construction site. The present study measures the stiffnesses and the tensile strains at the bottom of HMA for different axle loads throughout the year which is much better than MEPDG approach.

Vehicle classes 1-3, defined by Strategic Highway Research Program (SHRP) are discarded following MEPDG recommendation. Monthly average tensile strain for each type of axle load is used to calculate the allowable load repetitions. Damage ratio has been calculated using Eq. 3 (Huang, 2004).

$$D_R = \sum_{i=1}^{p} \sum_{j=1}^{m} \frac{n_{i,j}}{N_{fv,i,j}} \tag{3}$$

where D_R is the damage ratio at the end of a year, $n_{i,j}$ is the predicted number of load repetitions for axle type j in period i, $N_{fv,i,j}$ is the allowable number of axle load repetitions based on Eq. 1 for p being the number of periods in each year (12 in this study) and m being the number axle groups (1-3 in this study). The fatigue design life (D_L) is calculated based on Eq. 4 (Huang, 2004).

$$D_L = \frac{1}{D_R} \tag{4}$$

Using the above discussed procedure vehicle induced damage and fatigue design life is predicted which is presented in Table 1. Number of single, tandem and tridem axle loads are 1.13, 1.52 and 0.024 million respectively. HMA stiffness ranges 1380 MPa (200,000 psi) to 9315 MPa (1350,000 psi) throughout the entire year. Using Eq. 3 and 4, the vehicle induced damage ratio of 0.00011793 and design life of 8479 years are obtained. Though, the fatigue design life seems much greater than the usual value, it is quite reasonable to be so. The test section was over designed to accommodate the probable damage caused by sensors installation.

Vehicle and Thermal Loads

The design life predicted by considering the traffic load does not consider the thermal strain at the bottom of asphalt concrete. Thermal strain at the bottom of HMA has been measured from May 2012 to April 2013. To calculate the damage, the year is divided into twelve periods from January to December and the average value of each month is used in analysis.

Thermal strain fluctuates daily for day-night temperature variations and yearly for summer-winter temperature variations. Both characteristics are considered in this study. The daily and yearly thermal-induced strain fluctuation was calculated using Eqs. 5 and 6 respectively. The definition were proposed by Norman (1999) and supported by several other researchers (Al-Qadi et al. 2005, Bayat and Knight 2010).

$$\Delta\varepsilon\ (daily) = \varepsilon_{max,d} - \varepsilon_{min,d} \tag{5}$$

$$\Delta\varepsilon\ (yearly) = \varepsilon_{max,y} - \varepsilon_{min,y} \tag{6}$$

where $\Delta\varepsilon\ (daily)$, $\varepsilon_{max,d}$ and $\varepsilon_{min,d}$ are the daily thermal induced horizontal strain fluctuation, maximum and minimum horizontal strain at the bottom of HMA (m/m) and $\Delta\varepsilon\ (yearly)$, $\varepsilon_{max,y}$ and $\varepsilon_{min,y}$ are the yearly thermal induced horizontal strain fluctuation, maximum and minimum horizontal strain at the bottom of HMA (m/m) respectively.

Table 2. Determining Thermal Damage due to Daily Temperature Fluctuations

Periods	Stiffness, MPa	Average Thermal Strain (με)
January	9315 (1350 ksi)	254
February	7935 (1150 ksi)	348
March	6210 (900 ksi)	353
April	4485 (650 ksi)	388
May	2933 (425 ksi)	246
June	1380 (200 ksi)	456
July	1518 (220 ksi)	245
August	2070 (300 ksi)	269
September	3105 (450 ksi)	282
October	4485 (650 ksi)	305
November	6210 (900 ksi)	261
December	7935 (1150 ksi)	246
Measured Thermal Fatigue Life, $N_{ft} = 0.113[0.1\left(\frac{1}{\varepsilon_{tt}}\right)^{5.79}\left(\frac{1}{E}\right)^{2.03}]$		
January		2657747
February		594453
March		900224
April		1008158
May		33414475
June		4330929
July		130223322
August		40388395
September		13493192
October		4062265
November		5171512
December		4429427
Damage Ratio, D_R		0.000156654
Design Life (years)		6383

Horizontal strain at the bottom of HMA should be separated for vehicle induced strain and thermal induced strain. If both of these added together to determine envelop of strain it overestimates the damage. The reason is that vehicle produced strain develops at higher frequency of loading and thermal strain at lower frequency.

Fatigue life models for both of these strains are completely different. Therefore, the total damage should be calculated based on Eq. 7.

Total Fatigue Damage = Vehicle induced damage + Daily thermal induced damage + Yearly thermal induced damage (7)

Table 2 lists the results for calculating the thermal damage due to daily thermal fluctuations. The daily minimum and the maximum tensile strains are measured 245 and 456 με respectively. Allowable load repetitions were calculated based on Eq. 2. Using Eq. 3, the daily thermal induced damage ratio of 0.000156654 is obtained. Using Eq. 6 the yearly average strain variation is 1718 μm/m. The allowable load repetition for yearly single cycle thermal load is calculated using Eq. 2. The stiffness of HMA is used the average of twelve months' stiffness. The allowable load repetition and damage ratio for this strain is 159 and 0.0062728 per year respectively.

Vehicle and thermal induced damages are compared as presented in Table 3. Fatigue damage ratios produced by traffic, yearly and daily thermal fluctuations are $1.1x10^{-4}$, $6.3x10^{-3}$ and $1.6x10^{-4}$ respectively. It shows that consideration of thermal load decreases fatigue life from 8479 years (fatigue life for vehicle only) to 152 years.

TABLE 3. Comparisons of vehicle and temperature induced damages

Loads	Damage Ratio (D_R)
Vehicle Only	0.00011793
Yearly Thermal Cycle	0.006272825
Daily Thermal Cycle	0.000156654
Total D_R by Thermal Load	0.00642948
Total D_R	0.00654741
Combined Fatigue Life (year)	152
Comparisons	
Damage by Vehicle	1.8%
Damage by Daily Thermal Fluctuations	2.4%
Damage by Yearly Thermal Fluctuations	95.8%
Total Damage by Thermal Load	98.2%

Table 3 also shows that the thermal load is responsible for 98.2% whereas vehicle produces only 1.8% of total damage. For thermal load, yearly thermal fluctuation is more harmful then daily temperature fluctuation. It can be observed that yearly and daily temperature fluctuations produce 95.8% and 2.4% of total damage respectively. The results presented in this study are based on the developed fatigue model in laboratory and measured stiffness and strain values in field from May 2012 to April 2013. The outcome is dependent of local weather, material and geometry of pavement used. In addition, longer data should be analyzed for better prediction of damages.

CONCLUSIONS

The following conclusions can be made from this study:

- Thermal damage is more critical than vehicle produced damage in fatigue life of asphalt concrete.
- The fatigue service life of I-40 pavement is 8479 years considering vehicle load only whereas considering thermal strain at the bottom of asphalt concrete the design life decreases to 152 years.
- Fatigue damage caused by thermal load is 98.2% whereas vehicle produces only 1.8%. Annual summer-winter temperature fluctuation produces 95.8 % of total damage whereas daily temperature variation causes only 2.4%.

ACKNOWLWDGEMENTS

This project is funded by the New Mexico Department of Transportation (NMDOT). Special thanks go to Dr. David Timm of NCAT, Auburn University for his cooperation in the installation of the sensors on the I-40 pavement in New Mexico.

REFERENCES

AASHTO T321-07. (2007). "Determining the fatigue life of compacted Hot-Mix Asphalt subjected to repeated flexural bending." *Standard Specifications for Transportation Materials and Methods of Sampling and Testing,* 27th Edition. American Association of State Highway and Transportation Officials, Washington, D.C.

Al-Qadi, I., Hassan, M. and Elsefi, M. (2005). "Field and theoretical evaluation of thermal fatigue cracking in flexible pavements." *Transp. Res. Rec.,* No. 1919: 87-95.

Bayat, A. and Knight, M. (2010). "Measurement and analysis of flexible pavement thermal-induced strains." *Transportation Research Board Annual Meeting 2010* Paper #10-3654.

Huang, Y. (2004). *Pavement analysis and design.* 2nd Edition, Pearson Prentice Hall, NJ.

Islam, M. R. and Tarefder, R. A. (2014). "*Comparing Temperature Induced Fatigue Damage to Traffic Induced Fatigue Damage in Asphalt Concrete*." *TRB Annual Meeting 2014*, CD-ROM Paper No. 14-3194.

Islam, M. R. and Tarefder, R. A. (2013). "Evaluating the Longitudinal and the Transverse Horizontal Strains at the Bottom of Hot Mix Asphalt." *International Journal of Scientific and Engineering Research*, Vol. 4, No. 3, pp. 1-5.

Jackson, N. M., and Vinson, T. S. (1996). "Analysis of thermal fatigue distress of asphalt concrete pavements." *Transp. Res. Rec.,* No. 1545:43-49.

Norman, D. (1999). *Mechanical behavior of materials: engineering methods for deformation, fracture, and fatigue.* Prentice Hall, Upper Saddle River, N.J.

Rajbongshi, P. and Das, A. (2009). "Estimation of temperature stress and low-temperature crack spacing in asphalt pavements." *J. Transp. Eng*., 2009, Vol. 135(10):745-752

Shen, W. and Kirkner, D. J. (1999). "Distributed thermal cracking of AC pavement with frictional constraint." *J. Eng. Mech.*, Vol. 125(5):554-560

Sugawara, T. and Moriyoshi, A. (1984). "Thermal fracture of bituminous mixtures." *Proc., Paving in Cold Areas*, Mini-Workshop, Japan: 291–320.

Experimental Study On Evaluation Standard Of Repair Mortar Performance For Rigid Pavement

Jie Yuan[1],Hao Hu[1],Yong Luo[2], Shan Yang[3], Xianzhi Shao[3]

[1] Key laboratory of Road and Traffic Engineering of the Ministry of Education, Tongji University, Shanghai 201804 China;yuanjie@tongji.edu.cn;hhjsu@126.com
[2] Shanghai CAAC New Era Airport Design and Research Institute Ltd 200335 China; dcaacluoyong@yeah.net
[3] China Airport Construction Group Corporation 100101 China

ABSTRACT: The mix proportions of common repair mortar for rigid pavement were recommended for the technical requirements. A series of tests on mechanical properties and volume deformation were undertaken to propose an evaluation criteria of repair mortar performance which could be a technical reference in the industry of rigid pavement repair. It was demonstrated from the results that epoxy resin mortar was excellent in strength, but fatigue resistance and volume deformation were deficient. In addition, sulphoaluminate cement mortar was similar to Portland cement mortar in all performances. Finally, structural and bond strength of phosphate cement mortar were higher compared to others and fatigue resistance and volume deformation were superior.

INTRODUCTION

Many rigid pavements were widely constructed in China during the last century. These pavement structures were influenced by environment seriously. Different decisions were proposed in the selection of proper repair materials due to structural rehabilitation. Among various available pavement materials, repair mortars greatly drew the attentions. There should be some high performance for repair mortars such as sufficient strength in structure and cohesion and small volume deformation under the influence of environment, while durability and workability of them in some small scattered construction were prominent. Therefore, it was essential to choose a relative economical repair mortar.

The test results of Portland and phosphate cement mortar indicated that the latter was 77-120% higher than the former in adhesive bending strength, while 85-180% higher in bond-slip strength (Qiao et al. 2009). Compressive and flexural strength of sulphoaluminate cement mortar were 45.5Mpa and 8.1Mpa respectively 28 days later. Bond strength reached to 4.78Mpa 14 days later (Meng and Ye 2010). Compressive and flexural strength of phosphate cement mortar were 50Mpa and 9.1Mpa respectively 3 days later and the shrinkage rate of it was below 2.89×10^{-4} which indicated that phosphate cement mortar was available in pavement rapid repair (Deng et al. 2011).

However there are few evaluation standards of repair mortar performance for

rigid pavement which hampers the selection of suitable repair mortar. In general, structural strength must be an evaluation index of mending materials for rigid pavement. Besides, bond strength and volume deformation are so important performance indexes for repair mortar that drew particular attention in the research. In this paper, a number of characteristics such as mechanical properties, bond strength and volume stability were measured by the experiments to study the performance of these four kinds of common repair mortars

MATERIALS AND MIX PROPORTION

52.5 Portland cement, sulphoaluminate cement and phosphate cement were obtained from Guangxi Huarun cement co., LTD, Shanghai ShuangHe special cement co., LTD and Hangzhou Zhonggang construction engineering co., LTD respectively. In addition, epoxy resin mortar consists of E-51 epoxy resin, SM593 curing agent and butyl glycerin shrink ethers diluter. Sand which was adopted conforms with Nation Standards (*GB178-77*) while crushed aggregate was marble ranged from 5 to 10mm.

After some admixture added and component ratio of repair mortar adjusted, the mix proportions of repair mortars were proposed by considering the development of strength, workability and economics in Table 1.

Table 1.Mix proportions of Repair Mortars

Portland cement mortar	Fine aggregate	Portland cement	Water	Water reducing agent		Accelerator	
				Type	Ratio	Type	Ratio
	3	1	0.4	Naphthalene	0.8%	$CaCl_2$	2%
Phosphate cement mortar	Fine aggregate		Phosphate cement		Fly ash	Water	
	1		0.8		0.2	0.12	
Sulphoaluminate cement mortar	Fine aggregate	Sulphoaluminate cement		Water	Water reducing agent		
					Type	Ratio	
	3	1		0.4	naphthalene	0.8%	
Epoxy resin mortar	Epoxy resin	Curing agent		Diluter	Quartz sand	Fly ash	
	100	30		10	400	200	

EXPERIMENTS AND TESTS

The flexural and compressive strength tests consulted *Method of testing cements-determination of strength (ISO)GB/T17671–1999*）, the flexural bond test refer to *Technical maintenance guidelines of civil airport pavement*, the drying shrinkage test to *Stand test method for drying shrinkage of mortar*（*JC/T 603-2004)* . And other experiments are as follows.

Experiment of Pull-off Bond

The pull-off bond test was employed to evaluate the bond strength between the repair mortar and concrete. The test setup was presented in FIG.1. The interface

between concert and mortar can reflect the bonding status.

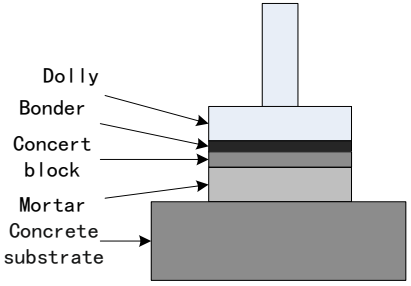

FIG. 1. Experimental Setup of Pull-off Bond Strength

The mix proportion of concert block and the concrete substrate was prepared with cement(whose strength grade is 42.5 according to ENV197-1-95), water, sand, and crushed aggregate by 1:0.5:1.65:3.08 (in weight).The cast substrate slab was prepared with a size of 40×40×4cm3 with the help of layered casting. 5/6 of the base layer thickness must be prepared before casting the remaining 1/6 of the surface layer thickness with 1 ‰ of cement of retarder citric acid sodium. Then, the surface concrete would be washed 10 hours later. Subsequently, the cast substrate slab was kept in curing room for at least 28 days. Before casting mortar over surface of substrate, the surface must be roughened by using a steel wire brush which was shown in FIG.2. In addition, the concert blocks were pieced as a size of 40mm×40mm×5mm from prism specimens of 4mm×4mm×16mm as shown in FIG.3.

The dolly shown in FIG.4 was made of stainless steel with a size of 45mm×45mm×20mm. It was bonded with concert block by the binder that was prepared with 618 epoxy, 593 curing agent and fly ash by 100:30:300. Meanwhile, flexible silica gel plate fabricated in a mould (400mm×400mm×5mm) with 16 holes as a size of 41mm×41mm×5mm for controlling the thickness of repair mortar which was shown in FIG. 5.

FIG. 2 Surface of Substrate

FIG. 3 Concert Blocks

FIG. 4 Measured Dolly

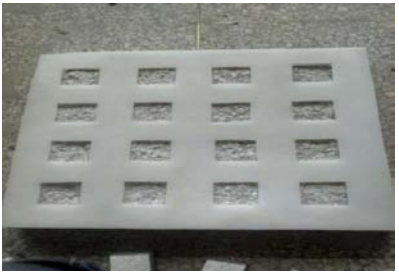

FIG. 5 Flexible Silica Gel Plate

The repair mortars prepared by recommended mix proportion were casted into the hole of flexible silica gel plate which was placed onto the surface of substrate. Then the measured dolly was attached to the repair mortar slightly one by one as FIG.6. Concert substrate was fixed with plate-girder of pull-off tester for pull-off bond strength measurement as FIG.7.

The pull-off bond strength was calculated by formula (1) as follows:

$$f_{AT}=\frac{T}{S} \tag{1}$$

Where f_{AT} is pull-off bond strength, MPa; T is failure load, N; S is bonded area, mm^2.

FIG. 6 Prepared Repair Mortar

FIG. 7 Pull-off Bond Strength Measurement

Experiment of Thermal-expansion Coefficient

Thermal-expansion coefficient tests were carried out on the 20mm×20mm×160mm specimens, with two small copper parts installed on both sides of moulds in advance. Before every specimen was dried to constant weight at the temperature of 100℃ in the oven, Portland and sulphoaluminate cement mortar were kept in the curing room for 28 days, while phosphate cement mortar and epoxy resin mortar were stayed in the air condition for 14 days. Then the reference length was recorded when the specimens cooled down to room temperature in the dryer. Finally the length of specimens was measured in every 10℃ higher (at least in the oven for 1hour) until temperature close to 100℃ as shown in FIG.8.

FIG. 8 Length of Specimen Measurement

The thermal-expansion coefficient was calculated by formula (2) as follows:

$$\alpha = \frac{L_0 - L_n}{(L_0 - l_0) \times (T_0 - T_n)} \tag{2}$$

where l_0 is the length between two cooper parts (mm); T_0 is the room temperature(℃); L_0 is the reference length(mm); T_n is the temperature after heating(℃); L_n is the length after heating(mm). The minimum scale value of micrometers is 0.01mm and the range of it is 10mm.

Experiment of Fatigue property

The specimens used for experiment of fatigue property were prepared like the ones for static load test. They were stored in a curing room at the temperature of (20±1)℃ and the relative humidity no less than 90% for 20-24 hours after demoulding. Then three-point bending tests were carried out with the sinusoidal wave whose frequency was 10Hz. This sinusoidal waveform is considered to close to the actual load waveform situation. The maximum stress was set to be 0.6, 0.7 and 0.8 of the flexural strength of mortars respectivly. The ratio of minimum stress and maximum stress was 0.1 shown in FIG.9. Sample number of fatigue experiment should not less than 5 at the same stress level. The samples were loaded repeatedly until they were damaged or it was over 1 million times.

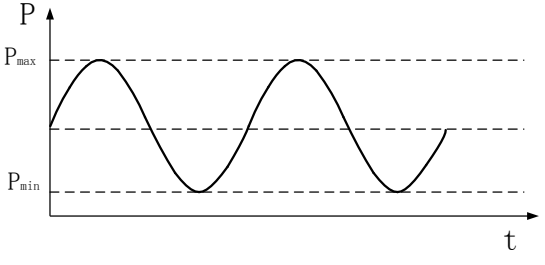

FIG. 9. Loading Mode of Fatigue Property Test

RESULTS AND DISSCUSSION

Flexural and Compressive Strength

As for rigid pavement, repair mortar must have enough flexural and compressive strength to avoid structural damage under the action of vehicle load. The flexural and compressive strength of common repair mortar were shown in Table 2. It indicated that phosphate cement mortar and epoxy resin mortar got a high compressive strength and flexural strength 1 hour after mixed which satisfied the standard of cement pavement design. However Portland and sulphoaluminate cement mortar were obviously lower than others in strength and reached a certain strength 1 day later. Besides, the early strength of the latter was superior to the former. However it was opposite 28 days later.

Table 2. Results of Strength Test of Repair Mortar

Material Types	Flexural/Compressive Strength (Mpa)					
	1h	3h	1d	3d	7d	28d
Portland Cement Mortar	—/—	—/—	5.60/24.48	6.46/39.89	7.23/49.05	8.32/59.44
Sulphoaluminate Cement Mortar	—/—	3.71/22.80	6.51/34.91	6.98/39.99	6.52/43.51	7.92/47.47
Phosphate Cement Mortar	7.81/61	8.2/54	8.6/56	9.8/64	10.9/79	11.8/81
Epoxy Resin Mortar	6.84/17.3	29.4/77.5	34.1/93.5	33.5/93.8	33.1/92.5	33.0/92.2

Flexural and Pull-off bond Strength

It is required that not only the structural strength of repair mortars should be high enough but also bond strength between original pavement and repair mortar is high too. The results of bond strength were shown in Table 3. It could be obtained that flexural bond strength of epoxy resin mortar was highest which reached to 9Mpa(flexural strength of concrete) 3 hour later, while it of phosphate cement mortar was more than 4.5Mpa 3 hours later and 9Mpa 7 days later. Sulphoaluminate cement mortar was similar to Portland cement mortar that was much less than the others in terms of flexural bond strength. Though it developed to more than 4.5Mpa 7 days later, but unfortunately it was almost 0Mpa 3 hours later.

Phosphate cement mortar had obviously higher pull-off bond strength which was more than 2Mpa 3 hours later and more than 3.6Mpa 1 day later than the rests except for epoxy resin mortar. The pull-off bond strength of Portland and sulphoaluminate cement mortar, by contrast, was less than 1Mpa 3 days later. The main reason why epoxy resin mortar was far less than phosphate cement mortar in pull-off bond strength 3 hours later might be that the early strength of the former was significantly affected by polymerization reaction heat, while the thickness of bonded epoxy resin mortar was just 5 mm which lead to the heat of polymerization reaction lower than flexural strength test.

Volume Stability

Drying shrinkage and thermal-expansion coefficient of repair mortar are another major concerns of rigid pavement repair because the success of any patch repair depends largely on overcoming the tendency of the patching material to deform after placement.

According to the results of thermal expansion coefficient experiment shown in Table 4, it indicated that the expansion rate of repair mortars almost increased linearly during the temperature growth. The thermal expansion-coefficient of the cement mortar except epoxy resin mortar was nearly the same (close to the thermal expansion coefficient of original rigid pavement which is 12.65×10^{-6} ℃$^{-1}$). However, thermal expansion coefficient of the epoxy resin mortar is four times greater than the Portland cement mortar. Therefore, the coordination of thermal expansion between the epoxy resin mortar and the original pavement should be taken into consideration when they are used for large area repair.

Table 3.Results of Bond Strength test of Repair Mortar

Material Types	Flexural/Pull-off Bond Strength（Mpa）			
	3h	1d	3d	7d
Portland Cement Mortar	—/—	2.0/0.1	3.5/0.4	4.8/—
Sulphoaluminate Cement Mortar	—/—	3.0/0.3	4.4/0.6	5.1/—
Phosphate Cement Mortar	4.6/2.0	6.4/3.6	8.2/—	9.1^{N}/—
Epoxy Resin Mortar	9.7^{N}/0.5	—/4.1	—/—	—/—

Note: Fractures on mortar meant the bond strength should be greater than it.

Table 4. Results of Thermal Expansion-coefficient Experiment

Material types	Expansion Rate(10^{-6})									Thermal Expansion coefficient(10^{-6} ℃$^{-1}$)
	20℃	30℃	40℃	50℃	60℃	70℃	80℃	90℃	100℃	
Portland Cement Mortar	0	135	243	388	563	693	782	897	1020	12.83
Sulphoaluminate Cement Mortar	0	178	261	421	505	617	729	846	958	11.21
Phosphate Cement Mortar	0	186	273	350	517	650	787	925	1043	12.74
Epoxy Resin Mortar	0	292	587	947	1369	1751	2099	2696	3305	42.23

Shrinkage of the repair mortar at early stage is a major cause of cracking, the results of the drying shrinkage ratio experiment were shown in Table 5. It indicated that Portland and Sulphoaluminate cement mortar were more sensitive to water than others, because the hydration products mainly contained CSH gel and

ettringite rather than struvite and magnesium phosphate amine stone from phosphate cement. While the epoxy resin mortar is glued by polymer.

Table 5. Results of the Drying Shrinkage Ratio Experiment

Material Types	Portland Cement Mortar	Sulphoaluminate Cement Mortar	Phosphate Cement Mortar	Epoxy Resin Mortar
Drying Shrinkage Ratio（10^{-4}）	3.89	3.21	1.29	1.89

Note: The results are measured after 7 days in the water then 42 days in the air.

According to the results above, phosphate cement mortar is the most stabile of all. Portland cement and sulphoaluminate cement mortar should be drawn more attention to the wet curing. However the wet curing for phosphate cement mortar is forbidden because too much water is harmful to strength.

Fatigue Test of Repair Mortar

It can be seen from the results of fatigue test of repair mortar shown in Table 6 that fatigue strength of phosphate cement mortar is significantly better than others and sulphoaluminate cement mortar have a shorter life on the condition of the high stress. The reason why the fatigue property of epoxy resin mortar is less than phosphate and sulphoaluminate cement mortar at the same stress condition, in spite of high strength, is the obvious difference of elasticity modulus between epoxy resin, sand and fly ash. Thus, it is easy to generate stress fatigue fracture in the interior of the sample. On the other hand, there should be more test researches for fatigue property of repair mortar in the future.

Table 6. Results of Fatigue Property of Repair Mortar Test

Materials	Flexural Strength(MPa)	Stress Ratio	Load Times
Epoxy Resin Mortar	33.0	0.8	845
		0.7	7710
		0.6	20748
Sulphoaluminate Cement Mortar	7.92	0.8	90
		0.7	9422
		0.6	390218
Phosphate Cement Mortar	11.8	0.8	2115
		0.7	139820
		0.6	＞1000000

Table 7. Evaluation Standard of Repairing Mortar Performance for Rigid Pavement

Material \ Property		Flexural Strength (MPa)	Compressive Strength (MPa)	Flexural Bond Strength (MPa)	Pull-off Bond Strength (MPa)	Drying Shrinkage (10^{-4})	Thermal Expansion coefficient (10^{-6} ℃$^{-1}$)
Portland Cement Mortar	3h	—	—	—	—	≤10	≤15
	3d	5.0	30	—	—		
	28d	6.0	40	4.5	2.5		
Sulphuraluminate Cement Mortar	3h	3.0	15	—	—	≤10	≤15
	3d	5.0	30	—	—		
	28d	6.0	40	4.5	2.5		
Phosphate Cement Mortar	3h	5.5	40	5.0	1.5	≤1.5	≤15
	3d	7.0	55	≥R0	≥Rb		
	28d	8.0	60	≥R0	≥Rb		
Epoxy Resin Mortar	3h	15	40	5.0	—	≤2	≤50
	3d	20	60	$\geq R0^N$	$\geq Rb^N$		
	28d	25	75	≥R0	≥Rb		

Note：R0 and Rb are the flexural strength and compressive strength of concert respectively.

Evaluation Standard of Repaired Mortar Performance for Rigid Pavement

When the repair mortar is used for rigid pavement, the structural strength of repair mortar must be sufficient and the bond strength between the repair mortar and original pavement should be high enough to avoid the structure damage. In addition, the difference of thermal expansion-coefficient and drying shrinkage between the repair mortar and original pavement lead to the discordance of volume deformation which can influence the repair quality in process of setting and hardening.

The compressive and flexural strength, flexural and pull-off bond strength, thermal expansion coefficient, and drying shrinkage are regarded as the indexes of performance evaluation standard of repair mortar for rigid pavement. It is also considered that repair mortar would be suitable for emergency rapid pavement repair and ordinary pavement maintenance, so the performance evaluation standard of 3h, 3d, 28d are shown in Table 7.

CONCLUSIONS

The mechanical properties and performance including compressive and flexural strength, bond strength, fatigue resistance and volume stability of four repair mortars were systematically studied in this paper. Based on the experimental results, following general conclusions can be drawn:

1) As for the repair mortars, bond strength and volume deformation as some performance evaluation indexes are more important than structural strength.

2) Due to the repeated action of vehicle load, fatigue resistance of repair mortar must be taken into consideration as another key performance evaluation index. However, it requires a further experimental research.

3) Evaluation standard of repairing mortar performance for rigid pavement

cannot be proposed by unified criteria because of the differences in properties of repair mortars. Therefore, the standards should be formulated respectively.

4) Epoxy resin mortar exhibits much better strength than other mortars. By contrast, the fatigue performance and the volume deformation have deficiencies. Portland cement mortar is similar to sulphuraluminate cement mortar in all aspects. Phosphate cement mortar has excellent performance in this evaluation especially in the fatigue property and the development of early strength.

REFERENCE

Morgan, D. R.(1996). "Compatibility of concrete repair materials and systems." *Construction and Building Materials.* v 10, n 1,p 57-67.

Santos, P. M. D.(2011). "Factors affecting bond between new and old concrete." *ACI Materials Journal.* Vol. 108, n 4,p449-456.

Fei, Q., Chau, C. K., and Li, Z. J.(2009). "Property evaluation of magnesium phosphate cement mortar as patch repair material." *Construction and Building Materials.* v 24, n 5,p 695-700.

Meng, X. Q. and Ye, Z. M .(2010). "Mechanical properties of sulphoaluminate cement repair mortar." *Journal of university of Jinan.* v 12, n 3,p 69-71.

Deng, H. W., Yang, Y. Z., and Gao, X. J.(2011). "Properties of phosphate cement mortar used as rapid-repair material." *Advanced Materials Research*. v 250-253, pt.2,p 1752-6.

The State Administration of Quality Supervision Bureau. *Method of testing cements-determination of strength (ISO)GB/T17671–1999*.

Civil aviation administration of China.(2010). *Technical maintenance guidelines of civil airport pavement*.

The Development and Reform Commission of the People's Republic of China. *Stand test method for drying shrinkage of mortar（JC/T 603-2004)*.

Shake Table Modeling of Laterally Loaded Piles in Liquefiable Soils with a Frozen Crust

Xiaoyu Zhang[1], M. ASCE, Zhaohui Yang[2], M. ASCE, Ph.D.,
and Runlin Yang[3], Ph.D.

[1] Staff Engineer, PND Engineers, 1506 W 36th Ave, Anchorage, AK 99508; rzhang@pndengineers.com
[2] Professor, Department of Civil Engineering, University of Alaska Anchorage, 3211 Providence Dr., ENGR 201, Anchorage, AK 99508; zyang@uaa.alaska.edu
[3] Associate Professor, Department of Civil Engineering, University of Science and Technology Beijing, 38 Xueyuan Rd, Beijing, China; yang_runlin@163.com

ABSTRACT: One of the important lessons learned from Alaska's major earthquakes in history is that the lateral spreading of frozen crust overlying liquefiable soils generated significant lateral forces and induced extensive bridge foundation damages. When the ground crust is frozen, its physical properties including stiffness and shear strength will change substantially. A shake table experiment was conducted to study the soil-pile interaction in liquefiable soils underlying a frozen crust. Cemented sand cured for a short period of time was found to possess similar mechanical properties of frozen soils and was used to simulate the frozen crust. Data collected from the shake table experiment was presented and analysed. The mechanism of frozen soil-pile interaction in liquefiable soils is discussed. It is concluded that it is important to account for the impact of frozen soil in the seismic design of bridge foundations in laterally spreading ground in cold regions.

INTRODUCTION

Liquefaction and associated ground failures have been commonly observed in past major earthquakes across the world and have caused extensive damages to existing infrastructures. A substantial portion of these ground failures and structural damages were direct results of or related to liquefaction induced lateral spreading. Lateral spreading is particularly damaging if a non-liquefiable crust rides on top of liquefied soil. Moreover, when the ground crust is frozen, its physical properties including stiffness and shear strength will change by orders of magnitude (Akili 1971; Stevens 1973; Haynes and Karalius 1977; Vinson et al. 1983; Zhu and Carbee 1983). What would be the impact to a bridge foundation if there is a frozen ground crust that is resting on a liquefied soil layer?

Lessons were learned from historical earthquakes in Alaska. In March 1964, Alaska experienced one of the largest earthquakes in recorded history: the Great Alaska Earthquake with a moment magnitude of 9.2. Numerous cases of bridge foundation damage associated with liquefaction-induced lateral spreading were reported in Southcentral Alaska after this earthquake. Ross et al. (1973) reported many observations indicating the liquefaction of

cohesionless soils and landslides. The following are a few direct quotations from the authors' report: "'mud' oozing up in cracks"; "road embankment collapsing to the level of flood plain"; "embankment sliding to river centerline"; "downstream movement of the footing and upstream tilt of the pier shafts"; and "piers shifting or tilting longitudinally toward the channel centerline". According to the statistical data, none of the then-existing foundation types was able to withstand the lateral forces, including cases where the superstructure had not yet been built.

Unfortunately, very limited studies have been carried out to study the impact of frozen crust on the built infrastructure. Recent research in Alaska and Iowa has identified the significance of frozen ground effects on the seismic responses of bridge foundations and validated the need for design guidelines to consider the effects of seasonally frozen ground (Sritharan et al., 2007; Yang et al., 2007; Yang et al., 2012; Zhang et al., 2012). There are no guidelines to account for the impact of frozen ground crust in the seismic analysis and design of bridge foundations.

Shake table experiments have been successfully applied in studying soil-pile interaction under liquefaction and liquefaction-induced lateral spreading conditions. Some examples of shake table experiments on soil-pile interaction include Cubrinovski et al. (2006), Shirato et al. (2008), Ueng (2010), and Yao et al. (2004). This paper presents the design, results and analysis of the shake table experiment conducted to investigate the mechanism and consequences of frozen crust-pile foundation interaction during earthquake-induced liquefaction and lateral spreading. Experiment model design, instrumentation plan, model preparation, frozen soil simulation, and recorded data including acceleration, pore pressure, and displacement time histories are presented. The bending moment induced on the pile was analyzed based on recorded strain data, and the mechanism of soil-pile interaction in liquefiable soils with a frozen crust is discussed.

SHAKE TABLE EXPERIMENT DESIGN

The shake table experiment was performed on a 3 × 3 m shake table. The payload capacity of the shake table is 10 tons, with a maximum acceleration ranging from 1.0 g (fully loaded) to 2.5 g (unloaded). FIG. 1 shows the soil-pile system set up in a 3 × 3 × 1.3 m (L×W×H) steel container. The container has a wall thickness of 4 mm with a frame support system welded to the outside. A steel pipe pile with an outer diameter of 5 cm and wall thickness of 0.175 cm was used to model a bridge pile foundation, typically used in Alaska, at a scale of 1:15. The pile was fixed at the bottom of the soil container and has a lumped mass of 250 kg on its top to simulate the inertial effect of the bridge superstructure. The soil profile consists of a 30 cm frozen soil crust overlying a 30 cm loose sand layer and a 60 cm medium dense sand layer. The crust has a 5° slope angle. A 25 cm wide opening between the left end of the frozen soil crust and the soil box was designed to mimic a river channel and allow the frozen crust to spread laterally during earthquake shaking. Water level was designed just above the interface between the loose sand and frozen soil to ensure that the sands were fully saturated. The sloping ground and river channel scenario resembles a typical topographical situation for a bridge site.

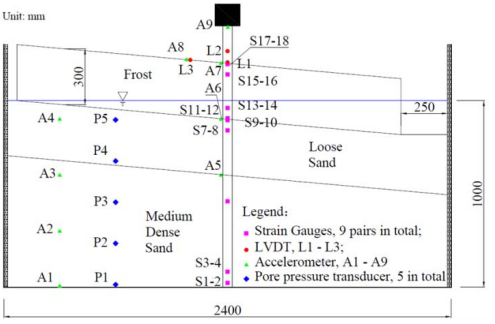

FIG. 1. Layout of the shake table model

FIG. 1 also shows that four types of transducers were used in this experiment: pore pressure transducers (5, identified by "P"), accelerometers (9, identified by "A"), strain gauges (9, identified by "S"), and LVDTs (3, identified by "L"). Accelerometers and pore pressure sensors were placed at different locations in the soil profile to record acceleration and pore pressure. Strain gauges were installed on the pile to measure the strain values for quantifying the loads, which is also one of the foci of this study. Considering that concentrated strains and moments might be generated by the frozen crust, more strain gauges were installed at locations close to the loose sand-frozen soil interface and the top of the frozen soil. Note the reference point for all LVDTs is the soil container; therefore, the measure displacement is relative displacement to the soil container box. Among the LVDTs, L3 was assigned to measure the frozen crust lateral displacement; L1 was assigned to measure pile deflection at the ground surface; and L2 was a backup sensor for L1 in case the expected strong interaction between the pile and the frozen crust damaged L1.

FIG. 2 presents the moment-curvature response for the pipe pile section. This curve was obtained by a moment-curvature analysis based on the following mechanical properties: steel yield strength 235 MPa, Young's modulus 200 GPa, and strain-hardening ratio 0.005. Assuming a yield strain of 0.2% and a rupture strain of 5% for the steel pipe, the yield bending moment (M_y) of the pile was determined to be 0.8 kN.m and the bending moment capacity (M_c), to be 1.06 kN·m.

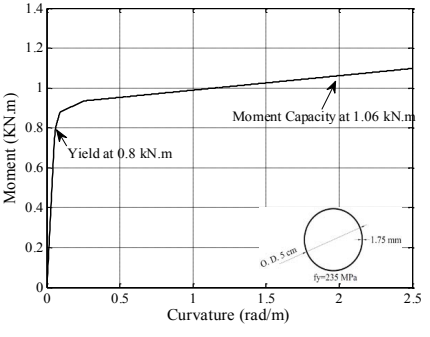

FIG. 2. The pile cross section and its moment-curvature curve

MODEL PREPARATION

The sand used in this experiment is characterized by an average particle size D_{50} of 0.33 mm. The loose sand layer has a saturated density of 1.7×10^3 kg/m^3 and relative density D_r of 40%, and the medium dense sand layer has a saturated density of 2.1×10^3 kg/m^3 and relative density D_r of 60%.

Due to laboratory facility limitation, cemented sand was used to simulate frozen ground crust. The sand-cement-water mix ratio by weight was 9:1:1.8. Key mechanical parameters including density (ρ), compressive strength (q_u), strain at 50% ultimate strength (ε_{50}), and Young's modulus (E) need to be comparable to those of frozen soil. Based on a number of experiments, it has been determined that a sand-cement mixture at a certain ratio after a 72-hour wet curing has comparable mechanical properties. Specimens for obtaining mechanical properties were made at the same time that the ground crust in the model was poured. Uniaxial compression tests were conducted under variable strain rates ranging from 1×10^{-6} to 3×10^{-6} s^{-1}. FIG. 3 shows the stress-strain curves obtained from four specimens. The mechanical properties of the four specimens are quite uniform, having the following average values: $\rho = 2.1\times10^3$ kg/m^3; $q_u = 0.51$ MPa; E = 310.1 MPa; $\varepsilon_{50} = 0.002$. Zhu and Carbee (1983) conducted laboratory tests of frozen Fairbanks silts at temperatures varying from -0.5 to -10°C, and reported q_u, E and ε_{50} values in the ranges of 0.4 ~17.3 MPa, 0.21 ~ 2.67 GPa, and 0.4×10^{-3} to 1.5×10^{-3}, respectively. By comparing the simulated frozen soil properties with those reported in Zhu and Carbee (1983), one can conclude that q_u and E of the simulated frozen soil specimens are within, but closer to, the lower bound of the range for frozen soils, and ε_{50} is within, but closer to, the upper bound of frozen soils. In other words, the simulated frozen soil used in this study is similar to frozen soils at relatively high sub-zero temperature. Note that simulated frozen soil exhibits a brittle behavior that is similar to concrete, while frozen soil typically shows a more ductile behavior.

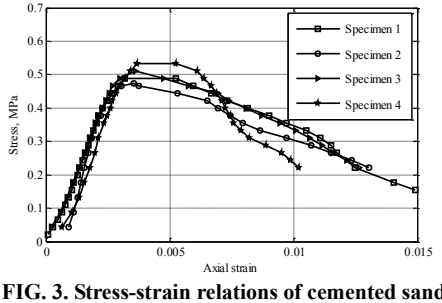

FIG. 3. Stress-strain relations of cemented sands

INPUT MOTIONS

The input motion experiment was performed by applying three stages of input motion, as shown in Table 1 and FIG. 4. In the first stage, the model was loaded by a sinusoidal wave and scaled-down acceleration time histories recorded at Pump Station #10 along the Trans-Alaska Pipeline System during the 2002 Denali earthquake, named "Sine Wave" and "Scaled Denali Earthquake," respectively. The sinusoidal wave had a peak acceleration of 0.03 g and the scaled-down Denali motion had a peak ground acceleration (PGA) of 0.15 g. The main purpose for these loadings was to check whether the model, instruments, and data acquisition system were functioning properly. Neither permanent deformation nor permanent bending moment was expected from these events.

Table 1. Input Motion Sequence

Test stage	Event name	PGA (g)	Duration (sec.)	Input Time (Local time)
#1	Sine Wave	0.03	20	8:20 a.m.
	Scaled Denali Earthquake	0.15	20	8:23 a.m.
#2	Japan Part 1	0.53	40	8:53 a.m.
	Japan Part 2	0.53	40	8:56 a.m.
#3	Scaled Japan Part 1	0.80	40	10:00 a.m.

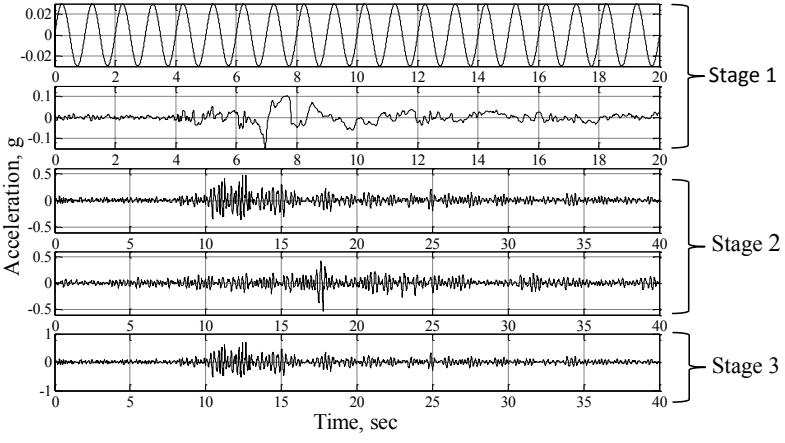

FIG. 4. Acceleration time histories of input motions

In Test Stage 2, after we ensured that the model, instruments, and data acquisition system were functioning properly, the model was loaded with acceleration time histories recorded at the AKTH04 station on the ground surface during the 2011 Tohoku Earthquake (M_w=9.0). This earthquake had a PGA of 0.53 g and duration of 80 sec. The source mechanism and magnitude of this earthquake are similar to those of the 1964 Great Alaska Earthquake. Due to the facility's limitations, however, the records for source mechanism and magnitude had to be split into two segments, named "Japan Part 1" and "Japan Part 2," respectively, and input to the shake table sequentially; a three-minute gap occurred in between to allow for this transition. Substantial permanent deformation and bending moment were expected from this stage of loading.

In Test Stage 3, the first portion of the Japan record with its PGA scaled up to 0.80 g was used as the excitation. This motion was input about one hour after Test Stage 2 to allow time for the excess pore pressure to drop to hydrostatic pore pressure. We expected that residual displacement and bending moment from Test Stage 2 would exist. The purpose of this stage loading was to induce larger displacement and gather pile performance data.

OBSERVATIONS OF MODEL BEHAVIOR

FIG. 5 shows four snapshots of the model during Test Stage 3 of this experiment. Cracks

started to form on frozen crust surface near the soil-pile interface after a few cycles of loading in Stage 2, as shown in FIG. 5a. As the test moved past the main shaking period, cracks gradually developed into a gap between the pile and soil and water rose to the ground surface from the gap and spilled out (FIG. 5b). At the end of Stage 2, the pile head tilted about 15 degrees towards the down-slope direction and the frozen crust laterally spread in the down-slope direction for about 2 cm. During Stage 3 loading, the frozen crust continued moving in the down-slope direction for about 1.2 cm and the pile head continued to tilt; water was seen spilling out of the gap long after the shaking ended. These phenomena indicated that considerable amount of excess pore pressure was generated in the sand layer during the shaking and full or partial liquefaction was induced in Stage 2 and Stage 3. Model excavation at the end of the experiment revealed that permanent deflection was found at about 0.28-0.30 m and 0.7-0.8 m below the ground surface, respectively, indicating the formation of plastic hinges during the experiment.

FIG. 5. Snapshots of the model during Test Stage 3 of this experiment: (a) crack formed near soil-pile interface, (b) gap formed between soil and pile, and water spilled out, (c) pile head tilted after a few cycles, and (d) lateral displacement of frozen crust observed.

RESULTS AND ANALYSIS

Sign Convention and Data Process

Results from Test Stage 2 are presented. The following sign conventions are defined to facilitate discussion: positive and negative depth values indicate the location above and below the ground surface, respectively; depth 0 m refers to the frozen ground surface. Displacement is defined as positive if it is along the downslope direction, and bending moment is defined as positive if it warps an element to the upslope direction in a "U" shape.

Recorded pore pressure data were first converted to excess pore pressure (EPP) by subtracting the hydrostatic pore pressure. Then the EPP ratio (r_u) was calculated by normalizing the EPP by the effective overburden pressure.

Assuming a linear distribution of strain along the pile cross section, measured strain data were converted to curvature by using Equations 1 and 2. Bending moment was evaluated by the moment-curvature relation of the model pile (see FIG. 2).

$$\phi = \frac{\varepsilon}{h} \tag{1}$$

$$\varepsilon = \frac{1}{2}(\varepsilon_t - \varepsilon_c) \tag{2}$$

where ϕ is the curvature; ε is the strain; ε_t and ε_c represent tension and compression strains obtained from symmetrically installed strain gauge pairs on the pile; *h* is the distance from the strain measurement point to the neutral axis of the section and the outer-radius of the pile was used for *h* in this study.

Data and Analysis

FIG. 6 shows the r_u time histories for Test Stage 2. At around 20 seconds, r_u began to build up quickly, when the first main shaking occurred. The corresponding maximum values of r_u for different depths are 31%, 39%, 41%, 33%, and 62% from the top to the bottom. The EPP buildup indicates partial liquefaction in the loose and medium dense sand layers. As mentioned, this earthquake record was input in two segments, with about 3 minutes of gap in between. A noticeable but not significant drop in the pore pressure time histories can be observed in FIG. 6. Again, spikes are observed in the r_u time history at the depth of -1.25 m. Despite these spikes, a clear trend in the EPP buildup can still be observed.

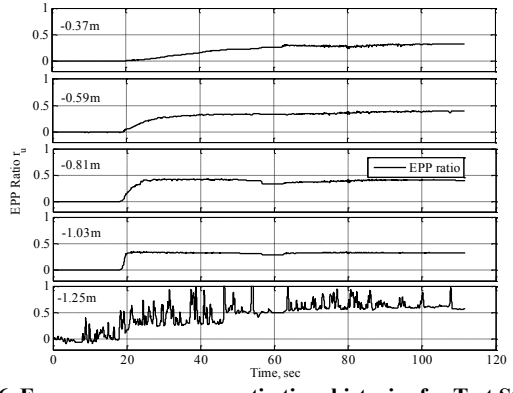

FIG. 6. Excess pore pressure ratio time histories for Test Stage 2

FIG. 7 shows the displacement time histories measured at two locations on the pile and at a "far-field" location on the frozen ground crust. Observe in FIG. 7 that the displacement for all locations was very small, up to 19 sec. into the shaking. After that time, displacement started to increase quickly at around 20 sec., which corresponds to the occurrence of the first peak of input motion. The displacement remained almost flat to the end of the first segment of shaking. It is clear that displacement of the pile continued at the end of Part 1 excitation, as indicated by the abrupt change in displacement during the 3-minute gap between the two

segments of loading. This displacement is likely due to tilting of the pile and the creep of the sand-cement mixture that was not fully cured. Such abrupt change is not present in the displacement time history recorded on the frozen crust. The displacement remained almost constant from the beginning of Part 2 shaking to 75 sec., and gradually increased until 80 sec. At 80 sec., a sharp increase is apparent in the displacement time history recorded on the frozen crust and in the time history recorded on the pile. Displacement kept increasing, although quite slowly, until the end of Part 2 shaking.

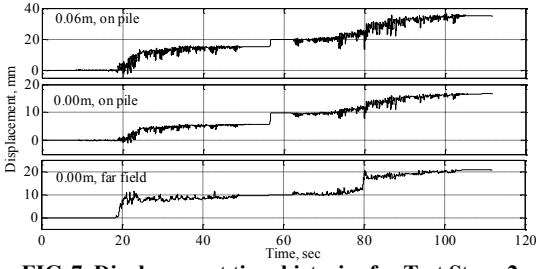

FIG. 7. Displacement time histories for Test Stage 2

The maximum lateral spreading of the frozen ground crust reached 2.1 cm, or 40% of the pile diameter. By comparing the displacement of the frozen crust with that of the pile at the ground surface, one notes that the frozen crust moved ahead of the pile, which implies that the pile deflection was driven primarily by lateral spreading of the frozen crust.

The bending moment envelope along the pile depth is shown in FIG. 8 to illustrate the location of possible plastic hinges. It is easy to see from FIG. 8 that the shaking formed two bending moment concentrations on the pile: one at the frozen ground crust-loose sand interface, and the other in the middle of the partially liquefied medium dense sand layer. The bending moments at both locations reached the pile's yield bending moment, indicating the formation of plastic hinges. The yielding of the pile at different times for these locations reveals the different mechanisms that are responsible for the formation of plastic hinges. The plastic hinge at the frozen crust-loose sand interface (at -0.29 m) started to form at the occurrence of the first peak of input motion (around 20 sec.), when the frozen crust lateral spreading was about 0.9 cm. It is very likely that this plastic hinge formed because of the large distributed load (soil resistance) applied on the pile by the laterally spreading frozen crust. Later, as lateral spreading of the frozen crust increased gradually, the bending moment actually dropped slightly, possibly due to yielding and creep of the cemented sand. A similar trend was observed in the bending moment time histories at the same depth after the occurrence of the second peak for like reasons. For the plastic hinge in the middle of the partially liquefied medium dense sand layer (-0.74 m), the bending moment started to form at the time of the second peak of input motion (around 80 sec.), when lateral displacement of the frozen crust reached it maximum value 2.1 cm. The bending moment remained high, while lateral spreading remained around 2.1 cm until the end of shaking. Apparently, this plastic hinge formation was due to lateral spreading of the ground crust.

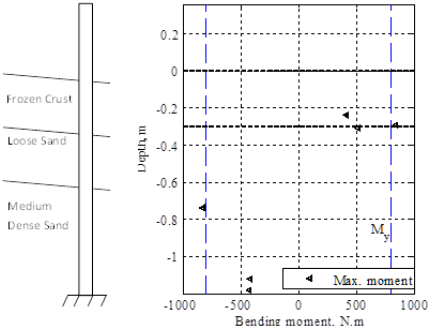

FIG. 8. Bending moment envelope along the pile depth for Test Stage 2

CONCLUSIONS

A model pile embedded in loose to medium dense sands underlying a frozen ground crust was built and a shaking table experiment was conducted to investigate the frozen ground crust-pile interaction during liquefaction-induced lateral spreading. Partially liquefaction was induced in the sands and a lateral spreading of 2.1 cm was induced in the frozen ground crust for loading Stage 2. Based on these recorded data and observations made during the experiment, the following conclusions can be made:

1) Frozen ground crust can be simulated by cemented sands. After wet curing for about 72 hours, the properties of cemented sand specimen demonstrated mechanical properties similar to those of frozen soils reported in literature.

2) Partial liquefaction was induced during the experiment with excess pore pressure ratio in the range of 30% to 60%. Water was observed spilling out from the gap formed between the frozen crust and pile. Considerable ground crust lateral spreading, i.e. 2.1 cm or 40% of the pile diameter, was induced in Test Stage 2.

3) Test data shows that two plastic hinges were formed during the shaking. One plastic hinge, located at the frozen ground crust-loose sand interface, started to form at the occurrence of first PGA. The other, located in the partially liquefied medium dense sand layer, started to form at the occurrence of second PGA, when the frozen ground crust laterally spreading reached its maximum value.

4) It was concluded that the plastic hinge at the frozen ground crust- loose sand was induced by the large shear force induced on the pile by the frozen ground crust, and the other in the partially liquefied medium dense sand layer was induced by laterally spreading ground crust and the confinement of the partially liquefied medium dense sand.

This study demonstrates that it is important to account for the large loads including shear and bending moment in the seismic design of bridge foundations in a liquefiable site. The results from this study can be used to calibrate a computer model and such model can be used to further the response of a large-scale pile under seismic loading for improving the design of full-scale piles.

AKCNOWLEDGEMENT

This research was jointly sponsored by the Alaska University Transportation Center and the State of Alaska Department of Transportation and Public Facilities under Project AUTC #410015. The authors are thankful to Mr. Elmer E. Marx, Bridge Engineer at the State of

Alaska Dept. of Transportation and Public Facilities, for his thoughtful comments provided for this study.

REFERENCES

Akili, W. (1971). "Stress-strain behavior of frozen fine-grained soils." *Highway Research Record: Frost Action and Drainage.* No. 360: 1-8.

Cubrinovski, M., Kokusho, T. and Ishihara, K. (2006). "Interpretation from large-scale shake table tests on piles undergoing lateral spreading in liquefied soils." *Soil Dynamics and Earthquake Engineering*, 26(2-4): 275-286.

Haynes, F.D. and Karalius, J. A. (1977). "Effect of temperature on the strength of frozen silt." *CRREL Report 77-3*, Cold Regions Research and Engineering Laboratory. Hanover, New Hampshire.

Kostadinov M. V. and Yamazaki F (2001). "Detection of soil liquefaction from strong motion records." *Earthquake Engineering Structure Dynamics*, 30(2):173-93.

Ross, G. A., Seed H. B., and Migliaccio, R. R. (1973). "Performance of highway bridge foundations." *The Great Alaska Earthquake of 1964* (Engineering), National Academy of Sciences, 190-242.

Sritharan, S., White, D. J., and Suleiman, M. T. (2007). "Effects of seasonal freezing on bridge column-foundation-soil interaction and their implications." *Earthquake Spectra*, 23(1): 199-222.

Stevens, H. W., 1973. "Viscoelastic properties of frozen soil under vibratory loads." *North American Contribution to the Second International Conference on Permafrost*. Yakutsk, Siverua, U.S.S.R., 400-409.

Shirato, M., Nonomura, Y., Fukui, J., and Nakatani, S. (2008). "Large-scale shake table experiment and numerical simulation on the nonlinear behavior of pile-groups subjected to large-scale earthquakes." *Soils and foundations*, Japanese Geotechnical Society, 48 (3): 375-396.

Ueng, T.S. (2010). "Shaking table tests for studies of soil liquefaction and soil-pile interaction." *Geotechnical Engineering Journal of the SEAGS & AGSSEA*. 41(1): 1-10.

Vinson, T.S., Wilson, C.R., and Blonader, P. (1983). *Dynamic properties of naturally frozen silt.* National Academy Press, 1983, 1315-1320.

Yang, Z., Dutta, U., Xiong, F., Zhu, D., Marx, E., and Biswas, N. (2007). "Seasonal frost effects on the soil-foundation-structure interaction system." *ASCE Journal of Cold Regions Engineering,* 21(4): 108-120.

Yang, Z. and Zhang, X. (2012). "Shake table experiments of bridge foundation in liquefiable soils." *Report* to the Alaska University of Transportation.

Yao, S., Kobayashi, K., Yoshida, N., and Matsuo, H. (2004). "Interactive behavior of soil-pile-superstructure system in transient state to liquefaction by means of large shake table tests." *Soil Dynamics and Earthquake Engineering.* 24: 397-409.

Zhang, X., Yang, Z., and Li, Q. (2012). "Analysis of laterally loaded piles in liquefiable soils with a frozen crust using p-y approach." *Cold Regions Engineering 2012: Sustainable Infrastructure Development in a Challenging Cold Environment (Proc. 15 Int'l Specialty Conf. Cold Regions Engineering)*, Eds. Brian Morse and Guy Dore. 456-466.

Zhu, Y. and Carbee, D. L. (1983). "Uniaxial compressive strength of frozen silt under constant deformation rates." *Cold Regions Science and Technology*, 9: 3-15.

Climatic Parameter TMI in Subgrade Soils

Er Yue[1], Lizhou Chen[1], Rifat Bulut[2], and Qi Cheng[3]

[1]Graduate Student, School of Civil and Environmental Engineering, Oklahoma State University, Stillwater, Oklahoma 74078
[2]Associate Professor, School of Civil and Environmental Engineering, Oklahoma State University, Stillwater, Oklahoma 74078; rifat.bulut@okstate.edu
[3]Associate Professor, School of Electrical and Computer Engineering, Oklahoma State University, Stillwater, Oklahoma 74078; qi.cheng@okstate.edu

ABSTRACT: This paper evaluates historical climatic data acquired from Mesonet weather stations across Oklahoma for pavement applications. Thornthwaite Moisture Index (TMI), a climatic parameter, is widely used in geotechnical engineering as well as other disciplines to evaluate the changes in moisture conditions in near surface soils in the unsaturated zone. It has become an important parameter for predicting the equilibrium soil suction beneath the moisture active zone, as well as the depth to constant suction. This paper employs three different TMI calculation methods (Thornthwaite 1948; Thornthwaite and Mather 1955; and Witczak et al. 2006) and produces TMI-based contour maps for Oklahoma using the climatic data from Mesonet stations. The results are analyzed and compared within the three methods. The evaluation of the analysis indicates that caution should be exercised when adopting a TMI-based approach in predicting climate-related unsaturated soil parameters (e.g., depth to constant suction and equilibrium soil suction).

INTRODUCTION

The paper describes three methods for calculating Thornthwaite Moisture Index (TMI) based on the Thornthwaite (1948), Thornthwaite and Mather (1955), and Witczak et al. (2006) studies, and presents TMI-based contour maps from these methods. The same climatic data, obtained from Mesonet weather stations in each seventy seven counties in Oklahoma, have been used in creating the contour maps. Monthly average temperature and monthly total precipitation data from 1994 to 2011 are used for the TMI calculations. The climatic parameter is based on long term weather data and is indicative of the dryness or wetness of a region. For example, if TMI is greater than zero, the area is regarded as wet and the area is considered dry if TMI is less than zero.

TMI, originally developed by Thornthwaite in 1948, is determined by annual water surplus, water deficiency, and water need following a water balance approach. The

calculation of TMI is based on a period of one year using monthly weather data. The calculation of TMI by Thornthwaite (1948) approach is computationally intensive. On the other hand, the methods given by Thornthwaite and Mather (1955) and Witczak et al. (2006) are relatively simple and only consider annual precipitation and potential evapotranspiration computed on a monthly basis.

TMI is a simple climatic parameter and is easy to determine with, in many cases, readily available data from local weather stations. The parameter has the appeal of relevance to moisture conditions of a site, and thus, has been correlated with the depth of moisture active zone (depth to constant suction) and the equilibrium suction (Fityus et al. 1998). However, the review of literature indicates that there are discrepencies between the established correlations in the literature. It is believed that those differences are coming from the TMI calculation methods, and to some extent from the local soil and weather conditions.

BACKGROUND

The Thornthwaite Moisture Index (TMI) has become an acceptable climatic parameter in geotechnical engineering because of its relative simplicity and practicality, and it has been used in engineering practice with success over the last several decades. Russam and Coleman (1961) developed a relationship between soil suction at depths below the moisture active zone and the TMI. Edris and Lytton (1976) studied the effects of climate on subgrade soils in Texas using the TMI for predicting the equilibrium soil suction beneath the pavements using the relationships developed by Russam and Coleman (1961). Wray (1978) adopted the TMI for predicting the horizontal moisture variation distance for slabs-on-ground foundations. McKeen and Johnson (1990) employed the TMI parameter in the estimation of the unsaturated soil moisture diffusion rates in subgrade soils. Fityus et al. (1998) employed the TMI as a predictor for determining the depth of seasonal moisture change in unsaturated soils in Australia. Recently, Perera et al. (2004) expanded on the work of Russam and Coleman (1961) and introduced a model to predict suctions beneath pavements using the TMI and basic soil index properties.

The original TMI given by Thornthwaite (1948) is based on an annual water balance calculation using records of long term climatic parameters such as precipitation, temperature, and estimated potential evapotranspiration. The moisture balance is determined in terms of precipitation, evaporation, water storage, deficit, and runoff. The water balance is computed by month. The process begins by calculating the difference between precipitation and corrected evaporation. If the difference is larger than zero, it is added into storage up to a maximum value. The amounts exceeding the maximum storage are considered as runoff. On the other hand, if the difference between the precipitation and corrected evaporation is less than zero, it is deducted from the storage up to zero. The amounts lower than zero are defined as deficit. A detailed analysis of the Thornthwaite (1948) method is given by McKeen and Johnson (1990). Later, Thornthwaite and Mather (1955) modified the original Thornthwaite (1948) equation by eliminating the water balance approach and reducing the amount of data required and computational effort in determining the climatic index. Recently, Witczak et al. (2006) offered a slightly different version of the Thornthwaite and Mather (1955) equation as part of a NCHRP research study for the Mechanistic

Empirical Pavement Design Guide (MEPDG). These models are described in the following section.

THORNTHWAITE MOISTURE INDEX

Thornthwaite (1948) defined a moisture index (known as the Thornthwaite Moisture Index or TMI) as a relative measure indicating the wetness or dryness of a particular region. The TMI has been a popular and attractive parameter in the geotechnical engineering community due to the fact that the data required for its determination are usually readily available from local weather stations and it is based on a simple climatic model as compared to some of the rigorous models in the literature (Edris and Lytton 1976; McKeen and Johnson 1990). Thornthwaite (1948) equation is given as:

$$TMI = (100R - 60D)/PE \tag{1}$$

where, D is the moisture deficit; R is the runoff; and PE is the net potential for evapotranspiration. TMI calculations are based on a period of one year with monthly values of precipitation, adjusted potential evapotranspiration, storage, runoff, and deficit by conducting a moisture balance approach. The calculation process requires the total monthly precipitation, average monthly temperature, initial and maximum water storage values, the day length correction factor, and the number of days for each month. The precipitation and temperature values can be obtained from the local weather stations. The maximum water storage is a function of the soil type and the initial water storage depends on the climate and site condition. The day length correction factor is a constant for a given month and location (latitude). Thornthwaite (1948) adopted a relatively simple model for the calculation of the adjusted potential evapotranspiration as compared to some of the sophisticated (yet complex in terms of the parameters involved) models available in the literature. The heat index for each month is determined using the mean monthly temperatures as follows:

$$h_i = (0.2t_i)^{1.514} \tag{2}$$

where, h_i is the monthly heat index and t_i is the mean monthly temperature. The annual heat index is simply calculated by summing the monthly heat index values as:

$$H_y = \sum_{i=1}^{12} h_i \tag{3}$$

where, H_y is the yearly heat index. The unadjusted potential evapotranspiration is then determined for each month as follows:

$$e_i = 1.6\left(10t_i/H_y\right)^a \tag{4}$$

where, e_i is the unadjusted potential evapotranspiration for a month with 30 days and a is a coefficient given by:

$$a = 6.75 \times 10^{-7}H_y^3 - 7.71 \times 10^{-5}H_y^2 + 0.017921H_y + 0.49239 \tag{5}$$

The unadjusted potential evapotranspiration is then corrected for the location (latitude) and the number of days in the month as:

$$PE_i = e_i(d_i n_i/30) \quad (6)$$

where, PE_i is the adjusted potential evapotranspiration for the month i; d_i is the day length correction factor (provided in McKeen and Johnson 1990); and n_i is the number of days in the month. A detailed explanation of the original TMI calculation process is given by McKeen and Johnson (1990) and Fityus et al. (1998). Equation 1 was later modified by Thornthwaite and Mather (1955) and is given as:

$$TMI = 100(P/PE - 1) \quad (7)$$

where, P is the annual precipitation. The potential evapotranspiration (PE) is determined using the same Thornthwaite (1948) model described above. As part of the NCHRP 1-40D research project for the development of the MEPDG, Witzack et al. (2006) modified Eq. 7 as follows:

$$TMI = 75(P/PE - 1) + 10 \quad (8)$$

TMI CONTOUR MAPS

TMI contour maps are produced based on the three models, Eqs. 1, 7, and 8, mentioned above using the climatic data obtained from seventy seven Oklahoma Mesonet weather stations representing seventy seven counties in the state. Contour maps consist of lines connecting points of equal values of TMI for a certain region. To create the contour maps of TMI, the method of Inverse Distance Weighting (IDW) has been applied in ArcGIS software. IDW is a type of interpolation scheme with a known scattered set of points. Having the TMI values for the seventy seven points (representing climatic data for the seventy seven counties in Oklahoma), the values to unknown points are calculated with a weighted average based on the available TMI values.

The original TMI calculations based on Eq. 1 are related to maximum water storage as well as the initial water storage. The original TMI maps produced by Thornthwaite (1948) were based on the assumption that the maximum water storage of 10 cm regardless of the soil type. Studies (i.e., Russam and Coleman 1961; Aitchison and Richards 1965; Wray 1978; and others) that established correlations between the TMI and unsaturated soil parameters (i.e., depth to constant suction and equilibrium suction) were based on the original TMI map using a maximum water storage of 10 cm. In order to make a comparison and to use the same established correlations for the equilibrium soil suction and depth to constant suction, a TMI contour map was constructed using the original Thornthwaite (1948) equation with the maximum water storage of 10 cm. The map is depicted in Fig. 1.

Using the same climatic data obtained from the seventy seven Mesonet weather stations across Oklahoma, TMI contour maps using Eq. 7 and Eq. 8 were also obtained and are shown in Fig. 2 and Fig. 3, respectively. Although there are similar TMI

contour patterns in the three maps (e.g., Figs. 1, 2, and 3), there are some significant differences in the TMI values across Oklahoma. This clearly emphasizes the importance of the methodology employed in the calculation of the TMI and the use of those values in the prediction of the moisture active zone. Therefore, caution should be exercised when attempting to predict a climate-dependent unsaturated soil parameter (e.g., depth to constant suction and equilibrium soil suction) from a TMI contour map.

Table 1 gives a number of TMI values selected from Figs. 1, 2, and 3 representing different climatic regions in Oklahoma. As it was mentioned above, the three TMI prediction models resulted in different values even though they showed similar trends across Oklahoma. However, Table 1 indicates that the differences between the original Thornthwaite (1948) and Witczak et al. (2006) methods are relatively small as compared the results based on the Thornthwaite and Mather (1955) method.

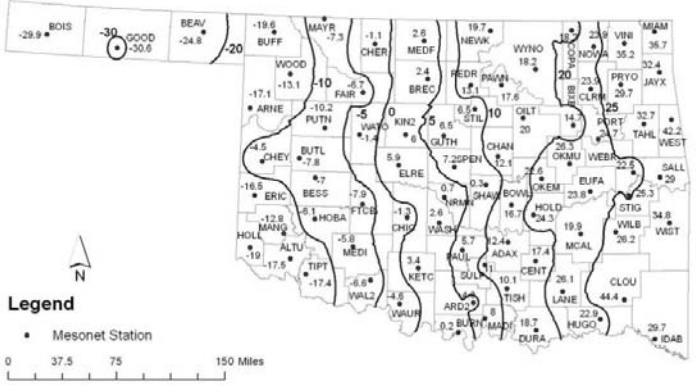

FIG. 1. TMI Contour Map Based on Thornthwaite (1948) Equation.

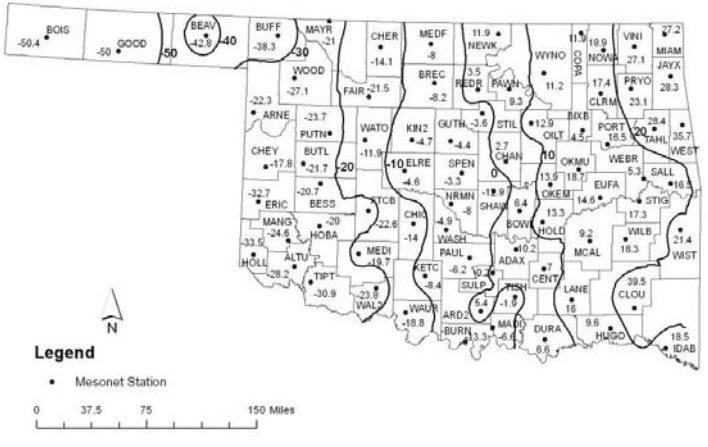

FIG. 2. TMI Contour Map Based on Thornthwaite and Mather (1955) Equation.

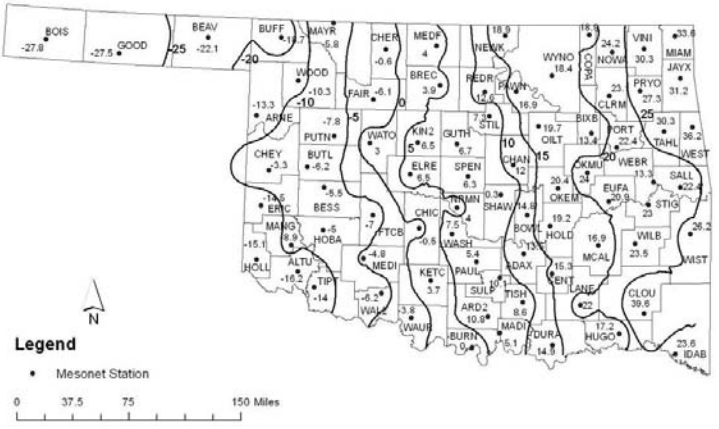

FIG. 3. TMI Contour Map Based on Witczak et al. (2006) Equation.

Table 1. Comparison of TMI Values Between Different Methods and Climatic Conditions.

Weather Station	Dry Climate		Equilibrium Climate		Wet Climate	
	BUFF	HOLL	MEDF	ARD2	MIAM	IDAB
Thornthwaite (1948)	-19.6	-19.0	2.6	4.3	35.7	29.7
Thornthwaite and Mather (1955)	-38.3	-33.5	-8.0	5.4	27.2	18.5
Witczak et al. (2006)	-18.7	-15.1	4.0	10.8	33.6	23.6

TMI IN ENGINEERING PRACTICE

TMI is widely used in Australia for the design of footings in expansive soils, and has been endorsed by the Australian standard AS 2870 (Fityus et al. 1998). The correlation between TMI and the depth to constant suction has been established over the years from field observations, site monitoring, and experience (Aitchison and Richards 1965; Fityus et al. 1998). They have proposed a correlation between the climatic classification, TMI and depth to constant water content as given in Table 2.

McKeen and Johnson (1990) conducted a comprehensive theoretical analysis of the moisture diffusion process in unsaturated soils for the prediction of the depth to constant suction, and attempted to correlate this depth with TMI. The analyses indicated that depth to constant suction varies from about 1.2 m to about 10 m depending on different climatic and soil conditions. McKeen and Johnson (1990) also reported correlations between TMI and moisture active zone from field observations and experience. These correlations are given in Table 3.

Table 2. TMI and Depth to Constant Suction Classification in Australia Based on Thornthwaite and Mather (1955) model (from Fityus et al. 1998).

Climate Classification	TMI	Depth to Constant Suction (m)
Wet Coastal/Alpine	>40	1.5
Wet Temperate	10 to 40	1.5 to 1.8
Temperate	-5 to 10	1.8 to 2.3
Dry Temperate	-25 to -5	2.3 to 3.0
Semi-arid	<-25	3.0

Table 3. TMI versus Depth to Constant Suction for Several Cities in US Based on Thornthwaite (1948) model (from McKeen and Johnson 1990).

Site	TMI	Depth to Constant Suction (m)
Amarillo	-55.6	3.7
Dallas	-30.5	2.1-4.6
Houston	45.7	1.5-3.0
San Antonio	-40.6	3.0-9.1
Jackson	76.2	3.7
Gallup	-81.3	1.2
Denver	-25.4	3.0

Comparison of the results from Table 2 and Table 3 indicates that the correlations between TMI and moisture active zone (depth to constant suction) could be misleading. For instance, for wet climates with TMI values larger than 40, the Australian method limits the constant suction depth to 1.5 m, while it can be between 1.5-3.0 m for a TMI value of 45.7 as suggested by McKeen and Johnson (1990). This simple analysis clearly indicates that it is very important to realize the limitations of such correlations. In the literature, these correlations are simply known as the TMI versus depth to constant suction regardless of the methods used in deriving them. However, as far as a consistent methodology is adopted, TMI can still confidently be used to predict ranges of those depths. Applications of TMI in predicting moisture active zone and constant suction have been widely used for pavement design and evaluation in Texas (Gay 1994; Lytton et al. 2004).

CONCLUSIONS

This research paper has evaluated historical climatic data from weather stations in Oklahoma and obtained Thornthwaite Moisture Index (TMI) contour maps using three different approaches. The analysis of the different approaches with the results of the correlations between TMI and moisture active depth clearly indicates that caution should be exercised in adopting a methodology (a TMI analysis model) for the prediction of the climatic-related unsaturated soil parameters. The TMI methods can

be improved further with more rigorous models for the computation of the potential evapotranspiration.

ACKNOWLEDGEMENTS

The authors thank and acknowledge the support provided by the Oklahoma Transportation Center and the Oklahoma Department of Transportation.

REFERENCES

Aitchison, G.D. and Richards, B.G. (1965). "A Broad Scale Study of Moisture Conditions in Pavement Subgrades throughout Australia." *Moisture Equilibria and Moisture Changes in Soils Beneath Covered Areas*, Butterworths, Sydney.

Edris, E.V. & Lytton, R.L. (1976). "Dynamic Properties of Subgrade Soils, Including Environmental Effects." *Research Report No. TTI-2-18-74-164-3*, Texas Transportation Institute, College Station, Texas.

Fityus, S.G., Walsh, P.F., and Kleeman, P.W. (1998). "The Influence of Climate as Expressed by the Thornthwaite Index on the Design Depth of Moisture Change of Clay Soils in the Hunter Valley." *Conference on Geotechnical Engineering and Engineering Geology in the Hunter Valley*, Conference Publications, Springwood, Australia: 251-265.

Gay, D.A. (1994). "Development of a Predictive Model for Pavement Roughness on Expansive Clay." *Doctoral Dissertation*, Texas AandM University, College Station, Texas.

Lytton, R.L., Aubeny, C.P., and Bulut, R. (2004). "Design Procedure for Expansive Soils." *Research Report No. FHWA/TX-05/0-4518-1*, Texas Transportation Institute, College Station, Texas.

McKeen, R.G., and Johnson, L.D. (1990). "Climate Controlled Soil Design Parameters for Mat Foundations." *ASCE Journal of Geotechnical Engineering*, Vol. 116 (7): 1073-1094.

Perera, Y.Y., Zapata, C.E., Houston, W.N., and Houston, S.L. (2004). "Long term moisture conditions under highway pavements." Geotechnical Engineering for Transportation Projects: *Proceedings of Geo-Trans 2004. ASCE Special Publication No. 126.*

Russam, K. and Coleman, J.D. (1961). "The Effect of Climatic Factors on Subgrade Moisture Conditions." *Geotechnique*, Vol. 3 (1): 22-28.

Thornthwaite, C.W. (1948). "An Approach Toward A Rational Classification of Climate." *Geographical Review*, Vol. 38 (1): 54-94.

Thornthwaite, C.W. and Mather, J.R. (1955). "The Water Balance." *Publ. Climatol.*, Laboratory of Climatology, Vol. 8 (1): 104 p.

Witczak, M.W., Zapata, C.E., and Houston, W.N. (2006). "Models Incorporated into the Current Enhanced Integrated Climatic Model for Used in Version 1.0 of the ME-PDG." *NCHRP 9-23 Project Report*, Arizona State University, Tempe, Arizona.

Wray, W.K. (1978). "Development of a Design Procedure for Residential and Light Commercial Slabs-on-Ground Constructed on Expansive Soils." *Doctoral Dissertation*, Texas A&M University, College Station, Texas.

Performance Evaluation of Superflex Modified Thin Asphalt Overlay

Xudong Hu[1,2], Qisen Zhang[3], Sheng Zhao[4], Wei Chen[5],
Yan Sun[2] and Liangyun Tao[2]

[1] PhD candidate, School of Civil Engineering, Central South University, Changsha, China, 410072; sailor24@126.com
[2] Lecturer, Dept. of Transportation Engineering, National University of Defense Technology, Changsha, China, 410072; sailor24@126.com
[3] Professor, School of Transportation Engineering, Changsha University of Science and Technology, Changsha, China, 410004; 13808418373@139.com
[4] Graduate Student, Civil & Environmental Engineering, University of Tennessee, Knoxville, Tennessee, USA, 37996; szhao2@utk.edu
[5] Engineer, Hunan Transportation Department, Changsha, China, 410072; 5514614@qq.com

ABSTRACT: The use of thin asphalt overlay is an effective way in preserving and maintaining the road surface. In this study, the virgin asphalt was mixed up with Superflex modifier at varied concentrations to get the modified asphalt overlay, and the optimum modifier content was 15% by weight of the total mix. Aggregate gradation of the overlay was acquired by means of volume method, and the optimal asphalt content was obtained through Marshall mix design. The performance of the modified overlay mixture evaluated in the laboratory included high-temperature stability, moisture susceptibility and skid resistance. In order to investigate the effects of different thickness levels and structure patterns, four thin overlay sections were paved on route G321 in Guangdong, China. Deflection, skid resistance, permeable performance and roughness were inspected four times in the following six years. The laboratory test results showed that all the testing indices satisfied the criteria specified in China. The field inspection data proved that the thin asphalt overlays evaluated in this study performed well in terms of skid resistance, permeable performance and roughness in every section, without sharp damage on the surface. It can be concluded that the Superflex modified asphalt mixture can be used as thin overlay and this technology is worth popularizing.

INTRODUCTION

Although the structures of most cement concrete pavements are in good condition in terms of the ultimate strength, there are some surface function damages occurring, such as exfoliation, slippage and poor roughness after several years' service. The pavement could recover from the surface function damage by reducing the influence of elevating the pavement and economizing the construction resources. According to previous construction experiences, however, thin asphalt overlay might be a better solution to this problem. It can improve the smoothness of the road surface, relieve the pressure of road investment and serve as an effective preventive measure for road maintenance, which is, in addition,

adapted to the tendency towards low-carbon economy.

LABORATORY EXPERIMENTAL PROGRAM

Virgin Asphalt

Esso 70# (Penetration grading system) was chosen as the virgin asphalt. It is now widely used in highway construction in hot and rainy areas. This asphalt is frequently used to produce SBS modified asphalt. The SHRP classification indices of Esso 70# virgin asphalt are listed in Table 1. The testing indices of Esso 70# satisfied AASHTO specifications according to Table 1. In the meanwhile, this asphalt can be graded as PG 64-22 or even higher grade following SHRP grading system.

Table 1. Esso 70# Virgin Asphalt SHRP Indices

Item		Unit	Criteria	Result	Method
64℃ Dynamic Shearing, G*/sin δ		kPa	≥1.0	1.465	AASHTO T315-04
Residue after RTFOT[1] 64℃ Dynamic Shearing, G*/sin δ		kPa	≥2.2	2.571	AASHTO T240-03 AASHTO T315-04
Residue after PAV[2]（100℃）25℃ Dynamic Shearing, G*/sin δ		kPa	≤5000	2544	AASHTO R28-02 AASHTO T315-04
Residue after PAV （-12℃）	Creep	MPa	≤300	256	AASHTO R28-02 AASHTO T313-04
	m Value	/	≥0.3	0.313	

Notes: [1]Rolling thin film oven tests. [2] Pressurized aging vessel.

Modified Additive

Superflex modifier is a mixture of modified asphalt with natural dust particles. The Superflex modifier used in this study was produced in TMA Company in Indonesia (Figure 1). The main advantage of this modifier is better cohesiveness and high-temperature stability. Superflex modified asphalt was made by mechanical blending Superflex modifier with virgin asphalt. Some of the test indices of Superflex are listed in Table 2.

Superflex modifier is similar to Trinidad Lake Asphalt (TLA) in ambient temperature which has high viscosity. Three concentrations (10%, 15% and 20% by total weight) of the modifier were chosen in this study in order to verify the optimum modifier content claimed as 15% by TMA. Table 3 presents the results of some basic tests conducted on the modified binder. It can be seen that 15% is the optimum modifier content since penetration, ductility, softening point and elasticity recovery rate of the modified binder containing 15% Superflex meet the criterion of SBS I-D of China with viscosity satisfying the standard of modified asphalt in Japan.

FIG. 1. Superflex Modifier.

Table 2. Superflex Modifier Test Indices

Item	unit	Result	Method
Penetration（25℃,100g,5s）	0.1mm	42	T 0604-2000
PI	/	5.9	
Softening Point (R&B)	℃	>100	T 0606-2000
Ductility（5℃）	cm	21	T 0605-1993
Recovery of elasticity	%	85	T 0662-2000

Table 3. The Conventional Test Results of Superflex Modified Asphalt

Virgin Asphalt		Esso 70#			
Superflex modifier content		0%	10%	15%	20%
Penetration（100g,5s）（0.1mm）	25℃	70	66	64	62
Ductility（5cm/min）（cm）	15℃	0.6	6.4	7.6	8.1
Softening point	℃	48.0	51.0	68.5	74.5
Mass loss after RFOT	（%）	0.07	0.02	0.05	0.02
Ratio of penetration after RFOT（25℃）	（%）	70.5	78.2	78.8	86
Rotary viscosity（135℃, 27,100RPM）	（Pa·s）	0.33	1.03	1.439	2.109
Elasticity recovery rate （25℃）	（%）	4.0	19.0	29.0	34.0

Mix Design

The coarse and fine aggregates were sieved according to AASHTO T30, which were all from Luohong stone ground in Zhaoqing, China. The gradation of filler and three types of aggregates are presented in Table 4. The specified gradation range was also provided by TMA. The synthetic gradation satisfied the demand of the specified range as shown in Figure 2.

Table 4. Gradation of the Aggregates

Sieve Size (mm)	The mass percentage of passing through the sieve size(%)										
	16	13.2	9.5	4.75	2.36	1.18	0.6	0.3	0.15	0.075	<0.075

1# 9.5~13.2mm		99.6	97.3	47.3	0.5	0.1	0.1	0.1	0.1	0.1	0.1	0.0
2# 4.75~9.5mm		100	100	98.8	32.4	2.5	1.0	0.8	0.6	0.6	0.6	0.0
3# 0~4.75mm		100.0	100	100.0	95.1	69.8	55.3	41.6	21.7	13.7	9.4	0.0
filler		100.0	100	100.0	100.0	100	100	100	97.4	90.6	75.8	0.0
Design gradation		99.9	99.1	81.7	40.7	23.7	19.7	16.3	11.3	9.0	7.1	0.0
Specified	Upper limit	100	100	100.0	55.0	35.0	28.0	22.0	16.0	12.0	10.0	0.0
gradation	Middle level	100	100	87.5	45.0	27.5	20.5	16.0	11.0	8.0	7.0	0.0
range	Lower limit	100	100	75.0	35.0	20.0	13.0	10.0	6.0	4.0	4.0	0.0

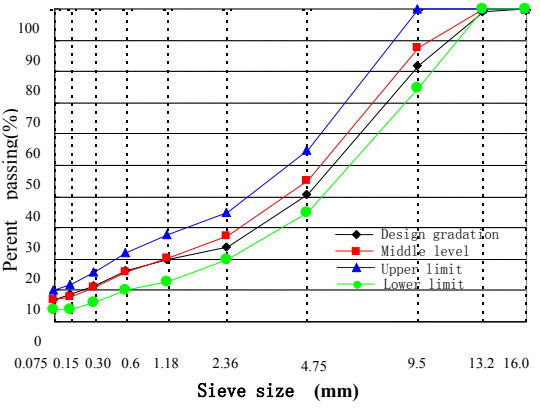

FIG. 2. Aggregate Gradation.

PERFORMANCE OF ASPHALT MIXTURE

High-temperature stability

The wheel rutting test was used to examine the dynamic stability and the high-temperature stability of mixtures. According to Chinese specifications, specimens of 300 mm by 300 mm by 50 mm were prepared and cooled down to ambient temperatures for 48 hours, then tested with rubber wheel load pressure of 0.7±0.05 MPa at 60℃ (traversing distance of 230mm, frequency of 42 times/min). The samples were tested in triplicate, and the results are shown in Table 5. Dynamic stability of modified asphalt mixture and virgin mixture are specified no less than 2,800/mm and more than 1,000/mm, respectively, according to the specifications. Table 5 shows that the high-temperature stability of the Superflex modified asphalt mixture satisfied the requirement of virgin mixture while did not satisfy that of modified asphalt mixture.

Table 5. The Results of Rut Test

Items	Dynamic Stability (time/mm)		C_v	Temperature	Tire forces
	Single Value	Average	(%)	(℃)	(MPa)
sample-1	1800	1862	19.4	60	0.7
sample-2	2250				

sample-3	1537

Moisture Susceptibility

Marshall specimens were made with 5.3% asphalt by weight of aggregate in order to test the moisture susceptibility of the mixture. As shown in Table 6, the residual stability reached 99.2% in accordance with the immersion Marshall test, indicating the water stability of superflex modified asphalt mixture met the demand of technical requirement of modified asphalt mixture. Therefore, the Superflex modified mixture showed good moisture resistance.

Table 6. The Result of Immersion Marshall Test

Asphalt –aggregate ratio	Density (g/cm^3)		Immersion for 30~40min					Residual stability (%)	Criteria (%)
	bulk volume	Theoretical value	Air Void (%)	VMA (%)	Asphalt saturation (%)	Stability (kN)	Flow value (0.1mm)		
	2.471	2.572	3.9	14.9	73.6	8.47	22.6		Ordinary
	2.477	2.572	3.7	14.7	74.8	8.57	27.8		asphalt
5.3	2.475	2.572	3.8	14.7	74.5	8.58	26.3		mixture
	2.471	2.572	3.9	14.9	73.7	9.35	22.7		⩽80
	2.463	2.572	4.2	15.2	72.1	9.40	20.9	99.2	Modified
									asphalt
Average	2.471	2.572	3.9	14.9	73.7	8.87	24.1		mixture
									⩽85

Skid Resistance

Samples in triplicate were made to obtain friction coefficient, texture depth and water permeability so as to examine the skid resistance. The results are shown in Table 7-9 and it can be seen that friction coefficient, construction depth and seepage coefficient of the mixture met the requirements. In addition, the mixture also showed good stability against sliding.

Table 7. The Result of Friction Coefficient Test

Sample No.	Tilting apparatus						Friction coefficient	Criteria
	1	2	3	4	5	average		
1	71	72	70	71	70	70.8		
2	67	66	67	66	68	66.8	70	⩾45
3	72	71	73	70	71	71.4		

Table 8. The Result of Texture Depth Test

Sample No.	Average diameter D(mm)	Texture depth $T_D = \frac{1000V}{\pi D^2/4}$ (mm)		Criteria
		single	average	
1	231	0.60		
2	225	0.63	0.63	⩾0.55
3	220	0.66		

Table 9. The Result of Water Permeability Test

Sample No.	The initial volume $V_1(ml)$	The last volume $V_2(ml)$	The initial time $t_1(s)$	The last time $t_2(s)$	Permeability coefficient $C_W = \frac{V_2 - V_1}{t_2 - t_1} \times 60$ (ml/min) single	Permeability coefficient $C_W = \frac{V_2 - V_1}{t_2 - t_1} \times 60$ (ml/min) average	Criteria (ml/min)
1	100	500	0	974	24.6		⩽80
2	100	500	0	1018	23.6	24.2	(for Stone
3	100	500	0	982	24.4		Matrix Asphalt)

FIELD SECTION TESTING

Project Selection

The selected project was to conduct pavement preventative maintenance on national highway 321(G321), from K159+480 to K160+090, a two-way four lanes road with the width of 18-meter, located in Zhaoqing, China. This area has a subtropical monsoon climate with an annual average temperature of 21.2℃, which is hot and rainy. The annual rainfall capacity is 1650-millimeters and the largest daily rainfall capacity is 317-millimeters. The spring and summer are rainy seasons.

Structural Concepts

Delaying or preventing cracking is critical when asphalt mixture is paved on top of the old cement concrete pavement as thin overlay. Four sections were constructed in the field. The stress absorbing layer was constructed in section B and section C in order to verify the impact of the thin overlay on preventing cracking. The thickness of the overlay in section A and section B was 4 cm, and was changed to 3cm in section C and section D in order to test the optimal thickness. The structural concepts are shown in Figure 3.

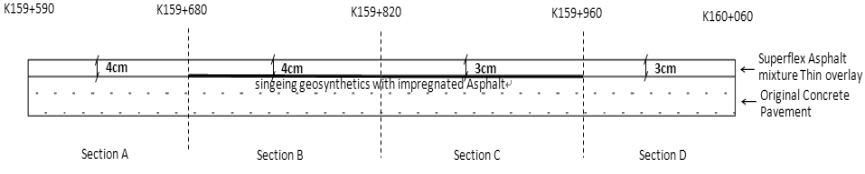

FIG. 3. The Structure of the Test Road

Inspection and Analysis

The field project was finished on May 12, 2006. It has been inspected and observed four times, on May 14, 2006, Oct 26, 2006, Jul 2, 2009 and Mar 31, 2012, respectively (which are labeled as I, II, III, and IV in Figure 4-7). Benkelman beam, Permeameter, British pendulum tester and straightedge (3m) were used to inspect deflection, skid resistance, permeable performance and roughness, respectively. The results are listed in Figure 4-7. According to the test results, the performance of every section declined over time, but it was observed

that the pavement performance indices of all sections of thin overlay met Chinese design requirements after six years' operation. Meanwhile, the Superflex modifier excelled in improving moisture susceptibility and skid resistance of the asphalt mixture. The technical indexes among four sections were not significantly different, which meant the 3cm depth of Superflex modified asphalt mixture met the performance requirements of thin overlay. In addition, the roughness of section B and C with geosynthetics was inferior to that of section A and D, mainly due to the use of less rough geosynthetics during construction.

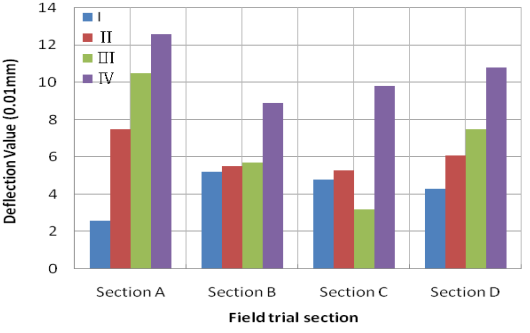

FIG. 4. Comparison of the Deflection Values for Various Sections.

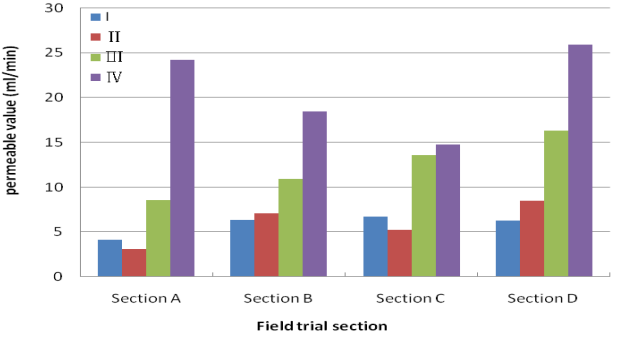

FIG. 5. Comparison of the Permeable Values for Various Sections

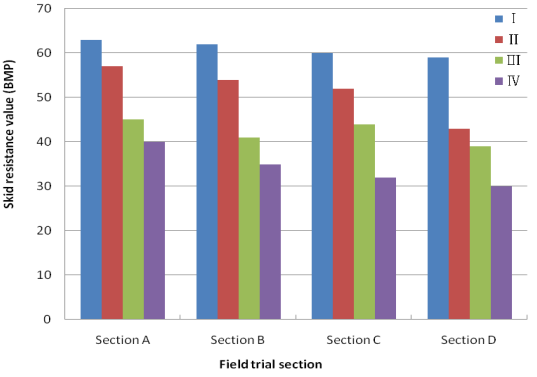

FIG. 6. Comparison of the Skid Resistance Values for Various Sections

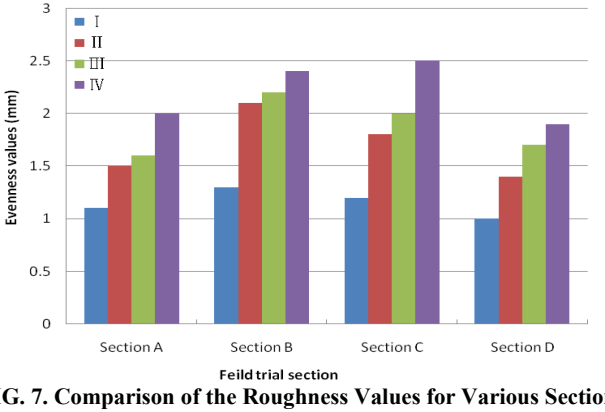

FIG. 7. Comparison of the Roughness Values for Various Sections

CONCLUSION

In this paper, Superflex modified asphalt was evaluated to be used as thin overlay. The performance of the Superflex modified asphalt mixture was evaluated in the laboratory for high-temperature stability, moisture susceptibility and skid resistance. All the testing indices were in accordance with the specifications, except for high-temperature stability. According to different thickness and structure patterns, four thin overlay sections were paved in the field. Then evaluation of deflection, Skid resistance, permeable performance and roughness was conducted on the field sections and every section was qualified with no sharp damage seen on the surface. Conclusions can be drawn as follows:

1. According to the experiments on virgin asphalt mixed with Superflex modifier in different concentrations, 15% Superflex was verified as the optimum modifier content for the binder selected in this study. The penetration, ductility, softening point and elasticity recovery rate of the mixed Superflex modified asphalt met the criterion of SBS I-D of China. In addition, viscosity satisfied the standard of modified asphalt in Japan.

2. Superflex modified asphalt mixture can meet the technical requirements for water stability of modified asphalt but not for high temperature stability, while satisfied the criteria for virgin mixture.

3. As time went on, the performance of every section declined, but the pavement performance indices of all overlay sections satisfied Chinese design requirements after six years of operation. The Superflex modified asphalt mixture excelled in improving moisture susceptibility and skid resistance compared to ordinary asphalt mixture.

4. The technical indexes of four sections were not significantly different. 3cm depth of Superflex modified asphalt mixture met requirements of pavement performance for thin overlay. The technology of the thin overlay presented good function and is worth popularizing.

REFERENCES

Rasmussen, R.O. and Rozycki, D. (2004). *NCHRP Synthesis 338: Thin and Ultra-thin Whitetopping*. Transportation Research Board, National Research Council, Washington, D.C.:3-9.

Pretorius, F. J., Wise, J. C., and Henderson, M. (2004). "Development of Application Differented Ultra-thin Asphalt Friction Courses Southern African Application". *8th Conference on Asphalt Pavement for Southern Africa*. Sun City, South Africa: Paper012.

McGhee, K. H. (1994). *NCHRP Synthesis of Highway Practice 204: Portland Cement Concrete Resurfacing*. Transportation Research Board, National Research Council, Washington, D.C.,73 p.

Tritsch, S.L. (1995). "Whitetopping Technique Revives Burgeoning Kansas Thoroughfare." *Report PA-135*, Fiber mesh Division, Synthetic Industries:324-331.

Rasmussen, R.O., et al. (2003), "Performance and Design of Whitetopping Overlays on Heavily Loaded Pavements", *Final Report for Concrete Pavement Technology Program Task 3(99)*, Vols.5, Federal Highway Administration, Washington, D.C.:521-530.

Performance of Paving Fabric Reinforced Asphalt Mixture

Peng Li[1], Jenny Liu[2], M. ASCE, Mike Samueloff[3], David Jones[4]

[1]Lecturer, College of Highway, Changan University, Xian, Shanxi, China, 710064, Phone: +8618681824903, Email: pengli_ak@qq.com
[2]Associate Professor, Department of Civil and Environmental Engineering, University of Alaska, Fairbanks, AK 99775-5900, Phone: 907-474-5764, Fax: 907-474-6030, Email: jliu6@alaska.edu
[3]TenCate Geosynthetics & Industrial Fabrics, Paving Division, 3930 Gatwick Drive, Troy, MI 48083, Phone: 248-250-7714
[4] TenCate Geosynthetics & Industrial Fabrics, 365 South Holland Drive, Pendergrass, GA, Phone: 706-693-1734

Abstract: The paving fabrics as interlayers have been used in asphalt overlays in a variety of design and construction situations for more than three decades. A number of positive benefits have been identified such as waterproofing control for base and subgrade protection, improved fatigue resistance, and reduced reflection of existing cracks, etc. In cold regions such as Alaska and other northern states, pavements are more prone to distresses due to extreme climatic conditions. A study has been conducted to explore how paving interlayers function in asphalt pavements in Alaska. This paper presents laboratory investigation of performance of asphalt mixtures reinforced with three types of paving fabrics. These three types of paving fabrics included two biaxial fabrics (i.e. PGM-G100/100 and PGM-G50/50) and one newly developed multi-axial reinforced paving composite, PGM-G^4. The performance tests included asphalt retention, grab strength, shear strength, permeability, and indirect tension (IDT). The results showed that adding paving fabric can increase pavement structure stiffness, greatly reduce the permeability and also provide good resistance to low temperature cracking. The multi-axial PGM-G^4 paving composite provided the best overall pavement performance.

INTRODUCTION

Asphalt overlay is the most effective way of maintenance and rehabilitation to recover the pavement performance (Hall et al. 2002). However, asphalt overlay is subjected to the reflective cracking and increasing the thickness of overlay would only postpone the propagation of such cracking (Browning 1999; Hughes and Somers 2000; Amini 2008).

The paving fabric can provide stress relieving membrane to absorb the reflective cracking (Lytton 1989, Prieto et al. 2007, Penman and Hook 2008) and reinforcement to increase overall structure stiffness and effectively spread load horizontally (Austin

and Gilchrist 1996). Due to its ability of asphalt absorption, nonwoven materials have remarkable crack relieving function (Marienfeld and Baker 1999). In addition, the fabric could also provide a waterproofing barrier and drainage system to dissipate water through sideway (Marienfeld and Baker 1999; Correia et al. 2011). Thus, using paving fabric can improve the pavement performance after overlay, extend service life and save maintenance cost in long run.

The interlayers primarily used for pavement reinforcement application and available in the market are manufactured as biaxial. Biaxial grids with equal strength in both the machine and cross machine directions allow stress transfer mainly in longitudinal and transverse directions. The new PGM-G^4 paving composite invented by TenCate Geosynthetics contains multi-axial fiberglass filament yarn, which changes the aperture geometry from a rectangular to a quad angular grid structure. This unique feature improves the structure radial stiffness and efficiently distributes stress from surface layer to geogrid throughout the full 360^o. This unique feature could deliver optimal asphalt concrete (AC)/grid interaction and more efficient reinforcement, which leads to lower cost, longer lasting and more reliable asphalt pavements by improving performance, increasing service life, and extending maintenance and rehabilitation intervals.

In cold regions such as Alaska and other northern states, pavement and paving fabrics are more prone to distresses due to severe climatic conditions. A study has been conducted to explore how paving interlayers function in asphalt pavements in Alaska. The performance of asphalt mixtures reinforced with three types of paving fabrics were investigated in the laboratory. These three types of paving fabrics included two biaxial fabrics (i.e. PGM-G100/100 and PGM-G50/50) and one newly developed multi-axial reinforced paving composite, PGM-G4. Preliminary results of laboratory performance tests including asphalt retention, grab strength, shear strength, permeability, and indirect tension (IDT) were presented in this paper.

MATERIALS

In this study, the hot mix asphalt (HMA) was laboratory blended mixtures according to the job mix formula (JMF) used for Rich Hwy North Pole Interchange paving project located in North Pole, Alaska. The nominal maximum aggregate size (NMAS) was 12.5mm. The JMF was designed using Marshall mix design method. The mix had an optimum binder of 5.4% and the design air void was 4% with 16% voids in mineral aggregate (VMA). The maximum theoretical density was 2.483g/cm^3. PG 64-34 polymer modified binder was used. The aggregate and binder were collected form the same sources as used in the paving project. Three types of paving fabrics were used, including two conventional biaxial fiberglass yarn paving composite (PGM-G100/100 and PGM-G50/50), and one multi-axial fiberglass yarn paving composite (PGM-G^4) (FIG.1). Both PGM-G100/100 and PGM-G50/50 contain the same type of nonwoven material. PGM-G100/100 has three fiberglass yarns in each direction and PGM-G50/50 has two.

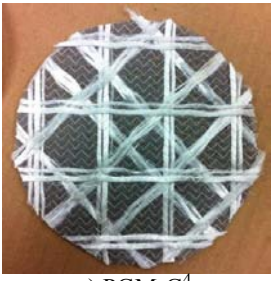
a) PGM-G[4]

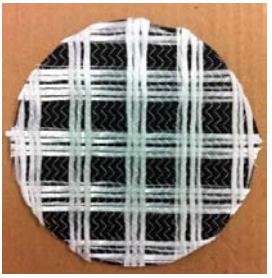
b) PGM-G100/100

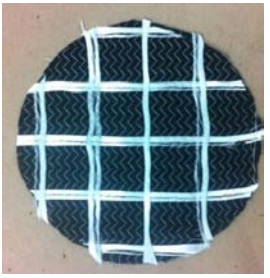
c) PGM-G50/50

FIG. 1. Paving Fabrics Used for Specimen Fabrication

LABORATORY TESTING

Asphalt Retention of Fabrics

The asphalt retention tests were performed on three types of paving fabrics according to ASTM D6140. Fabrics were cut into the sizes of 100 mm (4 in) in width and 200 mm (8 in) in length. Four specimens were made for each type of fabric. The weight of each specimen was measured and recorded. Specimens were then submerged in the asphalt binder for 30 minutes. Due to higher viscosity of modified binder, the conditioning temperature was increased from 135°C (ASTM D6140) to 145°C. This temperature was chosen according to the compaction temperature specified in the JMF, in which PG 64-34 modified binder was used. Then, saturated specimens were hung in the oven at 145°C for 30 minutes and then rotated 180° and hung for additional 30 minutes. The weights of saturated specimens were measured and recorded again. The weight difference per unit area was then calculated as the asphalt retention on the unit area.

Grab Strength Tests of Fabrics

Grab strength tests were performed to measure the breaking load of fabrics using grab method according to ASTM D4632. For PGM-G100/100 and PGM-G50/50, fabrics were cut into the size of 25 mm by 200 mm and for PGM-G[4], the fabric was cut into the size of 41 mm by 200 mm, to cover the width of one grid apertures. 12 samples were made for each type of fabric. Both original and saturated fabrics were tested. The method used to saturate specimens was same as the one used in asphalt retention test. During the testing, the specimen was grabbed at both ends and the tensile load was applied along the direction of specimen. The breaking loads were measured and recorded.

Shear Test

The shear tests were performed to measure the shear strength among the interface between layers. Two types of fabric were used, PGM-G[4] and PGM-G100/100,

because PGM-G100/100 and PGM-G50/50 used same nonwoven material and the installation of fiber glass on both paving composites were similar. Specimens of 120 mm in height and 150 mm in diameter were compacted using the Superpave gyratory compactor (SGC), with paving fabric placed in the middle of specimens. The number of gyration was adjusted to achieve the target air voids of 4% listed in the JMF. The tack coat (PG 64-34 binder) was applied and the rates used for PGM-G100/100 and PGM-G[4], were 1.22 liter/m^2 and 0.86 liter/m^2, respectively according to the manufacturer's recommendation. For each fabric, two types of specimens were made: one with glass side of paving composite facing down and another with nonwoven side of paving composite facing down. By comparing the results from these two types of specimens, one could determine the best way to place the fabric in the pavement to ensure strong bonding between paving fabric and AC. As shown in FIG.2, the specimen was held in a shear fixture during testing, and the vertical load was applied on the top part of the specimens at the rate of 12.5 mm/min until specimens were sheared apart.

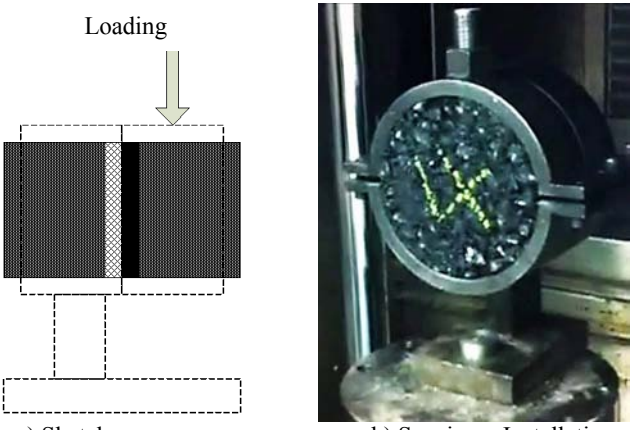

a) Sketchy b) Specimen Installation

FIG. 2. Shear Testing Setups

Permeability

Permeability, or coefficient of permeability, is the rate at which a porous material will transmit water under a hydraulic gradient (Kanitpong et al. 2001). The permeability tests were performed using a flexible wall permeameter according to ASTM PS 129-01 (2004). The control group was regular HMA without paving fabric. According to the recommendation from Georgia DOT (GDT 2011), the specimens with the height of 75 mm and target air void of 6% were compacted using the same process as the one used for shear test. FIG. 3 shows the testing setup for the permeability test. Before testing, the specimen was saturated using vacuum. Then, it was taken out and the surface of the specimen was dried using rag. The petroleum jelly was applied on the side of specimen for sealing to prevent water leaking from

the side of the specimen. When the specimen and permeameter was assembled, water was filled into the plastic tube to reach the 500 cm^3 mark (62 cm in height, h_1). Then the draining valve was opened. After 30 min, the water head was read and recorded as h_2. The test was performed twice on the same specimen. The permeability was calculated based on Darcy's law as shown in Eq. 1.

$$k = \frac{aL}{At} \ln\left(\frac{h_1}{h_2}\right) t_c \quad \text{.....(1)}$$

where,

k = coefficient of water permeability, cm/s
a = inside cross-sectional area of inlet standpipe, cm^2 (7.92 cm^2)
L = average thickness of test specimen, cm
A = average cross-sectional area of test specimen, cm^2 (176.7 cm^2)
t = average elapsed time of water flow between timing marks (h_1 and h_2), s
h_1 = hydraulic head on specimen at time t_1, cm
h_2 = hydraulic head on specimen at time t_2, cm
t_c = temperature correction for viscosity of water (1.0 for 20°C)

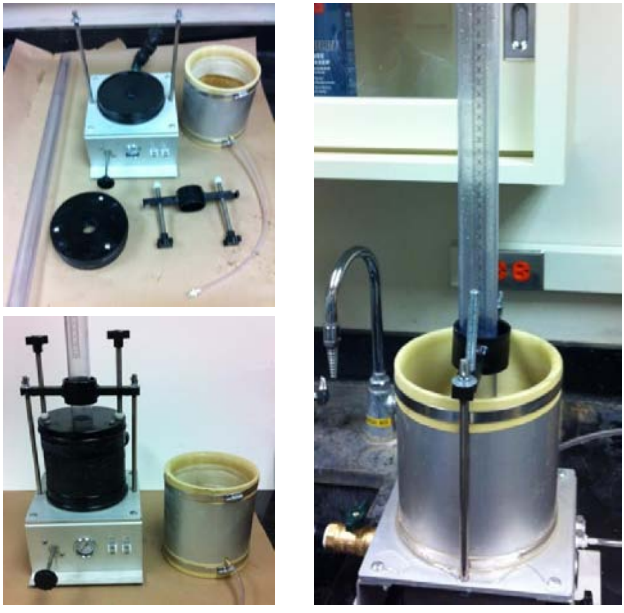

FIG. 3. Permeameter

Indirect Tension Test

IDT creep tests were performed on control HMA (without paving fabric), PGM-G[4], PGM-G100/100, and PGM-G50/50 treated specimens at 20°C, -10°C and -30°C to

evaluate low temperature performance of mixtures. The specimen fabrication process was the same as the one used for the shear test, except that specimens were cut into the thickness of 50 mm. During testing, a vertical load was applied along the radial direction of the specimen, and a horizontal tensile stress was generated in the center of the specimen. A constant load of 12 kN, 1.5kN and 0.15 kN were used at -30°C, -10°C and 20°C, respectively. The total loading period was 1000s.

TESTING RESUTLS

Asphalt Retention

The nonwoven fabric is made of polypropylene, which has an affinity for asphalt binder, due to the similar chemical composition of polypropylene and asphalt binder (TenCate™ Geosynthetics North America 2011). Such property ensures the tack coat asphalt could be bound into fabric providing a moisture barrier and a stress relieving membrane. The tack coat spreading rate was determined according to asphalt retention, which indicated how much asphalt binder was necessary to saturate the fabric. Table 1 summarizes the asphalt retention results for all three fabrics. Among three types of fabrics, PGM-G^4 had the lowest asphalt retention and followed by PGM-G50/50 and PGM-G100/100. PGM-G100/100 and PGM-G50/50 used the same type of nonwoven material and fiber glass could only absorb a little asphalt binder. Therefore, these two types of fabric had the similar asphalt retention. The typical asphalt retention of paving fabric (136 g/m^2 density) was 0.91 liter/m^2 (Amini 2005) and the results obtained from this study were close to this value.

Table 1 Summary of Asphalt Retention (PG 64-34, 145°C)

	PGM-G^4	PGM-G50/50	PGM-G100/100
Asphalt Retention (liter/m^2)	0.828	1.236	1.281

Grab Strength of Paving Fabric

The grab strength is important to constructability and performance of water barrier and reflective cracking control (TenCate™ Geosynthetics North America 2011). Strong fabric would benefit the pavement performance under a high traffic loading and in a cold climate. Table 2 summaries the braking tensile load of the saturated and unsaturated paving fabrics. The highest breaking load was obtained on PGM-G100/100, which was mainly contributed by the three yarns of reinforcement fiberglass. PGM-G^4 had the second highest breaking load. All specimens showed an increase of breaking tensile load after saturation and PGM-G^4 had the highest strength increase after saturation.

The results also indicated that the grab strength of fiberglass reinforced fabric was mainly contributed from fiberglass. As the yarn of fiberglass increased, the strength increased. In addition, during testing, the tensile load was applied along the direction

of fiberglass. For conventional biaxial composite, PGM-G100/100 and PGM-G50/50, if the loading direction was 45^o to the direction of fiberglass, their grab strength would be much lower, because there was not fiber glass installed in this direction. Meanwhile, PGM-G^4 with multi-axial fiberglass could provide same grab strength in 45^o direction which enable more efficient stress distribution within the pavement structure.

Table 2 Saturated vs. Unsaturated Breaking Tensile load (N)

	PGM-G^4	PGM-G50/50	PGM-G100/100
Saturated	2290	2023	4071
Unsaturated	1941	1926	3783
% Difference	18%	5%	8%

Shear Strength

After shear tests, all specimens were sheared off along the glass side of fabric indicating the interface between glass side and HMA was the weak side (FIG. 4). Based on such observation, the fabric needs to be placed with glass side facing down to have a direct contact with tack coat to improve the bonding strength.

a)PGM-G^4 b) PGM-G100/100

FIG. 4. Specimens after shear testing

The shear strength is summarized in FIG. 5. For PGM-G^4 and PGM-G100/100 treated specimens, "_G" stands for that the glass side of fabric was facing down during compaction, and "_N" stands for that nonwoven side of fabric was facing down. It can be seen that the specimens with glass side of fabric facing down had the higher shear strength and the value could be up to 80% higher than the strength of specimens with nonwoven side facing down. Therefore, during the field application,

the fabrics need to be placed glass side facing down to achieve the maximum interface bonding strength. In addition, specimens with PGM-G^4 fabric, which had less fiberglass, had higher shear strength than those with PGM-G100/100. Fiberglass could only absorb a little asphalt and its surface was slippery, which provided less shear resistant and bonding strength than nonwoven materials.

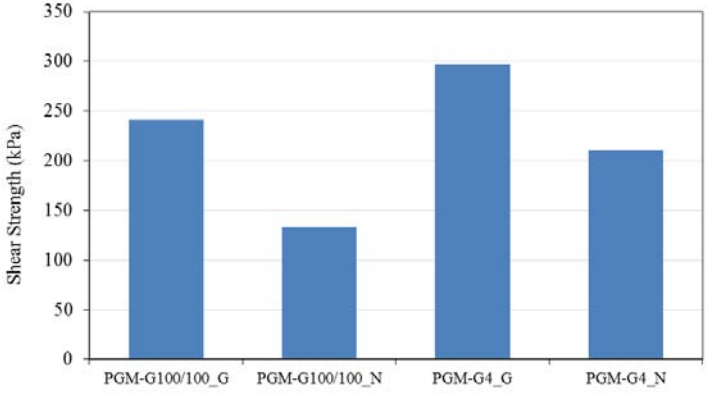

FIG. 5. Summary of Shear Strength

Permeability

Permeability is an important property of HMA, which highly correlates to the moisture susceptibility and durability of asphalt pavement. The recommended maximum acceptable permeability is 125×10^{-5} cm/s (Maupin 2000). FIG. 6 summarizes the effect of paving fabrics on permeability of HMA. The permeability values of all specimens were less than the recommended maximum acceptable permeability, 125×10^{-5} cm/s. The average permeability of control group is 18.5×10^{-5}cm/s. The paving fabric greatly reduced the permeability of HMA specimen. The permeability of paving fabric treated specimens was about 1/10 of that of control group. The lowest permeability was obtained from PGM-G100/100 treated specimens, followed by PGM-G^4 treated specimens and PGM-G50/50 treated specimens.

Indirect Tension Test

The creep compliance is a viscoelastic property of HMA. It is used in the mechanistic empirical flexible pavement design guide (MEPDG) to calculate the thermal stress at low temperatures (ARA, Inc. 2004). For certain stress, the creep compliance can be determined as the ratio of strain to stress at a certain time. The creep compliances at different loading temperatures obtained from IDT creep tests are summarized in Table 3. In general, fabric treated specimens had lower creep compliances than control materials. At 20^{o}C, PGM-G^4 treated specimen had the lowest creep compliance, which was only about half of control group's creep

compliance. At the lower temperatures, i.e. -10°C and -30°C, the creep compliance of three types of fabric treated specimens were close.

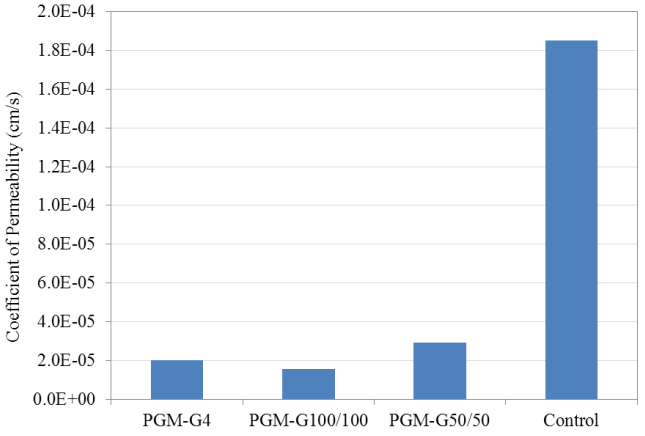

FIG. 6. Permeability Testing Results

Table 3 Summary of Creep Compliance (1/MPa)

Temperature (°C)	Material	Time (s)						
		10	20	50	100	200	500	1000
20	Control	4.90	18.39	46.22	68.08	90.64	121.33	145.55
	G4	5.23	12.31	25.03	35.19	46.20	63.59	78.94
	G50	7.96	19.87	34.17	44.58	55.30	70.97	83.98
	G100	5.09	14.54	30.74	44.70	60.00	82.36	100.45
-10	Control	0.27	0.34	0.60	1.04	1.31	1.71	1.84
	G4	0.19	0.26	0.52	0.81	1.00	1.16	1.23
	G50	0.19	0.26	0.45	0.70	0.90	1.11	1.24
	G100	0.14	0.19	0.40	0.63	0.82	0.97	1.06
-30	Control	0.09	0.09	0.11	0.14	0.17	0.20	0.20
	G4	0.06	0.07	0.08	0.11	0.15	0.17	0.16
	G50	0.05	0.05	0.07	0.10	0.14	0.16	0.17
	G100	0.05	0.05	0.06	0.09	0.13	0.15	0.15

The viscoelastic behavior of HMA is dominated by temperature. It can be seen from FIG. 7 that as temperature dropped from 20°C to -30°C, the creep compliance decreased more than 400 times for all mixtures. HMA with lower creep compliance and lower creep rate would be more prone to low temperature cracking. Though all mixtures showed decreased creep compliance with the decrease of temperature, at very low temperatures, the mixtures with paving fabrics had comparable creep

compliances compared with the control mixtures. On the other hand, adding paving fabric to HMA greatly reduced the temperature sensitivity of the material, especially for PGM-G[4], which was mainly contributed by the multi-axial fiberglass.

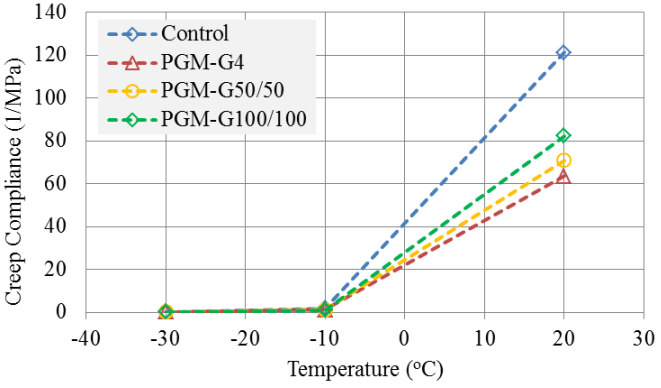

FIG. 7. Effect of Temperature on Creep Compliance (500s)

In cold regions, asphalt pavement suffers from low temperature cracking due to thermal contraction. HMA with higher creep compliance and higher creep rate would be less prone to low temperature cracking. However, it is worth noting the creep compliance of fabric treated specimens was the combination of HMA and saturated paving fabric. The creep compliance and strength of HMA itself would not change since the fabric was only placed at the interface. The reduction of creep compliance of fabric treated specimens indicated that the applied load mostly was carried by fabric and the load on the HMA was reduced. Fig. 8 shows the creep curves of horizontal tensile strain for four types of material at three different temperatures (i.e. 20°C, -10°C and -30°C). At 20°C, the creep strain of PGM-G[4] treated HMA was about half of the control group's strain at the end the test. At lower temperatures, i.e. -10°C and -30°C, the creep strain of fabric treated specimens were at least 10% lower than the control group's strain. In addition, the effect of adding fabric was more significant as loading time increased. At the beginning of the test (within initial 50s), all the curves almost overlapped on each other, indicating that saturated paving composite had lower creep rate and the difference of creep rate between HMA and paving composite could be the primary reason for the reduction of creep strain on the treated specimens.

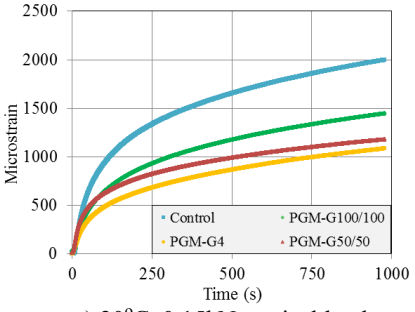

a) 20°C, 0.15kN vertical load

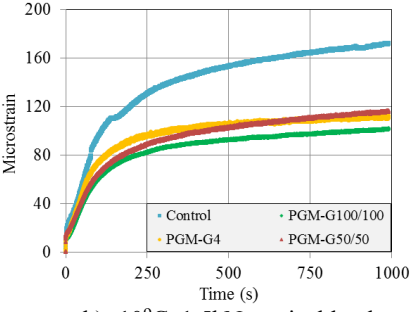

b) -10°C, 1.5kN vertical load

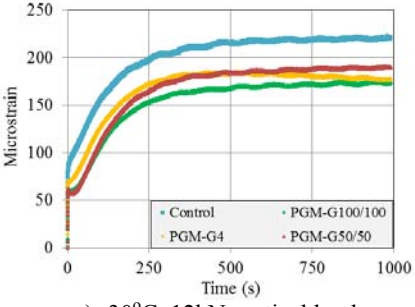

c) -30°C, 12kN vertical load

FIG. 8. Summary of Horizontal Creep Strain

In the field, for pavement without any cracks, which can be considered as an infinite band structure along the direction of the road, low temperature would only impose thermal stress on the pavement but no thermal contraction strain. Therefore, adding paving fabric may not contribute to thermal cracking resistance. However, contraction strain would be generated under low temperature, especially for locations where cracks exist. Under this kind of situation, fiberglass reinforced paving fabric could provide extra resistance to the thermal contraction. Even after thermal cracks occurred, the asphalt saturated paving fabric could maintain its integrity and continued to provide a moisture barrier to the underlying pavement (Davis and Miner 2010).

CONCLUSION

In this study, asphalt retention, grab strength, shear strength, permeability and IDT tests were conducted to investigate the material properties of paving fabrics and performance of asphalt mixtures reinforced with three types of paving fabrics.

PGM-G^4 paving composite had lowest asphalt retention and therefore lowest spreading rate among these three types of paving fabrics. PGM-G100/100, which had three yarns fiberglass in each direction, had the highest grab tensile strength and PGM-G^4 was the second.

The shear test results indicated that the fabrics need to be placed glass side facing down to achieve the maximum interface bonding strength in the field application. The permeability of all specimens was less than the recommended maximum acceptable permeability, 125×10^{-5} cm/s, and addition of paving fabrics greatly reduced permeability: the permeability of paving fabric treated mixtures was about 1/10 of that of control mixture.

Fabric treated mixtures had lower creep compliance than control mixture. At 20^{o}C, PGM-G^{4} treated specimen had the highest creep stiffness, which was doubled than the value of control group. At low temperatures, paving composite could provide extra resistance to reduce the thermal contraction in cracked pavement.

In a summary, this laboratory investigation identified performance improvement of asphalt mixtures due to the reinforcement of paving fabrics. Overall multi-axial PGM-G^{4} paving composite provided best pavement performance among three types of fabrics investigated. Further study will be performed to investigate the effect of paving composites on the dynamic modulus of HMA, with is a critical parameter for structural analysis and pavement design. Test sections in the field will be established and monitored to validate the laboratory findings.

REFERENCE

AASHTO T166 (2008). *Standard Method of Test for Bulk Specific Gravity of Compacted Bituminous Mixes, Using Saturated Surface Dry Specimens*. American Association of State and Highway Transportation Officials,

Amini, F. (2005). *Potential Applications of Paving Fabrics to Reduce Reflective Cracking*. Jackson State University, Jackson, Mississippi, 45 p.

ARA, Inc. (2004). "Guide for Mechanistic−Empirical Design of New and Rehabilitated Pavement Structures." *NCHRP Report No. A-37A,* Transportation Research Board, Washington, DC.

ASTM, (2004) "Standard PS 129–01 Standard Provisional Test Method for Measurement of Permeability of Bituminous Paving Mixtures Using a Flexible Wall Permeameter." *ASTM International*, West Conshohocken, PA.

Austin, R.A., and Gilchrist, A.J.T. (1996). "Enhance Performance of Asphalt Pavements Using Geocomposites." *Geotextiles and Geomembranes* 14, 175-186.

Browning, G. (1999). "Evaluation of Soil Moisture Barrier." *Final Report,* Report No. FHWA/MS-DOT-RD-99-21&23, Mississippi Department of Transportation, Jackson, MS.

Correia, N. d. S. and B. d. S. Bueno (2011). "Effect of Bituminous Impregnation on Nonwoven Geotextiles Tensile and Permeability Properties." *Geotextiles and Geomembranes* 29(2): 92-101.

Davis L., and Miner J. (2010). "Chip Sealing Over Paving Fabric in Various Climatic Conditions." *First International Conference on Pavement Preservation,* Newport Beach, CA.

Department of Transportation State of Georgia (2011). *GDT 1* www.dot.ga.gov/doingbusiness/TheSource/gdt/gdt001.pdf

Maupin, G. W. J. (2000) *Investigation of Test Methods, Pavements, and Laboratory Design Related to Asphalt Permeability*, Virginia Transportation Research Council, Charlottesville, VA.

Ghazavi, M. and Roustaei, M. (2013). "Freeze–thaw performance of clayey soil reinforced with geotextile layer." *Cold Regions Science and Technology* 89(0): 22-29.

Hall, K. T., Correa, C. E., and Simpson, A. L. (2002). "LTPP Data Analysis: Effectiveness of Maintenance and Rehabilitation Options." *NCHRP Web Document*, Issue 47, 332 p.

Hayden, S. A., Humphrey, D. N., Christopher, B. R., Henry, K. S., and Fetten, C. (1999). "Effectiveness of Geosynthetics for Roadway Construction in Cold Regions: Results of a Multi-Use Test Section." *Geosynthetics '99: Specifying Geosynthetics and Developing Design Details*, Boston, MA.

Hughes, J. J. and Somers, E. (2000). "Geogrid Mesh for Reflective Crack Control in Bituminous Overlays." *Final Report,* Report No. PA 200-013-86-001, Pennsylvania Department of Transportation, Harrisburg PA.

Lytton, R. L. (1989). "Use of geotextiles for Reinforcement and Strain Relief in Asphalt Concrete." *Geotextiles and Geomembranes* 8, 217-237.

Marienfeld, M. L. and Baker, T.L. (1999). "Paving Fabric Interlayer as a Pavement Moisture Barrier." *Transportation Research Circular: Journal of the Transportation Research Board E-C006*, 1-13. Washington.

Penman, J. and Hook, K.D., (2008). "The Use of Geogrids to Retard Reflective Cracking on Airport Runways, Taxiways and Aprons". *Pavement Cracking Mechanisms, Modeling, Detection, Testing and Case Histories*, London, 713-720.

Prieto, J. N., Gallego, J., and Pérez, I. (2007). "Application of The Wheel Reflective Cracking Test for Assessing Geosynthetics in Anti-reflection Pavement Cracking Systems". *Geosynthetics International,* 14, 287-297.

TenCate™ Geosynthetics North America (2011). *Important Physical Properties for Paving Fabrics.* http://www.tencate.com/amer/Images/tn_pavfab_tcm29-9648.pdf.

Using Statistical Method and Viscoelasticity to Control Low Temperature Performance of Asphalt Mixtures during Construction

Chun-Hisng Ho [1]

[1] Assistant Professor, Department of Civil Engineering, Construction Management & Environmental Engineering, Northern Arizona University, Box 15600, Flagstaff AZ 86011, email: chun-hsing.ho@nau.edu

ABSTRACT: Thermal cracking has been a severe issue in asphalt pavements in the cold regions. In the past years, a number of studies have been done using materials testing and statistical methods to give ways for quality control and quality assurance (QC/QA) in asphalt construction. However, these volumetric measurements (density, air voids, thickness, etc.) obtained from materials testing cannot accurately reflect actual mechanical information of the asphalt materials such as relaxing thermal stresses; the factor influencing low temperature cracking of asphalt concrete. This paper presents a statistical approach associated with viscoelasticity using the Bending Beam Rheometer (BBR) to evaluate the construction quality of the asphalt mixtures at low temperatures. An asphalt paving project in Utah was used in the research. Asphalt samples collected from the job sites were shipped back to the laboratory where specimens were tested using the BBR. Creep compliance from the BBR tests were used to perform viscoelastic modeling, and subsequently, the relaxation modulus was integrated to create a band of a confidence interval with the upper limit (UL) and the lower limit (LL). Based on the statistical principle, if any relaxation modulus curve from the field fell out of the range formed by the UL and LL, the construction quality could be considered as a dispute and needs further investigation. If the relaxation modulus curve from the field is located within the band, then it means that the quality of the mixtures meets the requirement. This approach gives a comprehensive review of the construction quality in asphalt pavements at low temperatures.

INTRODUCTION

Thermal-induced cracking of asphalt pavements in cold regions (such as Colorado, Utah, Montana, Idaho, Northern Arizona, etc.) has been critical to state highway agencies. According to a report on the investigation of low temperature cracking in asphalt pavements, US highway agencies spent approximately $ 45 billion dollars in 2006 for pavement maintenance due to low temperature cracking (Marasteanu et al. 2007). However, the effectiveness of these maintenance activities has not been

significant in some cold climates. For example, thermal cracking has been a pavement issue in northern Arizona. Numerous thermal induced cracks have been observed on pavements along highway US 180 and SR 64. The same issues have been noticed in Salt Lake City, UT on the major corridors. These low temperature cracks have exposed a severe maintenance issue to state highway agencies such as Utah Department of Transportation (UDOT), Arizona Department of Transportation (ADOT) Flagstaff Regional office. The reasons that cause thermal cracking vary and may include complicated factors in the stage of design, construction, and maintenance. One can be attributed to the quality control process implemented in the field. During the QC/QA process, what issues can be questioned are:

1. From the statistical point of view, whether the mixtures placed in the field come from the same population like the one that was previously submitted to the laboratory?
2. Based on quality control purposes, could the asphalt mixtures cored/collected be shipped in a timely manner to a laboratory where specimens were tested for their thermal cracking resistance and the findings can be interpreted quickly to assist highway professionals and contractors in decision making?

At present, highway agencies have searched promising methods to evaluate the performance of asphalt mixtures based on the potential for low temperature cracking such that the above issues can be addressed.

Ho and Romero (2011; 2012) recommended using asphalt mixture beams in the Bending Beam Rheometer (BBR) as a way to assess thermal cracking of asphalt mixtures in the field. It is known the contractor must be responsible for construction quality including asphalt production in a plant and mixture placement in the field. Based on current quality control processes, asphalt mixtures collected or cored from the field are tested in a laboratory to see if all volumetric measurements met the requirements. Even though numerous statistical approaches have been used to provide guidelines for QC/QA, using volumetric measurements as part of QC/QA processes may not accurately reflect the low temperature performance of the asphalt mixtures. As a result, unexpected pavement deterioration in asphalt pavements could occur in the future. Hence, this paper presents an approach using statistics and mechanics to characterize the thermal-induced properties of asphalt mixtures that can be used by highway agencies and contractors to execute day-to-day mix design and quality control during asphalt pavement construction.

METHODS FOR QUALITY CONTROL IN THE FIELD

In 1992, the California Department of Transportation (Caltrans) embarked on an implementation plan to improve construction quality. Dobrowolsky and Bressette (1998) introduced quality control and quality assurance (QC/QA) specifications for asphalt concrete paving through a joint Caltrans/industry group. Cominsky et al. (1998) presented a QC/QA plan for field production of hot mix asphalt (HMA) and a description of two field-testing devices that support the Superpave Gyratory Compactor for QC practices; particularly, using the field shear device and the triaxial creep device for materials tested at intermediate and high temperatures. Parker and

Hossain (2002) developed a statistical QC/QA program based on data collected from asphalt content, air void content, and mat density measurements. Their work aimed at assessing accuracy and variability of data (i.e., asphalt content, air voids, and mat density) in compliance with the state agency's Superpave mix design standards. Al-Qadi and Lahouar (2004) evaluated the performance of ground penetrating radar (GPR) in estimating the layer thicknesses of flexible pavements for use in QC/QA during asphalt construction. As it can be seen, most of field tests are used to evaluate volumetric properties (density, air void, asphalt content, etc.) of asphalt specimens and do not consider the mechanical properties (relaxation modulus, creep compliance, stresses, strains, etc.) of the materials. Even if all volumetric properties of specimens met the requirements, the results (volumetric properties) cannot accurately reflect actual mechanical information of the materials such as relaxing thermal stresses; those factors influencing low temperature cracking of asphalt concrete.

Currently there are three available testing methods that have been used for the prediction of low temperature properties of asphalt mixtures: the Indirect Tensile Test (IDT) specified in the American Association of State Highway and Transportation Officials (AASHTO) standard T322 (2009), or the American Society of Testing and Materials International (ASTM) D6931-07 *Standard Test method for Indirect Tensile (IDT) Strength of Bituminous Mixtures* (2009), the Thermal Stress Restraint Specimen Test (TSRST), specified in the AASHTO standard TP10 (2007), and the Bending Beam Rheometer (BBR), specified in the AASHTO standard T313 (2009), or ASTM D6648-08 *Standard Test Method for Determining the Flexural Creep Stiffness of Asphalt Binder Using the Bending Beam Rheometer (BBR)*(2008). Several research projects by Ho and Romero (2011; 2012), Zofka (2007), Zofka et al. (2007; 2008a; 2008b) done in the past have suggested the BBR to be a good tool for quality control in the field based on its features such as quicker and easier operation, less expensive, and staff familiarity at most regional labs. More recently, Ho and Romero (2013) presented the process of BBR specimen preparation and the number of replicates for a valid BBR test. All above information presented are in support of using BBR for testing in QC/QA. This paper continues the research efforts and presents a statistical approach in conjunction with the BBR and viscoelasticity aimed at providing a promising method for quality control at low temperatures during asphalt pavement construction.

STATISTICAL ANALYSIS

Determination of Confidence Interval

The quality control is a process in which highway agencies and contractors review the quality of the asphalt mixtures involved in production and placement. This quality control process requires a systematic approach to set up standards/specifications reasonable and acceptable for both the highway agency and the contractor. For the statistics stand point, the process can be implemented by determining a confidence interval based on the mechanical testing results; in this case: BBR. The objective of a confidence interval is to provide an estimated range of values which is likely to contain a population parameter from field the sample data.

The confidence interval (CI) is defined as:

$$CI = \bar{x} \pm t_{n-1}^{*} \times \frac{S}{\sqrt{n}} \quad [1]$$

Where:

$\bar{x}$ is the mean of samples

t_{n-1}^{*} is a critical value depending on the particular significance level and n is the number of specimens tested.

S and n denote the standard deviation and degrees of freedom.

Coefficient of variation (CV) is expressed as:

$$CV = \frac{S}{\bar{x}} \quad [2]$$

Ho (2010) recommended the maximum CV should be less than 0.2 for a test to be reliable, so Eq. 2 can be rewritten as:

$$S = 0.2 \cdot \bar{x} \quad [3]$$

Combining Eq. 1 and Eq. 3, yields:

$$CI = \bar{x} \pm t_{n-1}^{*} \times \frac{0.2 \cdot \bar{x}}{\sqrt{n}} \quad [4]$$

Eq. 4 gives an estimated range to determine a confidence level (i.e., the upper limits and the lower limits) based on the BBR tests and relaxation modulus analysis.

$$\text{The upper limits (UL)} = \bar{x} \cdot \left(1 + t_{n-1}^{*} \times \frac{0.2}{\sqrt{n}}\right) \quad [5]$$

$$\text{The lower limits (LL)} = \bar{x} \cdot \left(1 - t_{n-1}^{*} \times \frac{0.2}{\sqrt{n}}\right) \quad [6]$$

Ho and Romero (2011) indicated that the right term of Eq. 4 shows the information of confidence interval parameters for a given sample size and their mathematical relation. Using the UL and LL, a band of confidence interval can be developed by which both the highway agency and the contractors have agreement upon the parameters such as a confidence level, and the number of specimens to be tested, so a QC/QA rule can be established.

This paper used a paving project in collaboration with Utah DOT to demonstrate the process of quality assurance for testing BBR specimens. It is also feasible to perform quality control if a contractor wants to use the BBR tests to guide the work.

Paving Project

To illustrate a QC/QA process, an asphalt paving project was selected in Utah. Before paving, a mix design formula with the nominal maximum aggregate size (NMAS) 12.5mm and PG 64-34 binder was sent to the Utah Department of

Transportation (UDOT) Central Materials Laboratory for approval. Once the mix design formula was approved, the contractor was then able to produce asphalt mixtures using the same formula in the plant. The mixtures produced were then transported to the job site. For the statistical analysis purposes, asphalt mixtures using the same mix design formula were produced in the University of Utah Materials Laboratory. Mixtures made at the University of Utah were referred to as a control group while asphalt mixtures collected in the field were used as a comparison group.

As it is typical for UDOT projects, the asphalt mixture was sampled behind the paver during construction and taken to the regional laboratory where it was reheated and compacted into the standard 150-mm diameter specimens using the Superpave gyratory compactor. The compacted specimens were then tested for density as a means to ensure that all volumetric properties (VMA, VFA, binder content, etc.) were met. Based on the laboratory reports, the mixes were satisfactory in meeting the volumetric requirements. Compacted specimens were then shipped to the University of Utah Materials Laboratory where specimens were tested at -24°C, which corresponds to the low temperature PG of the binder plus 10 degrees. The BBR was used to obtain stiffness information of specimens. The number of specimens and the corresponding coefficient of variance for each paving day are specified in Table 1. As it can be noticed, all CV values of the specimens from the field are less than 0.20, so the BBR results are considered valid to be used for further analysis. Details for specimen production please refer to Ho and Romero (2013) in reference.

Table. 1 Coefficient of variation of specimens for each paving day

Paving Day	Aug. 4	Aug. 5	Aug. 7	Aug. 8	Aug. 10	Aug. 11	Aug. 12	Aug. 13	Aug. 14
Number of specimens tested at -24°C	19	15	14	15	13	15	15	14	14
CV	0.17	0.20	0.13	0.14	0.18	0.17	0.17	0.13	0.13

After completing the BBR tests, the stiffness values of each paving day were saved in the computer and exported for analysis use. Based on the stiffness values, a series of box-and-whisker diagrams were created along all paving days as depicted in FIG. 1. Each box plot graphically expresses five components from the minimum observation, quartile 1, median, quartile 3, and the maximum observation.

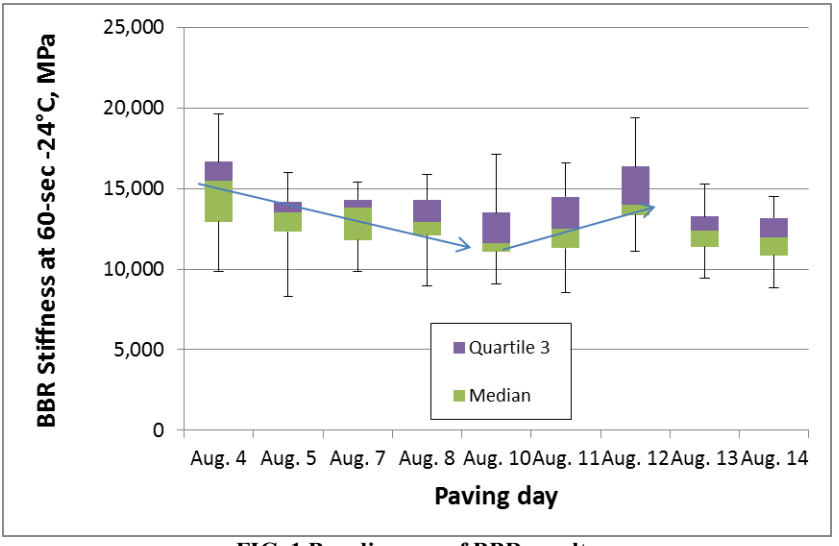

FIG. 1 Box diagram of BBR results

The box diagram distributions over the paving days give an initial examination for the low temperature properties of the asphalt mixtures in the field. By looking at the chart, it is noticed that the stiffness values decreased from August 4 down to August 10. This initial observation gave a problematic concern regarding the performance of the asphalt mixtures that might occur at low temperatures. Even though the stiffness increases after August 10, it can be argued that such a decrease raises suspicion of thermal cracking resistance on those paving days around August 10 (i.e., Aug. 8, 11, and 12). However, this is based on the observation on the physical properties of the asphalt specimens and it cannot completely indicate any potential mechanical behavior failure of the asphalt mixtures at low temperatures. Although the lab report showed that all volumetric properties met the requirements, however, the box diagrams in FIG. 1 raise a flag for an interest to look in depth at the construction quality. Thus, a further evaluation is needed. The next step was to investigate whether the construction quality of the asphalt mixtures on the above paving days meets the expectation for their thermal cracking resistance. To address this concern, a statistical analysis was used to create the band of confidence interval of the specimens and a series of viscoelastic modeling were performed to determine relaxation modulus of the asphalt specimens on selected paving days. This combined approach is to evaluate the construction quality of the asphalt mixtures by means of assessing their thermal resistance performance. The selection of field samples was on the paving days where the thermal quality of the mixtures has been questioned (Aug. 8, 10, 11, and 12). Based on the observation on Figure 1, viscoelastic analysis was performed on the asphalt specimens collected on August 8, 10, 11, and 12. The reason for these selections to be chosen was to first investigate the thermal performance on August 10 where the lowest stiffness was noticed. The analysis result on August 10 was then in

comparison with the viscoelastic behavior of the mixtures done on August 8, 11, and 12.

Creep compliance data from all production days were obtained from the BBR tests. Given the creep compliance on the selected paving days, relaxation moduli of the materials can be predicted. The determination of relaxation modulus is not the scope of the paper and since the viscoelastic analysis is available in numerous literatures and books, the relaxation modulus can be solved using the following equation (Ho and Romero 2011):

$$E(t) = \frac{1}{D_0 + D_1\Gamma(n+1)(1.786t)^n} \quad [7]$$

where $E(t)$=relaxation modulus at reduced time, t, D_0, D_1, n = power function parameters. Γ represents a gamma function.

Once the relaxation modulus in Eq. 7 was solved, the values of the relaxation modulus carried out in the laboratory were able to insert from Eq. 1 to Eq. 6 to create the relaxation modulus curve, the upper limits (UL), and the lower limits (LL) for the control group. This band shows a confidence interval with the corresponding confidence level (99%) that can be used to help evaluate the construction quality of the asphalt mixtures. Note that the confidence level can be decided based upon the agreement between the highway agency and the contractor before construction. In this research, 99% of confidence level was chosen. After the prediction of relaxation modulus is completed for the comparison group (specimens from Aug. 8, 10, 11, and 12), the curve was then incorporated into each confidence interval band in which the construction quality of the specimens from the field can be reviewed. FIG. 2 illustrates the schematic principle of the two groups used for quality control using relaxation modulus as a vertical axis and the time domain as a horizontal axis. It can be seen that the upper limits (UL) and the lower limits (LL) along with the relaxation modulus of samples (control group) define an estimated range of relaxation moduli (band). The relaxation modulus curve computed based on field samples is brought into the chart. The rule of thumb for the QC/QA is if the relaxation modulus curve from the field (comparison group) is out of the band, then the quality of the mixtures may need further investigation. If the relaxation modulus curve from the field is located within the band, then it means that the quality of the materials meets the requirement. Applying the algorithm presented above, the bands of confidence interval on August 5, 7, 8, 10, 11, and 12 paving days were created and displayed in FIG. 3a-FIG. 3f.

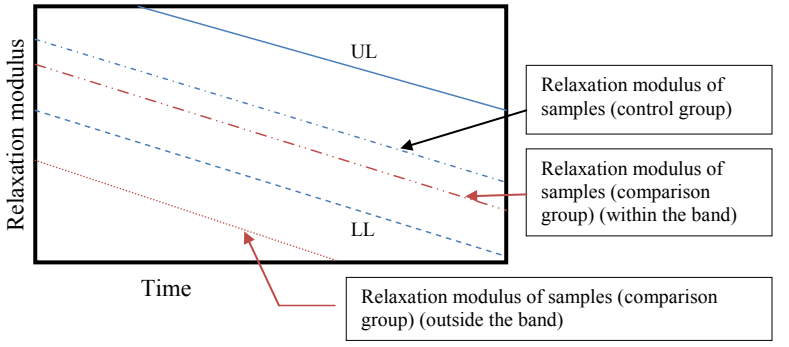

FIG. 2 Schematic illustrations for Quality Control

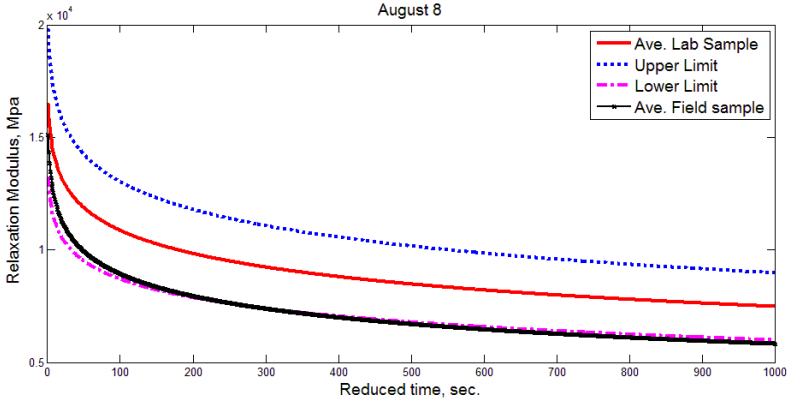

FIG. 3a: Confident interval for paving day August 8

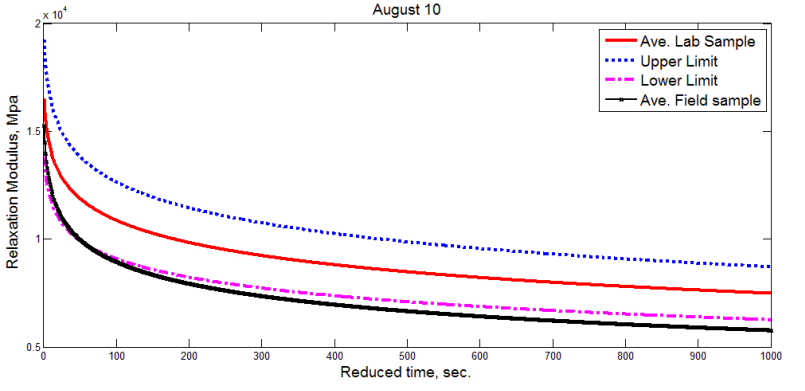

FIG. 3b: Confident interval for paving day August 10

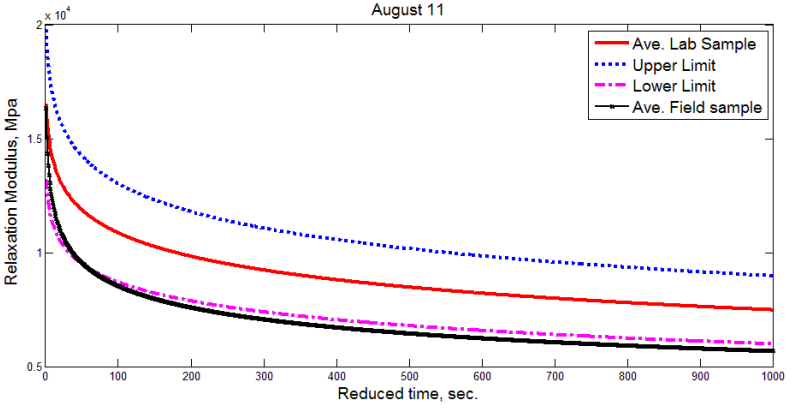

FIG. 3c: Confident interval for paving day August 11

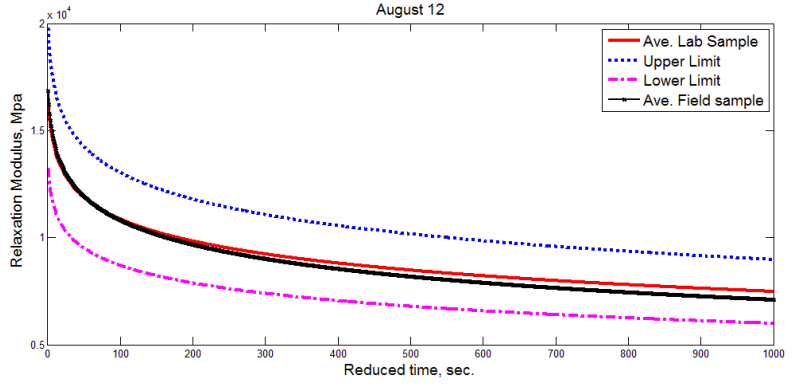

FIG. 3d: Confident interval for paving day August 12

Findings in FIG. 3a-3d provide the information for quality control of the asphalt mixtures on the four paving days. From a statistic point of view, the BBR results on the paving days need to be compared with the control group's such that the quality of asphalt mixtures on paving days can be confirmed. As previously mentioned, one of inconsistency issues is whether the mixtures placed in the field come from the same population like the one that was previously submitted to the laboratory? The approach presented in the paper could answer this question. By comparing BBR data from the field with the ones from the control group, the in-situ quality of asphalt mixtures could be evaluated. As has been shown in Figure 3b, the relaxation modulus curve from the field (comparison group) on August 10 fell out of the band indicating the construction quality may have statistically concerned. While it is not clear that the thermal stress of the asphalt mixtures on August 10 is less than that of the rest of

paving days, the statistical result otherwise has agreement with the observation in FIG. 2. It is also realized that the relaxation modulus curve (comparison group) (FIG. 3c) on August 11 is also located out of the band but close to the LL. While the stiffness values of the asphalt mixtures on August 11 did not reveal any potential dispute, the result in FIG. 3c otherwise brings attention on the quality of the mixtures that may be of interest to conduct a further assessment. The thermal performance on August 8 as shown in FIG. 3a was mostly on the edge of LL that indicates the thermal properties of the asphalt mixtures are satisfied but may keep close attention on their thermal cracking. The quality of the asphalt mixtures on August 12 is located within the band showing the quality of the mixtures meets the requirements. Note that since these charts in FIG. 3 are generated by statistical analyses, the scope of a band can change depending on the statistical parameters (confidence level and number of specimens tested). Note that the above analysis does not reflect the actual behavior of the asphalt pavements on site. Rather, the analysis is intended to provide an example of how to use BBR tests to perform QC/QA in asphalt pavement construction.

In practice, state highway agencies use a range of volumetric measurements as pay factors to pay for contractors for a given project. Given the same ideas, this paper provides a band of confidence interval that can be served as payment guidelines to help DOTs determine the quality of asphalt pavement construction and pay with full amount or partial. Before construction, both the highway agency and the contractors need to thoroughly determine these two parameters and specify them in the contract to avoid any disputes or conflicts during construction and payment. It should be emphasized that this paper tends to only provide a method that can be taken into consideration for QC/QA by the highway agency and the contractor. Any actions related to address the disputes of the paving quality were not included in the paper and should be based on the jurisdiction of any DOTs.

In general, the confidence interval associated with viscoelastic analysis can provide useful information to facilitate the understanding of thermal performance of the asphalt mixtures in pavement construction. This paper serves as an exploratory investigation using statistical approach associated with viscoelasticity with the intent to provide a methodology for QC/QA operations in asphalt construction. This paper is used to help primarily with QA. Even though only quality assurance was implemented in this paper, it is feasible that the material testing methodology can also be used in quality control if the contractor is planning to use the BBR data to guide the work.

CONCLUSIONS

Even though numerous statistical approaches have been used to provide guidelines for QC/QA, using volumetric measurements as part of QC/QA processes may not accurately reflect the low temperature performance of the asphalt mixtures. As a result, unexpected pavement deterioration in asphalt pavements could occur in the future. Thus, a combined approach using box diagrams (for volumetric measurement) and a band of confidence interval (for viscoelastic analysis) is presented to address this issue. The paper reviews the existing literature on quality control and quality assurance in asphalt pavements and provides the guide that can be used to evaluate the construction control of the asphalt mixtures at low temperatures during pavement

construction. Field samples were collected and shipped back to the laboratory where specimens were tested using the BBR and the results were graphically shown in the box diagrams. Statistical analyses associated with a series of viscoelastic modeling were performed to create bands of confidence interval. This paper serves as an exploratory investigation using statistical approach associated with viscoelasticity with the intent to provide a method for QC/QA operations in asphalt construction. State highway agencies can consider using a range of confidence interval to pay for the contractors for a given project based on its construction quality. Based on the statistical analysis results, the following conclusions have drawn:

1. The box diagram distributions for all paving days give an initial screening to assess the physical properties of the asphalt specimens, so any anomaly can be quickly noticed. If any suspensions were found in FIG. 1, a statistical analysis using Eq. 1 through Eq. 6 associated with viscoelastic analysis (Eq. 7) can be used to further investigate the construction quality of the asphalt mixtures as presented in the paper.
2. As presented in the case study, stiffness values from BBR results gave an initial screening in terms of field observation. Once any dispute is settled, a further statistical analysis could be performed to investigate the mechanical properties of asphalt mixtures.
3. The rule of thumb for the QC/QA is if any relaxation modulus curve (comparison group) fell out of the range, the construction quality could be considered as a dispute and needs a further investigation. On the other hand, if the relaxation modulus curve (comparison group) is located within the band (between UL and LL) of a confidence interval, then the quality of the mixtures is considered satisfactory. The paving project demonstrated the applicability of using BBR tests associated with the band of a confidence interval for QC/QA. This approach gives a comprehensive review of the construction quality in asphalt pavements.
4. The statistical parameters (confidence level and the number of specimens tested) can influence the accuracy and variability of the statistical analysis. Before construction, both the highway agency and the contractors need to thoroughly determine these two parameters to avoid any disputes or conflicts during construction and payment.

REFERENCES

Al-Qadi, I.L., and Lahouar, S (2004). "Use of GPR for Thickness Measurement and Quality Control of Flexible Pavements." *Journal of the Association of Asphalt Paving Technologists*, Vol. 73, pp. 501-528

American Association of State Highway and Transportation Officials (2009). "Standard Test method for Indirect Tensile (IDT) Strength of Bituminous Mixtures." *Standard Specifications for Transportation Materials and Methods of Sampling and Testing T 322.* AASHTO 29th edition.

American Society of Testing and Materials (2007). *Standard Test method for Indirect Tensile (IDT) Strength of Bituminous Mixtures.* ASTM D6931-07.

American Association of State Highway and Transportation Officials (2009). *Standard Specifications for Transportation Materials and Methods of Sampling and Testing TP10.* AASHTO 29th edition.

American Association of State Highway and Transportation Officials (2009). "Determining the Flexural Creep Stiffness of Asphalt Binder Using the Bending Beam Rheometer (BBR)." *Standard Specifications for Transportation Materials and Methods of Sampling and Testing T 313*. AASHTO 29th edition.

American Society of Testing and Materials (2008). "Determining the Flexural Creep Stiffness of Asphalt Binder Using the Bending Beam Rheometer (BBR)." *ASTM D6648-08*.

Cominsky, R. Killingsworth, B., Anderson, R.M., Anderson, D.A., Crockford, W.W (1998). "Quality Control and Acceptance of Superpave-Designed Hot Mix Asphalt." Transportation Research Board. *NCHRP Report: 409*.

Dobrowolski, J. and Bressette, T (1998). "Development of Quality Control/ Quality Assurance Specifications by Using Statistical Quality Assurance for Asphalt Concrete Pavements in California." *Journal of Transportation Research Board* No. 1632, Transportation Research Record of the National Academies, Washington D.C., pp.13-21

Ho, C.H. (2010). "*Control of thermal-induced failures in asphalt pavements*." *Ph.D. Dissertation*, the University of Utah

Ho, C.H., and Romero, P (2011). "Using Asphalt Mixture Beams in the Bending Beam Rheometer: Experimental and Numerical Approach." *Journal of Road Materials and Pavement Design*, Vol. 12 No. 2, 2011, pp. 239-314.

Ho, C.H. and Romero, P (2012). "Using Asphalt Mixture Beams in the Bending Beam Rheometer: Utah Experience." *Journal of the Transportation Research Record* No. 2268, pp.92-97.

Ho, C.H. and Romero, P (2013). "A Material Testing Methodology for In Situ Quality Control of Low Temperature Performance in Asphalt Pavements." *Proceedings of the 2013 Airfield and Highway Pavement conference*, Los Angeles, CA, pp. 1018-1029.

Marasteanu, M., Zofka, A., Turos, M., Li, X., Velasquez, R., Li, X., Paulino, G., Braham, A., Dave, E., Ojo, J., Bahia, H., Williams, C., Bausano, J., Gallistel, A., and Mcgraw, J (2007). "Investigation of Low Temperature Cracking in Asphalt Pavements." *National pooled Fund Study 776*. MN/RC 2007-43, Minnesota Department of Transportation.

Parker, F and Hossain, S (2002). "Statistics for Superpave Hot-Mix Asphalt Construction Quality Control/Quality Assurance Data." *Journal of Transportation Research Board* No. 1813, Transportation Research Record of the National Academies, Washington D.C., pp.151-156.

Zofka, A., Marasteanu, M. O., Li, Xinjun, Clyne, T. R., and McGraw, J (2005). "Simple Method to Obtain Asphalt Binders Low Temperature Properties from Asphalt Mixtures Properties." *Journal of the Association of Asphalt Paving Technologists*, Vol. 74, pp. 255-282.

Zofka, A (2007). "Investigation of Asphalt Concrete Creep Behavior Using 3-Point Bending Test." *PhD thesis*, University of Minnesota, Minneapolis.

Zofka, A., Marasteanu, M., and Turos, M (2008). "Investigation of Asphalt Mixture Creep Compliance at Low Temperatures." *Journal of Road Materials and Pavement Design*, Vol. 9, pp. 269-286.

Zofka, A., Marasteanu, M., and Turos, M (2008). "Determination of Asphalt Mixture Creep Compliance at Low Temperatures Using Thin Beam Specimens." *Journal of the Transportation Research Board*, No. 2057, Transportation Research Board of the National Academies, Washington, D.C., pp. 134–139.

Investigation on Service Time and Effective Cost of Typical Pothole Patches in Tennessee

Qiao Dong[1], Mbakisya A Onyango[2] and Baoshan Huang[3]

[1]Postdoctoral Research Associate, University of Tennessee, 411 John D. Tickle Building, Knoxville, TN, 37996; qdong2@utk.edu
[2]Assistant Professor, University of Tennessee, 440A EMCS, Chattanooga, TN, 37403; Mbakisya-Onyango@utc.edu
[3]Professor, University of Tennessee, 419 John D. Tickle Building, Knoxville, TN, 37996; bhuang@utk.edu

ABSTRACT: Pothole repair is a commonly practiced pavement maintenance conducted by many state highway agencies. This study investigated the current practices of pothole repair and their cost-effectiveness. A nationwide questionnaire showed that the throw-and-go method is widely used because of its simplicity while semi-permanent technique is considered to be more cost-effective. The field survey showed that the throw-and-roll patches, placed in the winter time, deteriorated quickly in the first three months, whereas the patches that survived the first winter or that were repaired in the spring lasted much longer. Although semi-permanent repairs have higher one time repair cost due to increased equipment and labor cost, they were proved to be more cost-effective in a long term. The throw-and-roll applied in the spring season appeared to be the most cost-effective repair strategy, while including winter season throw -and-roll are less cost-effective. Avoiding patching in severe season and conducting preventive patching could potentially improve the cost-effectiveness.

INTRODUCTION

Background

Potholes on the surface of asphalt pavements significantly reduce pavement condition, and potentially impair traffic safety. Potholes results from interconnected alligator cracks that cause the pavement surface to break into small pieces that are pulled up by travelling wheels. (Miller and Bellinger, 2003) The formation of alligator cracks and potholes can be accelerated by freeze-thaw cycles due to the expansion of freezing water inside the pavement when temperature drops.

Pothole repair is one of the most frequently performed pavement maintenance activities by many state highway agencies. Various patching techniques with different

combinations of materials and procedures have been used to repair potholes. Generally, pothole patching can be classified into two types: temporary repair such as throw-and-roll and permanent repair like semi-permanent. Throw-and-roll simply includes placing materials and compacting with shovels or by passes of truck tires. Semi-permanent includes cleaning debris, paving and compacting mixture with vibratory compactors. Many highway agencies use the throw-and-roll procedure in winter for temporary repair which is then followed by the semi-permanent patching in summer as more permanent repairs (Wilson and Romine, 1993).

In addition to the traditional throw-and-roll and semi-permanent methods, Tennessee uses Bobcat mill-and-pave shown in FIG. 1. as a permanent pothole repair technique. Bobcat mill-and-pave procedure includes milling a strip of severely deteriorated pavement surface, usually along the wheel path or a whole lane width, by a "Bobcat" milling machine, and paving a new surface. It is a small scale mill and fill procedure, capable of repairing a series of potholes continuously appeared on pavement. Although this method consumes much more materials than traditional patches, it repairs a deteriorated road section in one operation and thus is more efficient and potentially more cost-effective since the new pavement lasts longer than the patches.

(a) Throw-and-roll (b) Semi-permanent (c) Bobcat mill-and-pave

FIG. 1. Typical pothole patches used in Tennessee

Previous Studies

Several studies have been conducted to evaluate the performance of various patching techniques through field and laboratory evaluations. (Thomas and Anderson 1986; Wilson and Romine 1993, 1994 and 2001; Prowell and Franklin 1996; Maher et al. 2001; Dong et al. 2013). The Strategic Highway Research Program (SHRP) H-106 project (Wilson and Romine, 1993, 1994 and 2001) was the most extensive study on this topic. Findings from the project include the information pertaining to the types and performance characteristics of repair materials and methods, as well as the proper ways of planning, constructing, and performance evaluation of pothole repair projects.

Annualized or effective cost analysis, similar to the life cycle cost analysis (LCCA), has been employed by previous researchers to evaluate the cost-effectiveness of patches. Thomas and Anderson (1986) calculated annualized cost of pothole patches based on a 2-year field survey. Their findings suggested that throw-and-go procedures, which are just placing the materials, cost approximately three times more than the rigorous procedures which involve cutting, cleaning, and compacting. Wilson and Romine (2001) estimated the effective cost based on expected patch service time and analysis period and found that throw-and-roll technique was more cost-effective than

the semi-permanent patches because of reduced labor and equipment.

Objectives and Scope

In 2011, Tennessee Departments of Transportation (TDOT) initiated a study to evaluate the cost-effectiveness of typical pothole repair techniques used in Tennessee. In the study, a nationwide survey is conducted to review the current practices of state DOTs on pothole repairs. The performance and effectiveness of various pothole materials and methods were investigated through both laboratory evaluation and field observation. This paper presents the findings from the DOT questionnaire on the practices of pothole repair as well as the long term survey of patches installed on Tennessee highways. Based on the service life, the effective costs of different pothole repair strategies were analyzed to evaluate their cost-effectiveness.

DOT SURVEY

The questionnaire, covering the pothole distress situation, patching methods and materials, cost-effectiveness and guidelines on pothole repair strategy, was developed and sent to the maintenance divisions of state DOTs. A total of 29 responses were received. For the needs of pothole repair, 89% of the 29 respondents consider potholes a problem in their states. No specific procedure has been adopted to quantify pothole repairs. Generally, a state spends between 0.03 to 50 million dollars, or an average of 5.5 million dollars on pothole repair annually.

Patching Methods

Most states use throw-and-roll as a quick and temporary fix and use a more permanent method later. Although the failure rate of throw-and-go method is high, it is widely used because it is easy to apply, especially on high traffic roads or in incremental weather. However, the throw-and-go technique is least used in 8 out of the 29 states. This is probably because the throw-and-go patches have high failure rate and thus are not recommended by state highway agencies. Hot mixed asphalt (HMA) mixtures account for around 60% of all the patching materials. The rest are bagged or stockpile cold mixture. In term of the patch performance, several respondents reported that repairs performed in good weather last longer than those performed in severe weather condition. The semi-permanent technique is considered to be the more cost-effective than throw-and-roll.

Guidelines on Pothole Repairs

Half of the responded states do not have criteria for selecting pothole repair techniques and a standard guideline on pothole repair program. In addition, although various techniques have been utilized by state highway agencies to repair potholes, no specific procedure has been developed to evaluate the effectiveness of pothole repairs. In 2012, a National Cooperative Highway Research Program (NCHRP) Synthesis 20-05/topic 44-04 was initiated to evaluate new pothole repair techniques and evaluate

their effectiveness. The preliminary survey also found out that 71% of respondents have no measure of pothole repair performance and 77% indicated the need of such measure. Therefore, a study on the effectiveness of pothole repair techniques is of high necessity.

INVESTIGATION OF SERVICE TIME

Installation of Field Patches

As practiced by many state DOTs, throw-and-roll methods are used in the winter season and semi-permanent patches are usually applied in the summer. In this study, a total of 79 potholes were patched on seven road sections in Tennessee, including 65 throw-and-roll patches installed in winter, 12 semi-permanent patches installed in summer and 2 Bobcat repair in winter. The throw-and-roll patches used four typical patching mixtures in Tennessee, including a fine-graded hot mixed asphalt (HMA) mixture, two cold bag mixtures and a cold stockpile mixture. The 12 semi-permanent patches all used HMA mixture but with different combinations of procedures such as cutting edges, infrared heating or spraying tack coat. Field surveys were performed 1, 3, 6, 12 weeks and then every 3 months after the installation. 14 months survey of the throw-and-roll patches was performed. Since the semi-permanent and Bobcat repairs were installed later, 10 and 5 months surveys were performed, respectively. Cutting edges, infrared heating and spraying tack cost seemed have no significant effect. No distress was observed on the semi-permanent and Bobcat patches.

Service Time of Throw-and-Roll Patches

The service status of patches were recorded and summarized in FIG. 2. It can be seen that almost 30% of the patches were worn out and replaced with a new patch only 1.5 months after patching. Those throw-and-roll patches deteriorated quickly in the winter, which is mainly due to the severe freeze-thaw cycling. At the end of the 14 months survey, 70% of the patches were all repaired. It is noted that only a small part of the repaired patches (1st replace) were re-replaced, indicating that the repaired patches tended to have a longer service life.

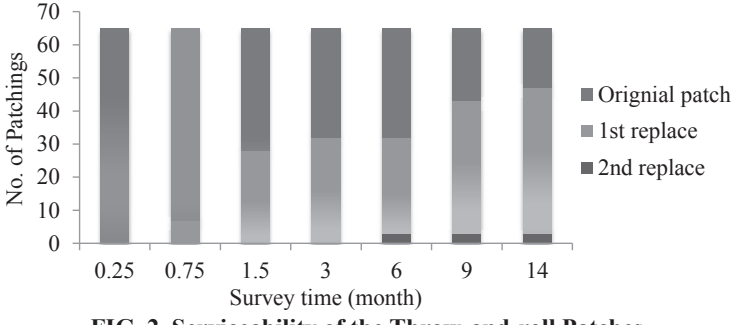

FIG. 2. Serviceability of the Throw-and-roll Patches

FIG. 3 shows the survival rate, which is the percentage of patches that are still in service, for the original and the first replaced patches. It can be clearly seen that the survival rate of original patches dropped quickly in the first three months in winter. After that, the survival curve tended to level off. This is because the patches survived the first winter were usually well compacted or fully cured for the cold mix and could last much longer. On the other hand, with the increase of time, the survival rate of repaired patch (1st replace) did not drop dramatically as the original patches. The repaired patches were mostly constructed in the spring and did not experience the severe freeze-thaw cycles in winter before they were cured and compacted. The survival curve of repaired patches seems similar with that of the original patches after the first three months. Half of the original patches failed in the first 6 months while majority of the repaired patches could last more than 12 months, indicating that they survived in the second winter.

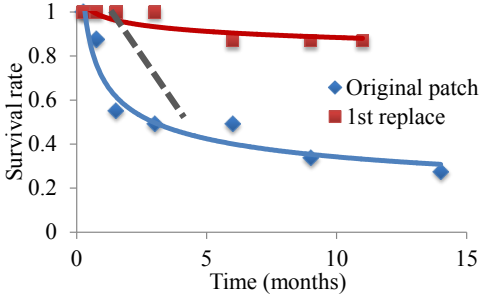

FIG. 3.Survival Curves of the Original and Replaced Patches

EFFECTIVE COSTS ANALYSIS

The main costs for pothole patching are material, labor, equipment, and user delay related to traffic control or lane-closure. Wilson and Romine (2001) pointed that material cost might be the least part of the total cost, and more expensive materials that were placed with less effort and last longer could reduce the overall cost, as well as the amount of re-patching needed. In the SHRP H-106 project, Wilson and Romine (2001) developed a template, which was adopted in this study to calculate the cost of one patching operation and the effective cost of multiple repairs in a specific analysis period based on the service life of patches.

Repair Cost

The materials, equipment, labor and user delay costs were collected with the help of TDOT maintenance engineers. The average repair costs for throw-and-roll, semi-permanent and bobcat patches with different combinations of procedures and materials are $1,210 ± 66, $3,135 ±96 and $4,865, respectively. The throw-and-roll patches cost much less than the semi-permanent patches due to the reduced equipment, labor and user delay. Although the unit costs of cold mixtures are higher than that of the

HMA, the total cost of HMA is slightly higher because HMA needs hot-truck to carry the materials.

Effective Cost

To evaluate the long term cost-effectiveness, the effective costs, which are the total costs for a specific analysis period, are calculated based on the one time repair cost and patch service time. Low effective cost indicates high cost-effectiveness. The expected service times of semi-permanent and Bobcat methods are 2 and 4 years, respectively. The expected service life of winter season throw-and-roll is 6 months while that of spring season throw-and-roll is 12 months. In this analysis, the analysis period is 4 years, which is the longest expected service life of a patch ("Bobcat" method). FIG. 4 shows the effective costs of different repair strategies. Those strategies are based on the service time and may not be exact the same as the actual operation. It can be seen that:

1. The 4 time spring season throw-and-roll is the most cost-effective strategy. This indicates that improving the quality of throw-and-roll patches could greatly increase the cost-effectiveness.
2. The Bobcat repair is cost-effective in long term. However, it can only be used for continuous occurred potholes not isolated ones.
3. Semi-permanent patches or the combination of semi-permanent and throw-and-roll in spring are also cost-effective repair strategies.
4. Repair strategies including winter season throw -and-roll are the less cost-effective. Therefore, it is recommended to avoid patching in the worst season. Preventive patching in advance could significantly improve the cost-effectiveness.

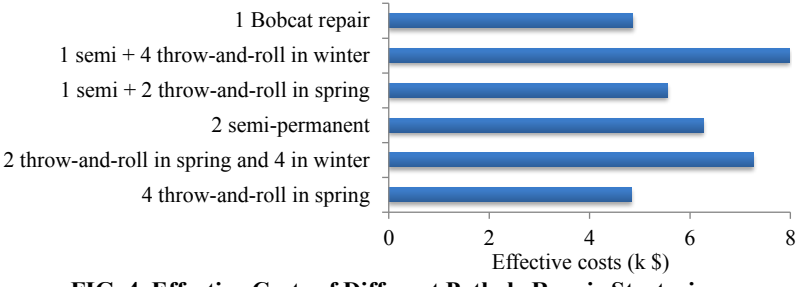

FIG. 4. Effective Costs of Different Pothole Repair Strategies

SUMMARY AND CONCLUSIONS

To investigate current practices on pothole repairs of state DOTs, a nationwide questionnaire was conducted. 89% of the respondents consider pothole repairs as a problem and an average of 5.5 million dollars is spent on pothole repair annually. The throw-and-go method is widely used because it is fast and efficient. Semi-permanent is considered to be more cost-effective technique. Most states use the throw-and-roll patches as winter season temporary repair followed by semi-permanent repairs.

Field survey on the service life of winter season throw-and-roll patches showed that

survival rate of patches dropped quickly in the first three months in winter. The average service life of those patches is only 6 months. However, the patches that survived in the first winter and the patches repaired in spring lasted much longer, with an approximate service life of 12 months. No distress was observed on the semi-permanent and Bobcat patches during the survey period.

The Bobcat and semi-permanent patches have higher one time repair cost due to increased equipment, labor and user delay. Based on the service time of different patching methods, the effective costs of different patching strategies were calculated to compare their cost-effectiveness. Bobcat, semi-permanent and spring season throw-and-roll repairs are cost-effective strategies, whereas winter season throw-and-roll patch is the least cost-effective. To improve the cost-effectiveness, it is recommended to avoid patching in the severe winter season and conduct preventive patching instead.

ACKNOWLEDGEMENT

The funding of this study was supported by the Tennessee Department of Transportation (TDOT). TDOT pavement maintenance engineers are especially acknowledged for their assistance in the field operation and cost data collection.

REFERENCES

Dong, Q., Huang, B., and Zhao, S. (2013). "Field and laboratory evaluation of winter season pavement pothole patching materials." *International Journal of Pavement Engineering*(ahead-of-print), DOI:10.1080/10298436.2013.814772.

Maher, A., Gucunski, N., Yanko, W., and Petsi, F. (2001). "Evaluation of pothole patching materials." *Report no. FHWA 2001-02*, New Jersey Department of Transportation and Federal Highway Administration U.S. Department of Transportation, Washington, D.C., USA

Miller, J. S. and Bellinger, W. Y. (2003). "Distress identification manual for the long-term pavement performance program (fourth revised edition)." *Report no. FHWA-RD-03-031.* Federal Highway Administration, Washington, DC.

Prowell, B. D. and Franklin, A. G. (1996). "Evaluation of cold mixes for winter pothole repair." *Transportation Research Record: Journal of the Transportation Research Board*, 1529(1), 76-85.

Thomas, H. and Anderson, D. (1986). "Pothole Repair: You Can't Afford Not To Do It Right." *Transportation Research Record*(1102).

Wilson, T. P. and Romine, A. R. (1993). "Innovative Materials Developemnt and Testing. Volume 2: Pothole Repair." *Report no. SHRP-H-353*. Strategic Highway Research Program, Washington, D.C., USA.

Wilson, T. P. and Romine, A. R. (1994). "Pavement Surface Repair Materials and Procedures: Training Program—Pothole Repair." *Report no. SS-20.* Strategic Highway Research Program, Washington, D.C., USA.

Wilson, T. P. and Romine, A. (2001). "Materials and Procedures for Repair of Potholes in Asphalt-surfaced Pavements--manual of Practice." *Report no. FHWA-RD-99-168*, Federal Highway Administration, Washington, D.C., USA.

Compaction Characters of Asphalt Mixture of Variable Thickness

Yunliang Li [1], Lun Ji [2], Jiuye Zhao [3], Yong Zhong [4], Zhenyu Xu [5], Yiqiu Tan [6]

[1]Associate Professor, School of Transportation Science and Engineering, Harbin Institute of Technology, Harbin, P.R. China,150090. liyl-hit@163.com.
[2]Associate Professor, School of Transportation Science and Engineering, Harbin Institute of Technology, Harbin, P.R. China, 150090. Jilun@hit.edu.cn.
[3]Master, School of Transportation Science and Engineering, Harbin Institute of Technology, Harbin, P.R. China, 150090. zhaojiuye89@126.com.
[4]Master, School of Transportation Science and Engineering, Harbin Institute of Technology, Harbin, P.R. China, 150090. zhongyong15@163.com.
[5]Master, School of Transportation Science and Engineering, Harbin Institute of Technology, Harbin, P.R. China, 150090. 344934300@qq.com.
[6]Professor, School of Transportation Science and Engineering, Harbin Institute of Technology, Harbin, P.R. China, 150090.Tanyiqiu@hit.edu.cn.

ABSTRACT: Compaction characters of variable thickness screed-coat material were investigated during the process of old cement road reconstruction. The compaction characters of asphalt mixture of variable thickness were studied under gyratory compaction test. Results show that asphalt mixture ATB 25 with different initial thickness have the same compaction character. However, residual void ratio of asphalt mixture with different initial thickness is different under the same compaction times. Based on void ratio of design and the relationship of compaction times and remaining void ratio, the relationship of compaction times and initial thickness was established. Through the results of gyratory compaction test, the optimum compaction temperature of ATB 25 is confirmed to be 140 ℃.

INTRODUCTION

With the development of road construction, there have been more and more road reconstruction and extension construction projects, and a major project in these is to overlay asphalt concrete on the old cement concrete pavement. Reviewed some application practices of reconstruction, using asphalt concrete overlay is one of the most available ways to reconstruct old cement concrete pavement(Lin et al. 2005, Liu et al. 2005, Chen, et al. 2005). This pavement structure, which asphalt mixture overlay on the old cement concrete pavement, is a special pavement structure type and become a research hotspot. Currently researches mainly focus on overlay structure design of the old cement concrete pavement, mechanical behavior(Leng et

al. 2009, Wang 2012, Yang et al. 2007; Zhang 2005, Yang et al. 2009, Zhu et al. 2011), material design of overlay structure, adhesion character of adjacent layers, reflection crack, and so on(Bian et al. 2012, Yuan et al. 2012, Wang et al. 2012, Mao et al. 2012, Jiang, et al. 2011). However, information on the effects of old cement concrete pavement with non-uniform thickness screed-coat on construction is limited. In fact, the effects cannot be ignored, especially in the process of reconstructing two-way road camber to one-way road camber; the problem of screed-coat of non-uniform thickness is more serious. Therefore, in the condition of screed-coat material with variable thickness, how to guarantee the uniform compaction is a problem that urgently needed to be solved. In this paper, the screed-coat material ATB 25 is designed. Through gyratory compaction test, the correspondence between compaction thickness and compaction effort is studied, and the relationship between asphalt mixture compaction thickness and compaction effort is established. This work can propose theoretical basis for asphalt mixture of variable thickness using uniform compaction.

RAW MATERIALS AND PROPOTION OF ASPHALT MIXTURE

Asphalt

Asphalt is Liao He 90# petroleum asphalt; specifications are shown in Table 1.

Table 1. Asphalt specifications

	Unit	Test value
Penetration (25℃,100g,5s)	0.1mm	86
Softening point	^{o}C	45.7
15℃ ductility	cm	>150
135℃ kinematic viscosity	Pa·s	0.275
Flash point	^{o}C	230
Solubility	%	99

Aggregates

Aggregates specifications are shown in Table 2, specifications can meet request of standard.

Table 2. Aggregate specifications

	Aggregate				
	1#	2#	3#	4#	5#
Crushing value（%）	19.3	18.8	-	-	-
Flat and elongated particles（%）	9.3	10.8	10.4	-	-
Soft aggregate content（%）	2.0	2.4	2.5	-	-
Adhesion grade	5	-	-	-	-
Sand equivalent（%）	-	-	-	-	72
Bulk volume density（g/cm^3）	2.69	2.68	2.73	2.716	2.55
Water absorption（%）	0.56	0.64	1.18	1.18	2.80
<0.075mm content（%）	0	0.2	0.2	1.1	12.5

Mix Design

Using the raw materials above to design the asphalt mixture ATB-25 with Marshall design method, gradation and Marshall test results are shown in Table 3 and Table 4.

Table 3. ATB-25 asphalt mixture Marshall test results

	Design value	Standard request
Asphalt-aggregate ratio（%）	4	-
Bulk volume Relative density	2.396	-
Actual measurement theoretical maximum density	2.531	-
Voidage VV（%）	5.3	3~6
Voids in the Mineral Aggregate VMA（%）	13.3	-
Saturation VFA（%）	60	55~70
Stability（kN）	23.46	≥15
Flow value（0.1mm）	42.7	-

Table 4. ATB-25 gradation

Gradation type	Accumulative residue(square hole sieve, mm)												
	31.5	26.5	19	16	13.2	9.5	4.75	2.36	1.18	0.6	0.3	0.15	0.075
ATB-25	100	94.9	77.3	70.8	64.5	52	38.9	28.1	20.4	15.5	9.9	7.6	5.3

COMPACTION CHARACTERS OF VARIABLE THICKNESS

The asphalt mixtures with five different initial thicknesses were employed in the gyratory compaction test. The initial thickness is respectively 69 mm, 99 mm,130 mm, 145 mm, and 188 mm. The relationship between initial thickness of the test-piece and compaction times is shown in Figure 1. The thickness decreases with increasing compaction times. The ATB asphalt mixture with different initial thickness

has different compaction curve. For the test-piece with 69 mm initial thickness, the thickness decreases rapidly in the first 40 compaction times, and then slowly. Especially after 60 compaction times, no evident decrement was observed. For the test-piece with 145mm, the similar tendency is observed. The test-piece thickness changes quickly before 50 compaction times, while it does not decrease after 80 compaction times. For the test-piece with initial thickness of 188mm, the thickness does not change after 100 compaction times. In terms of the compaction curve, the test-pieces with different initial thickness have the same tendency; these indicate that compaction character of asphalt mixtures is the same.

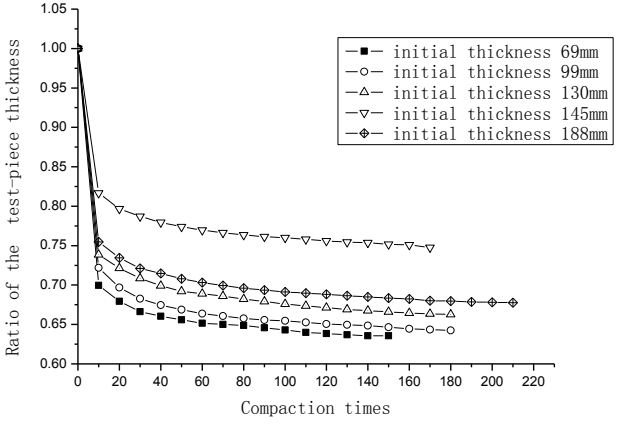

FIG.1. Compaction curves of five different initial thickness ATB-25

COMPACTION EFFORT OF VARIABLE THICKNESS

In order to analyze the compaction effort of asphalt mixture with variable thickness, volume parameters of ATB 25 mixtures test-pieces with five different initial thicknesses were measured under the same compaction effort through gyratory compaction test. TROXLER 4140 Gyratory Compactor was employed in this test, and the compaction times were 125. The results are shown in Table 2, ATB 25 voidage increases with the increase of thickness under the same compaction effort. This indicates that there should be a proper and reasonable compaction effort for the asphalt mixture ATB-25 with different thickness.

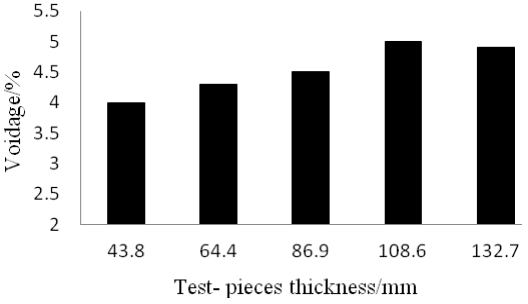

FIG.2. Voidage of asphalt mixture with different thickness

To gain the compaction effort of asphalt mixture with different thickness, 150 gyratory compaction times were employed to compact the test-pieces with thickness of 44mm, 64mm, and 108mm. The test-pieces with initial thickness of 44mm, 64mm, and 108mm were recorded thickness at 30, 75, 125 and 150 compaction times. 225 gyratory compaction times were employed to compact the test-pieces with thickness of 86mm and 132mm, all the test-pieces with initial thickness of 86mm and 132mm were recorded thickness at 75, 125, 175, 225 compaction times. Volume parameters after the gyratory compaction are shown in Figure 3. It can be seen that voidage of mixture ATB 25 decreases with increasing compaction times. Considering target voidage of 5%, the optimum gyratory compaction times of asphalt mixture ATB-25 with the thickness of 44mm, 64mm, 86mm, 108mm, 132mm are confirmed to be 65, 73, 103, 115 and 132 in Figure 3, respectively, which can meet the degree of compaction and evenness. The relationship of thickness and compaction times is shown in Figure 4.

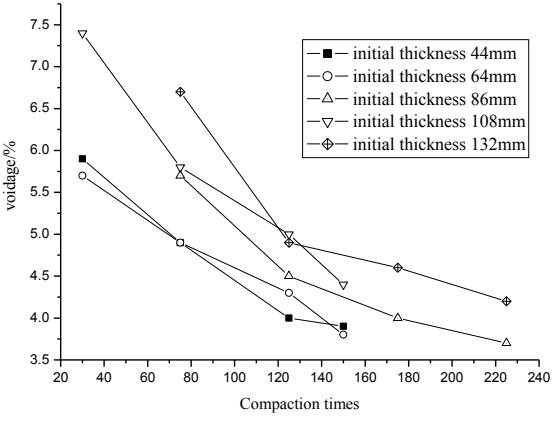

FIG.3. Curve of relationship between compaction times and asphalt mixture ATB-25 with different thickness

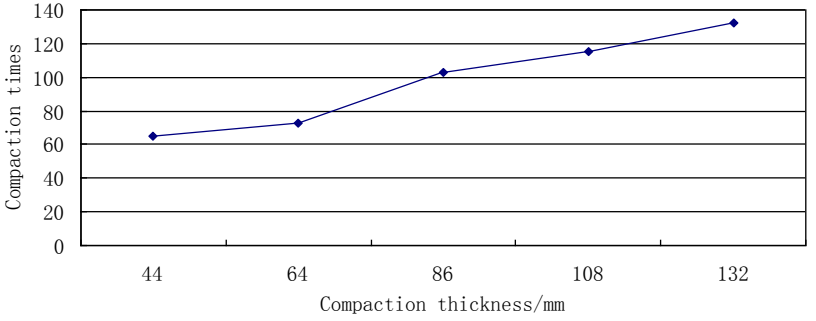

FIG.4. Compaction times of gyratory compaction test-pieces with different thickness

Regression analysis was adopted to analyze data in Figure 4 and Eq. 1 was gained to express the relationship of structure thickness and compaction times.

$$n = 0.799h + 28.16 \quad (1)$$

Where n, h represent compaction times and compaction target thickness, respectively. This equation shows that the optimum compaction times of asphalt mixtures with variable thickness can be gained according to the target thickness. Compaction uniformity and surface smoothness of variable thickness asphalt mixtures can be guaranteed by this method.

OPTIMUM COMPACTION TEMPERATURE

To guarantee the optimum compaction effect during construction, ATB-25 compaction temperature was gained by volume parameters analysis under gyratory compaction test. Asphalt mixture ATB-25 was stirred under optimum asphalt-aggregate ratio and optimum mixing temperature, and then the mixtures were put into drying oven for one hour aging at 110°C, 120°C, 130°C, 140°C, and 150°C, respectively. In the following, the test-pieces were compacted by SGC with 125 compaction times. After cooling, volume parameters of test-pieces were measured. The compaction character parameters at different temperature were calculated according to the curve of gyratory compaction. The voidage of asphalt mixtures at different temperature is shown in Figure 5.

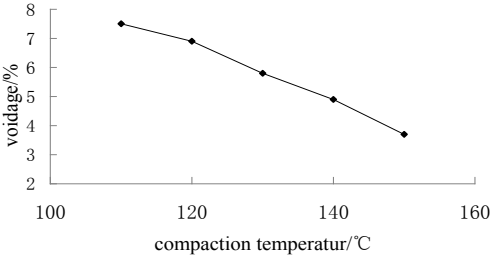

FIG. 5. Relationship between voidage and compaction temperature

Figure 5 shows that the voidage decreases from 7.5% to 3.7% with the increasing compaction temperatures from 110°C to 150°C. It indicates that the mixture becomes more and denser as the compaction temperature increases.

For construction temperature, asphalt should have favorable flowability. However, when temperature can meet the construction requirements, it is also no necessary to increase the construction temperature. To gain the optimum construction temperature, the optimum temperature can be defined as the highest temperature of the mixture viodage which is smaller than the design voidage. According to the design voidage 5.3% in Table 3, 140°C compaction temperature can meet the construction requirements. So, the optimum compaction temperature of ATB-25 is 140°C.

CONCLUSION

Through gyratory compaction test, the compaction characters of asphalt mixture ATB-25 of variable thickness were studied. Results indicate that asphalt mixtures ATB-25 with variable initial thickness have the same compaction characters. However, under the same compaction times, asphalt mixture with different thickness has different voidage, the larger thickness of asphalt mixture, the larger voidage it will have. According to design voidage and the relationship of compaction times and residual voidage, the relationship of compaction times and initial thickness was established, which can meet the standard requirement of voidage. Meanwhile, the optimum compaction temperature of asphalt mixture ATB-25 is confirmed to be 140℃ through test.

REFERENCES

Lin, X., Lin, Y., Pan, X., and Zheng, T. (2005). "Research on composite pavement of cement concrete and bitumen concrete." *Journal of BeiHua University*. 6(4):372-374.

Liu, H., Luo, X., and Dong, J. (2005). "Mechanism analysis of mechanics of ac overlays on old cement concrete pavements." *Highway*.11:77-80.

Chen, S., Zheng, M., and Yang, B. (2005). "Thermal stress influence factors of asphalt overlay on cement concrete pavement cracking slab." *Journal of Traffic*

and Transportation Engineering. 5(3):25-30.

Leng, Z., Al-Qadi, I. L., Carpenter, S. H., and Ozer, H. (2009). "Interface bonding between hot-mix asphalt and various Portland cement concrete surfaces." *Transportation Research Record*. 2127:20-28.

Wang J. (2012). "Analysis the control techniques of reflection crack on asphalt overlay of old cement concrete pavement." *Applied Mechanics and Materials*. 204-208:1945-1948.

Yang, B., Liao, W., Chen, S., and Wang B. (2007). "Numerical simulation analysis of stress-absorbing layer to relieve stress concentration in asphalt concrete overlay." *Highway*. 11:106-109.

Zhang, P. (2005). "Defence methods for reflective cracks in existed cement concrete black pavement." *Journal of Changan University*. 25(3):16-44.

Yang, D., Zhao, W., Li, L., and Qi, J. (2009). "Analysis of reflection cracks of asphalt concrete overlay over used cement concrete pavements by finite element analysis." *Journal of Huazhong University of Science and Technology*. 37(1):61-64.

Zhu, D., and Jia, X. (2011). "Analysis and simulation of interlayer damages in asphalt pavement overlay cement concrete slab." *Pavements and Materials: Recent Advances in Design, Testing, and Construction. Proceedings of the 2011 GeoHunan International Conference*. 192-199.

Bian, C., Song, J., and Liu, Z. (2012). "stress analysis of asphalt overlay on old cement pavement by impact of rolling technology." *Advanced Materials Research.* 446-449:3185-3190.

Yuan, Y., Wan, H., Wen, S., and Zhan, W. (2012). "Mechanical analysis on asphalt mixture overlaying on old cement pavement disengaged in the corner." *Proceedings of the 2nd International Conference on Electronic and Mechanical Engineering and Information Technology.* 666-669.

Wang, H., Wu, Y., and Ye, S. (2012). "Analysis of the mode of crushing and stability in old cement pavement during asphalt overlay project." *Applied Mechanics and Materials*. 204-208:1941-1944.

Mao, H., Zhuang, P., Zang, Y., and Yi, X. (2012). "Stress characteristic analysis of repaving asphalt pavement structure on old cement road." *Advanced Materials Research.* 594-597:1377-1381.

Jiang, Y., Jiang, S., and Li, Y. (2011). "The stress analysis on the asphalt overlay bottom at the seams of old cement concrete pavement." *2011 International Conference on Electric Technology and Civil Engineering.* 5630-5633.

Shear resistance performance evaluations of rubber asphalt waterproof adhesive layer on bridge deck

Lun Ji[1,2], Yunliang Li[3], Haipeng Wang[4], Lei Zhang[5], Yiqiu Tan[6]

[1]Associate Professor, School of Transportation Science and Engineering, Harbin Institute of Technology, Harbin, P.R. China, 150090; Jilun@hit.edu.cn.
[2]Visiting scholar, Dept. of Civil and Environmental Engineering, University of Alaska Fairbanks, Fairbanks, AK, 99775-5900; Lji2@alaska.edu
[3]Associate Professor, School of Transportation Science and Engineering, Harbin Institute of Technology, Harbin, P.R. China;150090; liyl-hit@163.com.
[4]Ph.D. Candidate, School of Transportation Science and Engineering, Harbin Institute of Technology, Harbin, P.R. China, 150090; wanghaipeng1@126.com
[5]Ph.D. Candidate, School of Transportation Science and Engineering, Harbin Institute of Technology, Harbin, P.R. China, 150090; hit.andy@foxmail.com
[6]Professor, School of Transportation Science and Engineering, Harbin Institute of Technology, Harbin, P.R. China, 150090; Tanyiqiu@hit.edu.cn.

ABSTRACT: Shear resistance performance between asphalt concrete surfacing and cement concrete is very important to guarantee the service life of deck paving. Insufficient shear resistance will result in some premature damage, such as cutting-slippage, folding, spalling, and loose. Shear resistance performance of rubber asphalt waterproof-adhesive layer was evaluated with oblique shear experiment under common design high-low temperature condition（20℃, 50℃ and -10℃）. With the different effect of loading rate and rubber asphalt spraying quality, shear resistance performance was evaluated with indexes such as maximum shear stress (τ_{max}), shear resistance energy (E_t) and ultimate shear deformation (δ_b). Results show that shear resistance performance of rubber asphalt waterproof adhesive layer under three different temperature conditions are significantly different. Under high temperature: τ_{max} and E_t decrease significantly when temperature varies from 20℃to 50℃; meanwhile the two indexes are affected by rubber asphalt spraying quality insignificantly; the fundamental factor determining shear resistance ability is interaction ability between rubber asphalt and concrete surface. Under -10℃: Rubber asphalt waterproof-adhesive layer shows elastic properties; the relationship between shear stress and shear deformation shows general linear; δ_b decreases significantly, but shear stress is great enough to improve E_t to an increased result. So the spraying quality and shear resistance ability can be determined and evaluated by the three indexes (τ_{max}, E_t, δ_b) tested by oblique shear experiment.

INTRODUCTION

The waterproof-adhesive layer plays an important role in cement concrete bridge pavement. The adhesive strength of the layer between the cement concrete

deck and the asphalt pavement may affect the bridge's service performance directly.

Suitable waterproof-adhesive layer can enhance the integrity between pavement and bridge deck to improve the coordination deformation and joint bearing ability, which can improve the mechanical state of pavement layer and prevent water seep into bridge deck.

Many studies about waterproof-adhesive materials have been carried out by researchers. There are many kinds of waterproof- adhesive materials such as modified emulsified asphalt, SBS modified asphalt, epoxy asphalt, asphalt waterproof coiled material, water soluble waterproof solvent and so on (Zhong and Li 2008). Bonding performances of modified emulsified asphalt, SBS modified asphalt and solvent-based adhesive were studied and optimum spraying quality of several materials is determined by tensile and shear test (Yang et al. 2003). The adhesive performances of the JS elastic waterproof mortar, epoxy resin and SBS (Styrene Butadiene Styrene) modified asphalt was studied by Wang et al. (2006). The adhesive performance of thermal spray SBS modified asphalt, cement based waterproof coating and AWP22000 bridge deck waterproof coating gluing were studied by Liu et al. (2010). Materials' mechanical performances were evaluated by drawing and shearing test.

Because of good deformation ability and adhesive performance, rubber asphalt can satisfy the functional requirements of waterproof-adhesive layer. Bridge deck pavement's service condition is harsher than road pavement; however, the mechanical response mechanism of waterproof-adhesive layer under different temperature conditions is unclear. In this study, rubber asphalt was used as adhesive material. And the shear resistance performance was evaluated under different temperatures, loading rates and binder spraying quantities.

EXPERIMENT

Shear resistance performance is very important to the bonding performance of interlayer bonding materials. Waterproof- adhesive layer should have enough shear resistance strength to ensure that premature damage do not occur in the waterproof-adhesive layer under the shear stress (Wang et al. 2009; Oscarsson and Said 2012; Uzan and Motola 2006; Hu and Qin 2011; Mohammad et al. 2002; Tajdini et al. 2012; Shan et al. 2012). In order to evaluate the bonding strength of adhesive material under different loading rates and temperature conditions, the oblique shear experiment device was designed. The shear stress of rubber waterproof-adhesive layer was tested and analyzed.

Test principle and indexes

The principle of oblique shear experiment was shown in FIG. 1. The test device includes loading plate, bearing plate and roller. The upper and lower bearing plates under vertical load are relatively sliding in the horizontal direction. The slip boundary is provided by the roller. The relative sliding of loading plates can produce shear stress for the adhesive layer. Shear stress can be expressed as Formula (1).

$$P = \frac{F}{A}\sin\alpha \tag{1}$$

Where, P is shear stress (MPa), F is pressure (N), A is bonding area (mm2), α is shear angle.

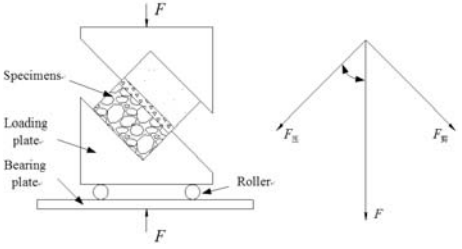

FIG.1. principle of oblique shear experiment

Evaluation indexes of shearing resistance ability are shown as follows:

(1) The maximum shear stress (τ_{max}) refers to the maximum shear value of structure shear test.

(2) The shear deformation resistance energy (E_t) can be expressed as formula (2).

$$E_t = \frac{1}{1000}\int_0^{\delta max} F(\delta)d\delta \tag{2}$$

Where, E_t is shear deformation resistance energy (J), δ is shear deformation (mm), $F(\delta)$ is shear stress when shear deformation is δ, and δ_{max} is maximum shear deformation (mm), which is fault deformation when stress-strain curve has no significant yield phase, or the end deformation of distortion when stress-strain curve has yield stage.

The ultimate shear deformation (δ_b) refers to the maximum shear deformation which can be withstood by specimens. The damage of viscoelastic material is unrecoverable if the shear deformation is larger than the ultimate shear deformation. The values can be fracture deformation when the stress-strain curve shows brittle fracture, or the middle deformation of yield stage when the yield stage exist in stress-strain curve.

Specimens

The specimen consists of cement concrete (50mm), waterproof-adhesive layer (10mm) and asphalt concrete (50mm). The preparation procedure of sample as follow: concrete slab with the thickness of 50mm is made firstly. Secondly, spraying rubber asphalt and crush stones on the surface of slab, then paving asphalt mixture on slab. Finally, the slab is cut into 90mm×90mm. Specimen used in test is shown in FIG.2.

Method

Actual device used in loading experiment is shown in FIG.2. MTS-180 was used as loading system. Specimen must be in experiment temperature for four hours before testing.

FIG.2. Oblique shear experiment device

EFFECT OF LOADING RATE ON τ_{max}

Loading rate has great influence on test results in mechanical experiments. The loading rates of 1mm/min, 5mm/min and 9mm/min were selected for shear testing. The experimental temperature was 20℃. The specimen characteristics and test parameters are shown in Table 1. The relationship between shear stress and shear rate are shown in FIG.3.

Table.1 Loading Rate and τ_{max}（MPa）

Loading rate（mm/min）	1	5	9
AC10 (spraying quantity is 2.0Kg/m^2)	0.91	1.19	1.39
AC16 (spraying quantity is 2.0Kg/m^2)	0.67	1.04	1.41
AC16 (spraying quantity is 2.4Kg/m^2)	1.06	1.21	1.45

FIG.3. shows that shear stress linear increased with loading rate varies in selected range of loading rate. And loading rate has great effect on τ_{max}. Considering the randomness of the vehicle acceleration, deceleration, the adverse conditions of structure as well as the feasibility of the experimental operation, 1mm/min was chosen as the loading rate under 20℃.

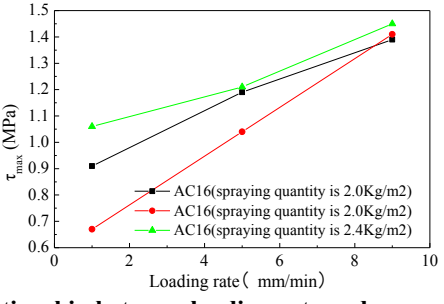

FIG.3. Relationship between loading rate and τmax under 20℃

OBLIQUE SHEAR EXPERIMENT AT DIFFERENT TEMPERATURE

Experimental Conditions

Tests were carried out under 20℃, 50℃ and -10℃ respectively. Rubber asphalt spraying quantities were 2.0Kg/m^2, 2.2Kg/m^2, 2.4Kg/m^2 and 2.6Kg/m^2 respectively. Asphalt mixture gradation used was AC-16. The τ_{max} would be significantly different when the loading rate was 1mm/min under 20℃ and -10℃ based on the above test. Therefore, 1mm/min was chosen as loading rate. Considering the rheological property effect, 5mm/min loading rate was chosen under 50℃.

Testing Results

Relationship between shear deformation and shear stress under different spraying quantities at 20℃

FIG.4 shows that the relationship of deformation and stress is almost linear at the initial stage of loading. Stress reaches to the max value with shear deformation increasing. The deformation varies between 1.5mm and 4mm when stress reached to the max value. Rubber asphalt has great deformation ability and can meet the bonding layer coordination deformation requirement.

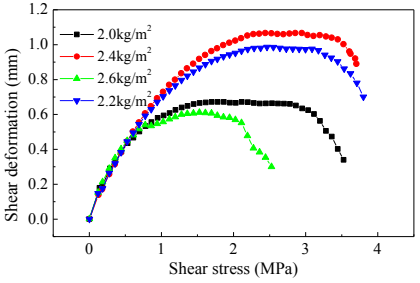

FIG.4 Deformation-stress curves of different spraying quantities at 20℃

Relationship between shear deformation and shear stress under different spraying quantities at 50℃

At the initial loading stage, shear stress and shear deformation show rough linear relationship. Nearby the τ_{max}, the Shear stress appears oscillation changes, after which, the shear stress falls down rapidly. For the different asphalt spraying content, the shear deformation – shear stress curves are very close. the viscosity of rubber asphalt decreases significantly compared with 20℃ ; The rubber asphalt also shows up the lubrication action, which results in the shear stress decreases; materials show some yield characteristics. In this case, asphalt spraying quantity had little effect on τ_{max} and E_t. It also shows that the fundamental factor in determining shear resistance ability at high temperature is the interaction ability between asphalt and adhesive surface.

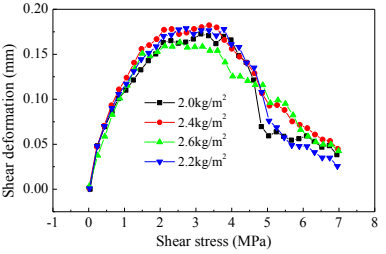

FIG.5 Deformation-stress curves of different spraying quantities at 50℃

Relationship between shear deformation and shear stress under different spraying quantities at -10℃

FIG.6 shows that the relationship between shear stress and shear deformation is linear. Materials present elastic properties and easy to failure in brittle. The stress-strain curve is not very smooth and appears zigzag, which is induced by the stress released when localized shear stress concentration appeared on the shear plane. The values of δ_b of specimens of rubber spraying quantity 2.0Kg/m^2, 2.2Kg/m^2, 2.4Kg/m^2 and 2.6Kg/m^2 are closed. The τ_{max} and δ_b increase when spraying quantity became lager. The aggregate coating effect is improved when spraying quantities lager than a certain value.

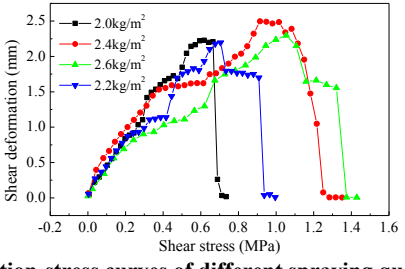

FIG.6. Deformation-stress curves of different spraying quantities at -10℃

Relationship between τ_{max} and spraying quantity

At 20℃, shear stress increases with spraying quantities increased at first, and decreases markedly with spraying quantities increased after peak value. It is because that cohesive force of gravel coating is small when asphalt spraying quantity is small, and becomes lager when asphalt spraying quantity increases gradually. However, when asphalt spraying quantity exceeds certain content, asphalt coating thickness increases and formats free sliding layer which will decrease the shear resistance ability. Therefore shear stress decreases when asphalt spraying quantity exceeds certain content.

Maximum shear stress decreases along with the increasing of experimental temperature. With the increasing of temperatures, the ratio of maximum shear stress changes from (3~5), 1 to (0.15~0.25). As shown in FIG. 7, under three

typical temperatures, each curve had an extreme point which located within 2.3~2.4 Kg/m^2.

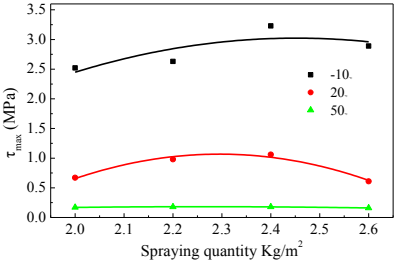

FIG.7 Strain-time curves of rolling process

The relationship between shear resistance energy and spraying quantity

According to shear stress and shear deformation, the relationship between load and displacement was determined, then energy absorption capacity of structure would be calculated, which was defined as shear resistance energy. This index would present the resistance capacity of shear and coordinate deformation for adhesive layer structure. Results are shown in Table.2 and FIG. 8.

Table.2 Shear Resistance Energy of Different Spraying Quantities (J)

Spraying quantity (Kg/m2)	2	2.2	2.4	2.6
-10℃	6.64	8.51	17.58	17.01
20℃	7.05	14.99	17.01	5.99
50℃	4.42	4.66	4.79	4.07

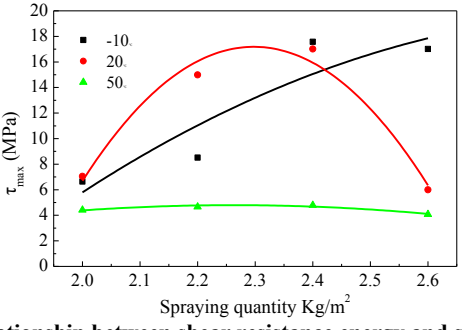

FIG.8 The relationship between shear resistance energy and spraying quantity

At -10℃, the influence of spraying quantity on shear resistance energy was not obvious, but had great effect on energy. At 20℃, there was an extreme point in energy curve; at 50℃, shear resistance energy was minimum compared with the other two temperature condition, and had less different between spraying quantity. At -10℃, when spray content was 2.4Kg/m^2, energy was similar to that of 20℃, it

was shear stress that had a great contribution to bear shear displacement. From all above, the most appropriate spraying quantity was 2.40 Kg/m^2.

The relationship between ultimate shear displacement and spraying quantity

Shear displacement shows the resistance capacity of displacement and compatibility of deformation. The max shear displacement for -10℃ is cracking point, while for 20℃ and 50℃, it is the middle point of yield part. Test results are shown in Table.3 and FIG.9.

Table.3 Ultimate Shear Displacement and Different Spraying Quantity (mm)

Spraying quantity (Kg/m2)	2	2.2	2.4	2.6
-10℃	0.56	0.69	1.08	1.09
20℃	2.28	2.73	2.94	1.5
50℃	3.13	3.19	2.94	2.97

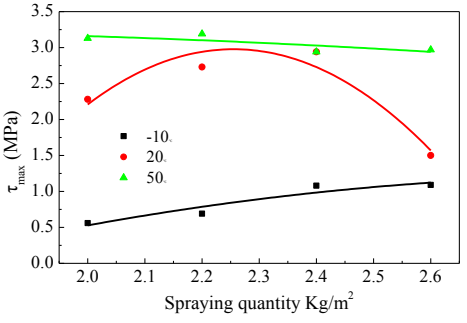

FIG.9 The relationship between shear displacement and spraying quantity

The τ_{max} decreases with the temperature decreasing. It is decreased 25~70%, compared to the results of -10℃ to 20℃. There was an extreme point at 20℃, around 2.3 ~2.4 Kg/m^2; after this point, the max shear deformation do not increase with the increasing of content, when spraying quantity was 2.6 Kg/m^2, strength decreased because of the extra asphalt. The diversity of the max shear deformation was not obvious at 50℃, comparing with 20℃, the max shear deformation entirely increases; the maximum increment is about one time than former.

CONCLUSIONS

1. In a determined shear rate arrangement, shear stress would linearly increase along with the increasing of loading rate. Shear rate had a great impact on shear stress.
2. At high temperature, viscosity of rubber asphalt adhesive layer decreases and liquidity increases, the maximum shear stress decreases obviously; the τ_{max} and E_t are less affected by spraying quantity of asphalt.

3. It shows a linear relationship between shear stress and shear deformation at low temperature. And materials exhibit elastic features.
4. Along with the decreasing of temperature, δ_b decreases obviously. E_t in low temperature is 25~70% of one in high temperate. At high temperature, δ_b is slightly difference with abnormal temperature, δ_b entirely increases as the spraying quantity increased, the maximum increment is one time more than the former one.
5. It is appropriate to adopt the oblique shear experiment to analyse the indexes of τ_{max}, E_t and δ_b, which are useful to evaluate shear resistance of waterproof adhesive layer.

References

Hu, C. H. and Qian, J. (2011). "Shear Stress Analysis of Long-span Steel Bridge Deck Asphalt Pavement using FEM." *International Conference on Multi-Functional Materials and Structures Engineering: Advanced Materials Research*: 12-17

Liu, L. P., Peng, Y. C., and Shao, J. (2010). "Study on essential performance of waterproof material on concrete bridge deck." *J. Building Materials*. 13(1):48-51.

Ma, Y. Q. and Liang, Z. L. (2007). "Study on Bridge deck pavement waterproof material selection and performance." *J. ROAD*. 6:101-103.

Oscarsson E. and Said S. (2012). "Assessment of ZSV in Asphalt Concrete Using Shear Frequency Sweep Testing." *J. Materials in Civil Engineering*. 24:1305-1309.

Mohammad, L. N., Raqib, M. A, and Huang, B. S. (2002) "Influence of asphalt tack coat materials on interface shear strength." *Transportation Research Record*. 1789: 56-65.

Shan, L. Y. and Tan, Y. Q. (2012). "Analysis of fatigue process of asphalt considering thixotropy." *China Journal of Highway and Transport*. 25(4):10-15.

Tajdini, M., Rostami, A., Karimi, M. M., and Taherkhani, H. (2012). "Evaluation of the geo-mechanical parameters of the interface between asphalt concrete and sand with applying direct shear test and numerical modeling." *Civil Engineering and Materials: Advanced Materials Research*. 587:116-121.

Uzan, J and Motola, Y. (2006). "Damage evaluation in simple shear tests with and without stress reversal of asphalt concrete." *Road Materials and Pavement Design*. 7:71-86.

Wang, W. H., Dai, Y. Y., and Sun, J. Y. (2006). "Test on waterproof on deck pavement of sea bridge." *China municipal engineering*. 120(4):36-38.

Wang, Y. L., Zhou, Y. L., Yao, A. L. (2009). "Test of shear and pull-off between asphalt and concrete on bridge deck pavement structure." *Journal of Chang'an University (Natural Science Edition)*. 29(6):15-18.

Yang, S. Q., Hao, P. W., and Liu, N. (2008). "The testing research for linking material of pavement interface about the bridge of cement concrete." *Journal of Hebei University of Technology*. 37(5):105-109.

Zhong, R. W. and Li, W. P. (2008). "Selection and application water-proof layer types of deck pavement." *Journal of Liaoning Provincial College of communications*, 10(4):17-18.

A Photogrammetric Method to Evaluate the Erosiveness of Fairbanks Silt with Different Treatments

Lin Li[1], Rodney Collins[2], Xiong Zhang[3], and Huayi Wei[4]

[1]Graduate Research Assistant, Department of Civil and Environmental Engineering, University of Alaska Fairbanks, Fairbanks, AK 99775-1157; lli10@alaska.edu
[2]Graduate Research Assistant, Department of Civil and Environmental Engineering Sciences, University of Oklahoma, OK 73071; rwcollins@ou.edu
[3]Associate Professor, Department of Civil and Environmental Engineering, University of Alaska Fairbanks, AK 99775-5900; xzhang11@alaska.edu
[4]Assistant Professor, School of Mathematics and Computational Science, Xiangtan University, Hunan, P.R. China, 411105; huayiwei1984@gmail.com

ABSTRACT: In Alaska, due to surface runoff from snow melt in spring, erosion is one of the most common hazards to cut slope and roadbed slopes. The traditional way to monitor erosion is performed by installing a fence to collect eroded soils carried by runoff. For this method, only total erosion for a specific area, which is the mass percent loss, could be obtained. The total and localized volumetric erosion were not available which made the runoff erosion less representative. In this paper, laboratory tests were performed to investigate the erosiveness of Fairbanks silt with different treatments which included geo-fiber, Envirokleen, and Soil-sement. A photogrammetric method was presented to monitor the runoff erosion which significantly reduced the cost and effort for the erosion monitoring.

INTRODUCTION

In Alaska, during springtime, melt water from snow and ice carrying soil and organics from the slump mass flows to the ditch and potentially to streams, wetlands, lakes and then into the sea. In the past few decades, regulatory agencies have refined and developed more stringent environmental regulations that prohibit such discharges. Consequently, there is a great need of research on the slope protection from erosion. Surface water from snow melt, can cause a big problem for roadbed and cut slopes especially those without surface vegetation. This cumulated erosion could trigger a slope stability problem when the frozen soil melts. In the past, most research efforts were on erosion due to water flow (Matsumoto et al. 2001, Curran and McTeague 2011, and Vandamme and Zou 2013). Some research efforts were on cut and roadbed slopes (APSC 1974, Vinson and Mchattie 2009). Since there is a lack of a cost-effective and accurate method to monitor the erosion, hazards due to erosion could not be quantitatively detected.

In this study, a photogrammetric method was proposed to monitor slope erosion due to surface runoff. Photogrammetry is widely used to determine the geometric properties of objects from photographic images. It offers the capability to capture three-dimensional (3D) points in sub-millimeter accuracy. As a noncontact 3D measurement technique, photogrammetry is used in different fields, such as topographic mapping, architecture, engineering, manufacturing, quality control, and geology. Photogrammetry was adopted to measure the erosiveness of Fairbanks silt with different treatments during the laboratory slope erosion tests.

EXPERIMENTAL DETAILS

The soil used in this research is sandy-silt which was collected at Great Northwest Inc. in Fairbanks, Alaska. Particle size distribution test was performed in accordance with ASTM D422 and presented as shown in Figure 1. The specific gravity of the soil was measured to be 2.76 according to ASTM D854. The maximum dry density and optimum moisture content of the tested soil were determined to be 1.84 g/cm^3 and 12% according to ASTM D1557.

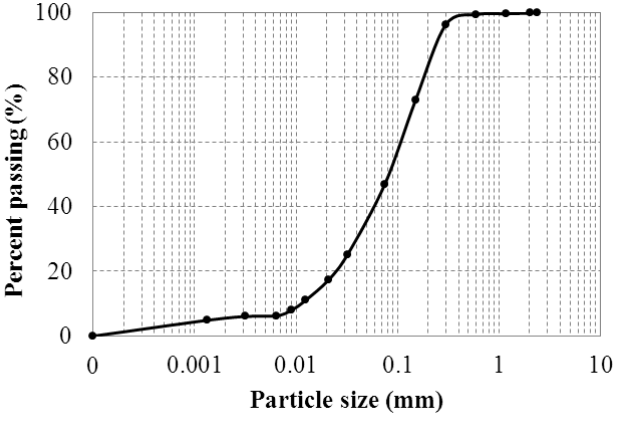

FIG. 1. Fairbanks silt particle size distribution

Laboratory Slope Erosion Test

To evaluate the erosiveness of Fairbanks silt with different treatments, geo-fiber, Envirokleen, and Soil-sement were added to the silt according to different configurations which are 6% water only, 6% water + 2% Soil-sement, 6% water + 0.5% geo-fiber, 6% water + 2% Soil-sement + 0.5% geo-fiber, 6% water + 4% Envirokleen + 0.5% geo-fiber. The fibrillated geo-fibers used in this project were 70 mm long. The non-traditional soil stabilization fluids used in this research included Envirokleen and Soil-sement, two products produced by Midwest Industries. The Soil-sement is a polymer emulsion type stabilizer which increases cohesion of treated soils. Envirokleen is classified as a synthetic fluid which was used to increase density

and cohesion of treated soils. Geo-fibers and the non-traditional liquid additives are described in more details by Collins (2011).

To simulate the natural erosion process on a slope before grass growth, a slope frame box (3 × 3.7 ft) with a gradient of 1.5:1 (h : v) was built as shown in Figure 2. Samples were prepared in the box and mixed by hand. Liquid additives (Soil-sement and Envirokleen) were added into the soil and blended until uniformly distributed. Geo-fibers were added after the soil was mixed with liquid and blended by hand until uniformly distributed. The test slope has hinges on one end to allow for compaction and soil placement to take place in a horizontal position. The soil was placed in the box in three layers and compacted using a 15.8 kg tamp. The soil surface was scarified before the placement of next layer to ensure good contact and uniformity throughout the sample. After all the prepared soil was placed in the test box, the top of the soil sample was screeded and the remaining soil was collected and oven-dried. The mass of the remaining soil was obtained by subtracting from the weight of the dry soil in the frame box. All soil samples with or without treatments were compacted in the frame box to a depth of 0.75 inch. As shown in Figure 2, a water reservoir was built at the top of the frame box to provide a constant water flow on the slope during the slope erosion test. Before testing, the water reservoir and the frame box (with soil sample inside) were well leveled. Then, the water reservoir was filled up with water. A constant water flow into the water reservoir was maintained to provide a constant water flow on the soil sample surface throughout the test. A large box was placed at the bottom end of the slope to collect all of the runoff during testing (Figure 2). The time used for running the test was determined based on several practice tests allowing for significant erosion to take place. In this test, total time of one minute was used.

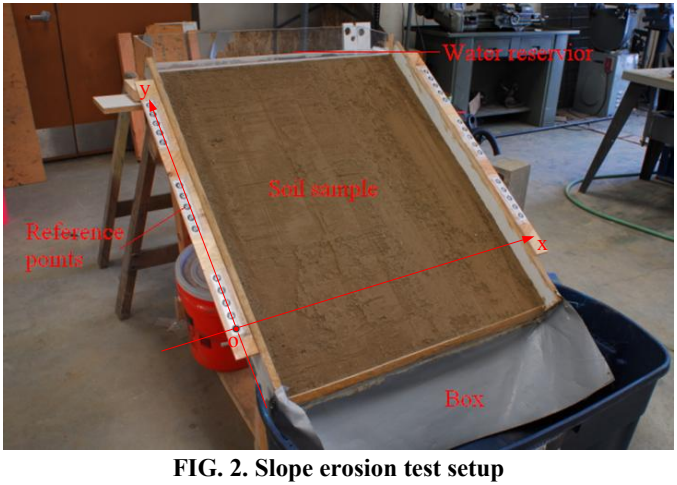

FIG. 2. Slope erosion test setup

Erosion Measurement

Nowadays, the rapid development in the field of digital camera technology and low-budget photogrammetric software products means that consumer cameras may be a

viable option for photogrammetric measurements. To perform the erosion measurement using photogrammetric method, a digital camera was required for photographing during testing. In this study a NIKON D7000 with a 50 mm fixed focal length lens (AF-S NIKKOR 50 mm f/1.4G) was used for image capturing. Photogrammetry principles can be described by Figure 3 using the ideal pinhole camera model. When a photograph is taken for an object, a 2D image is obtained and the depth of the object is lost. For the same object (Figure 3a), images taken from different positions are different due to perspective. The differences can be used to calculate the orientations of the camera where the images were taken. These camera orientations, together with the images, can then be used to reconstruct the 3D geometry of the object. In Figure 3a, perspective center (center of an ideal pinhole camera lens) of the left camera S_1 is set as the origin of an arbitrary coordinate system. Then, three coordinates of the perspective center S_2 (Xs, Ys, Zs) and directional angles (κ,ω,φ) are unknown for the right camera orientation. Usually the distance of any two points can be given as a scale, which reduces the unknowns to five. In Figure 3b, five equations can be established by identifying five pairs of corresponding points on the two images and the second camera orientation can be solved. Since there are numerous pairs (far more than five) of corresponding points on the two images, the redundancy in information can be used to perform an optimization analysis to accurately determine the camera orientation so that the errors in measurement are minimized. In addition, multiple images can be taken from different orientations with sufficient overlap, which can provide more redundant equations, to improve the accuracy of the result. Once the camera orientations are determined, a straight optical ray can be constructed from the photograph through perspective center of the camera to the point on the object as shown in Figure 3b (collinearity). The intersection of these rays (triangulation) then determines the 3D coordinates of a point. As a noncontact 3D measurement technique, photogrammetry is proved to be able to provide high accuracy measurements.

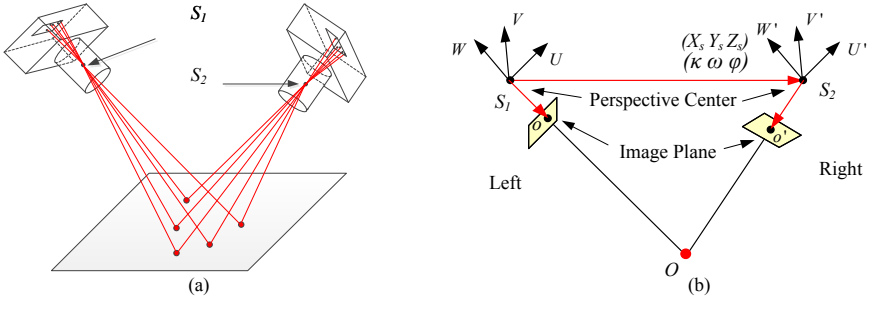

FIG. 3. Principle of Photogrammetry

For a photogrammetric measurement, camera calibration must be performed to reach high measurement accuracy. Camera calibration was performed by capturing a group of images for a point grid from different orientations. After calibration, the image sensor format size (23.9982 × 15.8961 mm), principal point (12.0865 mm,

8.1022 mm), focal length (f = 53.3864 mm) as well as some other distortion parameters were determined. For the measurements in this study, some reference points were placed at the both sides of the frame box (see Figure 2) for the buildup of the coordinate system as well as orientations of camera stations.

After specimen preparation as shown in Figure 2 or Figure 4a, several images for the testing system were captured before and after the erosion test. For image capturing, small aperture size (< F10) is suggested to ensure a longer depth of field for better image clarity. Also, a high shutter speed or a tripod is suggested to be used. Figure 4b is a picture of the soil specimen after erosion test. After the slope erosion test, the collected runoff was moved to a large pan and placed in an oven to measure the mass of the eroded soil. In all cases, the mass of the treatment material (either fibers or nontraditional liquid) was neglected in the measurement of eroded materials. The mass of the eroded soil divided by the mass of the soil in the frame box before the slope erosion test was the mass percent loss erosion.

After photographing, images obtained were processed for orientations of camera stations by marking and referencing the targets in different images. A coordinate system was built as shown in Figure 2. The origin was set to be the reference point at the lower left corner and the x and y axes were set to be parallel to the width and length directions of the frame box. The 3D coordinates of those reference points were determined through photogrammetric technique with a given scale. For each measurement, the 3D coordinates of these reference points were set to be the same. In this way, each measurement is compared in the same coordinate system. For the same sample, before and after the slope erosion test, two surfaces were obtained through the photogrammetric technique. Figure 5 presented the 3D reconstruction of the two surfaces for soil sample with 6% water + 2% Soil-sement + 0.5% geo-fiber. The volume between these two surfaces was the volume loss due to erosion. This volume divided by the volume of the material placed in the frame box before the slope erosion test is the volumetric erosion (volume percent loss).

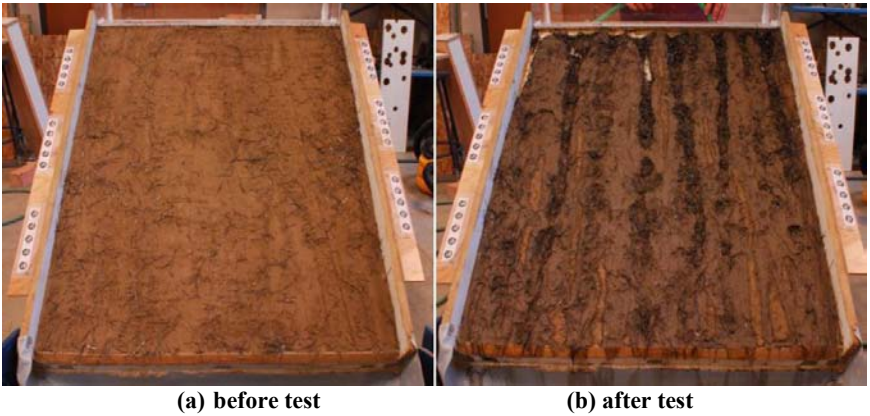

(a) before test **(b) after test**

FIG. 4. Slope Erosion Test (Silt + 6% W + 2% SS + 0.5% GF)

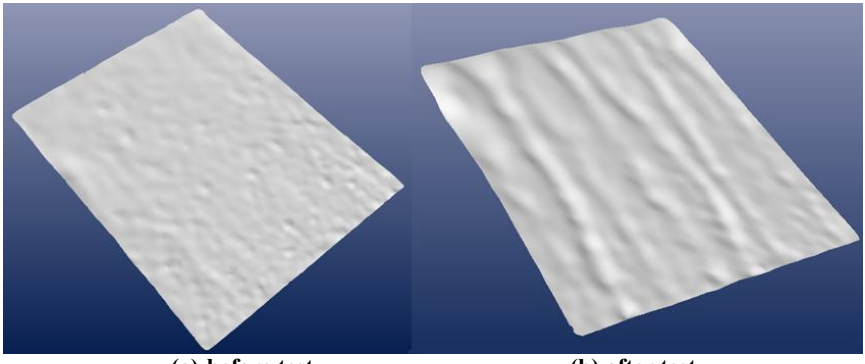

(a) before test **(b) after test**

FIG. 5. 3D reconstruction of sample surfaces (silt + 6%W + 2% SS + 0.5% GF)

TEST RESULTS AND DATA ANALYSIS

The laboratory slope erosion tests provided results that are critical in evaluating the performance of the erosion control methods prior to the onset of grass growth. Two samples were prepared for each treatment configuration including two untreated samples. The results show that there was a reduction in percent loss for treated samples compared to untreated samples. After all tests, erosion results were obtained and presented in Table 1. Both of the erosions (mass and volume percent loss) are the average of the two parallel tests.

Table 1. Slope Erosion Test Results for Fairbanks Silt with Different Treatments

Treatment	Dry density (g/cm^3)		% loss (mass)	% loss (volume)
	Sample 1	Sample 2		
6% Water	1.100	1.109	18.6	34.7
6% Water + 2% SS	1.080	1.054	16.1	25.5
6% Water + 0.5% GF	1.056	1.066	14.1	26.1
6% Water + 2% SS + 0.5% GF	1.097	1.051	11.8	27.3
6% Water + 4% EK + 0.5% GF	1.015	1.025	13.8	17.2

Initial dry density of all soil samples are also presented in Table 1. Soil samples with only 6% water content have the highest dry density and with 6% water content + 4% Envirokleen + 0.5% geo-fiber have the lowest dry density. Generally, it could be found that all treatments caused a reduction in percent loss of material. The reduction in volumetric percent loss is higher than that in mass percent loss. This is because of the volume change due to wetting brought by surface runoff. In terms of mass percent loss, the greatest overall reduction in percent loss came from the sample treated with 2% Soil-sement and 0.5% geo-fiber. However, for volumetric percent loss, the greatest percent loss was found to be the sample treated with 4% Envirokleen and 0.5% geo-fiber. Based on the mass percent loss results, the samples with geo-fiber caused greater reduction in percent loss than the samples without. The reason for the

effectiveness of geo-fibers is likely due to a root like structure that forms and tends to hold the sample together.

CONCLUSIONS

In this study, a photogrammetric method, which is time and cost-effective, was presented to monitor the erosion of soil slope under surface runoff in the laboratory. This photogrammetric method can detect both total and localized erosion, which is a complement of fence installation method. Through a series of slope erosion tests, erosiveness of Fairbanks silt varied with different treatment as well as their combinations. All treatments improved the natural erosion qualities of Fairbanks silt.

Besides being used for laboratory measurement, this photogrammetric method can also be applied to field erosion monitoring. However, a different focal length lens, which depends on the size of the erosion measurement area, is suggested to be used. Also, similar to laboratory measurement, some motionless reference points are required to build a coordinate system.

ACKNOWLEDGEMENTS AND DISCLAIMER

This study was funded by the AKDOT&PF and the Alaska University Transportation Center (AUTC). The authors gratefully acknowledge AKDOT&PF and AUTC for their financial support. The opinions expressed in this paper are those of the authors and do not represent the views of AKDOT&PF nor AUTC.

REFERENCES

Alyeska Pipeline Service Company (APSC). (1975). “Hess Creek Thermal Erosion Site - 1974 Evaluation.” *Report Number TE-006*.

Curran. J. H and McTeague. M. L. (2011). Geomorphology and bank erosion of the Matanuska River, south central Alaska: U.S. *Geological Survey Scientific Investigations Report* 2011–5214, 52 p.

Matsumoto. T., Kimura. M., and Ono. T. (2001) “Large-scale slope failure and active erosion occurring in the southwest Ryukyu fore-arc area.” *Natural Hazards and Earth System Science*, 1: pp. 203–211.

Vinson, T.S. and Mchattie, R.L. (2009). “Documenting Best Management Practices for Cutslopes in Ice-rich Permafrost.” *FHWA-AK-RD-09-01 Final Report*, Alaska Department of Transportation and Public Facilities Research Development, and Technology Transfer Library.

Vandamme. J. and Zou. Q., (2013). “Investigation of slope instability induced by seepage and erosion by a particle method.” *Computers and Geotechnics,* 48: pp.9-20.

Collins, R. (2011). “Stabilization of marginal soils using geofibers and nontraditional additives.” *MSc. Thesis*. University of Alaska Fairbanks, Fairbanks, AK.

Study on the Performance Deterioration of Asphalt Overlays on Rigid Runway Pavement- Case Study at Shanghai Hongqiao International Airport

Jie Yuan[1], Long Wang[2], Jian-Ming Ling[3] and Yong Luo[4]

[1]Associate Professor, Key Laboratory of Road and Traffic Engineering of the Ministry of Education, Tongji University, Shanghai 200092, China; yuanjie@tongji.edu.cn
[2]Master Degree Candidate, Key Laboratory of Road and Traffic Engineering of the Ministry of Education, Tongji University, Shanghai 200092, China; 071283@tongji.edu.cn
[3]Professor, Key Laboratory of Road and Traffic Engineering of the Ministry of Education, Tongji University, Shanghai 200092, China; jmling01@yahoo.com.cn
[4]Senior Engineer, Shanghai CAAC New Era Airport Design and Research Institute Ltd, Shanghai, 200335, China; caacluoyong@yeah.net

ABSTRACT: This paper analyzed the deterioration of performance of runway 18L-36R in three aspects: firstly, Pavement Condition Index (PCI) had been investigated since 2000 and the changes in dominant damage was analyzed. The results showed that there was a downward trend of PCI with a significant increase in length and quantity of reflective cracks. Secondly, the deflection basins from 2005 to 2009 were collected for comparison based on Heavy Weight Deflectometer (HWD) data (test date: 2005.11\2006.03\2006.08\2008.05\2009.10). And then the structural remaining life and Pavement Classification Number (PCN) were computed and analyzed based on the back-calculated results of structural parameters. It was found that there was little changes in PCN, but a significant reduction in structural remaining life. Thirdly, experimental results of core samples of asphalt overlay (2005.10\2008.05\2009.10) indicated that all the technical indexes of upper surface of asphalt overlays (overlaid in 2005) met the requirements， while the aging was more serious than other asphalt overlays (overlaid in 1991 and 1998 respectively). Moreover, the layer bonding condition between overlays and PCC changed from total bond to partial bond. Further analysis presented that material properties of overlay and bonding condition between overlays and PCC were main factors which influence the stress level in asphalt overlays and pavement bearing capacity. In conclusion, the performance of composite pavement deteriorated mainly for the property degradation of asphalt overlays.

INTRODUCTION

In 1964, Shanghai Hongqiao International Airport (SHA) opened for service. SHA is located in the west of Shanghai, approximately 13 km from city center. As an

important part of Hongqiao transportation hub, passenger traffic at SHA totaled 33 million in 2012 which ranked No.4 in China. Runway 18L-36R, one of the two runways at SHA, has been operated for about 50 years. Before 1991, it was a rigid pavement. In order to maintain normal operation, it has been overlaid for four times (1991\1998\2005\2011). The current structure is very complicated with four asphalt overlays on the original concrete pavement and a block-stone base. The typical structure of runway 18L-36R is shown in FIG. 1.

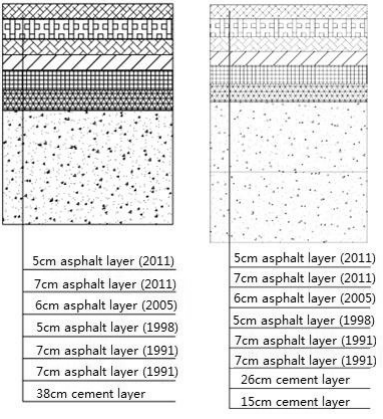

FIG. 1. Typical structure of runway

Since 2000, Runway 18L-36R had undertaken a series of detections and evaluations. Pavement detection items included non-destructive testing (NDT) with Heavy Weight Deflectometer (HWD), Pavement Condition Index (PCI) survey, destructive testing (DT) with core samples of pavement , pavement roughness testing and surface friction testing. These tests served two purposes: firstly, the basis for the timely pavement maintenance and repair was provided. Secondly, the design parameters for pavement overlay in the further studies could also be obtained.

This paper presented the approaches and methodologies of pavement evaluation in China. Based on the evaluation results, deterioration of performance of runway 18L-36Rwas analyzed.

PCI

FIG. 2 shows the crack development from 2002 to 2005. The cumulative length increased slightly from 2002 to 2004, but 2005 witnessed a sharp rise in data. Moreover, the reflective crack was the main type of all cracks investigated.

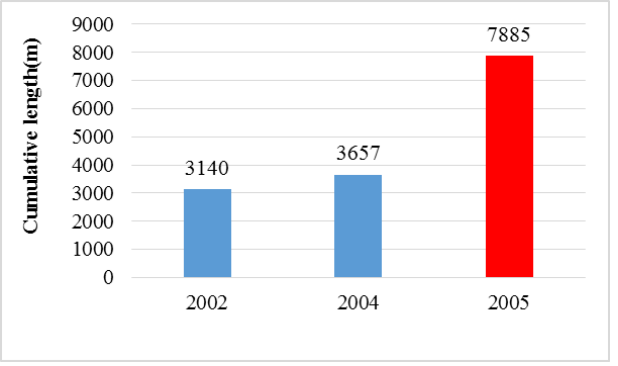

FIG. 2. Crack development from 2002 to 2005

FIG. 3 manifest the calculated PCI and its development trend from 2000 to 2004. It can be seen that the PCI in 2002 dropped sharply and the coefficient of variance increased significantly. As a result, a series of pavement maintenance was carried out in 2003.

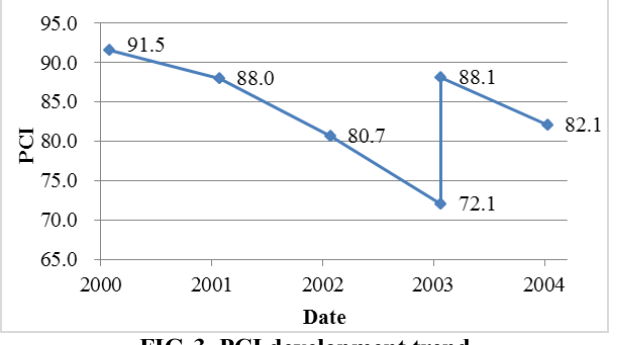

FIG. 3. PCI development trend

After overlaying in 2005, three times of investigations were carried out (2008.04\2009.03\2009.10). FIG. 4 shows the comparison of the length of cumulative cracks in these three investigations. Compared with the results of investigations before 2005, rutting was no longer the dominant type of damage, while the reflective crack was still the main type of damage. It also could be found that pavement cracks grow significantly in winter.

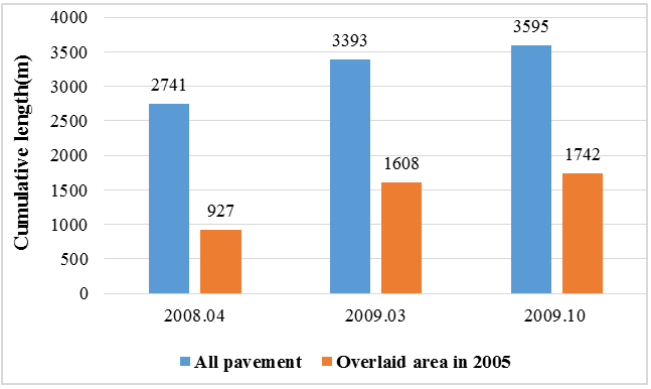

FIG. 4. Comparison in the length of cumulative cracks

According to the data analysis, not only the number of cracks increased significantly, but also the distribution of cracks became more widely. The distribution of cracks in three investigations (area overlaid in 2005) is shown in FIG. 5. Although the calculated PCI remained at a relatively high level, there was a downward trend of PCI with the significant increase in the length and quantity of reflective cracks.

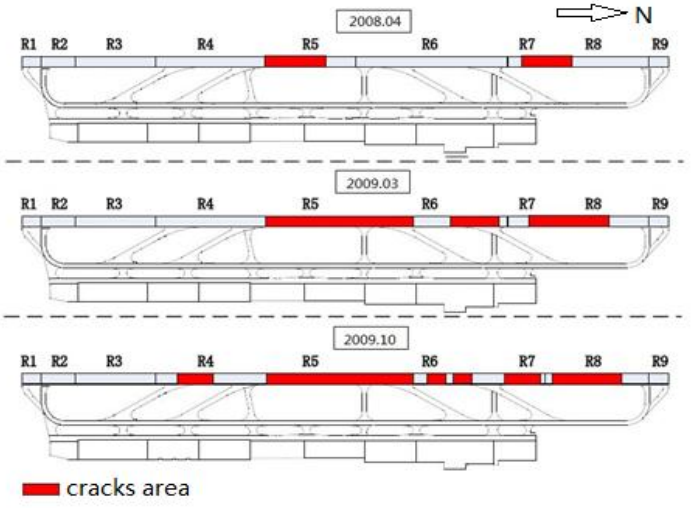

FIG. 5. Distribution of cracks

STRUCTURAL BEARING CAPACITY

As for its prominent capability of speediness, in-situ and nondestruction, NDT has been widely used in detection of pavement structural bearing capacity. At Shanghai Hongqiao International Airport, Heavy Weight Deflectometer (HWD) is the main

method of pavement structural bearing capacity testing. The runway were overlaid twice in 2005 and 2011 respectively, and over this span of 7 years, five times of HWD testing data were collected, which are shown in Table 1.

Table 1. HWD Testing Data of Runway 18L-36R

Test date and temperature	Sensor position (cm)	0	20	30	60	90	120	150	180	210	Load (KN)
2005.11 （23℃）	Average/μm	211	121	95	87	83	77	70	66	61	146
	Variance/μm	40	20	15	14	11	10	8	7	6	2
	Coefficient of Variance%	19	16	16	16	14	12	12	10	10	2
2006.03 （15℃）	Average /μm	155	100	85	81	76	71	66	61	56	144
	Variance /μm	25	14	11	10	9	8	7	7	6	2
	Coefficient of Variance%	16	14	13	13	12	12	11	11	11	1
2006.08 （27℃）	Average /μm	315	141	96	85	83	76	70	68	62	143
	Variance /μm	70	28	13	12	10	8	7	6	5	2
	Coefficient of Variance%	22	20	14	14	12	11	10	9	9	1
2008.05 （16℃）	Average /μm	156	97	84	79	75	69	64	60	55	145
	Variance /μm	36	18	13	11	9	8	6	6	5	2
	Coefficient of Variance%	23	18	16	14	12	11	10	9	9	1
2009.10 （16℃）	Average /μm	192	93	71	67	64	58	53	51	46	136
	Variance /μm	38	16	11	8	7	6	5	5	4	4
	Coefficient of Variance%	20	17	15	12	11	10	10	9	8	3

The comparison of deflection basins in five times of investigations can be seen in FIG. 6. The deflections at later seven points(D_2~D_8) in each test were close, while the deflections of D_0 (center of load plate) and D_1 (20cm from center of plate) in each test were different. This is mainly because the modulus of asphalt was very sensitive to the change of temperature, while the temperature had little influence on the structural performance of concrete slab and subgrade. Deflections near the center of load were affected largely by the modulus of surface, while deflections far from the center were affected mainly by the strength of subgrade. Because the changes in deflections at D_2~D_8 were not obvious, it could be seen that there was no significant deterioration in concrete slab and subgrade. However, if the influence of the temperature to the asphalt was excluded and only the test data of 2006.03（15℃）, 2008.05（16℃） and 2009.10（16℃）was analyzed, it could be seen that the deflection at D_0 in 2009 increased by 32%. Deterioration of asphalt parameter should happen between 2008 and 2009.

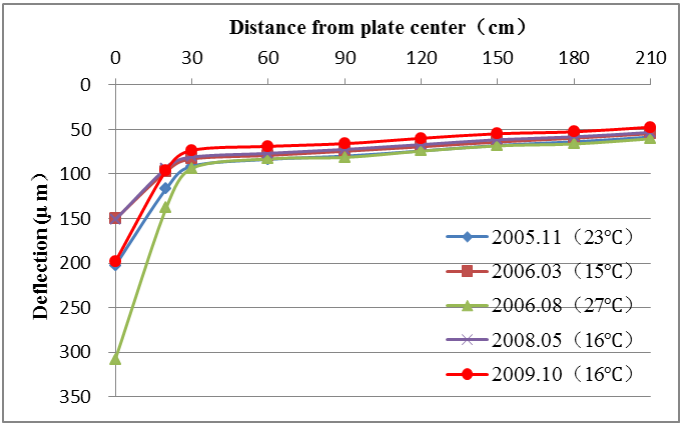

FIG. 6. The comparison of deflection basins in five times of investigations

In order to check the deterioration between 2008 and 2009, pavement structural parameter was back-calculated in accordance with the method of composite pavement back-calculation. The results are shown in Table 2.

Table 2. Results of Back-calculation

Date	Radius of relative stiffness /m	Elastic modulus of asphalt pavement /MPa	Elastic modulus of concrete slab /GPa	Bond coefficient	Modulus of subgrade reaction /MN/m^3
2009	0.99	1500	50	0.5	149
2008	1.00	1500	47	1.0	149

As is shown in the table, the bond condition between overlaid asphalt pavement and original concrete slab changed from total bond to partial bond. If the bond condition between structural layers gets worse, not only the deflection of pavement should be influenced, but also the load stress of asphalt overlay should increase significantly as the capacity of load diffusion by the original concrete pavement becomes poorer. In this way, deterioration of asphalt material would be accelerated.

PCN

The Aircraft Classification Number - Pavement Classification Number (ACN-PCN) method was published by International Civil Aviation Organization (ICAO) in 1983. All the members of ICAO are required to use this method to report pavement strength. In Appendix 2 of the ICAO Aerodrome Design Manual, Part 3, Pavements, procedures for determining the ACN are provided, while the calculation procedures

of PCN are not given.

In America, Boeing Company published Precise Methods for Estimating Pavement Classification Number in 1998. Then, Advisory Circular AC: 150/5335-5A of Federal Aviation Administration (FAA) was published in 2006. In 2011, AC:150/5335-5B and ComFAA 3.0 computer software were published. In China, the calculation procedures of PCN referred to AC: 150/5335-5A except the fatigue equation and the load position.

The PCN of runway 18L-36R was reported as: PCN / 52 / R / A / X / T.

Structural Remaining Life

In 2010, structural remaining life of runway 18L-36R was calculated in accordance with Design Methodology of Civil Airport of China. Because the original concrete layer was the main load diffusion layer of runway 18L-36R, the control index of design methodology of civil airport of China in structural life calculation should be fatigue cracking at the bottom of concrete slab. The calculated result of remaining life was 2.7 years.

MATERIAL PERFORMANCE

To analyze material performance of asphalt overlay, 16 core samples of pavement were collected in 2009. Core samples had reflected the thick of asphalt overlay in different time since 1991. The material on top surface was SMA16, AC16 was in the middle and AC20 was at the bottom. Specific conditions can be seen in FIG. 7.

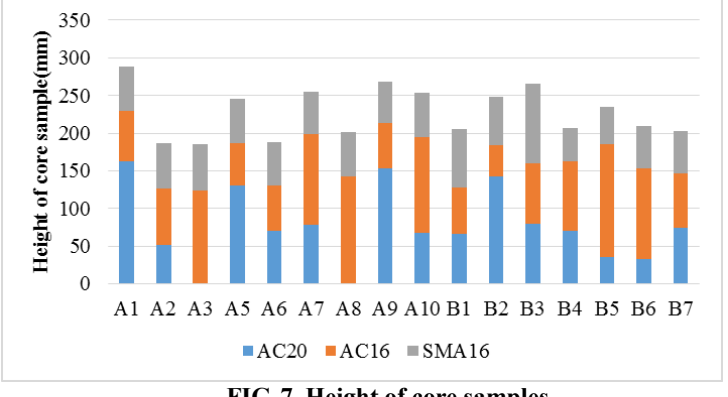

FIG. 7. Height of core samples

Table 3. Thickness of Asphalt Overlay

Layer	Average thick /mm	Max thick /mm	Min thick /mm	Coefficient of Variance %
Top (SMA16)	61.3	106.0	45.0	20
Middle(AC16)	88.8	150.0	42.0	35
Bottom(AC20)	95.2	172.0	33.0	47

From appearance and height of core samples, characteristics can be found as follow:

1) The integrity of core samples was good, no loose core samples were found.
2) Core samples consisted of three layers: two in 1991 and one in 2005. Because of milling in the process of overlaying in 2005, layer of overlay in 1998 was not found.
3) The bonding condition between overlayer in 2005 and older asphalt overlayer was good except that core sample of B4 got fractured. However, as the bonding condition between two overlayers in 1991 was poor, all five samples got fractured.
4) Cracks were top-down type basically.

Further analysis of material performance was based on laboratory test. Test items included air voids test, Marshall test, freeze-thaw splitting test, Cantabro loss test, asphalt content test and mixture gradation test based on the Pavement Evaluation Specification of Civil Airport (MHT 5024-2009). Test results are shown as follow:

Table 4. Technical Index of SMA16

Performance index	Test result	Technical standard	Comparison
Air voids (%)	6.2	3.5~4.5	Larger
Marshall stability（KN）	13.1	≥6.0	Satisfied
Strength ratio of freeze-thaw splitting residual（%）	82.8	≥80	Satisfied
Marshall residual stability（%）	88.5	≥80	Satisfied
Cantabro loss（%）	11.8	≤15	Satisfied
Asphalt content (%)	6.12	—	Satisfied
Mixture gradation	—	—	Aggregate bigger than 4.75mm beyond design limit

Table 5. Technical Index of AC16 and AC20

Performance index	Technical standard	AC-16	AC-20
Marshall stability（KN）	≥6.0	10.8	—
Strength ratio of freeze-thaw splitting residual（%）	≥80	66.2	70.0
Marshall residual stability（%）	≥80	75.9	—
Cantabro loss（%）	≤15	24.9	40.3
Asphalt content (%)	—	5.19	4.86

From test results shown above, it can be seen that:

1) Performance index of material SMA-16 (overlaid in 2005) was under control, but the mixture gradation changed and air voids of part area grew.
2) Mixture gradation of AC material overlaid in 1991 presented serious deviation. Water stability and loose-resistance ability could not meet the technical requirements. Technical index was close to asphalt macadam. Once waterproof ability and protection was lost from upper surface (SMA-16), rapid deterioration of asphalt overlay would happen.

In order to analyze the deterioration condition of asphalt overlay of runway 18L-36R, comparison of performance indexes of SMA-16 between 2005 and 2009 are shown in Table 6.

Table 6. Comparison of Performance Indexes of SMA-16 between 2005 and 2009

Performance index	Year 2005	Year 2009
Marshall stability（kN）	13.6	13.1
Cantabro loss（%）	7.7	11.8
Strength ratio of freeze-thaw splitting residual（%）	83.9	82.8
Marshall residual stability（%）	87.7	88.5
Air voids (%)	3.9	6.2
Asphalt content (%)	6.2	6.1

It can be seen that, after four years operation since overlaid in 2005, there had been little changes in water stability of SMA-16, while loose-resistance ability had reduced significantly. Considering that the air voids grew, factual asphalt content may reduce as well.

CONCLUSIONS

This paper analyzed the performance deterioration of runway 18L-36R from PCI，HWD and core sample experiments. Based on the analysis and experimental results obtained in the study, the following conclusions could be drawn:

1) There was a downward trend of PCI with a significant increase in length and quantity of reflective cracks.
2) With the growth of service life, the calculated structural remaining life based on HWD data decreases significantly.
3) Core sample experiments results showed that the changes of bonding condition between overlays and PCC and the property deterioration of overlaid material were the main factors which influence the bearing capacity of composite pavement.
4) The performance of composite pavement deteriorated mainly for the property degradation of asphalt overlays.

REFERENCE

Civil Aviation Administration of China.(2009). "Pavement Evaluation Specification of Civil Airport." (MH/T 5024-2009)

Civil Aviation Administration of China. (2010). "Specifications for Airport Cement Concrete Pavement Design." (MH/T 5004-2010)

Civil Aviation Administration of China.(2006). "Technical Standards for Airfield of Civil Airports." (MH 5001-2006)

International Civil Aviation Organization. (1983). "Aerodrome Design Manual, Part 3, Pavements."

Boeing Company. (1998). "Precise Methods for Estimating Pavement Classification Number."

Federal Aviation Administration. (2006). "Standardized Method of Reporting Airport Pavement Strength – PCN" (AC 150/5335-5A)

Federal Aviation Administration. (2011). "Standardized Method of Reporting Airport Pavement Strength – PCN" (AC 150/5335-5B)

Civil Aviation Administration of China.(1999). "Specifications for Asphalt Concrete Pavement Design of Civil Airports." (MH 5010-1999)

Inspection and Nondestructive Evaluation of Concrete Bridge with Environmental Deterioration

Jiong Hu[1], Soon-Jae Lee[2], Yoo-Jae Kim[3], and Mohamed Mahgoub[4]

[1]Assistant Professor, Department of Engineering Technology, Texas State University, 601 University Drive, San Marcos, TX 78666; jiong.hu@txstate.edu
[2]Assistant Professor, Department of Engineering Technology, Texas State University, 601 University Drive, San Marcos, TX 78666; sl31@txstate.edu
[3]Assistant Professor, Department of Engineering Technology, Texas State University, 601 University Drive, San Marcos, TX 78666; yk10@txstate.edu
[4]Assistant Professor, Department of Engineering Technology, New Jersey Institute of Technology, University Heights, Newark, NJ 07102; mahgoub@njit.edu

ABSTRACT: This paper presents a case study of inspection and evaluation of a concrete bridge located in southeast Texas. A significant level of deterioration of concrete columns in the bridge has generated public concerns regarding its structure integrity. Many environment-related factors including erosion, abrasion, wetting/drying, carbonation, freezing-thawing, chemical attack, and microbial-induced deterioration could all contribute to the deterioration. In this study, a visual inspection and a number of field tests were performed on columns of the bridge. Nondestructive evaluation (NDE) including hammer sounding, rebound hammer, ultrasonic pulse velocity, covering thickness, and half-cell corrosion potential analyses were performed in the comprehensive study to determine cause(s) of concrete degradation and ascertain the degree of deterioration.

INTRODUCTION

Deterioration and damage of reinforced concrete bridges has been a critical issue affecting their service conditions. In general, concrete bridge deteriorations are contributed by four major areas: chemical, physical, mechanical and biological (Delatte 2009). Chemical factors, generally caused by acid and salt, can be grouped into three major categories: (a) reactions leading to formation of expansive products, such as in the case of alkali-silica reaction, sulfate attack and corrosion of reinforcing steel in concrete; (b) cation-exchange reactions between aggressive fluids and the cement; (c) hydrolysis of the cement paste components by soft water. Physical factors of concrete deterioration/damage, generally caused by temperature and moisture change, heat, wind and water, can be grouped into two categories: (a) cracking due to normal temperature and humidity gradients, crystallization of salts in pores, structural loading, and exposure to extreme temperature such as freezing/thawing or fire; (b)

surface wear or loss of mass due to abrasion, erosion and cavitation from water flow. Mechanical factors can be grouped into two categories: (a) overloading by static and/or dynamic loads, such as those caused by earthquakes or extensive impacts or loads; (b) construction faults such as those from premature applications of load during construction. Biological factors including fungi, moss, and microbial, etc. can also cause internal or external concrete deterioration through physical and chemical interactions. It should be pointed out that the distinction among these causes is purely arbitrary. Many of the above-mentioned mechanisms are directly related to environment and often times these factors are superimposed on each other and concrete deteriorations are frequently caused by multiple reasons (Neville 1996; Mindess et al. 2003; Parameswaran et al. 2008; Peng and Stewart 2008; Roelfstra 2004; Shi et al. 2012; Papadakis et al. 2013; Neville 2004; Giannini et al. 2013).

Through a routine Texas Department of Transportation (TxDOT) inspection of a concrete bridge located at Alligator Bayou in Jefferson County, Texas, deterioration of concrete columns generated concerns of the structural integrity of the bridge. According to the location and service history of the bridge, causes including alkali-silica reactions, delayed ettringite formation, freeze-thaw damage, and fire damage can be easily ruled out. However, environmental-related deteriorations including erosion, abrasion, wetting/drying, carbonation, chemical attack, and microbial-induced deterioration are all possible cause(s) of the deterioration. In addition, extensive loads, and physical impacts could also result in the deterioration. A study is needed to identify the mechanism(s) of deterioration and evaluate the extent of it.

INSPECTION METHODS

Background Information Collection

Background information including age, mix design, climate condition, service condition, and history of incident (such as fire or physical impact) of the bridge was collected before the site investigation. The research team also determined the site investigation date according to information such as weather condition and accessibility.

Visual Inspection

Before on-site nondestructive evaluation (NDE), a visual inspection was performed to examine bridge column appearance and overall service condition. Information such as concrete cracking, spalling, delamination, efflorescence, softening of concrete and reinforcement corrosion was recorded. According to the preliminary visual inspection and accessibility, critical locations for NDE tests were also determined.

Field Inspection

In order to evaluate the level of concrete deterioration, a number of NDE tests were performed on bridge columns. Most tests including rebound hammer, half-cell corrosion potential, and covering thickness were performed at approximately 0.3-m intervals, starting at 0.15-m above water or ground level and up to 1.5-m above

(depending upon accessibility). At each measured height, five to seven measurements (within intervals of at least 0.15-m) were taken and the average reading from each nominal height were reported. Due to the high variable natural of the test, outliers (data with differences equal to or greater than 20% of the average value) from the rebound hammer test were removed, which accounts for approximately 1% of the total data used in the analysis.

Hammer sounding test was used to evaluate near surface concrete condition, mainly through surveying concrete columns by sounding to determine delamination in the concrete. The practice involves manually hit the concrete surface with a hammer and distinguish the sound upon contact. Generally speaking, solid sound is the indication of good concrete, and hollow sound is the indication of damaged concrete, mostly delamination. Because of the empirical nature of the test, hammer sounding test was only performed at selected location for general idea of concrete condition.

Rebound hammer, also known as Schmidt hammer test as shown in FIG. 1 was used to measure the hardness of the concrete surface. The rebound hammer measures the rebound of a spring-loaded mass impacting against concrete surface. The test hammer hits the concrete at a defined energy and its rebound is dependent on the hardness of the concrete. Tests were performed according to ASTM C805 "*Standard Test Method for Rebound Number for Hardened Concrete*" (ASTM 2008). By reference to the empirical conversion chart, the rebound value can also be used to determine the compressive strength (Malhotra and Carino 2004).

FIG. 1. Rebound hammer test.

The Ultrasonic Pulse Velocity (UPV) test as shown in Fig. 2 was performed on bridge columns to measure the velocity of an ultrasonic wave passing through the concrete, so as to estimate the degree of internal concrete deterioration. The method consists of measuring the time of travel of an ultrasonic pulse passing through the concrete being tested. Comparatively higher velocity is obtained when concrete quality is good in terms of density, uniformity, homogeneity etc. (Malhotra and Carino 2004). UPV tests were performed according to ASTM C597 "*Standard Test Method for Pulse Velocity through Concrete*", with direct transmission (ASTM 2008), i.e., two transducers lined up directly opposite each other on the column. 50K Hz frequency P-wave was applied in the measurement. An abrasive stone was used to remove the loss (soft) mortar on concrete columns prior to testing on an as-needed

basis, in order to expose the underlying concrete. Due to the extensive efforts needed for each test, the UPV test was performed only at selected locations.

FIG. 2. UPV test.

A covermeter (rebar locator) as shown in Fig.3 was used to locate rebar underneath concrete, i.e., covering thickness of concrete over rebars. The covering thickness of the concrete encircling the rebar was estimated through the measurement based upon an electromagnetic pulse-induction method. In the test, coils in the probe are periodically charged by current pulses and thus generate a magnetic field. Eddy currents are produced on the surface of electrically conductive material in the magnetic field, which induce a magnetic field in opposite directions. The resulting change in voltage can be utilized for the measurement and rebars that are closer to the probe or of larger size produce a stronger magnetic field (Malhotra and Carino 2004). Note that the measurements were only performed in the direction parallel to the main reinforcement direction (i.e., vertical direction) in this study.

FIG. 3. Covermeter test.

Corrosion activity was measured with a half-cell corrosion potential measuring device as shown in FIG. 4. The device is the same unit as shown in Fig. 3, yet with an exchangeable gauge that can also accept a half cell attachment. The measurement is associated with the steel corrosion rate, which can signal the severity of rebar

corrosion. The half-cell potential method measures the current flow (in the form of ion migration) through the concrete between anodic and cathodic sites accompanied by an electric potential field surrounding the corroding bar when there is active corrosion that exists. The corrosion potential of reinforcement was a qualitative measure through the evaluation of the potential difference between a standard portable half-cell, normally a Copper/ Copper Sulphate ($Cu/CuSO_4$) or Silver/Silver Chloride (Ag/AgCl) standard reference electrode placed on the surface of the concrete with the steel reinforcement underneath. Procedures as described in ASTM C876 "*Standard Test Method for Half-Cell Potentials of Uncoated Reinforcing Steel in Concrete*" were used (ASTM 2008), and the (corrosion) potential was measured against a silver/silver chloride reference half-cell in this study. The corrosion potential usually is presented as the voltage of current flow. With the silver/silver chloride half-cell used in the present study, a voltage higher than -120mV indicates a 90% chance of no active corrosion, a voltage lower than -270 mV indicates a 90% chance of active corrosion, while voltages between -120mV and -270mV indicate a uncertainty of active corrosion (Malhotra and Carino 2004).

FIG. 4. Half-cell corrosion potential test.

INSPECTION RESULTS

According to information collected prior to the site visit, the bridge to be inspected was constructed in 1952, and has served 58 years at the time of site visit. The concrete bridge is supported by a total of ten spans. While the east and west end spans were mostly in dry (land) condition and remain spans were generally exposed to fresh water body, bridge columns were reportedly under drying/wetting cycles due season changes. There were eight square shape columns in each span, with the cross section at approximately 360mmx360mm each. The bridge was located within an area with significant traffic from oil refinery plants. According to the weather condition, the site inspection was conducted on April 30th, 2010, with the temperature at 22.5^{o}C and relative humidity at 84.6% at the time the inspection started. Following section summarized results from the site inspection, detailed information of visual inspection, together with nondestructive testing results can be found at the project report associate with the study (Hu et al. 2011).

Site Condition and Visual Inspections

Due to seasonal changes, water level at the time of site inspection was approximately 0.15-m below the normal water level. The only two spans that were accessible during the site inspection were the east end span (span-1) and the second span from the east (span-2). While span-1 was not exposed to water, span-2 was exposed to water of approximately 0.25-m deep during the site visit.

(a) Overview of the bridge

(b) Overview of columns underneath the bridge

(c) Columns in east end span (span-1)

(d) Column with visible vertical cracking

(e) Column with peeled off concrete

(f) Column exposed corroded rebar

FIG. 5. Images of visual inspection.

As shown in Fig. 5, during the visual inspection, severe deterioration was observed throughout these bridge columns. Low to medium level of scaling and exposure of coarse aggregate was observed in all bridge columns, including columns in the two end spans that were mostly not directly exposed to water. In general, columns in the

two end spans have lower level of scaling (penetration depth less than 6-mm) comparing to columns in the remaining spans, which have medium level of scaling with penetration depth between 6- and 12.5-mm. Generally, the higher up from water level, the less degree of deterioration is observed. The observation is a good indication that the deterioration is likely driven by water movement and moisture level inside concrete. Cracks in vertical direction with up to 2-mm width and reached up to 1.2-m above water level was observed in approximately 40% of the columns. According to ACI 224, the extent of cracking in the bridge columns are significantly higher than the tolerable crack width of 0.30mm under humidity, moist air and soil condition (ACI 224 2001). Approximately 15% of the columns have corroded reinforcement exposure with chunks of concrete on the main rebar direction peeled off from concrete columns. No visible vertical cracking and/or peeled off concrete chunk was observed in columns in span-1.

Field Inspections

Hammer test was performed on concrete surface of three randomly picked concrete columns in span-1 and span-2 respectively. Results showed that even with surface scaling and losses of mortar, the remaining concrete is still in relatively sound condition.

Results from rebound hammer, UPV, and half-cell tests at different column testing heights are summarized in Figs. 6-7 respectively. In this paper, the number after the letter "S" referred to the span number from the east and the number after the letter "C" referred to the column number from the south. For example, the designation of "S1-C4" indicated that test results were from the fourth column from the south in the first span from the east. Heights using in the figures are the height above water level during site inspection.

Due to the high level of surface spalling, no valid UPV test data was obtained from columns in span-2. The UPV results from column 4 in span-1 showed that most of the measured wave velocity falling between 3,800 to 4,200 m/s, which indicated a good quality of concrete underneath the deteriorated surfaces (Malhotra and Carino 2004). However, no clear trend of relationship between UPV and height of testing location was observed.

Results of rebound numbers with test heights from approximately 0.2-m to 1.2-m above water level are shown in Fig. 6. It should be noted that rebound hammer test was not performed in low heights on columns in span-1, as the locations were not accessible with soil coverage. Rebound hammer test results were found to be highly scattered, and generally standard deviations increase at lower elevation, with up to a 50% variation observed in some locations, which is reasonable as the direct exposure of aggregate apparently increases the variation in test results. Rebound hammer tests indicated that in general, an increase of surface hardness with an increase in the height of the column, which is consistent with the observation that the deterioration is less severe when it is away from water level. Rebound numbers obtained from the test columns are mostly between 25 to 50, which is equivalent to compressive strengths of approximately 25 to 50MPa and indicated good concrete quality. Results also showed that even though there was no data available from rebound hammer tests in span-1 at

lower heights, there is no obvious difference between readings collected from span-1 and span-2.

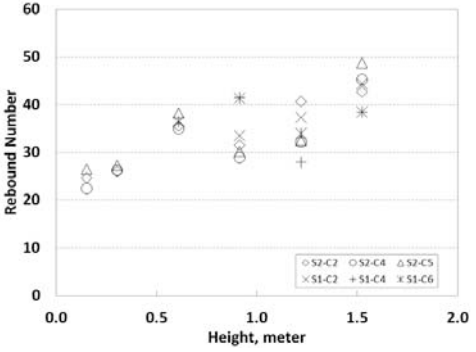

FIG. 6. Rebound hammer test results.

Results from half-cell corrosion potential tests as shown in Fig. 7 demonstrated a clear trend of decreasing corrosion potential with an increase in elevation. As expected, lower level of corrosion potential was observed in columns in span-1, as the columns are not directly exposed in water. Results also showed that high to medium levels of corrosion potential were found in both columns in span-2. High corrosion potential (i.e., corrosion potential less than -270mV) was observed at test locations below 0.5-m. The high level of corrosion potential is likely caused by a significant level of vertical cracking, which caused rebars more vulnerable to corrosion with the exposure of moisture and oxygen. Note that the trend of the decrease of corrosion potential with the increasing in height could also be affected by the moisture content, as dissolved oxygen and potential changes of concentration of chloride, sulfate or other ions in the concrete as one progresses upward from waterline will generally result in an increasing of reading of corrosion potential (i.e., less potential of corrosion).

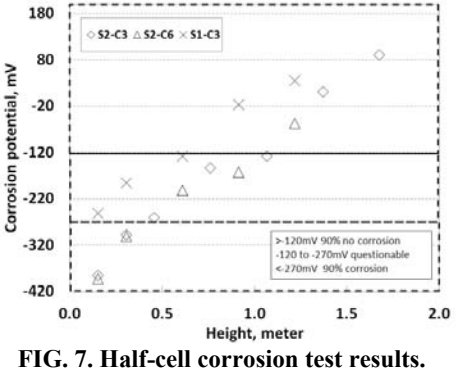

FIG. 7. Half-cell corrosion test results.

Covering thickness measurement showed similar covering thickness in columns in span-1 and span-2, with 51 to 75mm concrete covering in most test locations, except locations with direct reinforcement exposure. According to ACI building code, required concrete cover for corrosion protection is 51mm for concrete exposed to weather (ACI 318, 2008). Results indicated that even with low to medium level of surface spalling, concrete columns in the inspected bridge still provide sufficient cover thicknesses over reinforcement.

Deterioration Assessment and Analysis

As it was mentioned earlier, while various environmental factors might contribute to the deterioration of concrete in the bridge columns, some mechanism can be easily ruled out according to location of the bridge and the record of service history. Likelihoods of cause(s) of deteriorations are summarized in Table 1.

Table 1. Likelihood of Cause(s) of Deterioration

	Cause(s) of deterioration	Likelihood
Chemical	Alkali-silica reaction	Low
	Delayed ettringite formation	Low
	Sulfate attack	Medium
	Chemical deterioration	High
	Corrosion	High
	Carbonation	Medium
Physical	Wetting/drying	High
	Freezing-thawing	Low
	Erosion	Medium
	Abrasion	Medium
	Cavitation	Low
	Fire	Low
Mechanical	Physical impact	Low
	Extensive (traffic) load	High
Biological	Microbial-induced deterioration	Medium

As the bridge is located at southeast Texas, where the weather condition is general mild, freezing-thawing is not likely to be an issue. Good internal concrete condition from UPV test also indicated that the deterioration is not likely caused by alkali-silica reaction or delayed ettringite formation. The mild current in the water body also eliminate causes such as cavitation. There is also no record of fire damage and physical impact on the bridge and bridge columns. The wetting/drying cycles are believed to play an important role as the capillary forces could repeatedly draw water into micro-cracks in concrete. As the bridge is located within an area of significant traffic from oil refinery plants, the deterioration is likely due to three factors: (1) possible chemical deterioration due to the contamination of the water under the bridge from nearby oil refineries and possible coupled bio/chemical deterioration; (2) vertical cracking due to heavy loads applied on the bridge (James et al. 1987; Li et al. 2009); and (3) accelerated corrosion process due to the vertical cracking and high

moisture content in concrete from the capillary forces through dry-wet cycles in the columns. A laboratory analysis of sulphate, chloride and other chemical composition in water, bud and concrete, together with petrographic analysis of concrete samples might be needed to further determine the mechanism of deterioration.

While hammer sounding, rebound hammer, UPV and cover meter tests indicated that the remaining concrete in bridge columns are still in relatively good condition, observation of the high level of vertical cracking, peeled off concrete and measured high level of corrosion potential indicated that the bridge is not in a structural sound condition (Somerville 2008). Further action including repairing, strengthening, or full replacement of the bridge might be needed.

CONCLUSIONS

This paper presented a case study of field evaluation of a concrete bridge with suspected environment-related deterioration from various chemical, physical, mechanical and biological factors. A comprehensive study was conducted to identify concrete deterioration mechanisms and ascertain the degree of deterioration. In addition to visual inspection, NDE including hammer sounding, rebound hammer, ultrasonic pulse velocity, covering thickness, and half-cell corrosion potential analyses were used in the investigation. While further chemical and petrographic might be needed to determine the mechanism of concrete deterioration, results of the investigation indicated that the deterioration is likely due to the vertical cracking resulted from heavy loads applied on the bridge, high corrosion rate due to the cracking and high internal moisture content in concrete through wetting/drying, and possible chemical deterioration due to the contamination of the water under the bridge from nearby oil refineries coupled bio/chemical deterioration. Although NDE analysis indicated that concrete in the structure are still in fairly good condition, the extent of vertical cracking, loss of concrete and high corrosion potential of reinforcement indicated that further action might be needed to ensure the structural integrity of the bridge.

ACKNOWLEDGEMENTS

The authors wish to acknowledge the support of the TxDOT for funding this research. Special thanks are extended to TxDOT personnel for their support throughout this study, particularly Kevin Pruski as the project director, and William Pecht for the help during the field inspection. The authors would also like to thank graduate student Eom Cheol Tae for his involvement in the research.

REFERENCES

ACI 224 (2001). *ACI 224R-01: Control of cracking in concrete structures*, American Concrete Institute Committee 224, Farmington Hills, MI, 46p.

ACI 318 (2008). *ACI 318-08: Building code requirements for structural concrete and commentary*, American Concrete Institute Committee 318, Farmington Hills, MI, 456p.

ASTM (2008). *Annual Book of ASTM Standards*, ASTM (American Society of Testing Materials) International, West Conshohocken, PA.

Delatte, N. (2009*). Failure, distress and repair of concrete structures*, CRC Press LLC, Boca Raton, FL, 335 p.

Giannini, E., Folliard, K., Zhu, J., Bayrak, O., Kreitman, K., Webb, Z. and Hanson B. (2013). "Non-destructive evaluation of in-service concrete structures affected by alkali-silica reaction (ASR) and delayed ettringite formation (DEF) – Final report, Part I*," FHWA, FHWA/TX-13/0-6491*-1, 228p.

Hu, J., Hahn, D., Rudzinski, W., Wang, Z., and Estrada, L. (2011). "Evaluation, presentation and repair of microbial acid-produced attack of concrete*," FHWA, FHWA/TX-11/0-6137-1*, 215 p.

James, R.W., Zimmerman, R.A., and McCreary, C.R. (1987). "Effect of overloads on deterioration of concrete bridges." *Transportation Research Record*: 65-72.

Li, W., Sun, W., and Jiang J. (2009). "Review on damage and deterioration of concrete subjected to the coupling effect of fatigue load and environmental actions." *J. of the Chinese Ceramic Society*, 37 (12): 2142-2149.

Malhotra V.M. and Carino N.J. (2004). *Handbook on nondestructive testing of concrete*, 2nd edition, CRC Press LLC, West Conshohocken, PA, 384 p.

Mindess, S., Young, J.F. and Darwin, D. (2003). *Concrete*, 2nd ed. Prentice Hall, Upper Saddle River, NJ, 644p.

Neville, A.M. (2004). "The confused world of sulfate attack on concrete." *Cement and Concrete Research*, 34 (8): 1275-1296.

Neville, A.M. (1996). *Properties of concrete*, 4th edition. John Wiley and Sons, New York, NY, 844p.

Papadakis, V.G., Fardis, M.N. and Vayenas (2013). "Fundamental concrete carbonation model and application to durability of reinforced concrete." *Durability of Building Materials and Components: Proceedings of the Fifth International Conference*, 768 p.

Parameswaran, L., Kumar, R. and Sahu, G.K. (2008). "Effect of carbonation on concrete bridge service life." *J. of Bridge Engineering*, 13 (1): 75-82.

Peng, J. and Stewart, M.G. (2008). "Climate change, deterioration and time-dependent reliability of concrete structures." *Futures in Mechanics of Structures and Materials - Proceedings of the 20th Australasian Conference on the Mechanics of Structures and Materials*, ACMSM20: 559-565.

Roelfstra, G., Hajdin, R., Adey, B. and Bruhwiler, E. (2004). "Condition evolution in bridge management systems and corrosion-induced deterioration." *J. of Bridge Engineering*, 9(3): 268-277.

Shi, X., Xie, N., Fortune, K., and Gong J. (2012). "Durability of steel reinforced concrete in chloride environments: An overview." *Construction and Building Materials*, 30: 125-138.

Somerville, G. (2008). *Management of deteriorating concrete structures*, Taylor & Francis, New York, NY, 319 p.

Case History Analysis of Bridge Failures due to Scour

Cheng Lin[1], Jie Han[2], Caroline Bennett[3], and Robert L. Parsons[4]

[1]Project Geotechnical Engineer, Ph.D., Terracon Consultants, Inc., 2201 Rowland Ave., Savannah, GA 31404; clin@terracon.com
[2]Professor, Ph.D., P.E., University of Kansas, CEAE Department, Lawrence, KS 66045; jiehan@ku.edu
[3]Associate Professor, Ph.D., P.E., University of Kansas, CEAE Department, Lawrence, KS 66045; crb@ku.edu
[4]Professor, Ph.D., P.E., University of Kansas, CEAE Department, Lawrence, KS 66045; rparsons@ku.edu

ABSTRACT: Scour is a major cause for bridge failure. To understand the characteristics of bridge failures under scour conditions and provide useful information for scour countermeasure, this study reviewed and analyzed totally 36 historical cases of bridge failure due to scour, including their hydraulic, geotechnical, and structural conditions and failure modes. Based on the collected data, most of scour depths (i.e. up to 41%) ranged from 0.5 to 5 m, but the maximum scour depth could be up to 15 m. Local scour was accounted for 64% bridge failures, followed by channel migration (14%), and contraction scour (5%). Possible bridge failure modes due to scour included vertical failure, lateral failure, torsional failure, and bridge deck failure. Approximately 70% of bridge failures were lateral and vertical. The findings from this study can be updated when more cases of bridge failure under scour conditions are collected and/or become available.

INTRODUCTION

Scour removes soils around bridge foundations by flowing water, and thus reduces the capacity of bridge foundations. Scour events can cause damages to bridges thus posing a potential threat to public safety. According to Lagasse et al. (2007), 60% bridge failures in the United States resulted from scour.

To minimize bridge failures, the Federal Highway Administration (FHWA) has established a requirement that all state highway agencies should evaluate whether the bridges in their inventory are scour-susceptible. This study intended to characterize bridge failures due to scour based on the collected case histories. The bridge failures under scour conditions can result from combined factors including hydraulic,

geotechnical, and structural conditions. Analysis of these factors will help understand characteristics of bridge failure due to scour and provide useful information for selection of appropriate scour countermeasures.

In this study, 36 cases of bridge failures pertaining to scour were collected and their hydraulic, structural, and geotechnical conditions were analyzed. The collected case histories include 20 from New Zealand, 14 from the USA, and 2 from Canada. It should be pointed out that scour characteristics and possible damages highly depend on geological and climatic conditions. The conditions in other countries may be different from those analyzed in this study. The results from this study will be updated when more cases of bridge failures due to scour are collected and/or become available. This paper first reviews two classical cases (i.e. failures of the Schoharie Creek Bridge and the Hatchie River Bridge), and then analyzes the conditions for bridge failure and bridge failure modes in the scour events. This paper also briefly summarizes the remediation measures against scour damage.

FAILURES OF THE SCHOHARIE CREEK BRIDGE AND THE HATCHIE RIVER BRIDGE

Failures of the Schoharie Creek Bridge in the New York State and the Hatchie River Bridge in Tennessee have been widely known in the scour history and have been considered a driving force motivating extensive scour research in the United States. These two cases are thus discussed below in detail.

Failure of the Schoharie Creek Bridge

The Schoharie Creek Bridge collapsed in 1987, leaving 10 people dead. This bridge had two spans over the Schoharie Creek near Amsterdam, New York. The bridge suffered severe scour after a spring flood, which caused collapse of Pier 3 and subsequent Spans 3 and 4 (Storey and Delatte 2003). The 50-year flood event with a velocity of 4.6 m/s was a result of a combination of heavy rainfall and snowmelt [Wiss, Janney, Elstner Associates, Inc. and Mueser Rutledge Consulting Engineers (WJE and MR) 1987]. The high flood rate created an approximately 3 m deep scour hole around Pier 3. The Schoharie Creek Bridge was supported by spread footings with limited embedment into the riverbed. The spread footing under Pier 3 rested on highly erodible soils (i.e. layers of gravel, sand, and silt) (Thornton-Tomasetti 1987).

Causes of the bridge failure were investigated after the bridge collapse (Thornton-Tomasetti 1987; WJE and MR 1987). It was found that the collapse was attributable to a number of design and maintenance deficiencies, such as insufficient embedment of the spread footing, the erodible bearing soil layer, the use of erodible backfill for the footing excavation, and inadequate riprap protection, inspection, and maintenance. The scour was aggravated by a combination of other factors. For example, the flood velocity was higher than anticipated in the original design; debris accelerated downward scour; berms increased the floodwater under the bridge; and a high hydraulic gradient formed between upstream and downstream in the spring. Failure

was also related to insufficient design of the bridge structure for scour conditions. For example, the superstructure bearings allowed for the uplift and slide of the superstructure from the piers; simple spans without any redundancy were utilized; the lightly reinforced concrete piers had limited ductility; and deficient plinth reinforcement resulted in sudden cracking of the plinth instead of a hinging failure.

Failure of the Hatchie River Bridge

The Hatchie River Bridge near Covington, Tennessee failed in 1989. The failure killed nine vehicle occupants. The bridge collapsed during a flood event; the failure was characterized by the collapse of two adjacent pile-supported southbound column bents. Scour exposed friction piles under one column bent to water for a depth of 3 meters, resulting in the piles losing capacity to support the bent. The failure of the bridge was progressive from span settlement to complete span collapse within a time span of 45 minutes. As vehicles passed over the spans supported by one of the distressed column bents (Bent 70), the bent began to settle and leaned northward. In addition to the forces induced by the sliding of the heavy superstructure elements (up to 78 tons), lateral and vertical loads were added to Bent 70, resulting in continuous settlement and buckling of the friction piles. Later forensic investigation revealed that the piles deteriorated after being exposed to water over a prolonged period of time. A 25% reduction in the pile diameter was noted; this was hypothesized to be another primary reason for buckling failure (NTSB 1990; Thompson 1990; Jackson et al. 1991).

It was determined that a combination of channel migration and local scour directly contributed to the collapse of the Hatchie River Bridge. However, insufficient inspection was a human factor responsible for the bridge failure. Scour inspection had not reached the lowest level of the riverbed at the time before the collapse. In addition, evaluators failed to recognize the importance of the exposure of the friction piles. It is well known that friction piles are dependent on the surrounding soils to attain vertical capacity. Furthermore, a variety of overweight trucks permitted to travel across the bridge might have aggravated the collapse of the Hatchie River Bridge.

CONDITIONS ASSOCIATED WITH SCOUR-INDUCED BRIDGE FAILURES

Bridge scour is a complex process involving the interactions among flowing water, soils, and bridge structures. Thus, scour-induced bridge failures are associated with hydraulic, geotechnical, and structural conditions.

Hydraulic condition

Hydraulic condition consists of scour types, scour depths, and flow characteristics. In general, bridge scour includes local scour, contraction scour, general scour, and

channel migration. Local scour occurs around the bridge pier or foundation. Contraction scour is due to the contraction of flow area when the flow encounters obstruction. Contraction scour typically develops across the entire channel section. General scour refers to the long-term scouring of riverbed even without the existing obstruction such as bridges. Channel migration is a long-term erosion of river banks due to the flow tendency to migrate laterally.

A bridge may fail due to a combination of different scour types; however, one scour type is often the major cause to the bridge failure. As such, the case history analysis only associated the bridge failure with one scour type. Table 1 summarizes the distribution of scour types among scour-induced bridge failures. Table 1 shows that local scour is the dominant scour type among all the bridge failure cases examined in this study (accounted for approximately 64% bridge failures). The second dominant scour type is channel migration, which resulted in approximately 14% bridge failures. In contrast, contraction and general scour occurred less frequently.

Table 2 gives the range of scour depth observed at various bridges at failure. Scour depth was not always measured during or after bridge failures. Only 22 cases of bridge failures reported the scour depths. Table 2 shows that the scour depth ranged from 0.5 to 15 m. A shallow scour depth of 0.5 to 2.0 m was accounted for 16% of the 36 bridge failures. In these projects, bridges were mostly supported by shallow foundations. However, most of bridge failures (25% of total 36 cases) occurred at the scour depth ranging between 2.0 and 5.0 m. Bridge failures also occurred at greater scour depths but less frequently.

Table 1. Scour Types and Number of Bridge Failures

Types of scour	Number	Percentage
Local scour	23	64%
Contraction scour	2	5%
General scour	1	3%
Channel migration	5	14%
Not determined	5	14%
Total	36	100%

Scour damage often exacerbates when flood occurs. High stream velocity caused by flood tends to increase scour depth around bridge foundation. As a result, AASHTO (2007) requires that bridge scour should be investigated under flood conditions, i.e. design flood (100-year flood) and check flood (500-year flood). Floods are often accompanied by debris such as drifts, logs, and other debris along the river. Accumulation of debris around the bridge likely directs water downward and thus increases the scour depth. Also, debris accumulation increases lateral loads to bridges, and therefore increases the possibility of bridge failures. Figure 1 shows that 75% of scour-induced bridge failures were related to flood. Half of the bridge failures examined were bound up with debris. Flow with an angle of attack to the

bridge also influenced bridge stability because skewed flows tend to increase the rate of scour around the bridge, and also exert a torsional force to bridges. Flow toward a bridge may start with no angle of attack but gradually skews to the bridge if channel migration occurs. Figure 1 shows 44% bridge failures were associated with skewed flows.

Table 2. Scour Depth and Number of Bridge Failures

Scour depth (m)	Number	Percentage
0.5-2.0	6	16
2.0-5.0	9	25
5.0-7.0	2	6
7.0-10.0	3	8
10.0-15.0	2	6
Not determined	14	39
Total	36	100

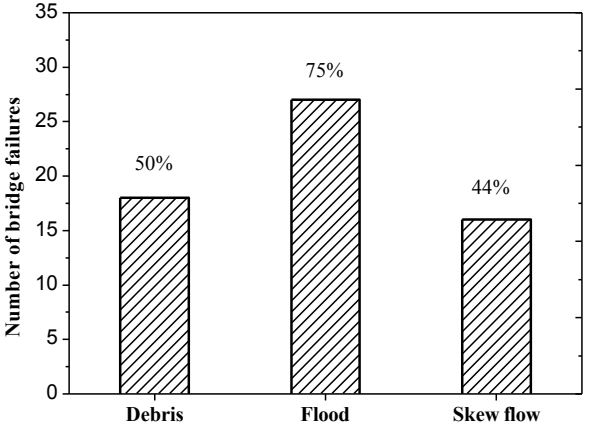

FIG. 1. Occurrence of debris, flood, and skew flow during bridge failures

Geotechnical condition

Geotechnical condition involves soil types and foundation types. Cohesionless soils are generally erodible as opposed to silt and clay. The time required to reach the maximum scour depth is approximately hours in sand, days in clays, months in glacial till and sandstone, years in limestone, and centuries in granite (Richardson and Davis 2001). Table 3 indicates most of bridge failures occurred in the erodible

riverbed materials, such as cobble/gravel and sand, while silt and clay contributed to 14% of total failures. Failure could also occur in mudstone/siltstone and earth loam but fewer cases were noted. The armored layers of gravels/cobbles are always deemed as non-erodible; however they may overlie erodible layer (e.g. silt or sand). In this case, scour can progress onto the underlying silt or sand

Table 3. Soil Types and Number of Bridge Failures

Soil types	Number	Percentage
Boulders	2	5
Cobbles / gravels	8	22
Armored gravels / cobbles	4	11
Sand or fine Sand with gravel or clay	5	14
Mudstone/siltstone	1	3
Silt/clay	5	14
Others (earth loam)	1	3
Not determined	10	28
Total	36	100

In terms of foundation types, shallow foundations are more susceptible to scour than deep foundations. Table 4 shows bridges supported by reinforced concrete piles have the highest percentage of failures. Spread footings contributed to the second highest percentage of bridge failure under scour events, followed by timber piles. Steel HP piles and unknown foundations claimed the lowest failures under scour conditions in the case studies examined.

Table 4. Foundation Types and Number of Bridge Failures

Foundation types	Number	Percentage
Spread footing	8	22
Concrete reinforced piles	15	42
HP Steel Piles	2	5
Timber piles	5	14
Unknown foundation	1	3
Not determined	5	14
Total	36	100

Structural condition

Table 5 summarizes bridge types pertinent to scour-induced failures. In the cases examined, bridge types have been documented in 22 of 36 cases. Failures of the slab-on-girder bridges were most encountered during scour events. Girder bridges with simply supported spans were more susceptible to scour than those with continuous

spans. In contrast to girder bridges, arch and truss bridges were less encountered in the cases examined.

Scour can initiate bridge failure at different structural components such as bridge deck, abutments, piers, or bridge foundations. Figure 2 illustrates failures of different structural components when the bridges were subjected to scour. In most cases examined, failures of bridge foundations triggered failures of bridge piers or abutments. As such, in Figure 2, foundation failures were considered as a part of pier and abutment failure. Figure 2 shows that pier failure was accounted for 61% the total failures, which is followed by abutment failure. Abutment failure was found to be influenced by channel migration and slope failure at the abutment. Others failures with lower percentage consisted of washout of bridge deck and bridge's tendency to fail by scour.

Table 5. Bridge Types and Number of Bridge Failures

Bridge types	materials	Number	Percentage
Arch	concrete	1	3
---	steel	1	3
Beam/Girder	concrete	7	19
---	steel	11	30
Box girder	concrete	1	3
Truss	steel	1	3
Not determined	-	14	39
Total		36	100

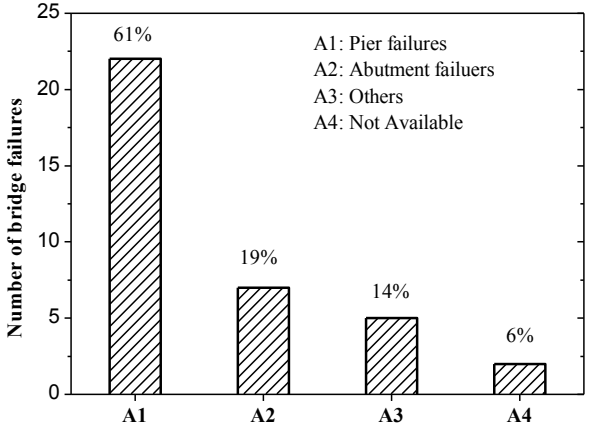

FIG. 2. Failures of bridge components due to scour

BRIDGE FAILURE MODES UNDER SCOUR CONDITIONS

Based on the assessment of the case histories, four failure modes were identified, including vertical failure, lateral failure, torsional failure, and bridge deck failure. Table 6 indicates that most bridge failures were associated with lateral failure, followed by vertical failure. In comparison, torsional failure and bridge deck failure were less encountered. The term *others* in Table 6 refers to a non-structural failure of a bridge, such as a slope failure at an abutment or washout of an approach to an abutment. Five of the 36 cases studied were classified as *others,* as channel migration produced intense scour to the approaches of the abutments.

The following section will characterize each of the failure modes.

Vertical failure

Bridge vertical failure under scour conditions could be attributed to a combination of factors such as inadequate soil support and pile instability. In general, bridge vertical failure due to scour could be generalized into four categories as noted in Figure 3. They consisted of inadequate bearing capacity of shallow foundation (Figure 3(a)), penetration of friction piles (Figure 3(b)), undermining of pile toe (Figure 3(c)), and pile buckling (Figure 3(d)).

Shallow foundations tend to lose their vertical bearing capacities when scour undermines the foundations and results in inadequate soil supports as shown in Figure 3**Error! Reference source not found.** (a). The Schoharie Creek Bridge is an example that scour undermined the bridge spread footings, causing the overall bridge failure.

Table 6. Failure Modes and Number of Bridge Failures

Failure modes	Number	Percentage
Vertical failure	11	30%
---Buckling	(2)	(5%)
Lateral failure	14	39%
---Structural hinging	(5)	(14%)
---Pushover failure	(4)	(11%)
Torsional failure	1	3%
Bridge deck failure	1	3%
Others	5	14%
Not identified	4	11%
Total	36	100%

Bridges on deep foundations can also fail under scour conditions as a result of inadequate vertical bearing capacity. For friction piles, the vertical bearing capacity is reduced due to the reduction of skin resistance when scour removes soil around the piles. Figure 3**Error! Reference source not found.** (b) illustrates the penetration of

friction piles as a result of inadequate vertical bearing capacity. As stated previously, the Hatchie River Bridge failed because the friction piles' skin resistance decreased as a consequence of scour. For end bearing piles, the piles lose their vertical bearing capacity when scour undermines the bearing layer (e.g. hard layer or bedrock) that the pile tips rest on, as seen in Figure 3**Error! Reference source not found.** (c).

Piles may also fail as a consequence of instability when scour increasingly removes the soils around the piles, resulting in an increase of the unsupported pile length, as seen in Figure 3**Error! Reference source not found.** (d). The slender piles tend to buckle under the axial load from the bridge superstructure or a combination of axial and lateral loads. Moreover, corrosion of the pile cross-section also contributes to the pile buckling failure. For example, corrosion resulted in approximately 44% reduction of cross-section of timber piles in the Hatchie River Bridge, (Thompson 1990), and 50% reduction of cross-section of steel HP piles in the I-10 Bridge over the Jourdan River in Mississippi (Avent and Alawady 2005). In terms of steel HP shapes, buckling can occur globally (flexural buckling) or locally (local buckling).

As indicated in Table 6, most vertical failures were associated with inadequate soil supports and to a less extent, were relative to instability issue.

Lateral failure

Lateral failure consists of pushover failures of piers, structural hinging of piles, kick-out failures of foundations, and excessive lateral movement of piers or foundations.

Pushover failures occur when transverse flood and debris loads incrementally add to bridge piers until bridge piers fail. Pushover analysis is a nonlinear static analysis by gradually increasing lateral loads until the collapse of the structure, as shown in Figure 4(a). In addition to causing pushover failure, debris tends to pressure the hydraulic flow downward, resulting in an even deeper scour hole. The greater scour depth in turns further lowers the pushover capacity of the bridge structure.

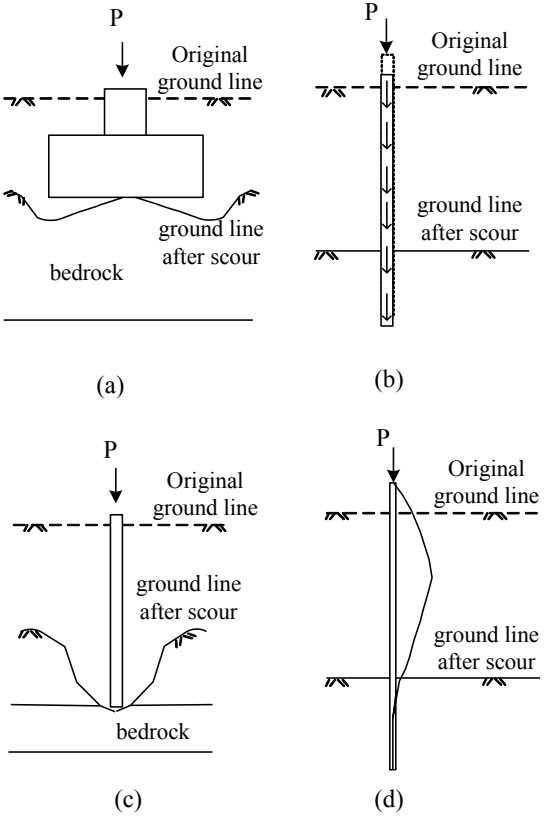

FIG. 3. Vertical failure of bridge foundations (a) undermining of footing base, (b) penetration of friction piles, (c) undermining of pile tip, (d) buckling of piles

Structural hinging occurs when transverse loads develop large bending moments to the structural elements when their boundaries are full or partial fixed, as seen in Figure 4(b). In the case studies examined, this failure mode was observed with the pier cap rotating towards the upstream direction (Melville and Coleman 2000). Piles with limited embedment into a pile cap may fail in a hinging mode due to inadequate bending moment resistance. In addition, floods carrying large and heavy debris such as stones may attack the piers or piles, resulting in a potential structural hinging (Melville and Coleman 2000).

Kick-out failure of foundations occurs when scour results in wash out of the piles from the location of pile tips, as depicted in Figure 4(c). Bridge that fails due to kick-out has relatively high lateral supports from superstructures but fails to sustain

adequate lateral capacity at the foundations. Shallow foundations are exceptionally susceptible to kick-out failures. Piles may also fail in kicking out once scour develops at a sufficient depth to mobilize pile tip laterally.

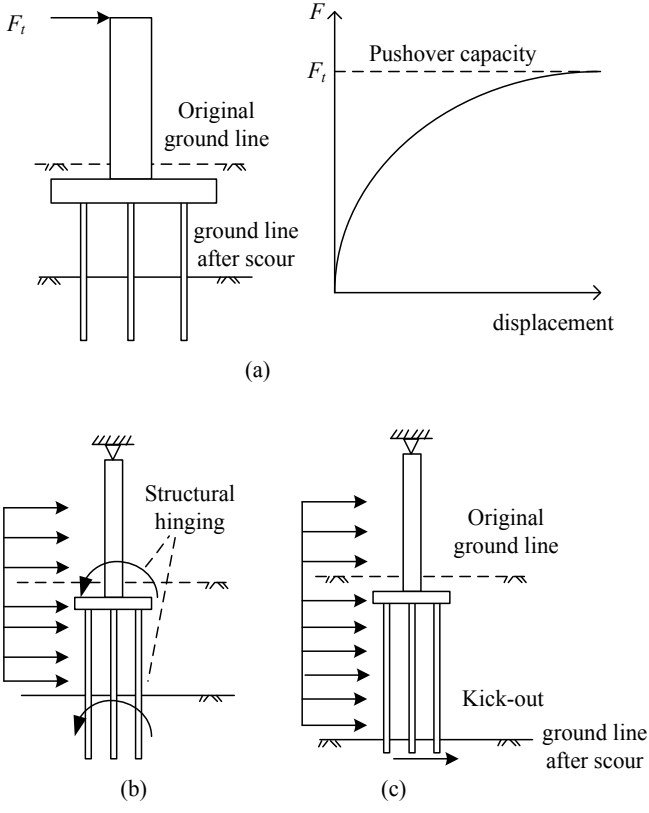

FIG. 4. Lateral failure modes of the bridge (a) pushover failure, (b) structural hinging, (c) kick out of foundations

Table 6 shows structural hinging failures accounted for 14% and pushover failures for 11% of the total failures.

Torsional failure

Torsional failure refers to a torsional (twisting) failure of the structure or structural components attacked by skewed flows. Flows with an angle of attack give arise to eccentric lateral loads and develop torques to bridge piers or abutments. In Table 6,

only one case had the bridge piles twisted (Melville and Coleman 2000), which was pertinent to torsional failure. Although torsional failure may not be a dominant failure mode, the torsion effect could co-exist with other types of bridge failures under skew flow conditions.

Bridge deck failure

Bridge deck failures may occur when bridge deck is outflanked by floods. Debris loads contribute to the washout of bridge deck in flood events. Bridge decks on simple-support spans are susceptible to the flood if the deck is not structurally attached to the superstructure elements. One among 36 examined cases was related to bridge deck failure as indicated in Table 6.

REMEDIAL WORK

Remediation of the bridge damage due to scour included retrofitting the damaged superstructure and foundation elements of bridges, and implementing scour countermeasures. Temporary Bailey bridges were built for those bridges whose spans were washed out or collapsed. Alternatively, some damaged bridges were forced to close and new bridges were constructed. Foundation rehabilitation included underpinning the damaged pile foundations with steel HP or pipe piles embedded to the competent soil layer. Deteriorated piles were replaced with sound piles, and in some cases, battered piles were constructed for the foundations to resist lateral loads. Grouting techniques were also used as remedial measures to fill the scour holes under spread footings.

It is also important to include scour protection and channel stabilization as a part of remedial work. Scour protection includes placing rock riprap and filter cloth on the riverbed under bridges. Channel stabilization includes stabilizing dikes to prevent the development of meander or realigning channels to establish smooth flows.

CONCLUSIONS

This paper reviewed case histories of bridge failures under scour conditions. Totally 36 cases were gathered and analyzed in terms of structural, hydraulic, and geotechnical conditions pertaining to scour-induced bridge failures. This paper also summarized bridge failure modes relative to scour and discussed scour remediation measures. Based on the analyses, the following conclusions can be drawn:

1) Local scour is the dominant scour type (i.e. 64%) responsible for bridge failure, followed by channel migration (14%) and contraction scour (5%). Most of scour depths (i.e. up to 41%) ranged from 0.5 to 5.0 m but the maximum scour depth could be up to 15 m.

2) Bridges in cohesionless soils were more susceptible to scour than cohesive soils. In the cases examined, most bridge foundations encountered were concrete piles (42%) and spread footings (22%).

3) Beam/girder bridges were most encountered in the cases examined. More failure or damage occurred at bridge piers than bridge abutments.

4) Bridge failure modes included vertical failure, lateral failure, torsional failure, and bridge deck failure. Among these failure modes, lateral failure (39%) was most prevalent, followed by vertical failure (30%).

REFERENCES

American Association of State Highway and Transportation Officials (AASHTO) (2007). *AASHTO LRFD Bridge Design Specifications.* 4th Ed., AASHTO, Washington, D.C.

Avent, R. R., and Alawady, M. (2005). "Bridge scour and substructure deterioration: case study." *Journal of Bridge Engineering*, 10(3), 247-254.

Jackson, L. E., Thompson, P. L., and Richardson, E. V. (1991). "Hatchie River and Schoharie Creek Bridge failures." *Proceedings of the 1991 National Conference on Hydraulic Engineering,* ASCE, 202-208.

Lagasse, P. F., Clopper, P. E., Zevenbergen, L. W., and Girard, L. W. (2007). "Countermeasures to protect bridge piers from scour." *NCHRP Report 593*, National cooperative highway research program, Transportation Research Board of The National Academies, Washington, D.C.

Melville, B. W., and Coleman, S. E. (2000). *Bridge scour*, Water Resources Publications, LLC, Highlands Ranch, Colorado.

National Transportation Safety Board (NTSB) (1990). "Highway accident report-collapse of the northbound U.S. route 51 bridge spans over the Hatchie River near Covington, Tennessee, April, 1989." Hydraulic, Erosion and Channel Stability Analysis of the Safety Board, Washington, D.C.

Richardson, E. V. and Davis, S. R. (2001). "Evaluating scour at bridges, fourth edition." *FHWA NHI 01-001 (HEC 18)*, Federal Highway Administration, Washington,D.C.

Storey, C., and Delatte, N. (2003). "Lessons from the collapse of the Schoharie Creek Bridge." *Proceedings of the Third Congress Forensic Engineering,* ASCE, San Diego, CA, 158-167.

Thornton-Tomasetti, P. C. (1987). "Overview report investigation of the New York State Thruway Schoharie Creek Bridge collapse." New York State Disaster Preparedness Commission.

Thompson, P. L. (1990). "April 1989 Hatchie River US-51 bridge failure." *Transportation Research Board*, 24-35.

Wiss, J., Elstner Associates, Inc. and Mueser Rutledge Consulting Engineers (1987). *Collapse of Thruway Bridge at Schoharie Creek*. Final Report Prepared for: New York State Thruway Authority.

A Benefit-Cost Analysis Toolkit for Road Weather Management Technologies

David Veneziano[1], Xianming Shi[2], M. ASCE, Lisa Ballard[3],
Zhirui Ye[4] and Laura Fay[5]

[1] Research Scientist, Western Transportation Institute, P.O. Box 174250, Bozeman, MT 59717-4250; david.veneziano@coe.montana.edu
[2] Research Professor, Department of Civil Engineering, Montana State Univeristy and Program Manager, Western Transportation Institute, P.O. Box 174250, Bozeman, MT 59717-4250; xianming_s@coe.montana.edu
[3] Principal, Current Transportation Solutions, PO Box 5651, Missoula, MT 59806-5651; lballard@currenttransportation.com
[4] Professor, Southeast University, China and Research Scientist, Western Transportation Institute, P.O. Box 174250, Bozeman, MT 59717-4250; jared.ye@coe.montana.edu
[5] Research Scientist, Western Transportation Institute, P.O. Box 174250, Bozeman, MT 59717-4250; laura.fay@coe.montana.edu

ABSTRACT: Highway agencies face increasing demands and customer expectations regarding mobility and safety during inclement weather, while confronting unprecedented budget and staffing constraints and a growing awareness of environmental challenges related to the use of chemicals and abrasives. To address these different issues, benefit-cost analysis is typically employed before making investment decisions. In the winter maintenance context, where the costs and benefits of road weather management tools can vary greatly, this presents a significant challenge to managers. This work presents an overview of a new benefit-cost analysis tool developed for winter maintenance practitioners to evaluate different equipment, operations and materials, including road weather management tools, in a streamlined, web-based environment. The toolkit was used to conduct two case studies of the use of Road Weather Information Systems (RWIS) and Maintenance Decision Support Systems (MDSS) for road weather management. The first case study examined the current use of RWIS statewide in Iowa and found that it produced an agency-specific benefit-cost ratio of 3.8 and a total ratio of 45.4. A second case study examined the potential use of MDSS in one subdistrict in Indiana found that a benefit-cost ratio for the agency would be 1.5, while the total ratio would be 3.0.

INTRODUCTION

Surface transportation in the United State is often threatened by the unpredictable character of weather, specifically “through visibility impairments, precipitation, high winds, temperature extremes, vehicle maneuverability, pavement friction, and

roadway infrastructure" (OFCM 2003). Recent years have seen "growing recognition of the effects of weather on the surface transportation system" (Strong et al. 2010) and this subject also deserves significant attention in the context of global climate change. Climate change and extreme weather have a profound impact on the U.S. infrastructure and transportation system.

The operators and maintainers of highway networks face increasing demands and customer expectations regarding mobility and transportation safety, especially during inclement weather, while confronting unprecedented budget and staffing constraints and a growing awareness of environmental challenges related to the use of chemicals and abrasives (Fay and Shi 2011, 2012, Pan et al. 2008, Shi et al. 2009, 2010a, 2010b, 2011, 2012, 2013, Staples et al. 2004). However, advances in road weather management in recent years, namely Road Weather Information Systems (RWIS) and Maintenance Decision Support Systems (MDSS), present an opportunity to provide agencies with significant benefits through reduced labor, material and other expenditures. To achieve these benefits however, agencies must first determine how significant these may be compared to the cost of an operation. The process required to make such a determination is benefit-cost (b-c) analysis. In the winter maintenance context, where various costs and benefits of road weather management tools can vary greatly, benefit-cost analysis presents a challenge to managers.

In light of this, a research need existed to develop benefit-cost analysis approaches for different winter maintenance practices, equipment and operations to streamline the process and assist maintenance managers in meeting the demand of identifying the benefits accrued versus the costs incurred. Work quantifying the costs and benefits of various aspects of winter maintenance has been completed to various degrees and was summarized by Fay et al. (Fay et al. 2010). As a result of existing evaluations, it was possible to develop a tool that could streamline benefit-cost analysis of these operations for agencies and provide indications of the benefits which they might hold in real-world applications. This work presents an overview of such a tool. RWIS and MDSS are the items selected to illustrate the process employed by the toolkit and to highlight the potential benefits that may be accrued using real-world data.

BACKGROUND

As indicated earlier, MDSS and RWIS are road weather management tools that hold many potential benefits for highway agencies. Consequently, past literature pertaining to these tools were identified to provide baseline information for the cost and benefit values from past studies that could be applied in developing a unified benefit-cost analysis approach for practitioners. Data from these efforts would be employed later in the development of streamlined approaches to compute their respective benefit-cost ratios. The following paragraphs summarize this information.

RWIS is one of the most widely applied systems that DOTs employ in making decisions related to treatment during winter storms. As expected for such a mature application, the costs, benefits and effectiveness of RWIS have been widely examined. Among the available literature related to RWIS costs, benefits and effectiveness is the work of Boslley (2001), Sullivan (2004), Lasky et al. (2006),

Ballard et al. (2002), Strong and Shi (2008), Ye et al. (2009a), Boon and Cluett (2002), McKeever et al. (1998), and Ye and Strong (2009).

RWIS systems have been found to be an effective tool for winter maintenance operations and are expected to produce cost savings throughout the lifetime of the installation. Given the extensive cost and benefit information available, several benefit-cost ratios were provided in the literature. Boslley, when examining the use of RWIS in general, determined that benefit-cost ratios between 1.1 and 5.0 were possible (Boselly 2001). Strong and Shi (2008) found that RWIS use in Utah produced a benefit-cost ratio of 11.0, while Ye et al. (2009a) determined use in Iowa and Nevada produced ratios of 1.8 and 3.2, respectively. Finally, Boon and Cluett (2002) determined RWIS use in Washington produced benefit-cost ratios between 1.4 and 5.0.

MDSS is an integrated software application that addresses the fundamental questions of *what*, *how much* and *when* in applying treatments according to the forecast road weather conditions, the resources available and local rules of practice (Ye et al. 2009b). In addition, MDSS can be used as a training tool as it features a *what-if* scenario treatment selector that can be used to examine how the road condition might change over a 48-hour period with the user-defined treatment times, chemical types, or application rates. A general overview of MDSS is presented by Smithson (2007), the National Center for Atmospheric Research (2008), NCHRP (2007), Mewes et al. (2005), Hart et al. (2008), with literature specifically discussing the costs, benefits, and effectiveness of MDSS presented by the work of Ye et al. (2009b, 2009c), Cluett and Jenq (2007), and Sugumaran et al. (2005).

Surprisingly, little published cost information was provided for MDSS in the literature. Still, benefit-cost ratios for MDSS were subsequently favorable, ranging between 7.11 and 8.67 in New Hampshire, 2.75 and 6.40 in Minnesota, and 1.33 to 2.25 in Colorado, as documented by Ye et al. (2009b, 2009c). These figures varied depending on the particular scenario employed in the respective analysis.

OBJECTIVE

The objective of this work was to develop that tool and investigate the resulting benefit-cost ratios of RWIS and MDSS using example data from agencies. The resulting work sought to address the existing gap of the lack of a straightforward tool that winter maintenance managers could use to complete benefit-cost analysis as well as to better understand the prospective benefits these operations held for agencies. Compared to traditional benefit-cost discussions related to RWIS and MDSS which have focused on one aspect of their benefits (materials savings, crash reduction, etc.) the new tool takes a more holistic approach by accounting for the many costs and benefits that arise from the use of each technology. The new tool bridges the gap between research and theory to produce a mechanism for practitioners which does not require a detailed background in areas such as statistics, economics, and so forth.

BENEFIT-COST ANALYSIS

When a financial value can be assigned to most of the costs and benefits of a piece of equipment, a practice or an operation, it becomes possible to compute a benefit-cost ratio. Benefit-cost ratios greater than 1.0 are generally desired. Given that winter maintenance items may entail long lives (e.g., RWIS and MDSS) that incorporate present and future (e.g., recurring maintenance) costs and benefits, there is a need to bring the values of all future costs and benefits accrued to a present value. A discount rate is employed to accomplish this. The discount rate is an opportunity cost value, or alternatively stated, the time value of money, which indicates how much money could be worth if invested in alternative ways.

For the purposes of this work, two approaches to selecting a discount rate were available. The first was to consider the Consumer Price Index (CPI) which the Office of Management and Budget (OMB) has recommended be based on the governmental borrowing rate of 7 percent. The average CPI inflation rate over the past 10 years has been 2.79 percent. Consequently, the discount rate would be 7.0 minus 2.79, or 4.21 percent through this approach. The second approach is to employ the Office of Management and Budget's (OMB, 2012) "Discount Rates for Cost Effectiveness, Lease-Purchase, and Related Analyses" guidance for a discount rate figure. Information compiled in December 2012 related to the nominal discount rate ranged from a 0.5 percent for a 3 year period to 3.0 percent for a 30 year period.

Using the project life and a selected discount rate, the values of costs and benefits are converted to both a present value and an annual value (or annual equivalent costs) by the following: present value = initial costs + present value of the annualized cost PV(A), where

$$PV(A) = \frac{A}{i} * \left[1 - \frac{1}{(1+i)^n}\right] \quad (1)$$

where

A = present value of annualized cost
i = the discount rate, and
n = number of years

If the discount rate is zero, then the annualized cost is simply PV(A) = A*n.

Once present and annual values are available for costs and benefits, it is possible to calculate the benefit-cost ratio. This is calculated by dividing present value benefits by present value costs, or annual equivalent benefits by annual equivalent costs. The benefit-cost ratio is calculated for agency-specific costs and benefits as well as total costs and benefits. Total costs and benefits include both those accrued by the agency, as well as from other sources, such as road users and society (via crash reduction, etc.).

TOOLKIT DEVELOPMENT

The tool developed to conduct benefit-cost analysis was web-based to provide the greatest availability to winter maintenance practitioners while also limiting the potential for errors to be made by users (e.g., changing a formula in a spreadsheet).

The toolkit was built to walk the user through a benefit-cost analysis in a series of steps. Based on the practice, equipment or operation selected by the user is presented with a series of web pages that represent the steps of benefit-cost analysis and require various item parameter, cost and benefit values to be entered. The data required for entry is straightforward and should be available based on agency practices. For data that is not available, guidance is provided on assumed values that can be entered.

The necessary data inputs for costs and benefits were established based on the literature discussed previously. In some cases, quantified values were not available; typically, these were related to society (environmental damage, reduced emissions, etc.). The toolkit still incorporated a mechanism for such values to be entered manually should they become available in the future.

CASE STUDIES

To establish what the benefit-cost ratios of these RWIS and MDSS would be for agencies with varying parameters (fleet size, coverage area, etc.), the benefit-cost toolkit was employed to conduct the case studies using information from the Indiana Department of Transportation (subdistrict level, i.e. a shed) and the Iowa Department of Transportation (entire state).

RWIS Case Study

The first case study examines the potential use of RWIS stations for the entire state of Iowa. Note that in this case study, RWIS is already in use for the state and the toolkit is being used to determine the benefit-cost ratio achieved through its implementation. The expected cost and benefit data is presented in Table 1.

For RWIS, general costs include the cost of alternative weather data from a data provider, the number of stations planned, or in this case, existing RWIS sites, the number of staff that are users, an average hourly labor rate (to estimate the costs for annual training), the hours of annual training required (per user), the annual cost of materials used in the jurisdiction being evaluated (in this case, statewide), the annual storm-related labor costs expended, the annual number of storm-related crashes that occur, and an average cost per crash. A 7 percent interest rate and 10 year life cycle were employed for the evaluation of RWIS. Agency, user and societal costs must also be considered. This includes the initial cost per RWIS station (e.g., equipment), installation, site preparation (included under installation costs in this case), communications installation cost per site and a central processing unit for the entire system. Annual costs include communications and maintenance to existing RWIS equipment. All of the data values associated with these costs are summarized in Table 1. No values for societal or user costs associated with RWIS were considered in this case.

The initial costs of RWIS, which are typical cost figures provided by the Iowa DOT from experience, were calculated as follows:

- RWIS Stations: \$50,000/site * 68 sites = \$3,400,000 (2)

- Installation costs: $4,00/site * 68 sites = $204,000 (3)
- Site preparation: none, included in installation cost (4)
- Communication installation: $50/site * 68 sites = $3,400 (5)
- Central Processing Unit: $4,000/unit * 2 units = $8,000 (6)
- Total initial costs:= ($3,400,000 + 204,000+ $3,400 +$8,000) - $450,000 (cost of forecast data) = $3,165,400 (7)

Table 1. RWIS Benefit and Cost Inputs

Project parameters	**Value**
Past/current weather data cost	$450,000
Planned/existing stations	68
Number of users	900
Hourly labor rate	$21.42
Hours of annual training	2
Annual material costs	$17,291,152
Storm-related labor costs	$4,626,720
Total annual storm-related crashes	8,346
Average crash cost	$33,700
Initial Cost Data	**Value**
Cost for each RWIS station	$50,000
Installation Cost	$3,000
Site preparations	$0
Communications installation cost per site	$50
Central processing unit	$4,000
Annual Cost Data	**Value**
Annual communications cost	$200
Annual maintenance cost	$2,550
Annual training cost	N/A
Annual Agency Benefits	**Value**
Reduced material usage	15%
Annual User Benefits	**Value**
Reduced crashes	10%

Note that the cost of forecast data is subtracted from the total costs, as this cost represents an expense that would have been incurred in lieu of the use of RWIS. Next, annual, or recurring costs were:

- Annual communications: $200/site * 68 sites = $13,600 (8)

- Maintenance: \$2,550/site * 68 sites = \$173,400 (9)
- Training: \$21.42/hour * 2 hours * 900 users = \$38,556 (10)
- Total annual costs: \$17,000 + \$173,400 + \$38,556= \$225,556 (11)

At this point, the initial cost must be converted to a constant annual payment before being added to the annual operating cost of RWIS to produce an annualized cost. This is accomplished by the following calculation:

- Annualized cost = $\frac{\$3{,}165{,}400 * 0.07\ (1+0.07)^{10}}{(1+0.07)^{10-1}}$ = \$450,681 (12)

The value of 0.07 is the interest rate, while 10 is the evaluation period. Using this result, the annualized cost is \$450,681 +\$225,556 = \$676,238. When using the present value equation presented in the Benefit-Cost Analysis section of this paper, the present value of RWIS costs is \$4,749,611. Based on this figure, the annual cost per RWIS site is \$751.

Following the establishment of costs, benefits must be established. For RWIS, the agency benefit is a reduction in annual material use and the user benefit is a reduction in crashes. These are reductions expressed as percentages guided by past findings documented in literature. The material use reduction of 15 percent is a conservative assumption based on a reported reduction of 40 percent achieved by the Idaho Transportation Department (ITD, 2009). Crash reduction guidance from the *Handbook of Road Safety Measures* indicates that the raising of winter maintenance standards can reduce Injury crashes by 11% and Property Damage Only (PDO) crashes by 30% (Elvik, et al. 2009). While the contribution of RWIS in these percentages is not broken out, one could conservatively assume that crash reductions attributed to the technology are 10 percent for both Injury and PDO crashes. No quantified benefits associated with the societal benefits of RWIS have been documented in past research.

To calculate the initial and annual value of benefits, the same approach employed for cost data is used. First, the material savings are calculated as:

- Material savings = \$17,291,152 (annual material exp.) * 0.15 (percent savings) = \$2,593,673. (13)

Savings from a 10 percent reduction in crashes are then calculated as:

- Crash savings = 8,346 (no. of crashes) * \$33,700 (avg. crash cost) * 0.10 (percent reduction) = \$28,126,020. (14)

The present value of the agency benefit from reduced material usage is then calculated as:

- Present value agency benefit = $\frac{\$2{,}593{,}673}{0.07}\ (1 - \frac{1}{(1+0.07)^{10}})$ = \$18,216,872 (15)

This figure equates to a benefit per site of $38,142. Using Equation 15 and substituting the value of annual crash savings for material savings, the present value of crash reduction benefits is $197,545,395, or $413,618 per site. The combined annual value of benefits is $30,719,693. When this value is substituted into Equation 15, the present value of all benefits is $215,762,267, or $451,760 per site.
Using the present value of agency benefits divided by the annualized agency cost ($18,216,872/$4,749,611), the benefit-cost ratio for the agency is computed as 3.8. This indicates that for every $1 spent on RWIS, the state is achieving a savings (primarily in material use) of $3.80. Similarly, the total present value of all benefits divided by the total cost of RWIS ($215,762,267/$4,749,611) produces a total benefit-cost ratio of 45.4. This indicates that for each $1 spent, a benefit of $45.40 was produced, including savings to society as the result of a reduction in crashes through better maintenance practices. These results compare favorable to those reported in literature (Fay, et al. 2010) where RWIS produced benefit-cost ratios between 1.1 and 11.0.

MDSS Case Study

The second case study examined the potential use of MDSS in one subdistrict in Indiana. This case study assumes MDSS is not already in use for the location. The expected cost and benefit data is summarized in Table 2.

Table 2. MDSS Benefit and Cost Inputs.

Project parameters	**Value**
Number of maintenance units	1
Number of computers per maintenance unit	1
Number of vehicles with mobile data collection units	5
Total number of vehicles	23
Total material cost per season	$373,186
Initial Cost Data	**Value**
In vehicle unit hardware	$2,000
Annual Cost Data	**Value**
Software costs or fees	$110
Communications	$200
Vehicle maintenance	$144
Administrative costs	$3,141
Training	$403
Annual Agency Benefits	**Value**
Reduced material usage	15%
Annual User Benefits	**Value**
Reduced crashes	15%

The evaluation begins with general project parameters, including the number of maintenance units in the jurisdiction, the number of computers that will receive MDSS software, the number of vehicles equipped with mobile data collection units, the total number of vehicles in the maintenance fleet, and the total material cost per season for the jurisdiction. Although not listed in the table, a 7 percent interest rate and 5 year life cycle were employed for demonstration purposes.

Next, thee initial and annual costs of MDSS are established. These consist only of the in-vehicle unit hardware cost. Next, the annual costs, including communications, software, and maintenance of MDSS equipment on each vehicle, administration costs and training costs are determined. All of the data values associated with these costs are summarized in Table 2. No societal or user costs were employed in this case. The initial costs of MDSS, which are typical cost figures provided by the specific subdistrict being considered in Indiana, were calculated as follows:

- In vehicle hardware : \$2,000/unit * 5 vehicles = \$10,000 (16)

Next, annual, or recurring costs were established, again using data provided by the Indiana DOT:

- Software: \$110/site * 1 computer = \$110 (17)
- Communications: \$200/year * 5 vehicles = \$1,000 (18)
- Vehicle maintenance: \$144/year * 5 vehicle = \$720 (19)
- Administrative cost: \$3,141/year (20)
- Training cost: \$403/year (21)
- Total annual costs: \$110 + \$1,000 + \$720 + \$3141 + \$403 = \$5,374 (22)

The initial cost is converted to a constant annual payment before being added to the annual operating cost by the following calculation:

- Annualized cost = $\frac{\$10{,}000 * 0.07\ (1+0.07)^5}{(1+0.07)^{5-1}}$ = \$2,439 (23)

The value of 0.07 is the interest rate, while 5 is the evaluation period. Using this result, the annualized cost is \$2,439 +\$5,374 = \$7,813. When using the present value equation presented in the Benefit-Cost Analysis section of this paper, the present value of MDSS costs is \$32,034. Based on this figure, the annual cost per MDSS vehicle is \$1,563.

Next, MDSS benefits are considered. For this case, the agency benefit is a reduction in annual material use and the user benefits are a reduction in crashes and reduced travel delays. These are percent reductions that may be expected based on previous research. The material use reduction of 15 percent is a conservative assumption based on a reported reduction of 40 percent achieved in Idaho (ITD 2009). User benefits are based on guidance from the *Handbook of Road Safety Measures* which indicates that the raising of winter maintenance standards can reduce Injury crashes by 11% and Property Damage Only (PDO) crashes by 30% (Elvik, et

al. 2009). It was assumed that crash reductions attributed to MDSS are 10 percent for both Injury and PDO crashes. No quantified benefits associated with the societal benefits of MDSS have been documented.

The same approach employed with respect to cost estimation was used to calculate the initial and annual value of benefits as follows:

- Material savings = \$373,186 (annual material exp.) * (5/23) (ratio of vehicle fleet equipped with MDSS) * 0.15 (percent savings) = \$12,169. (24)

Savings from a 15 percent reduction in crashes are then calculated as:

- Crash savings = \$81,127 (material savings) * * 0.15 (percent reduction) = \$12,169 (25)

Crash savings were found to be a percentage of materials savings in previous work (Ye, et al. 2009b), with a present value of agency benefits calculated as:

- Present value agency benefit = $\frac{\$12,169}{0.07}\left(1 - \frac{1}{(1+0.07)^5}\right)$ = \$49,895 (26)

This figure equates to a benefit per vehicle of \$2,434. Using Equation 26 and substituting the value of annual crash savings for material savings, the present value of crash reduction benefits is \$49,895, or \$2,434 per vehicle. The combined annual value of benefits is \$24,338. When this value is substituted into Equation 26, the present value of all benefits is \$99,791, or \$4,868 per vehicle.

Using the present value of agency benefits divided by the annualized agency cost (\$49,895/\$32,034), the benefit-cost ratio for the agency is computed as 1.6. These results indicate that for every \$1 spent on MDSS, the subdistrict is achieving a savings (primarily in material use) of \$1.60. Similarly, the total present value of all benefits divided by the total cost of MDSS (\$99,791/\$32,034) produces a total benefit-cost ratio of 3.1. This indicates that for each \$1 spent, a benefit of \$3.10 was produced. These ratios are similar to those reported in literature (Fay, et al. 2010), where MDSS produced benefit-cost ratios of 1.33 to 8.67.

CONCLUDING REMARKS

This work has provided a brief discussion of a new benefit-cost analysis tool developed for winter maintenance practitioners to evaluate different equipment, operations and materials. The approach employed by the toolkit was demonstrated in this paper through two case studies of the effectiveness of RWIS and MDSS in road weather management. The first case study examined the current use of RWIS statewide in Iowa. In examining this use, the toolkit estimated RWIS produced an agency-specific benefit-cost ratio of 3.8 and a total ratio of 45.4. A second case study examining the potential use of MDSS in one subdistrict in Indiana found an agency benefit-cost ratio of 1.6 and a total ratio would be 3.1.

In part, this work highlights the need for greater documentation of the different costs and benefits associated not only with RWIS and MDSS, but with all winter maintenance equipment, practices and operations. The documentation of such

information remains a significant gap in the winter maintenance community, and further research is necessary to establish the financial values of the different costs and benefits that are incurred by a particular item. Additional research is also warranted to better quantify some of the intangible benefits (e.g., societal benefits) such that benefit-cost analysis is more complete and accurate.

Over a longer period of time, factors such as climate change may play a significant role in the tools used for winter maintenance and for road weather management in general. In such instances, it will be of interest to evaluate how such changes impact the benefit-cost ratios for different aspects of winter maintenance. Once widely used by practitioners, the toolkit may also serve as a database in documenting the temporal and spatial evolution of the costs and benefits associated with various winter maintenance tools and help to better understand this question.

ACKNOWLEDGEMENTS

The authors wish to thank the Clear Roads pooled fund research project and its sponsor states of California, Colorado, Idaho, Illinois, Iowa, Kansas, Maine, Massachusetts, Michigan, Minnesota, Missouri, Montana, Nebraska, New Hampshire, New York, North Dakota, Ohio, Pennsylvania, Rhode Island, Utah, Vermont, Virginia, Washington, West Virginia, Wisconsin and Wyoming for the funding of this research. They also thank the numerous Clear Roads participants that provided guidance, input and feedback throughout the course of the toolkit's development. Finally, the authors thank the Iowa and Indiana DOTs for providing example data for use in the testing and demonstration of the toolkit. For more information on the toolkit, readers are encouraged to contact the Clear Roads Pooled Fund.

REFERENCES

Ballard, L., Beddoe, A., Ball, J., Eidswick, E. and Rutz, K. (2002). "Assess Caltrans road weather information systems (RWIS) devices and related sensors." *Research Report,* Western Transportation Institute, Bozeman, MT. 135 p.

Boon, C. and Cluett, C. (2002). "Road weather information systems: enabling proactive winter maintenance practices in Washington State." *Research Report,* Washington State Transportation Center, Seattle, WA. 126 p.

Boselly, S.E. (2001). "Benefit/cost study of RWIS and anti-icing technologies." *Research Report,* National Cooperative Highway Research Program, Washington, D.C. 37 p.

Cluett, C., and Jenq, J. (2007) "A case study of the maintenance decision support system (MDSS) in Maine." *Research Report,* ITS Joint Program Office, U.S. Department of Transportation, Washington, D.C. 51p.

Elvik, R., A. Hoye, T. Vaa, and M. Sorensen. *Handbook of road safety measures*, 2nd ed. Emerald Group Publishing, Bingley, United Kingdom, 2009. 1140 p.

Fay, L., Veneziano, D., Ye, Z., Williams, D. and Shi, X. (2010). "Cost-benefits of winter road maintenance tools: a renewed perspective based on recent research." *Transportation Research Record: Journal of the Transportation Research Board*, Vol. 2169: 174-186.

Fay, L., and Shi, X. (2011). "Laboratory investigation of performance and impacts of snow and ice control chemicals for winter road service." *ASCE Journal of Cold Regions Engineering*, 25(3): 89-114.

Fay, L., and Shi, X. (2012). "Environmental impacts of chemicals for snow and ice control: state of the knowledge." *Water, Air & Soil Pollution*, Vol. 223: 2751–2770.

Hart, R.D., Mewes, J.J., Hershey, B.W., Osborn, L.F., and Huft, D.L. (2008). "An overview of implementation and deployment of the pooled fund study maintenance decision support system." *Proc. Seventh International Symposium on Snow Removal and Ice Control Technology*, Indianapolis, IN. 229-239.

Idaho Transportation Department. (2009) "How Idaho's non-invasive RWIS network is paying for itself while helping to set new standards for improved service and operations." *Idaho Transportation Department Transporter*, Boise, ID.

Lasky, T.A., Yen, K.S., Darter, M.T., Nguyen, H. and Ravani, B. (2006). "Development and field-operational testing of a mobile real-time information system for snow fighter supervisors." *Research Report,* California Department of Transportation, Sacramento, CA. 90 p.

McKeever, B., Haas, C., Weissmann, J. and Greer, R. (1998). "A life cycle cost-benefit model for road weather information systems." *Transportation Research Record: Journal of the Transportation Research Board*, Vol. 1627: 41-48.

Mewes, J, Hart, R., Osborne, L., and Podoll, B. (2005) "The pooled fund study maintenance decision support system: a functional overview." *Proc. American Meteorological Society Preprint, 21st International Conference on Interactive Information Processing Systems (IIPS)*, San Diego, CA. 4 p.

National Center for Atmospheric Research (2008). "The maintenance decision support system (MDSS) project, technical performance assessment report, Colorado field demonstration – winter 2007-2008." *Research Report,* City and County of Denver, Colorado. 54 p.

National Cooperative Highway Research Program (2007). "Guidelines for the selection of snow and ice control materials to mitigate environmental impacts." *Research Report,* Transportation Research Board of the National Academies, Washington, D.C. 211 p.

Office of the Federal Coordinator for Meteorological Services. (2003). "Weather information for surface transportation: a national needs assessment report." *Research Report,* Office of the Federal Coordinator for Meteorological Services and Supporting Research, Silver Spring, Maryland. 302 p.

Office of Management and Budget (2012). "Discount rates for cost effectiveness, lease-purchase, and related analyses." *Research Report,* Office of Management and Budget, Washington, D.C.

Pan, T., He, X., and Shi, X. (2008). "Laboratory investigation of acetate-based deicing/anti-icing agents deteriorating airfield asphalt concrete." *Journal of the Association of Asphalt Paving Technologists (AAPT)*, Vol. 77: 773-793.

Shi, X., Fay, L., Yang, Z., Nguyen, T.A., and Liu, Y. (2009). "Corrosion of deicers to metals in transportation infrastructure: Introduction and recent developments." *Corrosion Reviews*, Vol. 27 (1-2): 23-52.

Shi, X., Fay, L., Peterson, M.M., and Yang, Z. (2010a). "Freeze-thaw damage and chemical change of a Portland cement concrete in the presence of diluted deicers." *Materials and Structures,* Vol. 43 (7): 933-946.

Shi, X., Liu, Y., Mooney, M., Berry, M., Hubbard, B., and Nguyen, T.A. (2010b). "Laboratory investigation and neural networks modeling of deicer ingress into Portland cement concrete and its corrosion implications." *Corrosion Reviews*, Vol. 28 (3-4): 105-153.

Shi, X., Fay, L., Peterson, M.M., Berry, M., and Mooney, M. (2011). "A FESEM/EDX investigation into how continuous deicer exposure affects the chemistry of portland cement concrete." *Construction and Building Materials*, 25(2): 957-966.

Shi, X., Goh, S.W., Akin, M., Stevens, S., and You, Z. (2012). "Exploring the interactions of chloride deicer solutions with nano/micro-modified asphalt mixtures using artificial neural networks." *ASCE Journal of Materials in Civil Engineering*, Vol. 24 (7): 805–815.

Shi, X., Fortune, K., Smithlin, R., Akin, M., and Fay, L. (2013). "Exploring the performance and corrosivity of chloride deicer solutions: Laboratory investigation and quantitative modeling." *Cold Regions Science and Technology*, Vol. 86: 36-44.

Smithson, L. (2007) "MDSS – the U.S. success story." *Proc. 2007 Annual Conference of the Transportation Association of Canada*, Saskatoon, Saskatchewan. 12 p.

Strong, C. and Shi, X. (2008). "Benefit-cost analysis of weather information for winter maintenance." *Transportation Research Record: Journal of the Transportation Research Board*, Vol. 2055: 119-127.

Staples, J.M., Gamradt, L., Stein, O., and Shi, X. (2004). "Recommendations for winter traction materials management on roadways adjacent to bodies of water." *Research Report,* Montana Department of Transportation. Helena, MT. 97 p.

Strong, C.K., Z. Ye, and Shi, X. (2010). "Safety effects of winter weather: the state of knowledge and remaining challenges." *Transport Reviews*, Vol. 30 (6): 677-699.

Sugumaran, R., Salim, M., Strauss, T. and Fulcher, C. (2005). "Web-based implementation of a winter maintenance decision support system using GIS and remote sensing." *Research Report,* Midwest Transportation Consortium, Ames, IA. 42 p.

Sullivan, J. (2004). "Road weather information system phase i." *Research Report,* Alaska Department of Transportation & Public Facilities, Juneau, AK. 78 p.

Ye, Z., Shi, X. Strong, C. and Greenfield, T. (2009a). "Evaluation of the effects of weather information on winter maintenance costs." *Transportation Research Record: Journal of the Transportation Research Board*, Vol. 2107: 104-110.

Ye, Z., Strong, C., Shi, X. and Conger, S. (2009b). "Analysis of maintenance decision support system (MDSS) benefits & costs." *Research Report,* South Dakota Department of Transportation Report, Pierre, SD. 143 p.

Ye, Z., Shi, X., Strong, C., Conger, S. and Huft, D. (2009c). "Benefit-cost analysis of maintenance decision support system." *Transportation Research Record: Journal of the Transportation Research Board*, Vol. 2107: 95-103.

Ye, Z. and Strong, C. (2009). "Cost-benefit for weather information in winter maintenance: technical memorandum 4 – secondary RWIS benefits." *Research Report,* Western Transportation Institute, Bozeman, MT. 152 p.